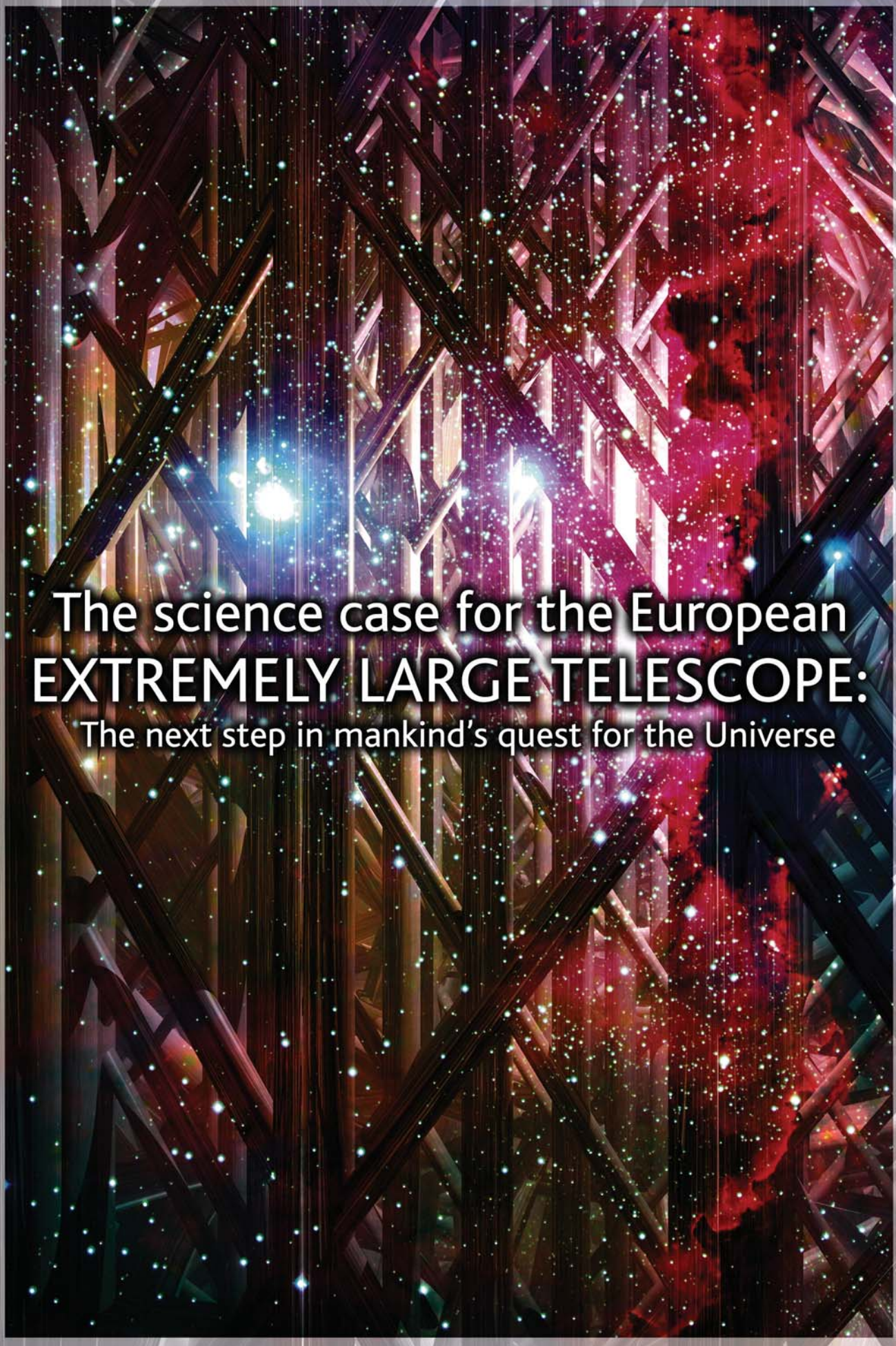

The science case for the European EXTREMELY LARGE TELESCOPE:

The next step in mankind's quest for the Universe

The science case for

The European Extremely Large Telescope

THE ESSENTIAL NEXT STEP IN MANKIND'S DIRECT OBSERVATION OF THE NATURE OF THE UNIVERSE, THIS WILL PROVIDE THE DESCRIPTION OF REALITY WHICH WILL UNDERLIE OUR DEVELOPING UNDERSTANDING OF ITS NATURE.

INDEX/CONTENTS

1 Executive summary

Science Case for the European Extremely Large Telescope

Astronomy is in its golden age. Since the invention of the telescope, astronomers have expanded mankind's intellectual horizons, moving our perception of the Earth from an unmoving centre of the Universe to being one of several small planets around a typical small star in the outskirts of just one of billions of galaxies, all evolving in an expanding Universe in which planets are common.

The nuclear energy sources which provide starlight are identified, and we know that the chemical elements of which we are made are the ash of that process: stardust. Exotic states of matter are known: neutron stars, black holes, quasars, pulsars. We can show that the Universe started in an event, the Big Bang, and see the heat remnant of that origin in the Cosmic Microwave Background. Tiny ripples in that background trace the first minute inhomogeneities from which the stars and galaxies around us grew. By comparing the weight of galaxies with the weight of all the visible matter, astronomers have proven that the matter of which we, the planets, the stars, and the galaxies, are made is only a tiny part of all the matter which exists: most matter is some exotic stuff, unlike what we are made of, not yet detected directly, but whose weight controls the movements of stars in our Galaxy. This 'dark matter' or 'unseen mass', whatever it is made of, is five times more abundant than are the types of matter of which we are made. Perhaps most exotic of all, some new force seems to be stretching space-time, accelerating the expansion of the Universe. The nature of this force, which controls the future of the Universe, remains quite unknown.

Astronomy is a technology-enabled science: progress in astronomy demands new technologies and new facilities. Astronomical telescopes and associated instrumentation are the essential tools allowing access to the widest and most comprehensive laboratory of all, the Universe we live in. Telescopes allow discovery of the new, and subsequent exploration of the whole range of known phenomena, from Solar System objects – planets, comets and asteroids, to the formation of stars and galaxies, extreme states of matter and space (e.g. around black holes) and finally to determine the global matter-energy content of our Universe. In the past half-century a new generation of telescopes and instruments allowed a golden age of remarkable new discoveries: quasars, masers, black holes, gravitational arcs, extrasolar planets, gamma ray bursts, the cosmic microwave background, dark matter and dark energy have all been discovered through the development of a succession of ever larger and more sophisticated telescopes.

In the last decade, satellite observatories and the new generation of 8- to 10-metre diameter ground based telescopes, have created a new view of our Universe, one dominated by poorly understood dark matter and a mysterious vacuum energy density. This progress poses new, and more fundamental, questions, the answers to some of which will perhaps unite astrophysics with elementary particle physics in a new approach to the nature of matter. Some discoveries, made using relatively modest technologies, will require vast increases in technology to take the next step to direct study. Each new generation of facilities is designed to answer the questions raised by the previous one, and yet most advance science by discovering the new and unexpected. As the current generation of telescopes continues to probe the Universe and challenge our understanding, the time has come to take the next step.

In the words of the Astronomer Royal for England, Sir Martin Rees,

"Cosmologists can now proclaim with confidence (but with some surprise too) that in round numbers, our Universe consists of 5percent baryons, 25percent dark matter, and 70percent dark energy. It is indeed embarrassing that 95percent of the Universe is unaccounted for: even the dark matter is of quite uncertain nature, and the dark energy is a complete mystery."

A small step in telescope size will not progress these fundamental questions. Fortunately, preliminary studies indicate that the technology to achieve a quantum leap in telescope size is feasible. A telescope of 50-metre to 100-metre diameter can be built, and will provide astronomers with the ability to address the next generation of scientific questions.

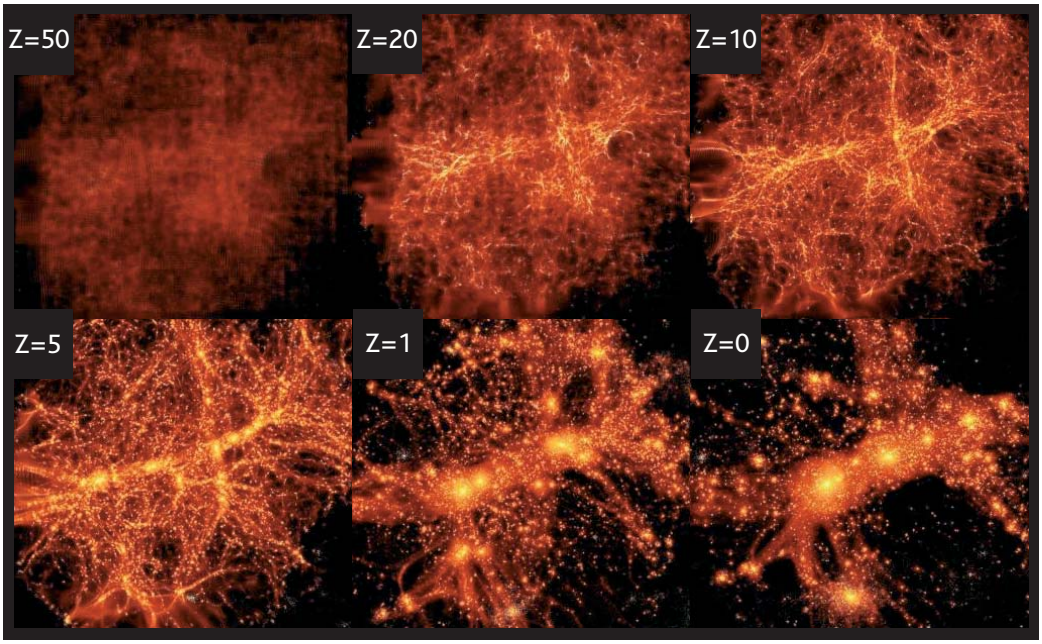

Simulation showing stages in the formation of the galaxies in the Local Group in a cold dark matter scenario. Snapshots are shown at various times from the early Universe (z=50) to the present day (z=0).

Primary science cases
for a 50metre -100metre Extremely Large Telescope

Are there terrestrial planets orbiting other stars? Are we alone?	Direct detection of earth-like planets in extrasolar Systems and a first search for bio-markers (e.g. water and oxygen) becomes feasible.
How typical is our Solar System? What are the planetary environments around other stars?	Direct study of planetary systems during their formation from proto-planetary disks will become possible for many nearby very young stars. In mature planetary systems, detailed spectroscopic analysis of Jupiter-like planets, determining their composition and atmospheres, will be feasible. Imaging of the outer planets and asteroids in our Solar System will complement space missions.
When did galaxies form their stars?	When and where did the stars now in galaxies form? Precision studies of individual stars determine ages and the distribution of the chemical elements, keys to understanding galaxy assembly and evolution. Extension of such analyses to a representative section of the Universe is the next great challenge in understanding galaxies.
How many super-massive black holes exist?	Do all galaxies host monsters? Why are super-massive black holes in the nuclei of galaxies apparently related to the whole galaxy? When and how do they form and evolve? Extreme resolution and sensitivity is needed to extend studies to normal and low-mass galaxies to address these key puzzles.
When and where did the stars and the chemical elements form?	Can we meet the grand challenge to trace star formation back to the very first star ever formed? By discovering and analysing distant galaxies, gas clouds, and supernovae, the history of star formation, and the creation history of the chemical elements can be quantified.
What were the first objects?	Were stars the first objects to form? Were the first stars the source of the ultraviolet photons which re-ionised the Universe some 200million years after the Big Bang, and made it transparent? These objects may be visible through their supernovae, or their ionisation zones.
How many types of matter exist? What is dark matter? Where is it?	Most matter is transparent, and is detectable only through its gravitational effect on moving things. By mapping the detailed growth and kinematics of galaxies out to high redshifts, we can observe dark matter structures in the process of formation.
What is dark energy? Does it evolve? How many types are there?	Direct mapping of space-time, using the most distant possible tracers, is the key to defining the dominant form of energy in the Universe. This is arguably the biggest single question facing physical science.
Extending the age of discovery...	In the last decades astronomy has revolutionised our knowledge of the Universe, of its contents, and the nature of existence. The next big step may well also be remembered for discovering the unimagined new.

1.1 Astronomy with a 50metre – 100metre telescope

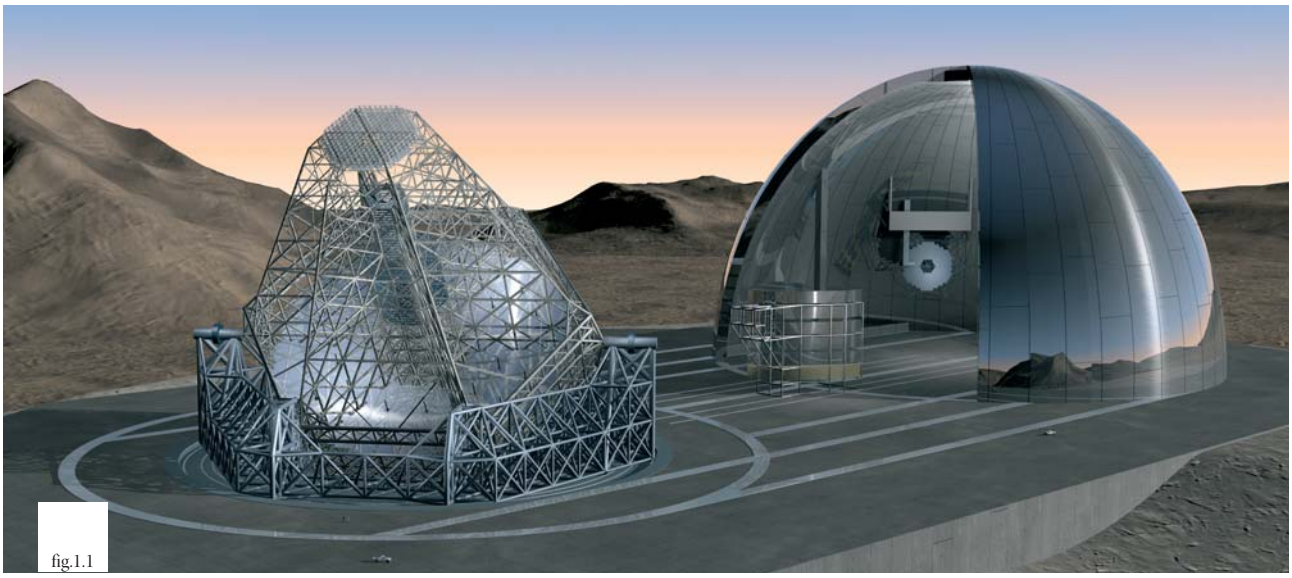
fig.1.1

Concepts for 50-100m ELTs. Above: the OWL (OverWhelmingly Large) Telescope, a design for a 100m-class telescope proposed by ESO (Gilmozzi 2004, Dierickx et al 2004).

The science case for 50m–100m diameter telescopes is spectacular. All aspects of astronomy, from studies of our own Solar System to the furthest observable objects at the edge of the visible Universe, will be dramatically advanced by the enormous improvements attainable in collecting area and angular resolution: major new classes of astronomical objects will become accessible to observation for the first time. Several examples are outlined in the following sections. Furthermore, experience tells us that many of the new telescope's most exciting astronomical discoveries will be unexpected: indeed the majority of the science highlights of the first ten years of the first 10m telescope, the Keck, such as its part in the discovery and study of very high redshift, young 'Lyman-break' galaxies, were entirely new, violated received wisdom, and, being unknown, were not featured in the list of science objectives prior to the telescope's construction.

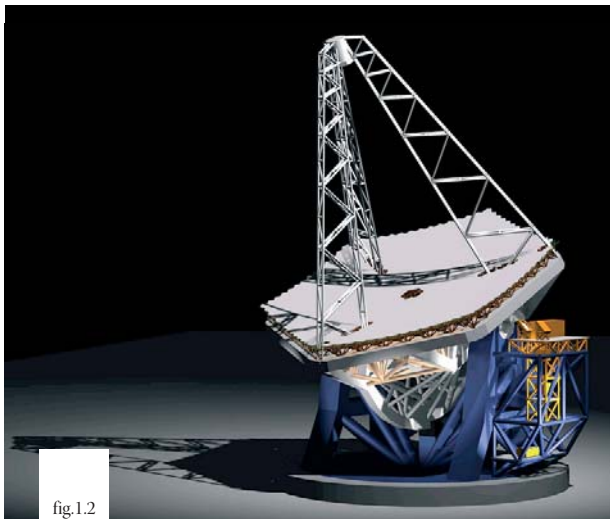
fig.1.2

The Euro-50 concept (Andersen et al., 2003, 2004).

The vast improvement in sensitivity and precision allowed by the next step in technological capabilities, from today's 6–10m telescopes to the new generation of 50–100m telescopes with integrated adaptive optics capability, will be the largest such enhancement in the history of telescopic astronomy. It is likely that the major scientific impact of these new telescopes will be discoveries we cannot predict, so that their scientific legacy will also vastly exceed even that bounty which we can predict today.

2 Introduction

In the following three chapters we describe the science case for a 50m-100m aperture Extremely Large Telescope. We divide the extensive science case into three broad areas: Planets and Stars (Chapter 3), Stars and Galaxies (Chapter 4) and Galaxies and Cosmology (Chapter 5). These divisions were chosen to reflect a change in the way astrophysics will be approached in the era of Extremely Large Telescopes. The traditional astronomical categories appropriate to currently available facilities divide the subject into three almost distinct disciplines, broadly Planets, Stars and Galaxies. In the Extremely Large Telescope era we will study planets around stars other than our own Sun, study individual stars in galaxies far beyond our own Milky Way, and begin detailed study of galaxies at cosmological distances. The context of these studies, in an era when particle physics, fundamental physics and astrophysics are increasingly merging into a single Grand Challenge, is discussed in Annex B.

Before describing these exciting possibilities, we first give a brief summary of the technological performance of Extremely Large Telescopes, which must be delivered to make these exciting scientific advances feasible.

2.1 The power of Extremely Large Telescopes

Current adaptive optics systems on 8-m class telescopes have recently demonstrated performance close to the theoretical diffraction limit. Figure 2.1 shows the diffraction limits for 8m, 30m and 100m telescopes compared to the typical sizes of astronomical objects. While 8m telescopes can resolve large regions within galaxies (between 300 and 1000pc in size) at redshifts around unity, Extremely Large telescopes can, given appropriate adaptive optics capability, resolve structures of a few tens of parsecs in size, the approximate size of a major star forming region, at similar redshifts.

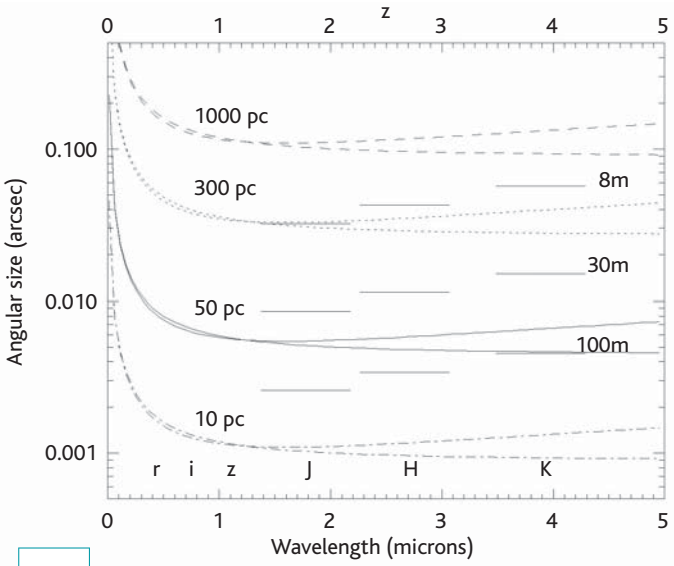

fig.2.1

The theoretical diffraction limits (1.2 λ/D) for 8m, 30m and 100m telescopes are plotted at three wavelength values corresponding approximately to the J, H and K infrared bands (horizontal bars). Also plotted are curves of projected angular size as a function of redshift for objects of various physical sizes (10pc, 50pc, 300pc and 1kpc) for two sets of cosmological parameters : $(\Omega_M, \Omega_\Lambda)=(0,0)$ and (0.3,0.7) for the lower and upper curves respectively.

A smaller diffraction limit combined with increased light-collecting aperture translates into great gains in sensitivity as telescope diameter is increased, particularly for unresolved point sources. This is largely because of the reduced contribution from sky noise when the size of the image is reduced. For example a 100m telescope with perfect diffraction-limited images would reach about 8 magnitudes fainter for point sources than an 8m telescope that delivers 0.5 arcsec images, for the same signal-to-noise and exposure time (in the near IR). In this simple scaling argument, we have assumed perfect diffraction-limited images (Strehl = 1). Even with a moderate Adaptive Optics (AO) correction that results in the majority of the light falling inside a 0.1 arcsec aperture, a 100m telescope would give a gain of 4.5 magnitudes for point sources compared to an 8m telescope producing 0.5 arcsec images, a factor of 60 in intensity (see Table 2.1).

Image size	8m	30m	100m	Comments
0.5 arcsec	0.0	1.4	2.7	Seeing limited
0.2 arcsec	1.0	2.4	3.7	
0.1 arcsec	1.7	3.2	4.5	
Strehl (K) = 0.2	0.6	3.5	6.1	e.g. Multi-conjugate AO
Strehl (K) = 1.0	2.4	5.2	7.8	Theoretical limit

Table 2.1

Gains in magnitude for the same signal-to-noise and exposure time when observing unresolved sources in the background-limited regime. The gains are shown relative to an 8m telescope delivering 0.5 arcsec images.

2.2 Telescope design requirements

This science case is being developed in parallel with a European Extremely Large Telescope design study (a four year program which began in March 2005), and the relevant OPTICON Joint Research Activities, which are developing the appropriate technological capabilities. We have listed design requirements for the telescope resulting from each part of the science case throughout the document, and where possible we have included simulations to demonstrate the potential of Extremely Large Telescopes for specific science applications. Naturally the science case and requirements will continue to evolve as the scientific and technical studies progress.

In many cases we have been able to consider the dependence of the science achievable on telescope aperture. These results are summarised for a few key science cases in Annex A.

Highlight Science Cases
for a 50m-100m Extremely Large Telescope

The science case presented in this document demonstrates the very wide range of applications for an ELT. Of these a few stand out as "highlights" and have generated particularly high levels of enthusiasm and discussion among the European ELT science group. These highlighted cases are:

(1) Terrestrial exoplanets (Section 3.1.1)

(2) Resolved stellar populations in a representative section of the Universe (Sections 4.2 and 4.3)

(3) First light and the re-ionisation history of the Universe (Section 5.2)

These are seen as some of the most exciting prospects for ELTs precisely because they push the limits of what can be achieved, and they will provide some of the most technically challenging specifications on telescope design. The boundaries of what is achievable in these scientific areas (and others) will not be known exactly until the ELT is in operation, although more precise feasibility assessments will be possible when the technical studies described above are complete. We now present the science case that we believe is within range of a 50–100m ELT based on our current understanding of the technical issues.

3 Planets and Stars

Introduction

Stars have focused the interest of astronomers for centuries. A great variety of observations have driven our knowledge of the processes leading to star formation, of how the interplay between gravity and nuclear reactions determine stellar evolution, and ultimately, the physical principles that explain the existence of some of the most exotic states of matter in the Universe: neutron stars and black holes. In spite of the undeniable progress made during the last few decades in understanding how stars form and evolve, essential questions remain for which the collecting area and angular resolution of an extremely large optical/infrared telescope will prove decisive. Many of these questions deal with the earliest and the latest stages of stellar evolution, plagued by significant unknowns.

Determining the entire stellar mass spectrum in the cores of molecular clouds or measuring the dynamical mass spectrum of black hole/neutron stars in binary systems are areas in which major changes may be required in the currently accepted scenario for star formation and evolution, and which present great observational challenges for the current generation of very large telescopes. Current limitations in the present understanding of star formation are directly related to the lack of high sensitivity, high spatial resolution observations in star forming regions, where 1 AU in the nearest regions at 100 pc corresponds to just 10 milli-arcsec. Probing such regions in the optical and infrared with the few milli-arcsec resolution provided by an E-ELT will most likely unveil the nature of processes that form stars in the cores of molecular clouds. It will also probe the conditions for formation of protoplanetary disks and the ubiquity of planet formation.

The recent discovery that at least 7% of Solar-type stars host giant planets at separations of less than 5 AU has opened a new domain for research. With current very large telescopes, it may well be possible to directly image massive giant planets, but only around a few specific types of objects, such as very young stars or brown dwarfs. However, to establish a complete picture of the formation of planetary systems, direct imaging and characterisation of planets around stars in various evolutionary stages is needed. In particular, in order to understand whether or not the architecture of our own Solar System is a common occurrence, detailed observations of stars similar in mass and age to the Sun must be obtained. These observations will require the higher angular resolution and collecting area of an E-ELT. Such a telescope will not only be a crucial tool for our understanding of the formation and evolution of planetary systems, but also for the exploration of our own Solar System, where planets and their moons will be studied with resolution comparable only to those of space missions.

An E-ELT will be capable of detecting giant planets (Jupiter to Neptune-like) orbiting at separations smaller than 1 AU around thousands of stars up to distances of 100 pc, including many in the nearest star forming regions. The ultimate goal, however, is the detection of terrestrial planets around Solar-type stars, orbiting in the so-called “habitable zone”, the region around a star where liquid water may exist on the planetary surface and therefore favourable to the emergence or existence of life approximately as we know it. For reference, the Sun’s habitable zone is about 0.15 AU wide, centred on the Earth’s orbit at a radius of 1 AU. The very high angular resolution of an E-ELT, combined with efficient techniques for suppressing the bright light of the parent star, may allow the detection of earth-like planets around hundreds of Solar-type stars at distances less than 50 pc. Once discovered, the

enormous light collecting capabilities of such a telescope will also enable studies of their atmospheres in search of indicators of biological activity.

In the following sections, we present a selection of science cases that will be addressed with an E-ELT. The science cases start with the study of exo-planets, before moving on to studies of our own Solar System, and then the lives of stars from birth in molecular clouds to their end points as neutron stars and black holes.

3.1 Exoplanets

An E-ELT will be a uniquely powerful facility for the study of extrasolar planets, from detection, through characterisation by spectroscopy, to elucidation of their evolution. Parts of this topic may be accessible to smaller ground-based telescopes; however, only a 50–100m diameter telescope will have the critically important potential to *discover terrestrial planets by direct imaging* and to characterise them by *spectroscopy of their atmospheres*. This is an undertaking which is not practicable for a significantly smaller facility, but one which is of the utmost scientific and philosophical importance. For this reason, the potential contribution of an E-ELT to the study of extrasolar planets is presented here in some detail.

3.1.1 Highlight Science Case: Terrestrial planets in habitable zones – "Exo-earths"

The detection of terrestrial planets like the Earth relies on their being illuminated by their parent star. An Earth-like planet in an Earth-like orbit around a Solar-type star within a few tens of parsecs from the Sun would, on its own, be more than bright enough to be detected by an E-ELT. However, light coming from a parent star directly is enormously brighter than that reflected by the planet: in the case of the Solar System, the Sun is ~10^{10} times brighter than the Earth at visible and near-infrared wavelengths. In order to stand any chance of success, it is therefore necessary to minimise the effects of this "glare" by concentrating the light of both the planet and the star into the smallest possible points, thereby allowing them to be detected separately.

3.1.1.1 "Exo-earths" around Solar type stars

At any given distance from the Solar System, the parameter space over which target exoplanets are accessible to an E-ELT will be determined by two effects. The brightness of the starlight reflected by the planet falls off with increasing orbital distance from its parent star: this limits the detectability of an exoplanet very distant from its parent star, even though it is well separated from it. At the other extreme, the bright inner structures of the stellar image created by the telescope, including superspeckles, diffraction rings, and so on, will drastically reduce the sensitivity at angular separations less than about 20 milli-arcsec for a 100m telescope. This corresponds to an orbital radius of 1 AU at 50 pc, 5 AU at 250 pc or 50 AU at 2500 pc. In the latter two instances, the low level of illumination by the parent star combined with the attenuation due to the distance of the system from the Earth, implies that only self-luminous exoplanets will be detectable (see Figure 3.4 on page 14).

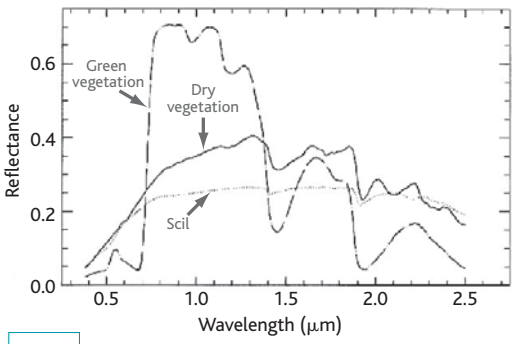

fig.3.1

(From Arnold et al 2002): Reflectance spectra of photo-synthetic (green) vegetation, non-photosynthetic (dry) and soil (from Clark 1999). The so-called vegetation red edge (VRE) is the green vegetation reflectance strong variation from ~5% at at 670 nm to ~70% at 800 nm. This edge has been detected in the global spectrum of the Earth (Arnold et al 2002).

However, at closer distances, an E-ELT will be capable of a vast range of exoplanetary investigation, covering planets both outside and inside a star's habitable zone. In particular, a 100m diameter E-ELT would yield a relatively large angular separation between the central diffraction peak of a star and its habitable zone, making it possible to image terrestrial-like exoplanets there in the face of the stellar glare, as discussed in more detail below.

3.1.1.2 Spectroscopic signatures of life: biomarkers

The near-infrared J band centred at a wavelength of 1.25μm is nearly optimal for the detection and characterisation of potential terrestrial exoplanets. The band contains and is bounded on both sides by strong spectral absorption features due to water in the Earth's atmosphere. However, the very same features are an extremely important diagnostic of conditions on exoplanets, since liquid water is arguably essential for carbon-based life with a generally terrestrial-like chemistry.

In the centres of the stronger telluric absorption bands, saturated lines will obscure any potential signal from an exo-earth. However, there are numerous unsaturated but nevertheless strong and narrow lines in the wings of the band which can be used. The changing doppler shift (up to ~50 km/s) as the Earth and an exoplanet orbit around their respective stars will cause the water lines in the respective atmospheres to shift in and out of wavelength synchronisation with respect to one another, making it possible to detect the exoplanet lines and measure their strength.

Similar techniques can be used to seek for the "B" absorption complex of oxygen at 760 nanometres at far-red optical wavelengths.

It is by now well accepted that significant amounts of free oxygen in the atmosphere of an exoplanet would be a strong indicator of the presence of photosynthetic biochemistry. More directly, plant life on the Earth gives rise to the so-called "vegetation red edge" (VRE) at 725 nanometres (see Figure 3.1), where the exact wavelength and strength of this absorption shoulder depends on the plant species and environment.

The detection of any such feature in the spectrum of an exoplanet would clearly be extremely important: even though the chances are very small that another planet has developed exactly the same vegetation as Earth, it would still be very interesting to find a type of vegetation different from terrestrial vegetation, and if a VRE is detected at a position incompatible with any shoulder in the libraries of mineral spectra, it would be a promising signature of a non-terrestrial biology. In a more general sense, an exoplanet with appropriately exotic chemistry would be quite likely to exhibit other, perhaps totally unexpected, spectral features in its spectrum. It is clear that such studies will constitute one of the most exciting potential applications of an E-ELT.

3.1.2 Simulations of planet detection with ELTs

The detection and characterisation of exoplanets, especially terrestrial ones, is a potentially highly rewarding goal of an E-ELT, but also an extremely challenging one. Thus, before building such a telescope, it is crucial that high fidelity simulations of the telescope, its auxillary systems, and instrumentation be made.

Figure 3.2 shows two representative simulations of the adaptive-optics corrected point spread function (PSF) of a 100m diameter telescope at near-infrared wavelengths (see, e.g. Le Louarn et al. 2004). The compact, diffraction-limited central core is surrounded by diffraction spikes and a diffuse halo of residual starlight not be fully corrected by the AO system. Any much fainter exoplanets in orbit around such a star must then be detected against this structured emission.

Figure 3.3 then shows a simulation of an exoplanetary system containing a Jupiter-like planet and an Earth-like planet, as they would be imaged by a 100m diameter E-ELT at visible wavelengths (Hainaut, Rahoui, & Gilmozzi 2004). In their study, Hainaut et al. calculated the signal-to-noise of planet detections over a range of parameter space in Strehl ratio, telescope size, distance to the planetary system, and observing wavelength.

The simulation includes an AO-corrected PSF which includes a full model of the telescope (including segmented primary and secondary mirrors), atmospheric turbulence, and a representative AO system with a single deformable mirror. In this case, the central star has been subtracted to permit the planetary images to be seen in the figure, although subtraction is, in principle, not necessary to make a detection. In practice, however, it is likely that additional contrast-enhancing methods will be used, such as coronography, nulling interferometry, extreme-AO, and simultaneous differential imaging. At the very least, a simple coronograph would probably be required to protect the detector from the high flux levels in the core of the stellar image. Note that, if by chance, a planet were concealed under one of the diffraction spikes, the rotation of the alt-az mounted telescope relative to the sky (or, equivalently, of the PSF structure, especially the diffraction spikes, relative to a detector array in

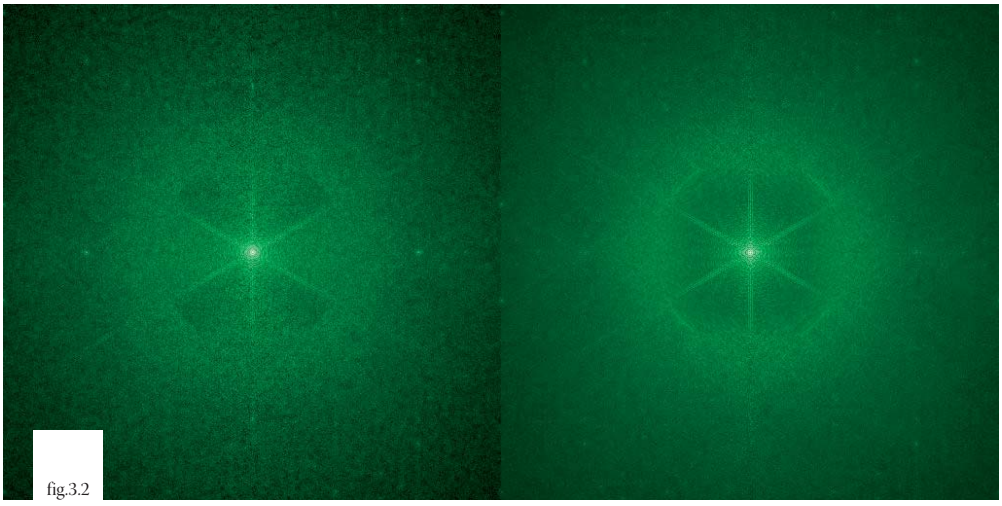

fig.3.2

Examples of simulated AO-corrected point-spread functions for the OWL 100m telescope by the ESO AO group (see, e.g. LeLouarn et al. 2004). The images are 1.7 arcsec on a side and are displayed on a logarithmic scale to show the complex structures present around the central peak, against which any potential exoplanet must be detected. The compact central spike is surrounded by the soft AO halo. Further out, the diffraction structures from the secondary mirror supports and the segmented primary and secondary mirrors are seen. These PSFs are calculated at 2.2μm assuming uncorrected seeing of 0.7 arcsec. Left: assuming a visible (R-band) Shack-Hartmann wavefront sensor. Right: assuming an infrared (K-band) pyramid sensor. The Strehl ratio for the left-hand PSF is 69%, while it is 76% for the right-hand one.

an instrument supported on a rotator) would soon unmask it. Slightly less tractable would be the case of a planetary system seen nearly edge-on. In this instance, the planet would spend a significant fraction of the time closer to the star than its maximum elongation: it would be necessary to wait a few months until its orbital motion took it clear again.

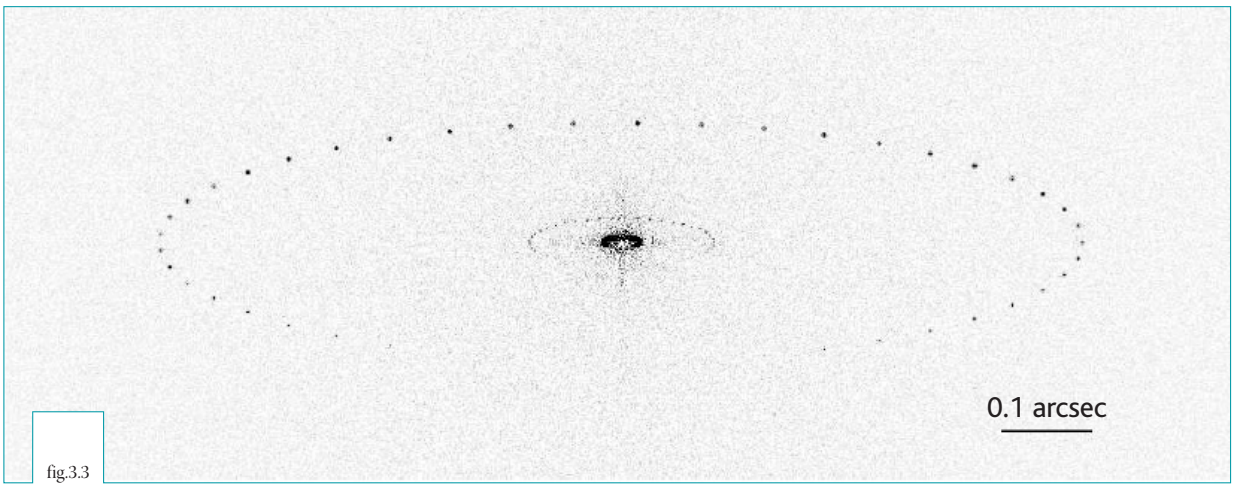

fig.3.3

A simulated time-series image of a Solar System analogue, containing a Jupiter-like and an Earth-like planet at a distance of 10pc. The system has been "observed" at a number of epochs as the planets go around in the 15 degree obliquity orbits to illustrate the phase effect. Each epoch is represented by a 100 ksec exposure in the V-band with the OWL 100m telescope, based on PSF simulations similar to those shown in Figure 3.2. The PSF of the central star has been subtracted from the image. (From Hainaut, Rahoui, & Gilmozzi 2004).

3.1.2.1 On-going simulations

Given the crucial importance of such simulations, it is important to note that several European groups are working independently and in collaboration to understand the physical limitations of ground-based observations of exoplanets. Although this work is ongoing, current results suggest that the exoplanet science cases presented in the present chapter are within the capabilities of a 50–100m diameter E-ELT. The European ELT Design Study started in March 2005 should deliver more detailed simulation results and key technology developments, both of which will be crucial to deriving realistic sensitivity limits for exoplanet science.

Some of the exoplanet studies being carried out in Europe are listed here, along with the particular physical effects each is considering. Annex B contains a discussion of the complementarity of proposed ground-based E-ELT exoplanet observations with space-based planet-finding missions such as ESA's Darwin and NASA's TPF-C and TPF-I.

Notes on Design Requirements
– detection and study of Exo-earth planets

Observation Type: High-contrast imaging and low-resolution spectroscopy

Field of View: Of order 1 arcsec x 1 arcsec

Spatial Resolution: Very high-Strehl ratio (70–90%) adaptive optics

Spectral Resolution: R~500–1000

Wavelength Range: 0.6-1.4μm

Target Density: On the order of 1000 targets around the sky

Dynamic Range constraint: 10^{10} contrast in brightness between star and an Earth-like planet; aim to detect planets at as close as ~30 milli-arcsec from the star

Telescope Size: As large as possible for spatial resolution and collecting area; 100m class telescope needed to study Earth-like planets

Date constraint: Multiple observations needed for confirmation

Other comments: Coronography and other contrast-enhancing methods will probably be used as required

- ESO Adaptive Optics Group – continued simulations of realistic PSFs for the 100m OWL as a function of wavelength, including a full telescope model, atmospheric turbulence, segmented mirror, and so on (see Figure 3.2 and Le Louarn et al. 2004). Also considering the effects of different wavefront sensing methods.
- Rahoui, Hainaut, & Gilmozzi (ESO) – extension of the simulations shown above (e.g. Figure 3.3) to include the effect of speckles and correction of speckles using simultaneous differential imaging, specifically in the context of exoplanet detection with ELTs, and with the OWL design used as a test case. The effect on planet detection signal-to-noise of various Strehl ratios, telescope size, wavelength, are being considered, along with the effect of exo-zodiacal light.
- European ELT Design Study – simulations relevant for exoplanet detection will be generated as part of the instrumentation, wavefront control, and AO work packages.
- Durham University AO group (UK) – working with ESO on simulations of AO on ELTs.
- O. Lardiere et al. – studying the effects of actuator pitch, telescope size and choice of site on imaging contrast, with and without coronography (see, e.g. Figure 3.4 and Lardiere et al. 2003). Also examining the effects of anti-aliasing to provide further gains in contrast.
- P. Salinari et al. (Arcetri) – simulations of the effects on contrast of piston errors and other effects such as pupil and segment shape.
- A. Chelli (Obs. Grenoble) – simulations of planet detection limits for ELTs, including the effects of non-stationary speckles.
- R. Gratton et al. – simulations based on performance of current instruments and predictions for the VLT-CHEOPS planet-finding project.
- T. Hawarden (UKATC) – estimates of speckles from segment piston errors.
- A. Ardeberg et al. (Lund Observatory) – investigating the effects for the case of a 50m diameter telescope

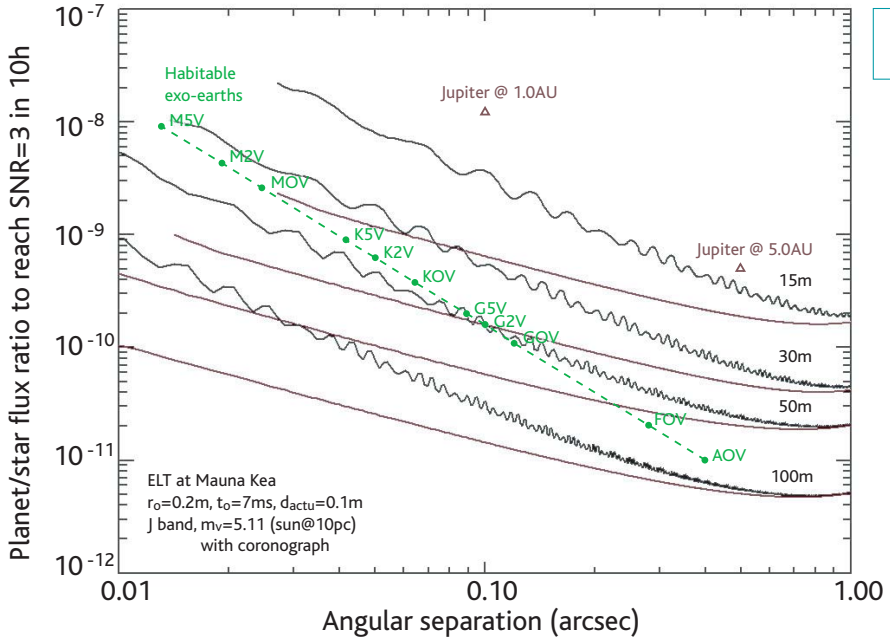

fig.3.4 Observable planet-star flux ratio at a signal-to-noise ratio of 3 in 10hrs (36 ksec) in the near-infrared J-band as a function of the planet-star angular separation. Results are shown for telescopes with diameters ranging from 15m to 100m. Habitable terrestrial planets orbiting main-sequence stars of various spectral types (at a distance of 10pc from the Sun) are plotted, along with "cold" and "warm" Jupiter-like planets. (From Lardiere et al. 2003).

3.1.3 Giant planets: evolution and characterisation

Viewed from a distance of 10 parsecs, our own, relatively old (4.5 Gyr) planetary system would be seen only in reflected sunlight at visible and near-infrared wavelengths. The largest planet, Jupiter, would have a visible V-band magnitude of 26.3 and a near-infrared J-band magnitude of 25.2 and thus be hard to detect against the glare of the Sun. However, when relatively young, gas giant planets radiate away excess energy from their formation and are thus self-luminous, making them potentially much easier to detect.

For example, at 1 Gyr, a 5 Jupiter-mass (M_J) would have roughly the same radius as our present-day Jupiter, but have an internally-heated effective temperature of ~350 K, even at 5 AU from its parent star. Models predict that such a planet would have a J-band magnitude of 21.7 and thus be some 25 times brighter than Jupiter at that wavelength. This would be a fairly faint source for present-day 8m class telescopes without even considering the nearby parent star, but a trivial observation for a 100m telescope even with the parent star present.

Indeed, it will be possible to detect Jupiter and super-Jupiter mass planets at increasingly larger distances with an E-ELT, by choosing sources in progressively younger clusters. For example, the Hyades lies at 46 pc and is 600 Myr old, while the Pleiades are more distant at 120 pc, but are younger at just 100 Myr. The nearest star forming regions, including Taurus-Auriga, Lupus, Chamaeleon, Corona Australis, and Orion, are further away at 150 to 450 pc, but contain stars as young as 1 Myr old, thus ensuring that any gas giant companions remain detectable. A key point to keep in mind, however, is that the apparent angular separation between the stars and their planets will be decreasing: 5 AU in Taurus-Auriga is just 35 milli-arcsec: here, the superb spatial resolution of an E-ELT will be crucial in resolving the planets from their stars.

An E-ELT will therefore permit the study of Jovian planets of a variety of sizes and ages, from nearby field stars to newly-formed stars in young clusters. Such observations will make it possible to carry out a rigorous verification of theories of the formation and evolution of large planets in a range of environments. A significantly smaller telescope than presently envisaged would be seriously limited in this work: the distances of the available clusters and star forming complexes place them beyond the reach of, say, a 30m facility, except for the study of the largest, super-Jupiters at large orbital radii.

Notes on Design Requirements

Observation Type: Imaging and spectroscopy
Field of View: Of order 1 arcsec by 1 arcsec
Spatial Resolution: 1–2 milli-arcsec
Spectral Resolution: 10–100
Wavelength Range: 0.5–2.5μm
Target Density: Thousands around the sky
Dynamic Range constraint: 10^7–10^8
Telescope Size: 50–100m

3.1.4 Mature gas giant planets

Although the direct detection of older, cooler Jupiter-mass planets is very difficult with present technology, their presence has been inferred around a large number (>150) of nearby, Solar-type stars via radial velocity observations. For obvious selection effect reasons, many of the earliest objects found were in very close, short-period orbits around their central stars, close enough to be substantially heated by the star. These so-called "hot Jupiters" are hard to explain in terms of current planetary formation theories, and the present paradigm is that they probably migrated to their present locations after forming at much larger distances from their parent star. Today, however, they are in very different environments from the gas giant planets in our own Solar System and will, in any case, be impossible to resolve from the glare of their parent stars. At somewhat larger

orbital radii, around the habitable zone for a Solar-type star, several "warm" Jupiters are now known, while a few exoplanetary systems are now known to harbour "cool" Jupiters, orbiting well beyond the outer edge of the habitable zone (Marcy et al. 2002; Naef et al. 2003; see Figure 3.5 opposite for the example of υ Andromedae) at 2.5 AU.

The range of warm and cold Jupiter systems explorable by an E-ELT depends on a combination of the required angular resolution to resolve a planet next to its star as and on the reflected flux from the star, both of which vary as a function of the star-planet separation and their distance from the Earth. Assuming a Jupiter-like reflectance spectrum for all gas-giant exoplanets, a 100m diameter E-ELT should be capable of directly imaging old, Jupiter-like planets orbiting at a few AU around Solar-type stars out to 100 pc distance from the Sun. Warm Jovian planets orbiting at ~1 AU, on the other hand, will be imageable out to perhaps 50 pc.

Notes on Design Requirements

Observation Type: Imaging and spectroscopy

Field of View: Few arcsecs

Spatial Resolution: Diffraction limited with high Strehl ratio

Dynamic Range constraint: 10^7–10^8 to within ~ 0.1 arcsec of the parent star.

Spectral Resolution: 10–100

Wavelength Range: 1–10μm

Target Density: Hundreds around the sky

Obtaining spectra of exoplanets does not fundamentally require that they be spatially resolved from the parent star, and a 100m E-ELT has the potential to secure spectra of cold giant planets out to ~20 pc and of closer-in, warm giants to beyond ~50 pc. Such spectra would enable a number of critical studies. The nature of the upper-atmosphere cloud particles can be determined (c.f. Marley et al. 1999), while secondary species such as NH_3 and CO can be utilised as tracers of atmospheric circulation via their chemistry. Deuterated molecules (with lines near 2.4, 4 and 8-10μm) can be used to determine deuterium abundances. These last enable an important diagnostic of the planetary mass, since sources exceeding 13 M_J will have depleted their deuterium as a result of nuclear burning in the planetary core. This will require detection of absorption bands which depress the continuum by less than 1%, a taxing problem for which only an E-ELT is likely to yield sufficient signal-to-noise.

3.1.5 Earth-like moons in the habitable zone

Radial velocity monitoring has uncovered a number of multiple planet systems including two or more gas giants. Figure 3.5 illustrates a system which contains Jovian planets approximating to all of the categories described above: the known planets of υ Andromedae include a "hot", a "warm" and a "cool" super-Jupiter (Butler et al. 1999). Systems similar to υAnd with gas giant planets in the habitable zone pose an intriguing prospect, namely that of terrestrial planet-sized moons in orbit around them which may offer a possible exobiological environment. Unfortunately, υAnd-b itself is slightly too close to its F6IV primary for habitability and, in any case, has an orbital eccentricity of ~0.4, inimical to the survival of life in its vicinity. Nevertheless, its presence indicates that a class of "warm" Jupiters with terrestrial moons may well exist. While an Earth-sized moon orbiting its parent super-Jupiter could not be resolved directly by a 100m E-ELT in imaging mode, there are several potential methods that would allow indirect detection of earth-sized moons as described below and which, in combination, would yield the moon albedo, mass, size, and orbit.

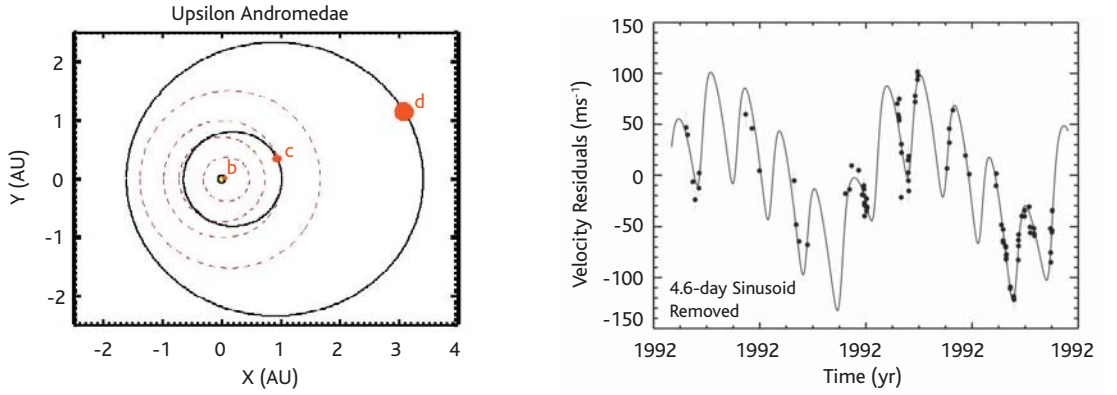

fig.3.5

Orbits of the three planets around the nearby Solar-type star υ Andromedae. The red dots mark the orbits of planets b, c and d. The dashed circles show the orbits of Mercury, Venus, Earth and Mars for comparison. Right: Measured radial (line-of-sight) velocities for υ And, showing the complex variations remaining after the strong effect of a ~1M_J planet orbiting at 0.06 AU from the star with a period of 4.6 days, a so-called "hot" Jupiter, has been removed. The remaining variations show the smaller amplitude and slower effects of two outer planets, one with 2 M_J orbiting at 0.8 AU (241 day period: a "warm" super-Jupiter) and the other with 4.6 M_J at 2.5 AU (1267 day period: a "cool" super-Jupiter). (Source: Butler et al. 1999). At the 13.5 parcsec distance of υ And, these two outer planets will be readily observable in reflected light with a 100m class telescope, even in spectroscopic mode.

3.1.5.1 Detection from reflex velocity measurements

If the parent Jupiter-like planet is bright enough to allow medium-to-high resolution spectroscopy, the reflex motion of the Jupiter due to a potential terrestrial moon may be detectable. For an Earth-mass moon orbiting a Jupiter-mass planet at the same distance as the moon is from Earth, the reflex velocity range is about +/– 60 m/s over a period of ~1 day. At 5 pc, a 100m E-ELT could secure spectra of the parent planet at resolutions of a few times 10^4, with S/N ~ 20, in a couple of hours. To detect the reflex motion due to the moon would require a long observing campaign (~600 hours) to acquire many such spectra. These would be analysed in phase bins around a hypothetical orbit, after accumulating enough spectra to build up the signal-to-noise to the required level (~100 per pixel per phase bin).

Notes on Design Requirements

Observing type: Reflex velocity measurements via mid- to high-resolution spectroscopy of a Jupiter-like planet

Spectral Resolution: A few x 10,000

Observing time: 20 hrs per observation. Several observations needed at different phases. About 600 hrs total.

3.1.5.2 Moon-induced astrometric wobble of the planet

In addition to perturbing the radial velocity curve due to the gas giant, the moon will also cause an astrometric wobble in the photocentre of the planet about their common centre of mass. For an Earth-mass moon lying on a Titan-like orbit around a Uranus-like planet at a distance of 10 pc from the Sun, the amplitude of the wobble would be ~0.5 milli-arcsec, or ~25% of the diffraction-limited width of the planet image for a 100m class ELT operating at a wavelength of 1μm.

Notes on Design Requirements

Observation Type: High-precision astrometric monitoring

Spatial Resolution: Diffraction-limited over very small field-of-view

Wavelength Range: Near-infrared, 1μm if possible

3.1.5.3 Spectral detection of terrestrial moons of giant planets

The spectrum of a Jupiter-mass planet at 1 AU from its parent star should show strong absorption of reflected starlight due to methane, ammonia, and gaseous and condensed water, resulting in a drop in its 2–4μm spectrum by a factor 10^4 (Sudarsky et al. 2003). By contrast, over the same spectral region, the spectrum of an Earth-like moon is likely to be almost flat. As the Earth/Jupiter surface area ratio is roughly 0.01, the reflected light from the Earth-like moon would dominate by a factor of ~100 in the 2–4μm region (Williams & Knacke 2005), making its spectral detection eminently possible.

Notes on Design Requirements

Observation Type: Low resolution spectroscopy

Spectral Resolution: R > 10

Wavelength Range: Near-infrared, 1–5μm

3.1.5.4 Mutual planet/satellite shadows and eclipses

Finally, when the parent star, the planet and its moon are nearly aligned, transits and eclipses can occur. When the moon transits between the star and the planet, it projects its shadow on the planet surface, making a dip in the planetary light curve. When the planet lies between the star and the moon, the latter disappears in the planet shadow in an eclipse, resulting in a dip in the global planet+moon light curve, with the same depth as the previous one, but with a longer duration. Figure 3.6 shows the resulting light curve for a maximum orbital elongation of the planet. The depth and duration of the mutual shadows and eclipses are modulated by the orbital revolution of the planet+moon system.

Notes on Design Requirements

Observation type: Photometric monitoring of planet flux to ~ few % precision

Wavelength Range: Near-infrared, 1–5μm

Date constraint: Monitoring observations over hours and days

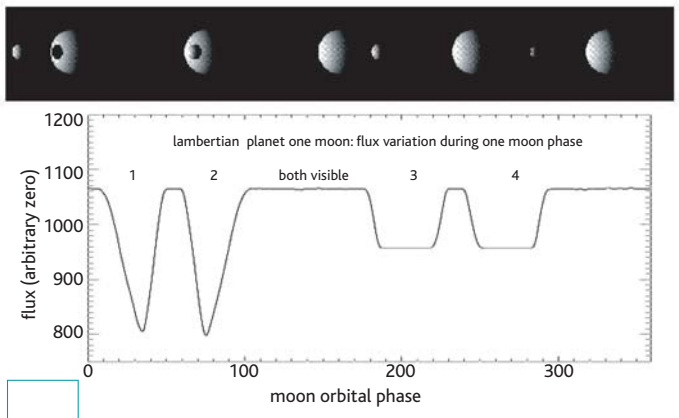

fig.3.6

Lightcurve of a Jupiter-like planet + terrestrial moon system in the case where the planet, moon and star are closely aligned. See also Schneider et al. (2003).

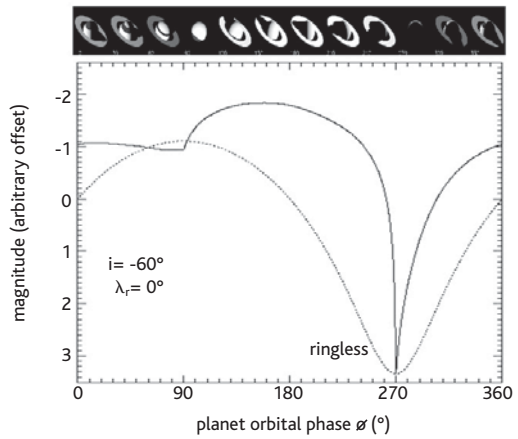

fig.3.7

Lightcurve of a ringed planet as a function of orbital phase (solid line) compared to that of a ringless planet (dotted line). The appearance of the ringed planet at the corresponding phases is shown in the series of simulated images above the graph. (Source: J. Schneider).

3.1.6 Rings around Extrasolar Planets

Most of the gas giants in our own Solar Sytem have accompanying rings of varying extent and density, with Saturn's being the most obvious prototype. Thus, it is entirely plausible that extrasolar gas giants will also sport rings. Such rings are expected to be readily detectable as they are larger than the planet: while the radius of a giant planet is roughly independent of mass at ~ 1 Jupiter radius, the radius of the rings is expected to scale approximately as the one third power of the planet mass. Thus, the rings around a 10 M_J planet would have a radius on the order of three times larger than those of Saturn and be ten times brighter (Arnold & Schneider 2004; Dyudina et al. 2005. See also JPL publication 01-008 "Biosignatures and planetary properties to be investigated by the TPF mission"). Indeed, the very existence of rings around a planet is an indirect proof of the presence of satellites in the same system, as rings are expected to have a short lifetime and to survive they must be replenished by dust or ice generated by the collision of small bodies.

The light curve of a ringed planet as it orbits its parent star is complex, depending on the relative size and albedo of the planet and rings, the 3D orientations of the ring plane and orbit, and the optical depth of the ring (Figure 3.7). The light curve can be analysed to yield the size of the rings, the optical depth, the albedo, and colour, while the spectrum of the ring system can be extracted from the planet+ring spectrum by using spectral features specific to the planet, planetary models, and the different orbital phase behaviour. The size and optical thickness constrain the density of the ring material, while the orientation gives a direct determination of the orientation of the planet, since from dynamical considerations, the rings necessarily lie in the equatorial plane of the planet (or, equivalently, perpendicular to its rotation axis).

Ring spectra would provide constraints on their composition and physical characteristics. The shape of water ice bands will, for instance, indicate the typical size of ring particles. Silicates and CH_4 will be revealed by their typical spectral features around 1 and 2μm, and 3.4μm respectively. An obvious expectation is that ice particles will be present only for rings around planets further away than a few AU from the star. The form of the scattering function will constrain the surface roughness of particles. Saturn's rings are essentially made of water ice, with no detected silicates, and it would be very illuminating to see if this is a universal character or if such rings can contain material other that water ice, including silicates and methane.

The combination of the shape of the light-curve and the spectrum should give a fair model of rings. Finally, if rings are present in a system, they can lead to an incorrect determination of the planet radius inferred from its thermal emission, as envisaged by future space missions such as Darwin. As described here, the ring and planet contributions can be separated in the reflected light regime at optical and near-infrared wavelengths.

Notes on Design Requirements

Observation Type: Repeated imaging and spectroscopy

Field of View: Single sources

Spatial Resolution: 10 milli-arcsec

Spectral Resolution: 100–1000

Wavelength Range: 0.5–4μm

Dynamic Range Constraint: The observations must achieve a contrast between the parent star and the planet of between 10^7–10^9, in order to characterise rings using 1% photometry.

Telescope Size: From 30m (for simple detection of rings) to 100m (for accurate characterisation)

3.1.7 Planets around young stars in the Solar neighbourhood

As discussed in Section 3.1.3, gas giant planets are substantially more luminous when they are young, radiating away their excess energy as they cool after formation. The same is also true for young terrestrial-mass planets. Thus, the existence of populations of young stars with ages in the range 10-600 Myr in the Solar neighbourhood, at distances of less than 50 parsecs from the Sun (see, e.g. Zuckerman et al. 2004), offers a unique opportunity to detect exo-earths and other planets at early stages of evolution. The contrast between the planet and its parent star is significantly more favourable for detection when young than later in life, when the star has reached its roughly constant main sequence luminosity but the planet has cooled down and is visible in reflected light only. An example of this is seen in Figure 3.8, a near-infrared image of a young (~10 Myr) brown dwarf in the nearby (~70 pc) TW Hydrae association, which shows a faint companion at roughly 55 AU separation which may have a mass of only a few M_J. An E-ELT will make it possible to image planets of this mass and lower around Solar-type stars in these associations, its spatial resolution being crucial to identify planets at much smaller separations, potentially in the habitable zone.

Characterisation of exo-earths around stars in this age range will allow us to explore the critical time domain associated with the beginning of life on our planet. It is very likely, as a consequence of the emergence of life, that major changes took place in the chemical composition of the Earth atmosphere during the first Gyr. An E-ELT will offer the possibility to track these dramatic changes in chemical composition from the pre-biotic to the biotic-dominated world by observing samples of exo-earths at different times of their early evolution.

Notes on Design Requirements

Observation Type: Imaging and spectroscopy
Field of View: Few arcsec
Spatial Resolution: 2 milli-arcsec
Spectral Resolution: 10–100
Wavelength Range: 0.6–10μm
Target Density: Few hundreds
Dynamic Range constraint: 10^8
Telescope Size: >50 m

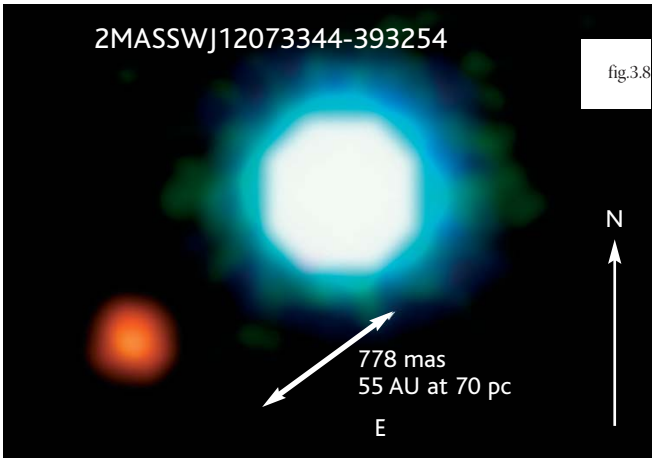

The young (~10 Myr) brown dwarf 2M1207 (centre) in the nearby TW Hydrae association. The fainter object seen near it at an angular distance of 778 milli-arcsec may represent the first direct image of an exoplanet. Further observations, in particular of its motion in the sky relative to 2M1207, are needed to ascertain its true nature. The image is based on H, K and L' images with the NACO AO facility on the VLT. The available infrared colours and the spectral data suggest that the companion may be a 5 MJ planet at ~55 AU from 2M1207. The surface temperature appears to be about 10 times hotter than Jupiter at about 1300K: the source is very young and still liberating considerable energy as it contracts and cools. It remains unclear how such an object can have formed so far from the parent star: it may be more appropriate to think of this as a binary brown dwarf system. (From Chauvin et al. 2004).

3.1.8 Free-floating planets in star clusters and in the field

Not all planetary-sized objects are in orbit around other stars: there is evidence for free-floating objects with masses in the range 3–10M_J in the ~1 Myr Orion Nebula Cluster and the 3–5 Myr old σ Orionis cluster (Lucas & Roche 2000; Zapatero-Osorio et al. 2000; McCaughrean et al. 2002; see Figure 3.9). These objects were probably not formed in circumstellar disks like true planets, but were much more likely born as very low-mass brown dwarfs via fragmentation near the tail of the stellar initial mass function. Their study is very interesting in its own right, since predictions of standard star formation theory are that opacity-limited fragmentation should not produce sources below a few Jupiter masses, and thus tracing the mass function at these limits will yield insight into the process by which very low-mass sources actually form. A 100m E-ELT would enable studies of the frequency and characteristics of young isolated sub-stellar objects with masses as low as Saturn in star forming regions out to several kiloparsecs, while young objects at the hydrogen-burning mass limit should be observable even out to Andromeda.

Studies of such objects will define the lower end of the initial mass function (IMF) for cloud fragmentation in a wide range of star forming complexes with different environments, including, for example, metallicity and will allow comparison with the evolution of similar-sized objects (i.e. young Jovian planets) which formed in orbits around stars. Because these objects can be studied out to considerable distances, a number of different star forming regions will be examined and relationships between the properties of the specific region and the sub-stellar (and stellar) initial mass function explored, for both captive and free-floating Jovian objects.

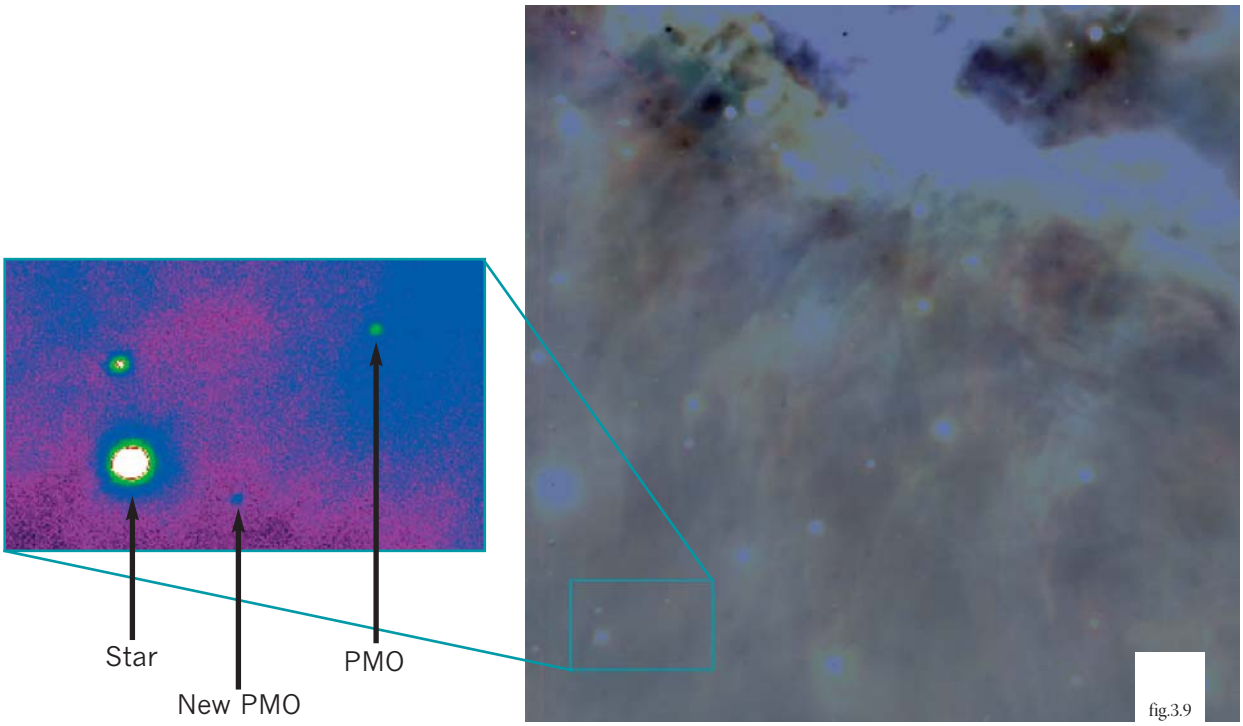

Right: A near-infrared image of the Orion nebula near θ^1Ori taken with the FLAMINGOS instrument on the 8m Gemini-South telescope. Left: A section of the image (corresponding to the green box in the right hand image) in which candidate planetary-mass objects (PMOs) have been identified (Lucas, Roche, & Riddick 2003).

Importantly, these free-floating sources can also be used as excellent proxies for "true" planets at the very earliest stages of their evolution, because their relative isolation makes them much easier to study than planets close to stars. Furthermore, older counterparts are likely to be present in the general field, populating the Solar neighbourhood. Such objects would have cooled down to very low temperatures and future mid-infrared surveys may detect significant numbers of these isolated planetary-mass objects down to a few times the mass of Uranus. An E-ELT will allow detailed photometric and spectroscopic characterisation, enabling us to study the whole domain of gaseous planets over a wide range of ages and circumstances, including the evolution of their physical properties (effective temperature, gravity, and chemical composition) from birth until ages older than the Solar System.

Notes on Design Requirements

Observation Type: imaging and spectroscopy
Field of View: few arcsec-1 arcsec
Spatial Resolution: 0.01arcsec
Spectral Resolution: 10–100
Wavelength Range: 1–10μm
Target Density: hundreds to thousands around the sky
Dynamic Range constraint: no
Telescope Size: >50m

3.2 Our Solar System

All bodies more distant from the Sun than Venus will be accessible to an E-ELT. For most Solar System work, the great potential of an E-ELT to lead a revolution in planetology lies in its extraordinary angular resolution, which will represent a quantum leap in our ability to examine the distant components of the Solar System in a regular, systematic and efficient manner. To illustrate this, Table 3.1 summarises the surface resolutions it will achieve:

Object	Surface Resolution (km)	Pixels across typical disc	Notes
Moon	0.003	~10^6	Illustrative
Mars	~2	3400	
Asteroids	3–7	~200	Ceres, Vesta
Jupiter	8	~500	Galilean moons
Saturn	15	~300	Titan
Uranus	30	~25	Ariel
Neptune	45	~90	Triton
Pluto	60	~90	
(20,000) Varuna	63	~15	Large Trans-Neptunian Object
(90377) Sedna	130	13	Most distant TNO

Table 3.1

Surface resolution at various Solar System bodies corresponding to the diffraction limit of a 100m E-ELT at a wavelength of 1μm.

These resolutions offer a dramatic leap forward for Solar System astronomy. An E-ELT will fill the huge gaps in our spacecraft-based knowledge of the surfaces of Solar System objects, doing the work of a flotilla of fly-by planetary probes. In particular, the telescope will throw open the barely-explored field of long-duration monitoring of objects where interesting changes with time are expected, at surface resolutions comparable to those offered by weather satellites in orbit around the Earth.

An E-ELT has immense potential for observational planetology: the great and dramatic archive of data, which has been returned by the probes and orbiters of space programmes of the world, could readily be multiplied several times in size and scientific utility after a decade of work by an E-ELT. The following sections illustrate just some of the particularly dramatic new results which are very likely to be obtained.

3.2.1 Mapping planets, moons and asteroids

Space probes have mapped at least one face of a fair fraction of the larger component bodies of the Solar System. However, how much can be missed in a simple flyby is well illustrated by Mariner IV's failure to detect the great valleys of Mars, arguably more important features than its impact craters for understanding its evolution and the dramatic significance of its ancient topography. Until now, only expensive and complex orbiters have stood a chance of producing a complete map of any object, but an E-ELT would be well-placed to make important inroads into this work.

The closest planet outside the Earth, Mars, has been well served with orbiters with linear resolving capabilities comparable to (and in one case superior to) those likely to be offered by an E-ELT. However, beyond Mars is the asteroid belt, containing a few hundred objects large enough for an E-ELT to yield important surface detail. Spatially-resolved spectroscopy with a linear resolution of 2–8 km and almost arbitrarily high spectral resolution would also be readily possible. An E-ELT will provide a database which will be an indispensable precursor to possible future exploitation of the raw materials offered by the asteroids.

3.2.1.1 Large and nearby asteroids

For the few hundred largest asteroids, complete surface maps, showing topography and geological indicators at surface resolutions of a few km, will be obtainable in a few minutes of observation of each, spread over a few days or weeks, depending on the asteroid rotation properties and axis orientations. The same will be true of the important near-Earth and Earth-crossing objects, which, being often much closer, will be observable at much higher surface resolution than main-belt asteroids.

A direct determination of shapes without the shape/albedo degeneracy which comes from unresolved lightcurve observations can be used to constrain thermal models which can then be used to probe the bulk properties of the object via their sub-surface thermal conductivity. Non-spherical shapes provide limits on the density and strengths of materials required to resist self-gravitational collapse into a sphere. Images will reveal large scale surface inhomogeneities, to constrain impact histories.

An E-ELT would also be able to detect companion objects down to a few metres in diameter in the Main Belt and orbital parameters will provide masses and the resolved images will determine diameters; from this information, densities can be derived, which are critical to understanding the structure, composition and evolution of the small bodies.

3.2.1.2 Small asteroids

Main-belt objects down to ~10 km across will be sufficiently resolved to determine details of rotational period, sizes, shapes, axis orientations and approximate surface distribution of geological components.

3.2.1.3 Major and minor moons

Many of the Solar System's planetary satellites are unstudied, while the many of the others have only a few images taken at a distance by a probe in an orbit not optimised for that body. These data sets will be completed, or in most cases superseded, by an E-ELT, with image sets offering near-complete multi-wavelength surface coverage and, in most cases, superior resolution.

3.2.2 Transneptunian objects (TNOs)

The larger TNOs will be resolved by an E-ELT with several pixels across their disk, with up to ~15 in the J band in the case of (20,000) Varuna, one of the largest currently known. E-ELT studies of TNOs will determine whether cometary activity occurs at these very large heliocentric distances, and if so, in what type of surface terrain. In the case of the larger TNOs for which good quality mapping is possible, synoptic studies over decade-long periods will allow the long-term evolution of the surfaces to be followed. Spectroscopy of TNOs down to a few tens of km in diameter will be possible at spectral resolutions comparable to or higher than the best spectra currently available for Pluto. This will identify surface ices and their physical states (mixture ratios and so on) and even accurate temperatures via the narrow 2.16μm feature of N_2. Such spectra will also allow geological mapping of the planetesimal surfaces and correlation of albedo features with specific materials.

One application for which an E-ELT is unlikely to have serious competition is spectroscopy of larger TNOs at resolutions around 10^5, which will permit the determination of the D/H ratios of the surface ices in these bodies. This ratio is known for the comets originating in the Oort cloud and it is of great interest to know whether the ratio is the same in the Kuiper Belt, which would imply similar thermal histories. The Oort cloud objects have higher D/H than the deep oceans on Earth: the question of whether the terrestrial hydrosphere was seeded from Oort or Kuiper belt is obviously of great interest.

3.2.3 Comets and the Oort cloud

The size distribution of objects in the outer Solar System constrains models of planetesimal accretion in the early Solar nebula and the subsequent collisional erosion of the surviving planetesimals once the giant planets had formed. This distribution is not well known, even for the larger objects, but ground-based searches with 8m class telescopes and possible future dedicated facilities will resolve this issue for objects larger than about 50–100km. An E-ELT will then make crucial "pencil-beam" surveys to detect objects orders of magnitude fainter, probing the trans-Neptunian size distribution down to objects less than 1km in size (V~35 at 40 AU), thereby linking objects in the present Kuiper belt with the nuclei of observable short period comets.

Long period comets are believed to have formed at 10–20 AU from the Sun before being ejected into the Oort Cloud. By following their evolution as they retreat from the Sun and de-activate, an E-ELT will be able to determine the size distribution of long-period comet nuclei without the uncertainties brought on by unresolved low-level activity at the 10–12 AU heliocentric distances to which they can be followed at present. Observing the fragments of cometary break-up such as occurred with Comet LINEAR in summer 2000 (Figure 3.10) is at the limit of present telescopes, but after such an event, an E-ELT will be able to probe the sub-nuclear structure of the parent: are comet nuclei composed of discrete and heterogeneous sub-nuclei?

Ideally, it would be desirable to begin watching "new" long-period comets while their surfaces are still pristine, but this may be difficult since it is the start of sublimation which generates a coma and makes them discoverable. However, dedicated searches could provide an E-ELT with early discoveries from which the volatile content of the nuclei can be determined via spectroscopy and from the sublimation temperatures of various ices. During perihelion passage, an E-ELT will be able to follow the detailed morphology of gas-dust jets on a kilometre scale, right down to the nuclear surface, revealing if the dust is released directly from the nucleus or from the gradual destruction of larger grains some distance from the surface.

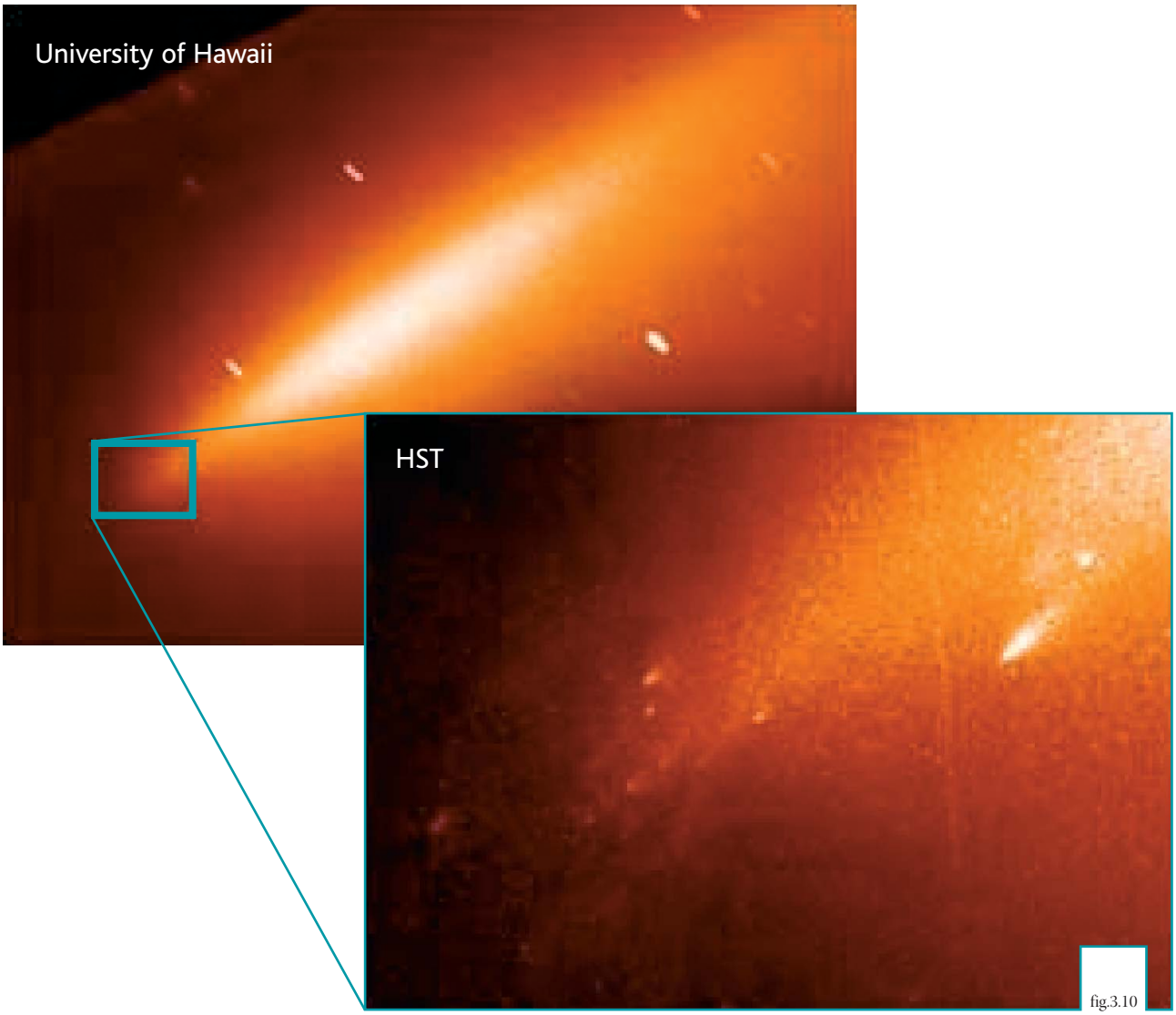

fig.3.10

The nucleus of Comet LINEAR disintegrated in July 2000. The Hubble Space Telescope and the 8m VLT were able to follow the fragments for a few days before they faded into invisibility. A 100m class E-ELT would be able to observe much smaller fragments in similar disintegrating comets, providing spectra to probe the internal physical and chemical structure of their nuclei. Figure credit: NASA, Harold Weaver (the Johns Hopkins University), HST Comet LINEAR Investigation Team, and the University of Hawaii.

3.2.4 Surface and atmospheric changes

Several Solar System bodies exhibit surface changes on timescales of days to years. Furthermore, all the Solar System bodies with true atmospheres show, or will show when examined in the sort of detail an E-ELT will offer, meteorological phenomena. These range from the rapid circulation in the great spot of Neptune, which frustrated interpretation on Voyager images, to the leisurely evolution of the Martian dust-storm season. All such studies will benefit immensely from the capability of an E-ELT to monitor changes on timescales from minutes to years, making it possible to study phenomena associated with the local equivalents of tropical storms or changes reflecting the impact of the Solar cycle.

At the resolution of a 100m E-ELT, the motions of cloud top features in the atmospheres of Jupiter, Saturn, Uranus and Neptune could be followed to an accuracy on the order of 1 m/s and less. A long-term study will allow the characterisation of the variability in the zonal circulation of these planets, and establish the range of motions in the meridional direction. Both are important to understand the origin of these circulations. The meteorology on these planets could be followed at the mesoscale range, allowing regional studies of vortices, convective storms, and waves. A long-term study of these phenomena could allow a better understanding of the atmospheric structure beneath the upper clouds. Also, high-resolution spectroscopy could be performed at regional scale in these planets which, in combination with imaging at selected wavelengths (e.g. the methane band filters in the red region), will make it possible to characterise the structure of hazes and clouds and their spatial and temporal variability.

For this atmospheric monitoring work, an E-ELT would be extremely powerful, particularly when realising that NASA and ESA have no space missions presently planned for Uranus and Neptune, at least.

Further Solar System surface and atmospheric studies of particular importance for planetology include:

1. Evolution of vulcanism on Io. The images secured by a 100m E-ELT will offer between ~900 (at visible wavelengths) and ~100 (thermal infrared) resolution elements across the surface of Io. In the visible and near-infrared, these images will be surpassed only by those secured on the nearer fly-bys of Galileo (Figure 3.11). Thermal-infrared images at these resolutions have never been secured. An E-ELT will open a new era of vulcanism studies on this moon, greatly enhanced by the powerful spectroscopic possibilities of the telescope.

2. Activation of the Centaurs. The Centaurs are objects orbiting between Saturn and Neptune. They are similar in size to large asteriods, but have icy compositions more akin to comets and, indeed, are probably giant comet nuclei in orbits which are evolving inwards from the Kuiper belt. Most appear to be currently inactive, but the prototype, Chiron, is known to have periods of comet-like activity, developing a faint coma. At their distances of > 10 AU, they are far too cold for water to sublimate, so the cause of the activity of Chiron is a puzzle, while the lack of activity on any object but Chiron is equally puzzling. An E-ELT will permit the determination of detailed surface compositions for all the Centaurs and will allow them to be monitored in detail as they orbit the Sun.

3. Development of surface activity on Triton. The structures generated by the gas geysers on Triton will be readily discerned in the ~100 pixel-wide optical/near-infrared images delivered by a 100m E-ELT and, along with thermal-infrared imaging and spectroscopy, should yield clues as to their influence on the evolution of the surface of that planetary-sized moon.

4. Synoptic studies of Pluto and Large Trans-Neptunian Objects. It is expected that Pluto's current tenuous atmosphere will freeze in the 2000–2020 period, although the timescales for this collapse are uncertain. If an E-ELT is available on that timescale, it will be possible to follow that process in detail on images and spectroscopy with ~100 resolution elements across the planet. Whatever the precise timescale for atmospheric collapse, an E-ELT offers the opportunity for synoptic monitoring

of the evolution of Pluto's surface over many years. No conceivable space mission can provide such an opportunity for many decades. A comparison with the NASA 'New Horizons' spacecraft is instructive, as it is the only planned mission to Pluto in the foreseeable future (Stern & Spencer 2003). Due for launch in January 2006, this small spacecraft will execute a high-speed (12 km/s) flypast of the Pluto-Charon system in 2015 or later. The mission will obtain ~1 km resolution images in the visible and ~7 km images in the near-infrared for a short time during closest approach, but Pluto's slow (6.4 day) rotation means that only part of the planet can be imaged at such high resolution. Complete mapping will be provided by a long focal length camera at a resolution of ~40 km for a few days prior to and after closest approach, allowing a single mapping of the entire surface at this resolution. However, should Pluto be in a dynamic state of atmospheric collapse during the flyby, no temporal studies will be possible and the final state of the surface will remain an enigma. An E-ELT could make such maps at will at almost any time, probing the temporal evolution of any large scale features seen by the New Horizons spacecraft during its flypast.

5. Atmospheric changes in Titan. Following the very successful Cassini-Huygens exploration, Titan should be one of the prime targets for an E-ELT. Observations at visible wavelengths will allow us to follow the seasonal and long-term variability of its dense haze layers, while observations at close to 1μm will reach the surface and lower clouds of methane. Combined with spectroscopy, these studies will bring a new perspective on the influence of the seasonal insolation cycle on Titan's "methanological" cycle.

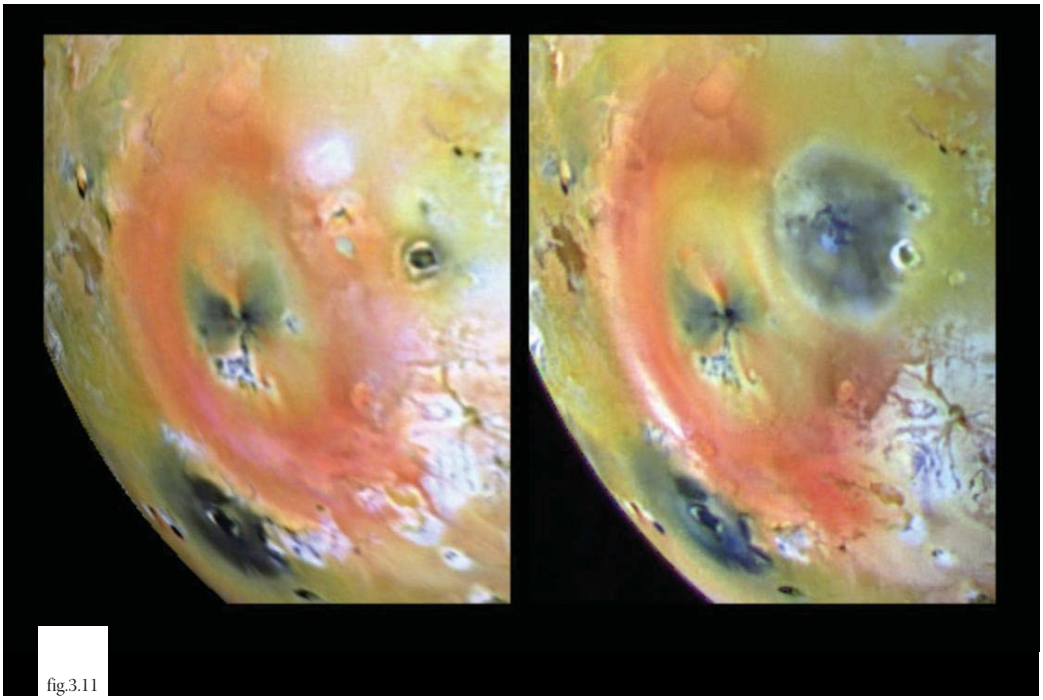

fig.3.11

Changes in the surface of Io observed by the Galileo spacecraft. The images were taken on April 4th and September 17th 1997. (Credit NASA/JPL).

Notes on Design Requirements

Observation Type: imaging and integral-field spectroscopy
Field of View: ~ 1 arcmin x 1 arcmin for larger planets. Smaller objects require only a few square arcsec
Spatial Resolution: As high as possible, with diffraction limited performance at 1μm desirable
Spectral Resolution: TBD
Wavelength Range: Visible to thermal-infrared
Date constraint: To observe the freezing of Pluto's atmosphere requires an E-ELT in operation before 2020

3.3 Stars and circumstellar disks

3.3.1 Formation of stars and protoplanetary disks

The so-called "nebular hypothesis" for the formation of the Solar System from a rotating, disk of gas and dust was proposed and elaborated upon by natural philosophers including Descartes, Kant, and Laplace, based on observations of the planetary motions in a Copernican context. The modern-day version of the nebular hypothesis for the formation of a single, low-mass star was outlined by Shu et al. (1987) and has since been substantially fleshed out by a wide range of observations. In brief, the scenario includes the following stages:

1. Condensations grow in molecular clouds.

2. An "inside-out" collapse commences when the density of a condensation reaches some critical value. This process proceeds on a timescale governed by the local sound speed.

3. A protostar forms, surrounded by an accretion disk, while both are deeply embedded within an envelope of infalling dust and gas.

4. Bipolar outflows form and are amongst the dramatic phenomena occurring during this phase. These have a separate and important impact on the surrounding cloud material on scales of several parsecs.

5. With the passage of time, the inflowing material falls preferentially onto the disk rather than the star and migrates inward to accrete on to the star.

6. In the late stages of formation, the disk may be fully dispersed by an energetic outflow and/or may agglomerate into planets.

However, the real story of star and planet formation is likely much more complex than this. It has been known for many years that most stars are actually in binary systems and more recent observations and large-scale numerical modelling suggest that the majority of young stars in the Galaxy today are being formed in dense clusters of tens to thousands of stars. A new, larger-scale, more holistic paradigm is now under development (see, e.g. MacLow & Klessen 2004), which begins with the formation of a giant molecular cloud as compressed shell of a large-scale turbulent flow, initiated by supernova explosions. The giant molecular cloud contains enough turbulent motion and energy to initially stabilise it against gravity, but the turbulence decays on a dynamical time scale to form smaller eddies, which also collide and trigger further compression forming clumps in which star clusters may form.

Eventually, the turbulent hierarchy forms dense protostellar cores which collapse to generate single or multiple protostars, most surrounded by circumstellar disks or circumbinary disks. The collapse commences either by turbulent dissipation or ambipolar diffusion of magnetic flux from the core, allowing gravitational energy to dominate. Observations of density profiles across several pre-stellar cores indicate that the collapse is probably not occurring in an inside-out fashion as in the Shu et al. scenario, but rather in an outside-in collapse mediated by turbulent dissipation.

At the same time, collimated jets and bipolar outflows may help remove some of the excess angular momentum to enable further accretion. The flows may also stir up the parent clouds and help to unbind them, thus limiting the star formation efficiency. Magnetic fields are important in generating these jets and outflows, and Alfven waves are likely to enable magnetic braking of the clumps and cores, further mitigating the angular momentum problem. The fields may also play a vital role in generating an effective viscosity in circumstellar disks, via the Balbus-Hawley instability.

In this new picture, many of the key "products" of star formation, such as the distribution of stellar masses and the fraction of stars with planetary systems, may arise through strong dynamical, radiative, and mechanical interactions between the cloud cores, protostars, and protoplanetary systems. However, a vast number of key questions remain unanswered and an E-ELT will make vital and unique contributions to solving many of them, allowing physical models of the star and planet formation processes to be tested and constrained in detail. In particular, the

ability of an E-ELT to deliver direct imaging and 3D imaging spectroscopy of complex and confused regions at extraordinarily high spatial resolution will make it possible to establish the density, temperature, and dynamical structures in the core inflow and accretion disk regions, to examine the structure and kinematics of the jet launching zone, and to investigate the stability of the launching mechanism. It will be equally important to observe the ongoing process of planet formation, to determine the fraction of disks that are forming planets, at which stage in the accretion process they form and how long it takes, how their masses are set, and to understand how typical our own Solar System is.

A fundamental limit on our ability to study the very youngest stars in detail is set by the distance to the nearest star forming regions. The closest molecular complexes where low-mass star formation is currently occurring, with source ages of 1 Myr or younger, are the ρ Ophiuchus, Taurus, and Chamaeleon complexes, all ~150 pc away, while the nearest centre of high-mass star formation is in Orion, at roughly 500 pc. On the other hand, at slightly later stages, on the order of 10 Myr, we are fortunate to have the TW Hydrae association of objects at roughly 50 pc, which offers a sample of pre-main-sequence T Tauri stars, in the late, possibly planet-forming, stages of their initial disk evolution. Table 3.2 shows how the diffraction-limited angular resolution of a 100m E-ELT maps onto linear resolution at various key distances for local star formation studies.

Table 3.2 Resolution of a 100m telescope at nearby targets.

Distance	**Target**	**Resolution** (res.el. per AU/*AU per res. el*).					
Pc		1μm	2μm	5μm	10μm	17μm	350μm
10		50	25	10	5	3	*7*
50	TW Hya assn	10	5	2	1	*2*	*35*
150	ρOph, Tau, Cham	3.3	1.7	*1.5*	*3*	*6*	*100*
500	Orion	1	*2*	*5*	*10*	*17*	*350*

At near-infrared wavelengths of 1–5μm, a diffraction-limited 100m E-ELT will offer spatial resolutions of 2–10 milli-arcsec. The shorter wavelengths in this range will include emission from the hottest dust and gas, i.e. from stellar photospheres, shocked and otherwise heated material, as well as scattered light from protostars themselves. Also visible will be hot gas in face-on or low-extinction circumstellar discs. At 2–2.5μm, molecular hydrogen and first overtone CO lines are available as diagnostics, while in the 3–4μm windows, polycyclic aromatic hydrocarbon (PAH) and other organic emission and absorption features, as well as the Brackett α line of ionised hydrogen are available. The 5μm window offers powerful diagnostics via the CO fundamental lines, coupled with extremely low dust extinction.

At mid-infrared wavelengths, a 100m E-ELT offers spatial resolution of ~20 milli-arcsec at 10μm, declining to ~40 milli-arcsec at 20μm, making it possible to study the warm, inner regions of circumstellar disks at temperatures around ~100–500 K generated by radiative heating of dust within few AU of the central star. A large number of emission and absorption features are also available in this wavelength range, in particular the silicate features at 9.7μm, and several potentially valuable diagnostic features in the pure-rotation lines of molecular hydrogen. While the 28μm 0–0 S(0) line is not accessible from the ground, the 17μm 0-0 S(1) line is and has already been detected in the circumstellar disk of the YSO binary GG Tau (Thi et al. 1999). This line arises in material at a few hundred Kelvin and is a particularly useful potential tracer of features in young, H_2-rich circumstellar disks.

3.3.1.1 Probing birthplaces

Stars and planets form within dark molecular clouds. Despite 30 years of study, however, relatively little is understood about the internal structure of these clouds and consequently the initial conditions that give rise to star and planet formation. This is largely due to the fact that molecular clouds are primarily composed of molecular hydrogen, which is virtually inaccessible to direct observation in its cold, quiescent state. Most of what has been learned to date has been derived from observations of trace H_2 surrogates, namely relatively rare molecules such as CO, CS, and NH_3 with sufficient dipole moment to be detected by radio spectroscopic techniques, and interstellar dust intermingled with the gas at a level of roughly 1% by mass, whose thermal emission can be detected by radio continuum techniques. Nevertheless, the uncertainties inherent in these techniques make it very difficult to construct an unambiguous picture of the physical structure of these objects and thus, in turn, yield only a sketchy picture of the way stars form.

An E-ELT operating at near- and mid-infrared wavelengths will bring the end of the "dark cloud era". Given the extraordinary sensitivity of an E-ELT at those wavelengths, where dust absorption is strongly reduced to begin with, virtually all but the very densest molecular clouds will become transparent. A careful analysis of the near-infrared light from background stars and/or galaxies seen through a molecular cloud will provide direct measurements of the dust column density in the cloud. Such measurements are free from the complications that plague molecular line or dust-emission data and will enable the construction of exquisitely detailed maps of cloud structure. More quantitatively, there are roughly 10^5 stars per square arcmin seen towards the plane of the Milky Way to a limiting K-band magnitude of 28, or about 300 stars per square arcsec. By measuring the extinction seen towards this background population via near-infrared colour excess, it will be possible to derive maps of the projected cloud structure with resolutions on the order of 0.1 arcsec, corresponding to a linear resolution of about 10 AU in the nearest star forming regions, over a dynamical range of $1 \leq A_v \leq 150$ mag or a factor of roughly 150 in column density.

The resolution of an E-ELT dust column density map of a molecular cloud derived in this way will be comparable to the resolution achievable by the ALMA millimetre interferometer measuring the dust and gas emission, although the E-ELT should have a substantially larger field-of-view. A more detailed analysis shows that the two facilities are highly complementary, as is the proposed E-ELT submillimetre camera SCOWL (see Annex B) to the ALMA continuum imaging. A comparison of ALMA molecular-line maps and dust emission maps with an E-ELT near-infrared column density map will allow the study of the chemistry of the star formation process and interstellar grain properties (e.g. grain emissivity properties, grain growth) on sub-Solar System size scales. The expected dynamic range and resolution will allow this type of study from the quiescent molecular material phase, through the pre-stellar and protostellar phase, ending with the dispersion of the parental molecular material by the newly-formed star. Such data will be very complementary to that obtained at mid-infrared and millimetre wavelengths in the very densest pre-stellar cores, with A_v of up to 500 mag, by the NASA/ESA/CSA JWST and ALMA, respectively.

Beyond this imaging work, the immense sensitivity of an E-ELT for spectroscopy in the near-infrared and especially in the mid-infrared will allow detailed studies of the chemical and dynamic properties of the quiescent cloud by absorption line spectroscopy in the spectra of background sources at high resolutions ($R \sim 100{,}000$). With current facilities, such experiments are limited to relatively rare but bright embedded objects as probes. But these embedded objects usually exert a strong influence on the surrounding cloud themselves, making it almost impossible to measure quiescent cloud properties away from such centres of activity. An E-ELT, on the other hand, will provide numerous sightlines through undisturbed, pristine molecular material, using much fainter but much more common normal background stars.

Notes on Design Requirements

Observation Type: Near- and mid-infrared imaging and spectroscopy

Field of View: Up to 1 arcmin x 1 arcmin; multiple sightlines for spectroscopy

Spatial Resolution: 2–10 milli-arcsec (near-infrared), 20–40 milli-arcsec (mid-infrared)

Spectral Resolution: Up to 100,000

Wavelength Range: 1–5μm and 10–20μm

Target Density: Up to ~300 per sq arcsec

Other comments: ALMA (resolution also reaching ~25 milli-arcsec at 1 mm over a 10 km baseline) will play a highly complementary role, being well suited to observing relatively high column densities of much cooler 20–100 K gas and dust.

3.3.1.2 Structure in inner disks

Current models of the evolution of young circumstellar disks within the central 30 AU, i.e. the radius of our own Solar System to Neptune, are almost completely based on theory and educated guesswork: observations are urgently needed in order to constrain and inform these physical models.

An E-ELT will be well able to resolve structures in this inner disk region at infrared wavelengths, offering sub-AU imaging out to 10μm in the TW Hya association and at wavelengths as long as 3-4μm out to the ρ Oph complex. Simple imaging of disks at high resolution offers an important start on these investigations. Especially in edge-on systems, detailed modelling and matches to the observed isophotes are expected to yield strong indications of the presence and nature of any embedded planetary bodies.

Gaps in disks are expected to be associated with planet formation, representing ranges of radii within which the accreting planet has swept up most of the disk material. Such gaps have been inferred in a number of systems from observations of deficient wavelengths in spectral energy distributions, but these

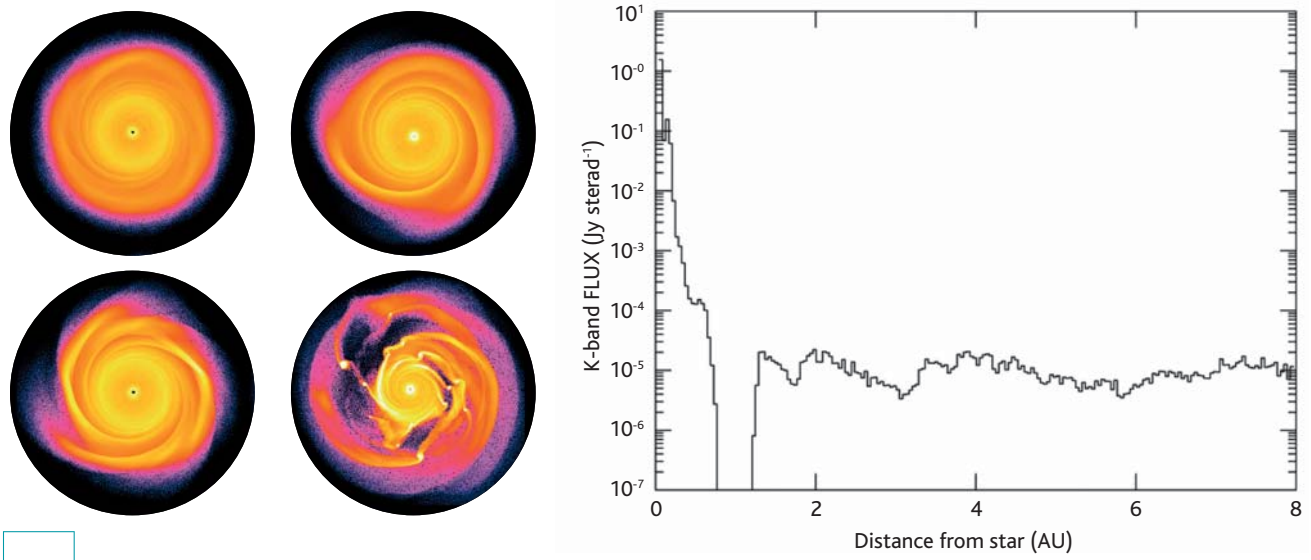

Fig.3.12

Left: Simulations from Mayer et al. (2004) showing the formation of gas giant planets via fragmentation of protoplanetary disks. Right: Simulated signal generated by an Earth-analogue orbiting a small star as it forms in a disk of material illuminated by the parent star. The disk brightness is shown on a logarithmic scale versus distance from the star; at the position of the terrestrial planet (1 AU), a dark lane is present (Kurosawa & Harries, University of Exeter).

inferences are notoriously model dependent: the successful observational demonstration of the existence of an annular gap in a young disk is a particularly desirable outcome. Such a feature is a near-certain indicator of the presence of a protoplanet and the width of the gap, if it can be measured or inferred, is a direct measure of the mass of the planet.

Such measurements may be possible by searching for signs of shocked emission where a supersonic flow is engendered by the planet's gravitational perturbation of the disk gas at the edges of the gap. Emission from the shocked locations, on either side of the gap, should be detectable in the 17μm line of H_2 and even if the gap is unresolved, the velocity shear across it will impose a clear signature on the observed emission line profile. An especially interesting possibility is open only to an E-ELT, namely following the emission locus as it orbits around the star: a 5 AU orbital radius is about 2.5 resolution elements at 17μm in the TW Hya association and about 1 element at ρOph, assuming a 100m E-ELT. There is also the prospect of resolving the emission locations in the intermediate lines of the pure-rotational series: the 0–0 S(3) line at 9.7μm, in particular, should be adequately strong and should be resolvable in TW Hya stars.

Beyond this, there is some prospect for an E-ELT to directly spatially resolve the emission loci on either side of the gap, if the gas is excited to high enough temperatures to lead to emission in the 1–0 S(1) line of H_2 at 2.12μm: a Jupiter-mass planet is expected to produce a ~ 1 AU gap at 5 AU radius; for a 100m telescope this is ~2 resolution elements wide at 2μm at the distance of the ρOph, Taurus and Chamaeleon complexes. Direct detection, and possibly, resolution, of planetary gaps should also be possible using ionised hydrogen Brackett α line emission from the diluted gas in the gap itself, which will be well resolved (~3 resolution elements) for Jovian planets in circumstellar disks in the TW Hya association. A face-on multi-planet system might, for example, resemble a bulls-eye in the light of this emission line.

Aside from planet formation, other important phenomena are concentrated in the previously-inaccessible inner parts of the disk. The region within 10 AU of a young star is likely to be the source of bipolar outflows, and is also the region where accretion may generate significant luminosity through shocks, at least in the younger disks. The dynamics in this region are dominated by rotation, accretion and outflow. However, the motions are likely to be complicated by convection (above the disk plane), non-axisymmetric features such as spiral density waves, and time-dependent highly-clumpy accretion. This region is also around the so-called "snow line", where water-ice will rapidly sublime, significantly affecting the chemical abundances and dust composition. Photoionisation is also likely to be important for molecular gas depletion in the faces of the disk exposed to the star. Dust agglomeration, preferentially in the densest parts of the disk plane, may substantially alter the visual extinction and hence the temperature. Finally, variations in molecular abundances with radial position in circumstellar disks will be compared with those seen in comets in our Solar System, offering some insight into the question of how typical the Solar System is.

Notes on Design Requirements

Observation Type: High spatial resolution imaging & spectroscopy

Field of View: Few arcsec

Spatial Resolution: Diffraction-limited at 2μm and beyond

Wavelength Range: Near- (2μm) and mid-infrared (10μm, 17μm) +Brackett α

Dynamic Range constraint: ~10^5 at a distance of ~0.1 arcsec (to be confirmed)

Telescope Size: 100m assumed (need best spatial resolution possible)

3.3.1.3 Embedded young stellar objects

The very earliest phase of protostellar formation is generally referred to as the Class 0 stage, where the newly-formed, cool object is so deeply embedded in the natal gas and dust that it is not detectable shortward of far-infrared and millimetre wavelengths. However, after ~10^5 yrs, the sources become visible at near- and mid-infrared wavelengths at the so-called Class I and Class II stages. The inner few AU of the disk will still, in most cases, be highly extinguished in the optical, but accessible to observations in the near-infrared, where the extinction is greatly reduced, while the temperature in the interesting inner few AU yields significant emission at mid-infrared wavelengths.

In order to trace the structural and chemical evolution of the gas and dust in these inner regions, as planetary systems start to form, diffraction-limited imaging observations resolution with a 100m telescope are required, yielding a linear resolution of ~3 AU in the closest star forming regions. Integral field spectroscopic observations at high spectral, as well as spatial, resolution are needed to understand the disk dynamics, with velocity resolutions of a few km/s (R~100,000) desirable. Working at such high spectral resolution also helps enhance the detectability of narrow spectral features against the bright continuum emission, with important targets again including the pure rotational H_2 line at 17μm and the CO fundamental lines at 4.6μm, along with numerous additional atomic, molecular, solid-state, and mineral tracers which will make it possible to determine the evolution of the physical conditions in the inner nebula. An E-ELT is required to deliver the necessary combination of high spatial and spectral resolution with extreme sensitivity.

Notes on Design Requirements

Observation Type: Mid-infrared imaging + 3D imaging spectroscopy

Spatial Resolution: Diffraction-limited at mid-infrared wavelengths

Spectral Resolution: R ~ 100,000

Wavelength Range: 5–20μm

3.3.1.4 Jets and outflows: dynamics and moving shadows

The present understanding of accretion and outflow in low-mass stars is largely derived from observations of relatively evolved T Tauri stars such as HH30 (Figure 3.14). Yet it is well known that much of the important evolution in the inner disk takes place at the much earlier Class 0 and Class I stages. The young protostars remove the bulk of the angular momentum and energy lost during the accretion process in the form of winds which are an order of magnitude more powerful than those seen in the optical Herbig-Haro jets from T Tauri stars.

Current jet models predict that they are launched and ejected from within the innermost few AU of a disk: at the nearest star forming regions, this corresponds to ~ 10 milli-arcsec, achieveable by an E-ELT at near- and mid-infrared wavelengths. While near-infrared H_2 and [FeII] line emission has now been detected from the

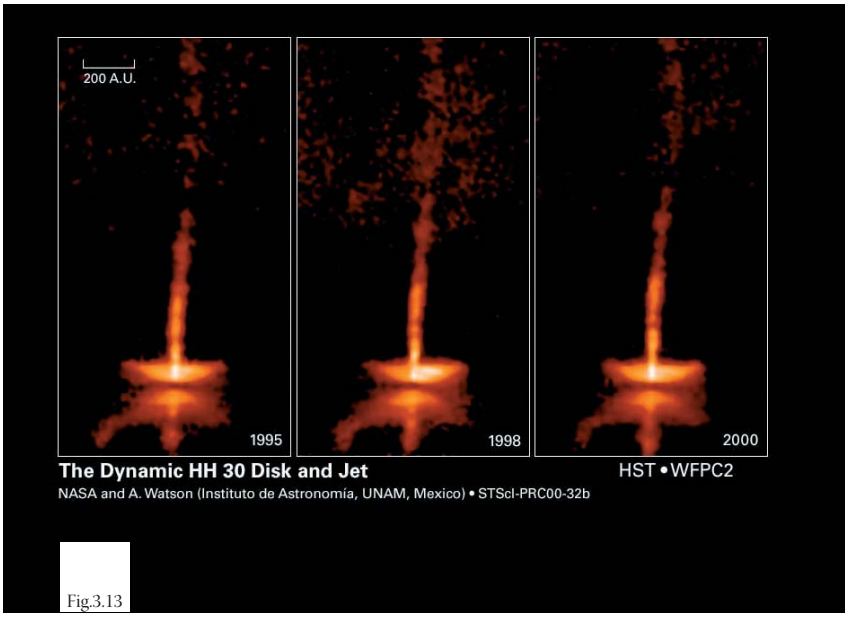

Fig.3.13

Images of HH 30, obtained with HST, showing changes in only a 5 year period in the jet of this star, which is about half a million years old. Credit: NASA and A. Watson (Instituto de Astronomia, UNAM, Mexico).

base of jets in Class I sources (Davis et al. 2003), these observations lack any spatial information. To gain a deeper insight into how the accretion and outflow are linked , and how the collimated jets and winds are launched and accelerated away, simultaneously high spatial (~ 1 AU) and spectral (~ 1 km/s) resolution observations using integral field spectroscopy are required in the lines of H_2 and [FeII] in the near-infrared for evolved Class II and III objects, and at mid-infrared wavelengths for the younger, more embedded Class I and, if possible, Class 0 objects.

Time-lapse imaging will be a key new facility to help disentangle outflows, shocks, and the disk dynamics in YSOs: it may no longer be useful to publish single images of a flow, as only a movie will be meaningful. An early example of the sort of results that might be achievable is the proper motion measurement of the jet clumps and the dark shadow on the disk in HH30, taken over 5 years with the HST (Figure 3.14). Typical outflow velocities in jets from young stars of ~100 km/s mean that proper motions of knots in outflows in star forming regions at 150 pc will be measurable within just a few days, assuming a diffraction-limited 100m E-ELT imaging in optical and near-infrared emission lines. Thus, over a year of regular monitoring on a weekly timescale, a detailed time-lapse movie of a given jet and its interaction with the ambient medium could be made. Furthermore, in systems like HH30 where the disk is also clearly visible in reflected light, the same monitoring experiment would trace changes in the illumination of the disk, effectively tracing out structure in the innermost sub-AU regions of the disk.

Notes on Design Requirements

Observation Type: Time-lapse imaging on weekly basis over ~ year

Spatial Resolution: Diffraction-limited at near-infrared wavelengths

Spectral Resolution: R ~ 100 (narrow-band filter imaging)

Wavelength Range: 0.5–2μm

3.3.1.5 Debris disks around other stars

Debris disks are the products of collisions of asteroid-sized bodies around main-sequence stars and at least 15% of such stars have significant amounts of this debris. These disks can be studied in scattered light at optical and near-infrared wavelengths, as well as in dust emission at far-infrared and millimetre wavelengths. At the latter wavelengths, facilities such as Spitzer, Herschel, and ALMA will make significant progress in our understanding of their origins and structure, but for a comprehensive study of such disks down to the low- mass limits of our own Solar System, a large and sensitive survey of nearby stars at high spatial resolution will be required.

An E-ELT operating with a sub-millimetre bolometer array camera could carry out such a survey and provide answers to important questions: does the mass of debris depend on the stellar age, spectral type, location; is there a continuous mass distribution of debris disks down to that of the Solar System; is our Solar System unique in having a low dust mass; how is debris (and hence asteroids) related to the presence of planets? For any given system, the frequency and mass of debris can be interpreted as the interval between catastrophic collisions of asteroids, which is then related to the bombardment rate of any habitable planets in the system.

Notes on Design Requirements

Observation Type: Sub-millimetre imaging

Field of View: 3 x 3 arcmin

Spatial Resolution: Diffraction limited to ~1" at sub-mm wavelengths; AO not required

Wavelength Range: 350-850μm; 2 or 3 atmospheric windows simultaneously

Target Density: All stars within 100pc

Dynamic Range constraint: >100:1 within 0.5"

Telescope Size: As large as possible for competitive collecting area and to avoid sub-mm confusion limit; 100m class telescope needed

3.3.2 The lives of massive stars

Massive stars are beacons, wreckers, and the engines of change within their Galactic environments. A major goal in astronomy is to achieve a good understanding of how these stars form, evolve, modify their environments, and die explosively, ending in neutron stars or black holes. High mass stars are so luminous that even with present telescopes, they can be picked out as individuals in galaxies well beyond the Local Group, while the HII regions that they ionise can be seen out to quite large redshifts. When OB stars more massive than ~8 $M_\odot$ explode as supernovae, they dramatically complete the process of deposition of kinetic energy and chemically-enriched matter in the local ISM that begins soon after they form. Furthermore, massive stars can also modify the formation and evolution of nearby low-mass stars and their protoplanetary disks, perhaps promoting formation of new stars via radiative implosion, while also ionising and evaporating disks, perhaps preventing planet formation.

Despite their enormous importance, however, their birth is poorly understood. The standard theory of low-mass star formation is very likely inapplicable to massive stars, as radiation pressure from a massive central protostar rapidly reverses accretion and sets an upper limit below ~10 $M_\odot$. Nevertheless, much higher-mass stars are observed, leading theorists to other models for their origin, including the coalescence of many lower-mass stars in the cores of very dense clusters (Bonnell, Bate, & Zinnecker 1998; Bally & Zinnecker 2005). On the other hand, some massive stars are seen to have very large, collimated outflows, suggestive that a disk is indeed involved in their formation. Another issue is the role of magnetic processes in high-mass star formation: peculiar behaviour displayed by the ~50 $M_\odot$ θ^1Ori C in Orion suggests that it is an oblique magnetic rotator (Babel & Montmerle 1997), suggesting that magnetic fields may be important.

As yet, however, there is no strong empirical evidence allowing us to discriminate between the various theories, in part because massive stars are born and evolve extremely rapidly, making them very rare and generally rather distant from the Earth. Also, they are very heavily embedded before they burst on to the scene as main sequence stars.

The main contribution of an E-ELT to this endeavour will be (i) the application of its high spatial resolution to Galactic studies of the birth and evolution of high-mass stars, perhaps in extremely dense clusters, (ii) the possibility to push the study of these objects out to a far richer variety of Galactic environments, a long way beyond the Local Group (see also the section on Stars and Galaxies), and (iii) using its near- and mid-infrared sensitivity to peer through the huge extinction surrounding very young, massive stars.

3.3.2.1 Early phases of evolution

Hot cores and compact HII regions within the Galaxy have been identified as sites containing very young luminous stars (less than ~10^5 years old), usually in compact clusters. These are spread throughout the Galactic spiral arms at typical distances of a few to 15 kpc, with only a few within 1 kpc, and thus high spatial resolution is at a premium when it comes to studying them, along with near- and mid-infrared sensitivity, in order to penerate the extinction.

Radio observations of free-free emission from ultra-compact HII regions imply length scales ranging between ~100 and 1000 AU or so. Existing 4– and 8–metre class telescopes are able to determine the stellar content of such regions in the Galaxy by near-infrared imaging (see, e.g. Henning et al. 2001) and spectroscopy. For the next step, however, narrow-band imaging and spectroscopic studies of the immediate environments of the exciting sources of ultra-compact HII regions are required on scales down to 10 AU or desirably 2 AU, the latter being possible with a diffraction-limited 100m E-ELT at near-

infrared wavelengths in Orion, the nearest site of this activity. Such observations will make it possible to search for direct evidence of merging in extremely dense clusters, and/or will resolve disks, if present, despite the intervening extinction.

Studying the outflows from young massive stars will also be important: an E-ELT can use its imaging spectroscopy capability at high spatial resolution, imaging in emission lines to trace the wind-wind, wind-cloud and wind-ISM interactions, and the associated photo-evaporative processes which may to dominate the evolution of lower-mass stars and their protoplanetary disks.

There is also a great degree of complementarity between an E-ELT and ALMA for the study of deeply embedded, young massive stars. ALMA will provide insights into the dust and molecular gas close to young massive stars, while an E-ELT will explore the ionised gas interior to this via infrared imaging, at finer angular scales than ever previously achievable.

Notes on Design Requirements

Observation Type: Narrow band imaging and imaging spectroscopy

Spatial Resolution: As high as possible

Wavelength Range: Near- and mid-infrared

Other comments: Complementary to ALMA

3.3.2.2 Mature phase outflows

The evolutionary trajectories of the most massive stars (greater than ~50 $M_{\odot}$) in the Hertzsprung-Russell diagram remain very poorly known. The most massive stars can lose most of their mass before exploding as supernovae, and such stars are the fastest-evolving and, in their evolved and exposed phases, the brightest, of all. They are also the dominant sources of enrichment in metal-poor environments. Examples of these still distinctly mysterious "top-end-of-IMF" objects include η Car, P Cygni and the Pistol Nebula exciting star near the Galactic Centre.

Key clues to the evolutionary status of such stars are their surface chemical compositions and those of their winds and ejecta. These can be probed by examining the relic nebulae surrounding objects such as η Car, which is embedded in a dramatic bipolar nebula (Figure 3.15) and is suspected to be double or even a triple system. However, there is no direct evidence for what lies at the core of a source like η Car or what happens when a system like this undergoes an outburst. An E-ELT will be able to monitor such objects via narrow-band imaging and 3D spectroscopy, resolving the smallest scales and following fine structure as it dynamically evolves and propagates outward. A 100m E-ELT will resolve circumstellar structures at η Car down to 10 AU in the near- and mid-infrared. This is roughly 50 stellar radii and thus such observations will be capable of revealing whether or not an ionised disc is present and may also be able to tell directly whether the star is in fact multiple.

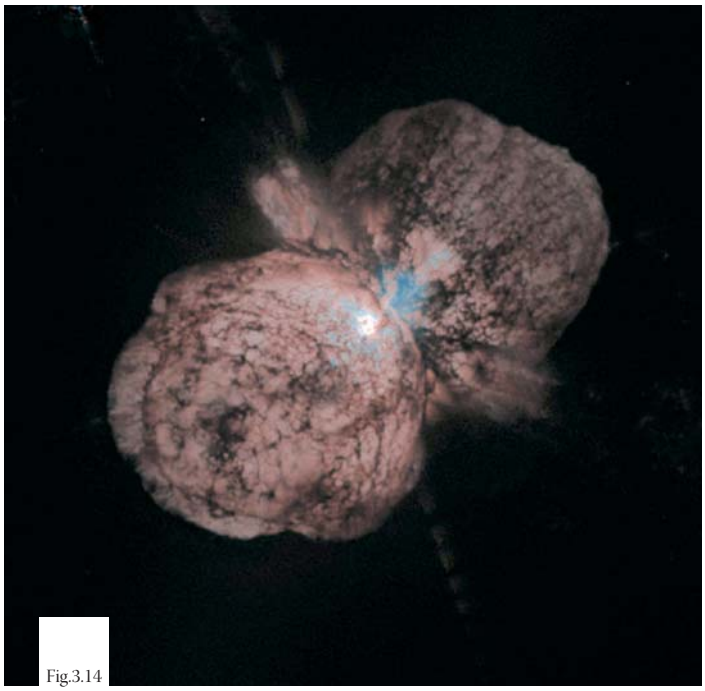

Fig.3.14

HST image of Eta Carinae (Credit: J. Morse and K. Davidson, NASA).

Long-term monitoring experiments will be important: shells may be expected to become observable within a few weeks of ejection and in more compact objects, within a few days

only. The high spectral resolution and sensitivity of an E-ELT are needed to reveal the kinematic details of the outflows, which, because of the low surface gravities of these extreme supergiant stars, tend to be very slow. In addition, spectropolarimetry is expected to prove critical for understanding these huge and complex systems, and here again the great collecting area and high resolution of an E-ELT will make it by far the most powerful available facility for carrying out these photon-starved observations.

Notes on Design Requirements

Observation Type: Narrow-band imaging and 3D spectroscopy

Spatial Resolution: Diffraction limited

Wavelength Range: Near- and mid-infrared

Other comments: Monitoring is an important aspect; spectro-polarimetry would also be very helpful

3.3.2.3 Normal and peculiar stars

If a 100m diameter E-ELT could be made diffraction limited in the optical, its resolution of ~ 1.5 milli-arcsec in the V-band would enable direct mapping of the surface of some types of nearby stars. Fracassini et al. (1981) lists ~100 stars with apparent diameters of 10 milli-arcsec or greater – an E-ELT could produce images with areas of ~100 pixels of the photospheres of each of these stars, which include the nearest red giants, first ascent red giant branch (RGB) stars and asymptotic giant branch (AGB) stars around 100 pc, and red supergiants around 1 kpc. Solar-type main sequence stars may be (marginally) resolved up to a distance of about 10 pc.

In this manner, it would be possible to directly see structure in the surface temperature and/or abundance pattern due, for example, to stellar spots related to emerging magnetic flux tubes or due to (super-)convection cells in the mantles of red giants. Magnetic fields may be directly mapped by means of integral field spectro-polarimetry from circular polarization (at typically an 0.1 percent level) in the wings of photospheric absorption lines. Narrow-band imaging or integral field spectroscopy will reveal chromospheric activity, for instance in the form of Hα filaments and protuberances. Mapping and monitoring the radial velocity pattern across the stellar surface will reveal differential rotation, inclination of the rotational axis, and/or (non-) radial pulsation of the surface. Because of the brightness of the sources and the modest contrast of structures against the surface (~1%), a Strehl ratio of near 90% would be required, an extremely challenging but rewarding problem at such short wavelengths. Seeing the surfaces of nearby Solar-type stars and red (super)giants will teach us a great deal about the structure and dynamics of stellar interiors, which is hitherto hampered by an incomplete understanding of basic physical principles such as turbulence, convection and the generation of large-scale magnetic fields.

Notes on Design Requirements

Observation Type: Imaging, IFU spectro-polarimetry

Field of View: Of order 1 arcsec

Spatial Resolution: Diffraction limited in optical (Hα); Strehl ratio ~90% desirable

Spectral Resolution: Up to R=100,000

Wavelength Range: Optical (Hα)

Telescope Size: 100m assumed for the best possible spatial resolution

Other comments: Monitoring is important

3.3.2.4 Asteroseismology

Stellar seismology (or asteroseismology) is a major tool for understanding the evolution of stars whose diagnostic power has been well demonstrated by ground and space-based observations of the Sun for 25 years. It has helped improve our physical knowledge of matter in the conditions of the Solar interior and confirmed that the origin of the neutrino flux discrepancy lay on the particle physics side of the equation in the existence of a neutrino mass. The theoretical understanding of asteroseismology is quite advanced, but observations remain a great challenge for several key reasons. Very long period observations, of the order of several weeks to months, are required on the same object, with a very high duty cycle (> 80%). Extreme stability is needed at the level of a few ppm in photometry and below 1m/s in spectroscopy, over timescales appropriate to the variations, i.e. a few hours. Finally, very large photon collecting power is necessary in order to achieve significant signal-to-noise for a useful sample of representative objects.

For this reason, only a few very bright stars have been studied to date. Improvements are expected from space missions (e.g. COROT), but advances there will be limited due to the small aperture of the telescopes. Fundamental advances in this field will require complete asteroseismological mapping of all kinds of stars of different ages, masses, and chemical composition, in homogeneous groups like open clusters, and over wider regions of the Galaxy.

The two techniques for asteroseismology are high-resolution spectroscopy or photometry at visible wavelengths. Spectroscopy permits one

Notes on Design Requirements

Observation type: Multi-object spectroscopy and eventually photometry

Field of view: 30 arcmin

Spatial resolution: Not relevant (no AO needed)

Spectral resolution: R~80 000

Target density: 500 per field

Dynamical range constraints: As large as possible: at least a few 10^5

Telescope size: Of the order of 100m

Observing time: Several weeks continuously

to reach a large variety of modes of oscillations, but only for slow rotators. A 100m E-ELT acting essentially as a flux bucket would make it possible to carry out studies on stars as faint as V=11, thus enabling the study of the internal structure of Solar-like stars in the Pleiades and in other open clusters.

In the case of photometry, ideal observations would be limited by the photon noise only, at which point 10^7 photons per second would need to be collected in order to detect Solar-like oscillations: for a 100-metre E-ELT, this would then correspond to V=17. However, in practice, such observations at precisions of a few parts per million are unreachable from the ground due to scintillation. One possibility for decreasing this noise component would be to site an E-ELT at a polar site, such as Dome C in Antarctica, where scintillation is greatly reduced. Furthermore, such a site would help address the other fundamental requirement of asteroseismological studies, namely that of extremely long time series observations and a high duty cycle.

3.3.2.5 Chemical composition: the challenge of chronometry

The most traditional task of astronomers has always been the measurement of time. Ancient astronomers were confronted with the difficult task of determining a precise calendar, predicting equinoxes, solstices, as well as eclipses of Sun and Moon. Modern astronomers face the challenge of measuring the age of the Universe itself and of its various observable components. Our current understanding of cosmology is that the Universe emerged from a hot and dense phase composed only of hydrogen, helium, and traces of lithium: all other elements have been synthesised elsewhere.

From this premise, one may immediately conclude that the abundances of chemical elements in an astrophysical object contain some information on the age of the object itself. Unfortunately, the evolution in time of most elements is rather complex, since many can be formed in different environments, with different time scales. In this respect, the simplest element is beryllium, its only production channel being through spallation of heavier nuclei, such as carbon, oxygen and nitrogen, by cosmic rays (Reeves et al. 1970). This process is "global" rather than "local", since the particles are transported on Galactic scales, which implies that the berillyum abundance is predicted to increase linearly with time, at least in the early phases of the formation of our Galaxy. Thus, in principle, the berillyum abundance may be used as a true "cosmic clock" (Beers et al. 2000; Suzuki et al. 2001).

Pasquini et al. (2004) have recently shown this to be the case by measuring Be abundances in unevolved stars of the globular cluster NGC6397 and determining the age of the cluster (Figure 3.16). Although this "Be age" turned out to be in excellent agreement with the age derived from isochrone fitting, it is strongly desirable to carry out further studies to check that the two "clocks" (beryllium and stellar evolution) agree over a range of ages and metallicities, and to obtain a clear view of the times of formation of the different globular clusters.

Unfortunately, such a programme is not feasible with 8m class telescopes. Beryllium must be measured in turn-off stars: it is destroyed at temperatures above 3.5 millions Kelvin and thus may be diluted as stars climb to the sub-giant branch and up the red-giant branch. Beryllium is measured using the resonance doublet at 313.1 nm, close to the atmospheric cut-off. At these wavelengths, the turn-off of NGC6397 (at V=16.5) is at the very limit of the capabilities of UVES at VLT, while most other globular clusters have fainter turn-offs. However, an E-ELT equipped with a high-resolution (R ~ 30,000) multi-object spectrograph will allow a major breakthrough.

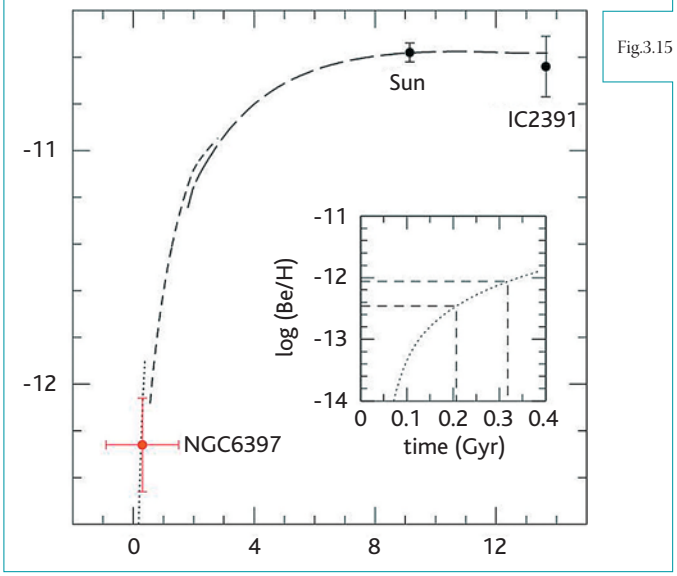

Fig.3.15

Evolution of Be with time in the Galaxy according to a three-zone Galactic chemical evolution model (Valle et al. 2002). The three curves refer to the halo, thick disk, and thin disk. The data points show the Be abundance in the young open cluster IC2602 (age 30Myr), the Sun (age 4.5 Gyr), and the globular cluster NGC6397 (age 13.9 +/- 1.1 Gyr). The model result is normalised to the Solar meteoritic abundance. The inset illustrates the use of Be as a "cosmic clock" to constrain the formation of NGC6397. The horizontal lines corresponds to the 1 sigma contours around the measured Be abundance. The cluster birth is constrained to the first 0.2-0.3Gyr after the onset of star formation in the Galactic halo. (From Pasquini et al. 2004).

Beryllium could be measured in all globular clusters with a turn-off brighter than V ~ 21, making it possible to span the whole range of metallicities spanned by globular clusters.

With such a solid calibration of the Be-chronometer, it would then be possible to envisage the age determination, on a star-by-star basis, for a large sample of field stars. This, in turn, would place firm constraints on the timescales over which the different Galactic components (thin disc, thick disc, halo, bulge) formed. The turn-off of the Galactic bulge is at V=20 and thus, in principle, a precise dating of these stars will be possible: it may become possible to establish if there is an age range in the bulge.

Radioactive elements offer another interesting chronometer. Heavy radioactive nuclei, such as ^{232}Th and ^{238}U, have lifetimes which are of the order of the age of the Universe and are thus suitable for dating ancient objects. Such nuclei are produced through rapid neutron captures: if the production ratio of any two nuclei produced in the process (of which at least one radioactive) is known, then the measurement of their present-day ratio provides a direct measurement of the time elapsed. To date, there is still considerable uncertainity on the site where the r-process occurs and therefore on the prevailing physical conditions. The fact that some ratios such as Th/Eu are not "universal" (Hill et al. 2002) is a strong indication that the r-process occurs under different conditions. In spite of this, it has been shown that the U/Th ratio is indeed a very good chronometer, since its dependence on the physical conditions under which the r-process occurs is small (see, e.g. Goriely & Clerbaux 1999; Goriely & Arnould 2001; Wanajo et al. 2002).

The use of this chronometer, however requires the measurement of Th and U, whose cosmic abundances are extremely low. Fortunately, there is a class of extremely metal-poor stars which show greatly enhanced abundances of r-process elements (Cayrel et al. 2001). Large surveys aimed at the discovery of more of these r-enriched stars are currently producing their first results (Christlieb et al. 2004).

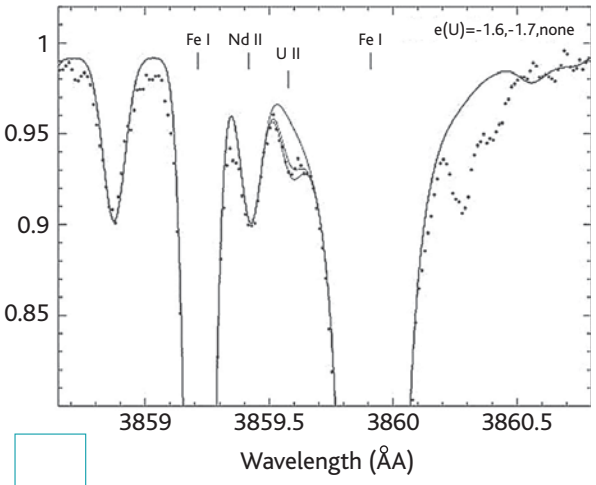

Fig.3.16

The U II line in CS 31082-001 (From Cayrel et al. 2004).

The measurement of U is very difficult and requires high-resolution high S/N spectra (Figure 3.17). With 8m telescopes, it will be possible to attempt the measure of U, and thus determine a radioactive age, in only a few stars. An E-ELT would be sensitive enough to measure the U abundance for stars to V=17 in one hour, enabling a true mapping of the halo to yield precise information on any age spread. An E-ELT could actually turn the radioactive dating of stars from a curiosity into a true working tool for the understanding of the Galaxy.

Finally, it is not known if r-enhanced stars are peculiar to our Galaxy or exist in other galaxies too. Assuming a survey could be carried out for candidate stars in the Local Group using 8m telescopes, measurement of the abundance of U in such stars is a task which may be accomplished only by an E-ELT.

Notes on Design Requirements

Observation Type: spectroscopic

Field of View: 30"

Spectral Resolution: 30000-150000

Wavelength Range: 300-700 nm

3.3.3 The death of stars

3.3.3.1 Mass function of black holes and neutron stars

The best-known examples of stellar black holes are those in the so-called low-mass X-ray binaries (LMXBs). These are X-ray transient systems formed by a compact object (either a black hole or a neutron star) and a slightly-evolved stellar companion. As a consequence of mass transfer from the secondary, these systems suffer transient outbursts which re-occur, typically, once every several decades. Exploring the properties of these systems requires time resolved spectroscopy to determine radial velocities. If these can be obtained not just for the compact object and its accretion disk, but also, in the infrared, for the companion star, the masses of each can be determined.

Many new transients will be detected by X-ray monitoring satellites in the coming decades. While the vast majority will be too distant to be observed by the current generation of ground based telescopes, VLT studies of nearby examples will explore the physics of the accretion disks and the properties of the highly-peculiar secondary stars. Determining the radial velocity curves, which have typical amplitudes of 400 km/s and orbital periods ~10 hrs, requires 20 or more spectra with S/N ≤ 10 and resolving power ~1000, distributed around the orbit. A typical LMXB secondary star has M_V ~ 8 or M_H~ 6; the tremendous light-gathering power of an E-ELT will allow it to secure suitable spectra in less than about 15 minutes out to distance of 50 kpc, permitting LMXB component masses to be determined throughout the Galaxy and the Magellanic Clouds. Such a data set will allow the determination of the distribution of masses among black holes and neutron stars and even its dependence on location and the heavy-element abundance of the parent Galaxy.

Notes on Design Requirements

Observation Type: Time-resolved spectroscopy

Spectral Resolution: R~1000

Wavelength Range: Near-infrared

Observing time: 20 x 15 minute spectra = 5 hrs on-source

Other comments: Time-resolved spectroscopy over a typical period of 10 hrs

3.3.3.2 Isolated neutron stars

Neutron stars have, to date, been studied mainly in radio and X-rays. However, to study the neutron star itself, as opposed to the accretion-flow emission in an X-ray binary, optical, highly time-resolved photometry and spectroscopy of an isolated neutron star may be the optimum. However, these objects are faint, with likely candidates having V > 26, and a search for nonradial oscillations, for example, with predicted periods in the range of milliseconds or hundreds of microseconds, will require the enormous light-gathering power only made possible with an E-ELT. Even then, such observations would be quite challenging: about 4 hours of observing in phase with the pulsar period would be required to build up a 300-point light curve of a V = 26 pulsar resembling that in the Crab Nebula, which has a 30 milli-sec period. Although, at first sight, it could appear that X-ray observations perhaps would be more suitable, their potential is limited by the limited number of X-ray photons that can realistically be collected over such short timescales by foreseen space instruments.

A detailed probing of neutron-star interiors would enable a better understanding of baryonic matter and is, of course, of considerable interest also outside astronomy proper. Other neutron-star related observations include the optical counterparts of millisecond pulsars, of relevance for pulsar physics and branches of radio astronomy.

Notes on Design Requirements

Observation Type: Highly time resolved optical photometry and spectroscopy

Field of View: Single, isolated targets

Spectral Resolution: R~100

Wavelength Range: optical

Telescope Size: As large an aperture as possible for time-resolved spectroscopy of faint sources

Observing time: Time-resolved spectroscopy, even at low resolution, would be a substantial challenge even for a 100m class telescope. Spectra at (say) 300 points around the cycle could be accumulated on a CCD by in phase charge transfer, but even at R ~100 many nights would be needed to accumulate a useful result (roughly a week to S/N ~ 5).

3.3.3.3 Black holes in globular clusters

Two classes of black holes are suspected to exist in globular clusters: objects of low (stellar) mass (LMBHs; M ~ 10 $M_\odot$) and those of intermediate mass (IMBHs; M ~ few x 1000 $M_\odot$). The former (LMBHs) are expected as the end products of the evolution of stars populating the uppermost end of the IMF, i.e. those with masses greater than roughly 30 $M_\odot$. If such remnants are formed without significant initial velocity kicks, the retention fraction is expected to be high and the holes constitute a dynamically important cluster sub-population (Kulkarni et al. 1993; Sigurdsson & Hernquist 1993). Depending on the shape of the upper IMF, most if not all globular clusters are expected to possess this population of up to several hundred LMBHs early in their life. Within ~1 Gyr of formation, most of the LMBHs within a cluster have settled through the process of mass segregation to form a centrally concentrated core. As the density of this core increases, so too does the frequency of multiple-hole interactions, resulting in the formation of BH-BH binaries and the ejection of single holes. Subsequent interactions harden the BH-BH binaries until eventually the recoil velocity is sufficient for ejection.

Several single holes are also expected to be ejected during this hardening process. Hence, it is thought that the LMBH population in a cluster completely depletes itself within a few Gyr. Nonetheless, the LMBH population is expected to inject significant amounts of energy into the stellar core in a cluster before depletion, both through the dynamical scattering of stars and the removal of BH mass from the cluster centre. N-body simulations show that this influence is in many cases enough to significantly alter (expand) the structure of the stellar core (Figure 3.18). Therefore, LMBHs likely represent an important (and often neglected) dynamical influence in the early and intermediate phases of star cluster evolution.

Intermediate Mass Black Holes in clusters are interesting because it is thought that such objects may represent the seeds of the very much more massive BHs observed at the centres of Galactic bulges. One possible formation mechanism for an IMBH in a cluster is through the process of runaway merging. This only occurs in very dense, very young clusters. In such clusters, the mass segregation time-scale for the most massive stars is very short, leading to a core collapse time-scale for these stars which may be shorter than the main sequence lifetimes of the stars themselves. During core collapse, the density of massive stars is sufficient that direct collisions may be initiated. The first collision leads to a massive merged object, which, with its increased interaction cross-section, is likely to undergo further collisions with massive stars. N-body simulations suggest this can lead to a runaway process resulting in the production of an object (possibly an IMBH) of mass up to 0.1% of that of the cluster (Portegies Zwart & McMillan 2002). If this were to occur in a cluster formed near to the centre of a Galactic bulge, it is thought that the in-spiral and subsequent destruction of the cluster can seed the bulge with an IMBH, which may later grow into a super-massive BH. Since runaway merging is by nature a stochastic process, and is particularly sensitive to cluster structure (it will not occur unless the relaxation time for massive stars is sufficiently short), IMBHs are not expected in all globular clusters. Nonetheless, because of their possible importance as the seeds of super-massive BHs, as well as their intriguing dynamical history, measurements of IMBHs in clusters are of considerable interest.

To date, there is only indirect and/or inconclusive evidence for IMBHs or populations of LMBHs in globular clusters. HST measurements suggest the presence of a ~2500 $M_\odot$ IMBH in the nearby globular cluster M15 (e.g. Gerssen et al. 2002) and a $2x10^4$ $M_\odot$ IMBH in the massive stellar cluster G1 in M31 (Gebhardt et al. 2002), although N-body simulations have demonstrated that neither detection requires the presence of an IMBH: each set of measurements can be explained by models with large central populations of stellar remnants such as neutron stars and white dwarfs (Baumgardt et al. 2003a,b). The only evidence for LMBH populations in globular

clusters is the observation (Mackey & Gilmore 2003a,b) that intermediate age clusters in the Magellanic Clouds possess a wide range of core sizes, and that this range apparently correlates with cluster age. This trend can, at least in part, be explained by the dynamical influence of LMBH populations (Figure 3.18); however, as yet not all other possible explanations have been ruled out.

The main problem in detecting the presence of IMBHs (or centrally concentrated LMBH populations) in globular clusters is that these objects have only small spheres of dynamical influence, and hence such studies are, at present, limited by resolution. The only way to establish beyond doubt the presence of an IMBH at the centre of a globular cluster, and accurately measure its mass, is through the direct dynamical analysis of stars lying within its sphere of influence. N-body simulations (Baumgardt et al. 2005) have shown that the radius of this sphere is given by $R_i/R_h \sim 2.5(M_{BH} / M_C)$ where R_h is the cluster half-mass radius, M_{BH} is the IMBH mass, and M_C the cluster mass. For a typical Galactic globular cluster, $R_h \sim 5$ pc and $M_C \sim 2x10^5$ $M_\odot$, so that $R_i \sim 0.1$ pc for a 2000 $M_\odot$ IMBH. For even the closest Galactic globular clusters this is a region only ~ 20 arcsec in diameter, while for the majority of the Galactic population the angular span is much smaller (~ 0.8 arcsec at 50 kpc). Because of this, crowding is severe and we are limited to obtaining measurements (spectra) of only the brightest available stars (or even worse, integrated spectra). This limits radial velocity samples per cluster to be small, reducing the confidence in any IMBH detection. While centrally concentrated populations of LMBHs likely have somewhat larger spheres of influence than do individual IMBHs, the Galactic globular clusters are too old to still possess significant LMBH populations. Rather, intermediate age star clusters in the Magellanic Clouds must be studied for direct detections of such populations. However, at distances of 50-60 kpc, crowding in these clusters again becomes too severe to allow meaningful measurements at present.

The availability of a 100m E-ELT would enormously enhance capabilities in this field of study. Assuming functional AO in the visible, diffraction-limited resolution of the order of one milli-arcsecond would be delivered, more than sufficient to fully resolve the central core of even the most crowded (or distant) Galactic and Magellanic Cloud globular clusters, all the way down the cluster luminosity function. Measurements of the nearby cluster M4 (e.g. Bedin et al. 2001) have shown the main-sequence hydrogen-burning limit to lie near $M_V \sim 15$. Such stars at the LMC distance would have $V \sim 34$ assuming typical extinction levels. With 10 hours of integration time on a 100m class telescope, these stars could be measured with S/N ~ 50. Hence, most, if not all, of the main sequence would be available for two types of measurements, in all clusters closer than 50 kpc. The two necessary sets of measurements are (i) obtaining accurate positions and proper motions for stars within the sphere of influence of any central IMBH or LMBH population; and (ii) obtaining radial velocity measurements for as many of these stars as possible. In combination, these measurements would define 5 of the 6 dimensions of cluster dynamical phase space, allowing a detailed analysis more than sufficient to establish the existence of an IMBH (or LMBH population).

The first set of measurements would be relatively straightforward given the exquisite resolution and enormous light-gathering power of a 100m class E-ELT. Assuming a central velocity dispersion of ~10 km/s, stars in a Magellanic Cloud cluster would exhibit proper motions of ~0.5 milli-arcsec per year due to internal dynamics, which would be easily detectable over a several year baseline. Closer clusters would of course have more easily measurable stellar proper motions. To be useful, the second set of measurements would necessitate radial velocities for significant numbers of stars, accurate to a few hundred metres per second. This can be achieved with moderate to high resolution spectra (R > 20,000), but would require a multi-object spectrograph or IFU for efficient observing.

For a 100m E-ELT, measurements with suitable S/N could be achieved with a few hours integration for V ~ 28 main sequence stars. This is significantly up the main sequence from the hydrogen-burning limit for clusters at Magellanic Cloud distances; however, such observations would still allow radial velocities to be obtained for many thousands of stars within each cluster core. The situation would, of course, improve dramatically for clusters closer to the Sun.It is worth emphasising that extending the study beyond the Galaxy is essential, as only at the Magellanic Clouds are the first available sample of intermediate age clusters reached: thus, only there can one begin to study evolutionary effects.

Hence, with a 100m class ELT the internal dynamics at the very centres of all globular clusters out to and including those in the LMC and SMC would be directly measurable, allowing secure detections of IMBHs in cluster cores, as well as the possibility of investigating the effects of low mass black hole populations in intermediate-age clusters.

Notes on Design Requirements

Observation Type: Imaging (repeated in order to measure proper motions) and spectroscopy (for radial velocities)

Field of View: 5 arcsec

Spatial Resolution: ~1 milli-arcsec

Spectral Resolution: R~5 (imaging) and R=20,000

Wavelength Range: Near-infrared (2μm) and visible. For spectroscopy CaII (830nm) would be beneficial.

Target Density: Crowded fields

Telescope Size: A 100m telescope is assumed in these calculations. This is needed for the highest possible spatial resolution and measurements of faint targets (V~34 for imaging, V~28 for spectroscopy)

Observing time: Proper motions require a minimum of 5 epochs x 10 hrs imaging per field. Spectroscopy requires a few hours per field. Total ~60 hrs per field. Note that if a star could really be found in close, it becomes a direct test of strong GR, so fully sampling orbital precession in the strong GR regime becomes viable: that would take maybe 100 epochs, but is unique science.

Date constraint: Proper motion measurements require multiple observations over a 10 year baseline.

Other comments: IFU or MOS would make the spectroscopic observations more efficient

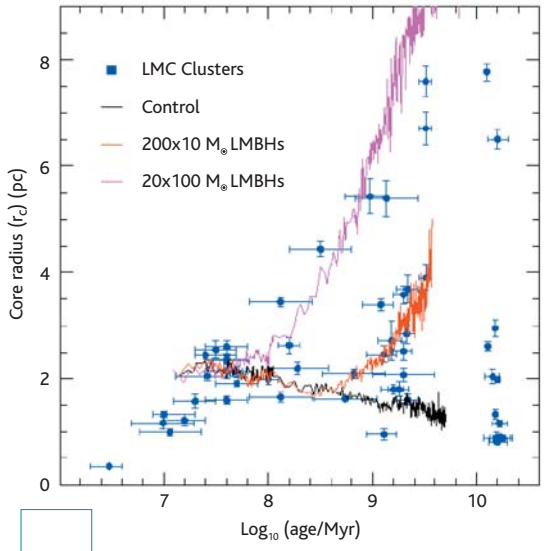

Fig.3.17

Core radius as a function of age for 53 clusters in the LMC. The spread in core radius increases strongly as a function of age. N-body simulations (overplotted) show that one possible explanation is the presence of significant low mass black hole populations in some clusters. The control run is a 10^5 Solar mass star cluster with no low mass black holes. The (observational) core radius shows a gradual contraction due to mass segregation. In contrast, an identical cluster with 200 x 10 $M_\odot$ low mass black holes shows moderate expansion as the holes concentrate in the core and eject one another. A population of more massive objects (20 x 100 $M_\odot$) shows even stronger evolution, although this cluster dissolves after only ~7 Gyr.

3.3.4 Microlenses: optical and near-infrared counterparts

Microlensing events toward the LMC and the bulge of our Galaxy have confirmed the existence of a population of MACHOs (Massive Compact Halo Objects) which may account for a significant fraction of the dark matter in the halo (Alcock et al. 1997). However, the nature of these lensing objects is unknown. Depending on its distance from the Sun, an E-ELT will be able to resolve the lens from the lensed star roughly a decade after the original lensing event. This will enable investigation of the lensing object by direct imaging and spectroscopy. If the lenses are old (cool) white dwarfs, as claimed, spectroscopic examination will provide an unique opportunity to date and trace back in time the various phases of the Galaxy halo. At 50 kpc, a 0.5 $M_{\odot}$, 15 Gyr old DA WD will have V ~ 32.

Identification of the lenses would permit the determination of their space motions (proper motions of 0.1 milli-arcsec/yr and radial velocities of 200–400 km/s are expected) and spectroscopic characteristics, providing unique information on the very early phases of our Galaxy and also on the physics of such very old degenerate objects.

Notes on Design Requirements

Observation Type: Imaging and spectroscopy

Spectral Resolution: R~100 (spectroscopy or narrow-band imaging)

Wavelength Range: Near-infrared (1–2.5μm)

Halo brown dwarfs are another possible class of MACHO lenses and could be directly imaged and spectroscopically examined up to distances of order 1 kpc in the Galactic halo. At 1 kpc, a 0.05 $M_{\odot}$ old brown dwarf may have J=28 and K=29 (Burrows et al. 1997). Very low resolution spectroscopy (R=100) or narrow-band filter imaging in the near-infrared of the faintest objects will be sufficient to measure the expected distinctive methane and possibly ammonia bands if the MACHOs are indeed brown dwarfs.

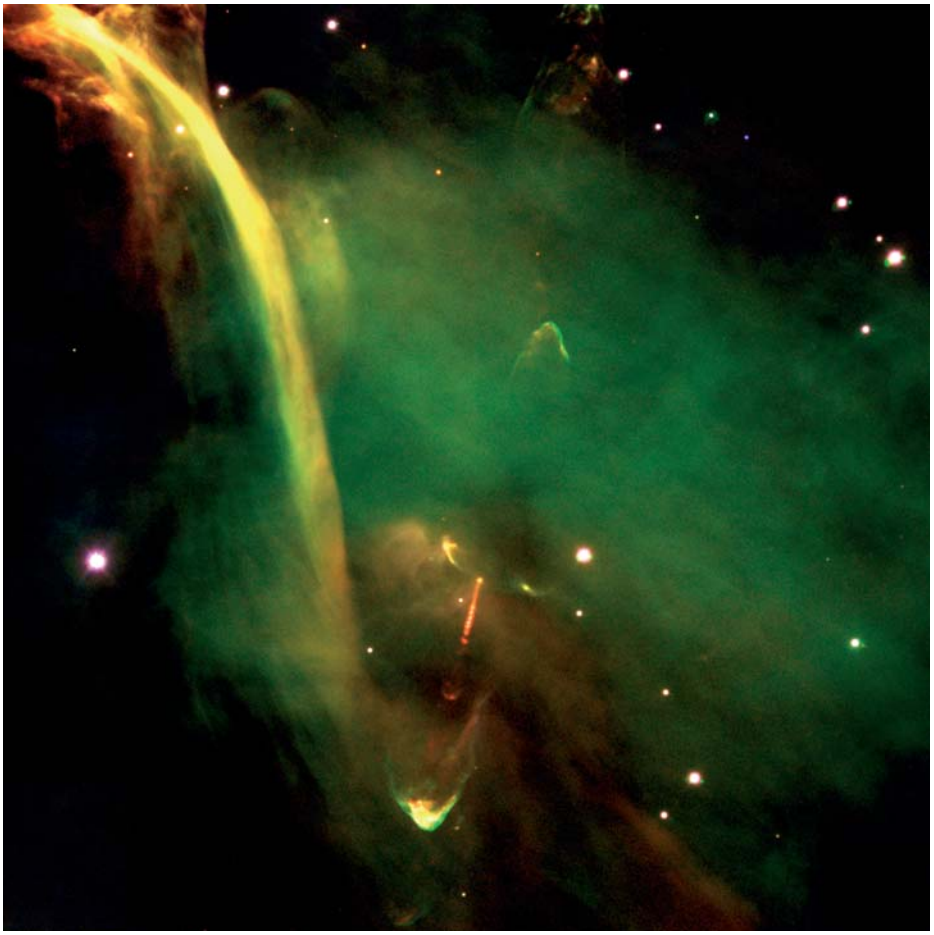

Protostar HH-34 in Orion. Three-colour composite of the young object Herbig-Haro 34 (HH-34), now in the protostar stage of evolution. Probing the physics of star and planet formation is a major challenge for the Extremely Large Telescope.

4 Stars and Galaxies

Introduction

A very large optical-infrared telescope will allow us to derive the important processes of galaxy formation and evolution in the full range of environments. Several complementary lines of attack are possible, directly connecting the present-day Universe with the high redshift Universe, where the old stars near the Sun formed. Both the star formation histories of galaxies and the mass assembly histories of galaxies will be elucidated. We know that interactions and mergers between galaxies occur and play a (probably crucial) role in determining the morphological type of a given galaxy, but we do not know what merged, or when it merged – how do the merging histories of non-baryonic dark matter and of baryons compare?

Similarly, stars clearly form(ed) at some rate from gas, but at what rate, where, with what stellar Initial Mass Function, and what were the effects of this star formation on the remaining gas? What is the connection between galaxies and the supermassive black holes at their centres? The unprecedented spatial resolution of a 50–100m telescope, comparable to those achieved by VLBI in the radio, will provide unique insight. Thus, E-ELT will provide the data that are required to underpin an analysis of the physical properties of galaxies over the age of the Universe.

A European ELT as envisaged is a critical component of a multi-faceted approach to understanding our Universe. GAIA will provide an astrometric capability that is impossible from the ground, supplying proper motions and distances. An ELT complements and thus strengthens the capabilities of ALMA, which focuses on analyses of the dust and gas content of galaxies.

In this Chapter we describe the impact that a 50–100m ELT will have on our understanding of the formation of galaxies in relation to their constituents, including gas, stars, star clusters and black holes. The following sections are arranged in order of increasing distance, starting with the interstellar medium (ISM) in our own Galaxy, on to resolved stars in galaxies beyond our own, and finally to star clusters and black holes at cosmological distances.

4.1 The Interstellar Medium

In the following sections we show how a 50–100m ELT could be used to study the physical properties of the interstellar medium (ISM), such as the density, temperature, structure and chemical content of the ISM, and even the physical properties of dust grains in neighbouring galaxies.

These studies would make use of photon-starved modes of observing, i.e. those which extract the most information from the incoming light: high and ultrahigh resolution spectroscopy; polarimetry and spectropolarimetry; ultrahigh signal-to-noise spectroscopy.

CO	4.67μm 1–0 fundamental
HCN	3μm $\nu 3$ fundamental
SiO	8.3μm 1–0 fundamental
NH_3	10.3μm $\nu 3$
C_2H_2	2.44μm, 3μm
SiH_4	11μm $\nu 4$
CH_4	3.3μm $\nu 3$

Table 4.1

A selection of simple molecules detectable in the near- and mid-infrared ro-vibrational transitions, in the circumstellar and interstellar environments.

4.1.1 Temperature and density probes in the thermal infrared

The ro-vibrational transitions of a range of molecular species occur in the 4 to 25 micron region of the infrared spectrum accessible from the ground (Table 4.1). These include species such as HCN, SiO and NH_3 which are also detectable at millimetre wavelengths through their rotational transitions, but also a number of species such as SiH_4, C_2H_2, and CH_4 which, because of their symmetry, can not be detected at radio wavelengths. The transitions of these species can probe a range of physical conditions: the symmetric top species can be used for temperature diagnostics while molecules with large permanent dipole moments, such as HCN and CS, can serve as density probes. Using these species we can build on results from the current generation of 4 and 8 metre telescopes by pushing to higher extinctions, higher resolutions and shorter wavelengths.

Notes on Design Requirements

Observation Type: spectroscopy

Spectral Resolution: R=10^4 up to 10^6. Many gaps in the high atmospheric extinction exist in the 16-25 micron region; some of these are very narrow and a resolving power of 1 million is needed to make significant progress in these regions.

Wavelength Range: Mid-IR: 7–25 microns

Other comments: Mid-infrared observations are heavily affected by telluric absorption (for example the detection of C_2H_2 lines around 7 and 13 microns (Lacy et al. 1989) undertaken at a resolving power of 10^4 required a substantial effort to flat field using the Moon; mid-infrared observations generally benefit from the higher dispersion which an ELT, with its greater light gathering, would make possible.

4.1.2 Fine structure in the ISM from Ultrahigh signal-to-noise spectroscopy

One current limit to high signal-to-noise spectroscopy is the ability to flat field the detection at the same time as being limited by the background photon flux. For example, the venerable CGS4 InSb detector on UKIRT can not be pushed much further than a flat fielding accuracy of 1 in 1000, as it is essential to keep the light from the source on as small a number of rows as possible. An ELT's light gathering power could be used to disperse a spectrum laterally across thousands of rows of a CCD or infrared detector, producing an immense gain in flat-fielding accuracy, roughly proportional to the square root of the number of rows used. At present, S/N of 1,000,000 is very hard to achieve in the presence of systematics; with an ELT it should be commonplace, for sources which are currently studied to S/N of a few hundred. With suitable choice of targets, this will bring within reach ultrahigh S/N studies of the fine structure in the interstellar extinction, and because each visitation will be very quick there is clear potential for monitoring this structure for changes and modelling those changes in the light of small-scale cloud structure in the local ISM. At present this work is very painstaking and slow, but the rewards may be a complete understanding of the structure and chemical content of the local interstellar medium.

Notes on Design Requirements

Observation Type: Ultra-high signal to noise spectroscopy

Date constraint: Monitoring needed to observe changes in small-scale cloud structure.

4.1.3 The high redshift ISM

The 217.5nm interstellar extinction bump, at redshift 1, is located in the blue part of the spectrum. At redshift 2 it is in the yellow-red. This feature has been well studied in the local ISM and when combined with measurements of the visible extinction curve can be related to the metallicity of the galactic environment of the dust. The possibility to directly detect the 217.5nm bump in samples of galaxies at redshift greater than 1 will give an independent measure of the metallicity of those early environments. Using background QSOs as silhouette sources, it should be possible to map out the carbonaceous dust content of the Lyman alpha forest.

Quasars behind dusty galaxies may permit studies to distinguish between massive and low/intermediate mass stars as sources of the carrier carbon grains; if these grains come from lower mass stars then the presence of significant production would be possible only if the age of the host galaxy is above a lower limit.

High redshift will bring currently inaccessible dust features into reach, for a price which even with the ELT would be modest compared to satellites. It is possible to find a system with high enough redshift that the EUV is redshifted into the optical window. A second resonance in graphitic grains (a prediction of models) beyond the Lyman limit would then be detectable. This might, of course, fall to hydrogen opacity in the Lyman alpha region.

UV lines in the regime between 1200A and 2000A can be used to measure both photospheric and interstellar abundances in galaxies. Large telescopes are beginning to open up the possibility of tracing metallicity and star formation at very long look-back times. Through optical spectroscopy in the visual and red, this is beginning to be exploited to redshift of order 2 using 8-m class telescopes to observe UV-luminous galaxies (e.g. de Mello et al. 2004), and to z>3 in lensed systems (Villar-Martin et al. 2004). Systematic work on representative samples at lookback times longer than 10.5Gyr will require larger apertures and equivalent spectroscopy capabilities in the near-infrared (see also Section 5.2).

Notes on Design Requirements

Observation Type: spectroscopy

Field of View: single sources

Wavelength Range: Near-IR

4.1.4 Measuring Dust properties via polarimetry

Multi-wavelength polarimetry of interstellar dust provides a key indicator of mean grain size. To just detect a linear polarisation of 1% (with a signal-to-noise of 3) requires a signal-to-noise on the received flux in excess of 400. This limitation has restricted polarimetry to the brightest objects and regions, but the technique is immensely powerful. ELTs rectify the photon starvation by providing the required photon flux. Possible projects include (i) dust properties and alignment in neighbouring galaxies, at the level of individual ISM clouds; (ii) the interstellar polarisation curve at high resolution (suitable for the definitive study of the relationship between dust and molecular carriers of interstellar features).

Notes on Design Requirements

Observation Type: Multi-wavelength Polarimetric measurements

4.1.5 Optical studies in heavily extinguished regions

The E-ELT's light grasp will open up the dark clouds to scrutiny at visible wavelengths for the first time. In many ways, the visible regime is better for studies of molecular abundances in these regions, with many well-understood diagnostics relevant to the sort of abundances modelled in the big codes. However, lines of sight through these regions are currently completely inaccessible. In our galaxy, optical studies of highly reddened stars in or behind dense clouds is certainly important, to determine properties which are currently estimated indirectly via observations at longer wavelengths; namely spectral types, ratios of total-to-selective extinction, molecular column densities, etc.

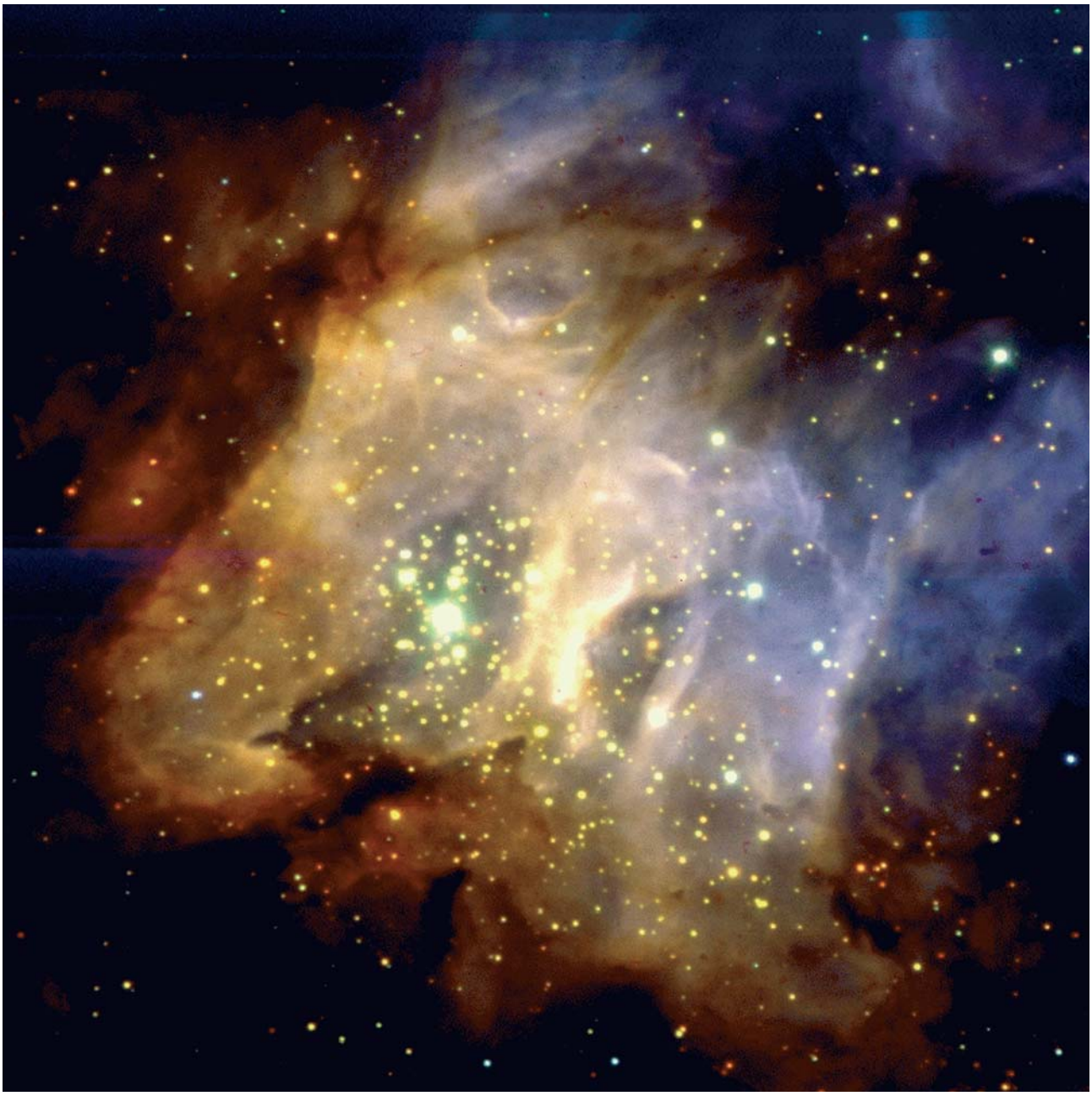

The star forming region RCW38. Massive young stars are forming here, illuminating the surrounding gas to make regions like this visible across the Universe to an Extremely Large Telescope. The massive stars explode as supernovae, creating and dispersing the chemical elements, and providing probes of the history of star formation, and the geometry of space-time.

4.2 Highlight Science Case: Resolved Stellar Populations

Galaxies are assemblies of baryonic material (stars, dust and gas) and non-baryonic "dark matter". The only component that directly retains observable information about star formation rates and metal enrichment rates – the evolution of the baryonic component – is the stellar population. This is because low mass stars have extremely long life times, comparable to the age of the Universe, and retain in their atmospheres the gas, with the elemental abundances intact, from the time of their birth. Thus, if the stars of different ages can be picked out of a stellar population, and this is most accurately done if the population is resolved into individual stars, then the star formation rate and metallicity at different times is directly measured. An individual star which can be accurately placed on a Hertzsprung-Russell Diagram (or the observed version, the Colour-Magnitude Diagram) can be given an accurate age and thus a place in the evolutionary history of the galaxy (see Figure 4.1). This requires accurate photometry: the measurement of luminosity and colour for each star. By the simple counting of stars of different ages in a Colour-Magnitude Diagram the rate at which stars are formed throughout time is directly obtained. Abundances can be measured from spectra of individual stars of known ages and thus the evolution of abundance of different elements can also be directly measured throughout time (see Figure 4.2 and Figure 4.3). The motions of the stars reveal the spatial distribution of the mass within the galaxy, and different stellar populations may have different kinematic signatures dependant upon the merger history of the galaxy (see section 4.6).

The separation of a galaxy into its individual stars for the detailed reconstruction of the history of its formation and evolution requires higher spatial resolution the further away or the more concentrated the stellar population. Distance also means that the stars become fainter, thus to carry out accurate photometry and spectroscopy of the individual stars a large telescope collecting area is required.

It is unfortunate that the Local Group of galaxies (LG) does not provide a sample of galaxies that is even reasonably representative. Indeed, even with space telescopes and the current generation of 8–10m telescopes, it is a challenge to obtain data of relevance to the evolution of the LG. With adaptive optics, current 8-10m telescopes do allow evolutionary studies of LG galaxies but for galaxies beyond the LG, these telescopes have too low a spatial resolution.

Our Galaxy and M31 are similarly classified and have been seen as quite comparable (Stephens et al., 2003). However, recently, significant differences have become obvious (Durrell et al., 2001; Ferguson et al., 2002; Brown et al., 2003; Burstein et al., 2004). The globular clusters of the Galaxy and M31 show many similarities but also striking differences (van den Bergh, 2000). New data indicate so far unknown characteristics of the Magellanic Clouds and M31, while the other Local Group galaxies are even less understood. Thus, even for the most nearby galaxies, we have no consistent picture of evolution. Furthermore, it is currently impossible to quantify the effect of environment on the formation and evolution of galaxies if we are restricted to studies in a very local area around one galaxy, our Milky Way, as we are at present. For a representative sample of galaxies, we must reach the Virgo Cluster of Galaxies with sufficiently high spatial resolution and light collection.

While the Virgo Cluster offers an ideal galaxy sample, at 16 Mpc it is ten times as far away as the most distant LG members and well beyond the reach of current telescopes even with adaptive optics. This is even more obvious for the Fornax Cluster of Galaxies at a distance of 20 Mpc. At the end of 2004, we remain far from having an adequate understanding of any external galaxy. This is clear from new results for our neighbour galaxies, the Magellanic

Clouds (Romaniello et al., 2004; Ferraro et al., 2004; Dall'Ora et al., 2004; González et al., 2004) as well as M31 and M33 (Salow and Statler, 2004; Burstein et al., 2004; Williams and Shafter, 2004; Ciardullo et al., 2004).

The spatial resolution of a diffraction-limited large optical telescope is critical to overcome crowding, and a 100m class telescope is required to study the brighter galaxies at their half-light radius – without it work is limited to the less representative outer regions where crowding is less of an issue. The more luminous elliptical galaxies and bulges are of lower surface brightness (Kormendy 1977), aiding this endeavour.

With an ELT, long-lived stars, comparable in mass to the Sun, may be resolved in galaxies out as far as the Virgo cluster. As shown in the following sections, one may obtain deep colour-magnitude diagrams and spectra of stars of all ages in all environments (with the exception of only the very dense inner regions). This would be the first opportunity to analyse in detail the stellar populations across the entire Hubble Sequence of galaxies, including ellipticals.

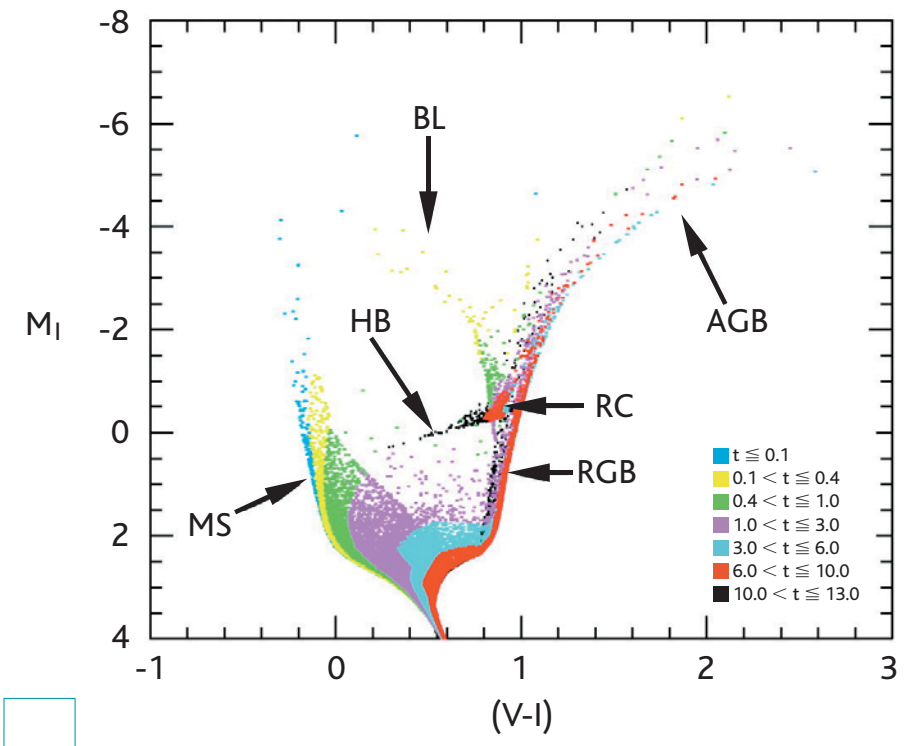

fig.4.1

Synthetic Colour-Magnitude Diagram computed using constant star formation rate from 13 Gyr ago to the present and with metallicity linearly increasing from Z = 0.0001 to Z = 0.02. The Bertelli94 stellar evolution library and the Lejeune et al. (1997) bolometric correction library have been used. Stars in different age intervals are plotted in different colours, and the colour code is given in the figure, in Gyr. Labels indicate the different evolutionary phases: BL – blue loop; HB – Horizontal Branch; RC – Red Clump; RGB – red giant branch; AGB – asymptotic giant branch; MS – main sequence. From Aparicio & Gallart (2004).

4.2.1 The Hubble Sequence: Understanding Galaxy Formation and Evolution

The age distributions for the oldest stars in galaxies across the Hubble Sequence have a particularly important role in constraining theories of galaxy formation. Determining the epoch of the onset of star formation in disks is a crucial constraint on hierarchical-clustering models, since currently the only mechanism to form large extended disks as observed, within Cold Dark Matter dominated models, is to delay their formation until after a redshift of unity (Weil, Eke & Efstathiou 1998; Thacker & Couchman 2001). This could be disproved by the identification of significant populations of old stars in disks at large galactocentric distances. Such observations could be achieved with a 100m-class telescope through deep Colour-Magnitude Diagrams for the inter-arm regions of disks, with an emphasis on the low surface brightness outer regions, out to the Virgo cluster. At even greater distances, identification of Blue Horizontal Branch stars in outer disks would be a significant constraint. Such data also constrains the law of star formation in disks (e.g. Ferguson et al 1998), since some models posit a "threshold" gas surface density before star formation occurs.

The age distributions of stars in bulges and ellipticals are obvious discriminants of theories of their formation. Were bulges to be associated with inner disks, as 'bar-buckling' models for bulges would predict (e.g. Combes et al. 1990), then the ages of inner disks and bulges should be more similar than if bulges and disks are separate and distinct. If bulges date from the last merger event that occurred with a mass ratio of close to unity, with the disk being accreted subsequent to that event (e.g. Kauffmann 1996) then one would expect that bulges surrounded by larger disks would be older than bulges surrounded by smaller disks. Further, in this picture ellipticals are just bulges that have not been able – either through lack of time, or through being in a crowded environment – to accrete a disk, and there should be strong similarities between bulges and ellipticals.

4.2.2 Chemical Evolution – spectroscopy of old stars

Spectroscopy allows us to delve more deeply into the chemical evolution of a galaxy using the chemical abundance ratios that are frozen in the unprocessed gas in the outer regions of red giant branch stars. This allows a direct measure of the metal enrichment of the gas out of which the star was formed at the time it was formed. Therefore, we can directly measure elemental abundances at different stages in the star forming history of a galaxy by looking at abundance ratios in stars with a range of ages.

It is possible to carry out spectroscopy of red giant branch stars at intermediate resolution (R=3000–8000) to measure the equivalent widths of strong lines of elements like Mg or Ca that have been empirically calibrated to relate to the metallicity (or iron abundance) of the star in which they are measured, e.g. the Ca II triplet absorption lines at 8500A (Figure 4.2). This is merely considered a metallicity indicator – it gives a rough estimate of the total enrichment of the star but no details about what may have enriched it to this level. For that, higher resolution spectroscopy of red giant branch stars is required (R>20000) where individual lines of many elements can be detected and interpreted (Figure 4.3).

Spectroscopy thus allows us to go one step further than Colour-Magnitude Diagram analysis, which, if Main Sequence Turnoffs (MSTO) are reached gives the most accurate age determination of the episodes of star formation in the life of a galaxy but it does not provide direct evidence for chemical evolution processes. Spectroscopy at sufficiently high resolution allows the measurement of a large variety of elemental abundances impossible from photometry alone. The combination of detailed Colour-Magnitude Diagrams and abundance ratios covering the whole age range of star

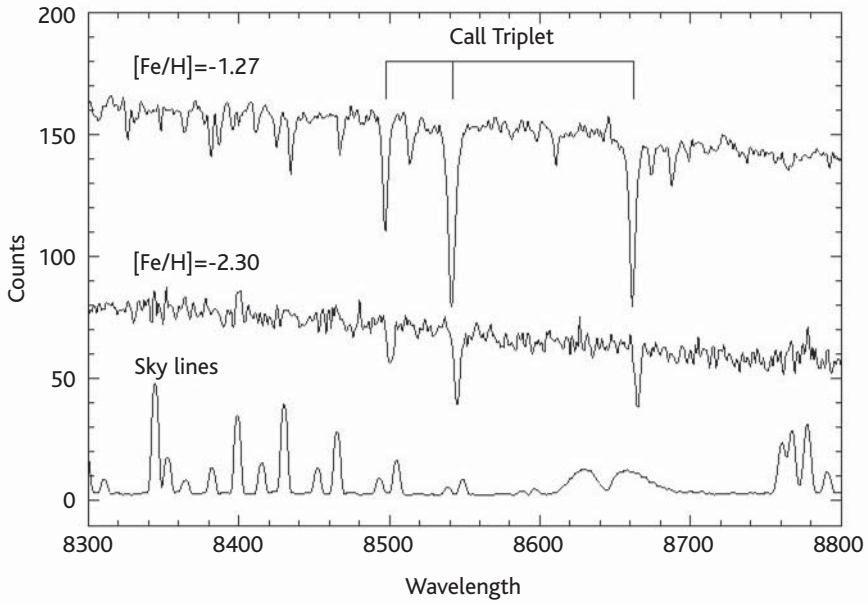

fig.4.2 Intermediate resolution VLT/FORS1 spectra of two stars with different metallicities in the Sculptor dwarf spheroidal galaxy taken in the CaII triplet spectral region. Also shown for comparison is the sky line distribution (although not to scale). From Tolstoy et al. (2001).

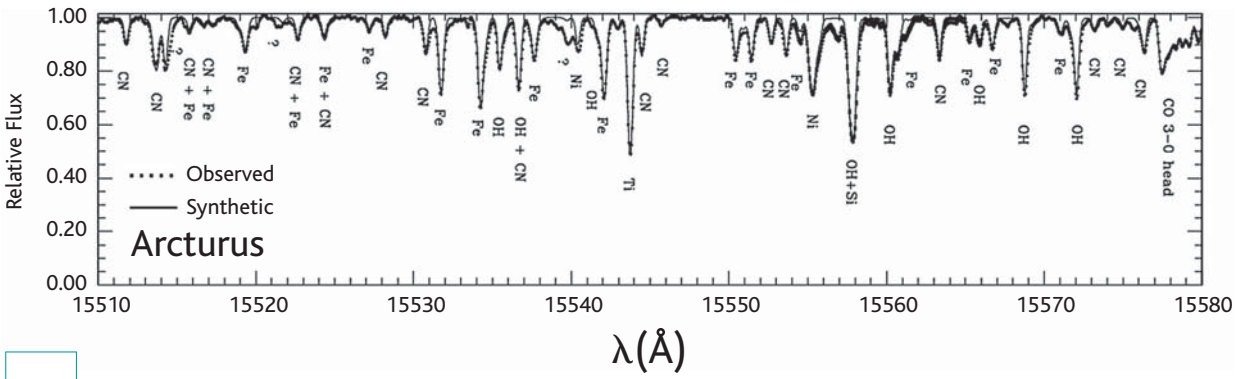

fig.4.3

A Gemini-Phoenix infrared high-resolution spectrum of the nearby star Arcturus. The observed (dotted line) and synthetic (solid line) are shown in the region 1.551-1.558 microns. From Melendez et al. (2003).

formation activity gives us detailed information about the exact relationship between star formation and metal enrichment in a galaxy. This can provide insights into the details of supernova enrichment of the interstellar medium with time and also the role of gas infall and outflow in the evolution of a galaxy.

Using abundance analysis we can thus address the questions of whether the Milky Way is a typical spiral galaxy, the Local Group a typical galactic environment. By measuring the distribution of ages, chemical abundances – including detailed elemental abundances – and accurate kinematics for a range of spiral galaxies in a range of environments this fossil record may be used to derive the two complementary aspects of galaxy formation and evolution – the mass assembly history and the star formation history. These are likely not to be the same, but are probably related through such effects as tidally-induced star formation. The mass assembly history is complicated since one really wishes to distinguish whether the mass being added is baryonic, non-baryonic, gas, stars etc. Evidence is written in the stellar kinematics, in that signatures of previous orbits can persist, particularly in angular momentum (see section 4.6), and in the stellar(atmospheric) chemical abundances, which are essentially unchanged throughout most of a star's life and so stars of different ages can be used to measure abundance ratio variation with time (see Figure 4.4). The star formation history is given in the age distribution, and this together with the chemical abundances allows chemical

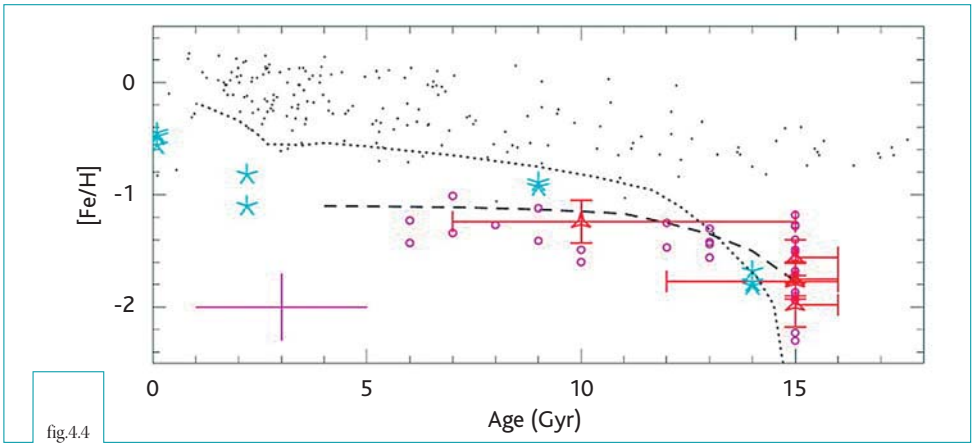

fig.4.4

Measured metallicities for individual stars in the nearby dwarf spheroidal galaxy, Sculptor. The CaII triplet metallicities from Tolstoy et al. 2001 are shown as small circles, where the typical error bar is noted in the lower left. Direct iron abundances from VLT/UVES spectra (Tolstoy et al 2003) are shown as red triangles with error bars. Also shown are LMC star cluster iron abundances from Hill et al. (2000) (blue stars) and the LMC chemical evolution model, by Pagel & Tautvaisene (1998) as a dotted line. The numerous small dots show the iron abundances in Galactic disk stars by Edvardsson et al.(1993). The dashed line is a model metal enrichment pattern from a Colour-Magnitude diagram based age distribution of the stars.

evolution models to be developed that constrain gas flows etc. and allow a test of the validity of star formation 'laws' (e.g. Wyse & Silk 1989; Kennicutt 1989; Gilmore & Wyse 1991).

From high-resolution spectra the most basic measurement that can be made is the iron abundance, [Fe/H], in the atmospheres of red giant branch stars. From high-resolution spectra numerous lines of Fe I and even Fe II can be measured, which allows the determination of an exceptionally accurate [Fe/H] value. From high-resolution spectra there are also a host of other elements for which an accurate abundance can be obtained. These give us additional insights into the details of past star formation processes in these galaxies (e.g. McWilliam 1997).

Light elements (e.g. O, Na, Mg, Al) allow us to trace "deep-mixing" abundance patterns in RGB stars. This is a very distinctive pattern of abundances that are markedly different in globular cluster giants and field stars. There are also the group of alpha-elements (e.g. O, Mg, Si, Ca, Ti). The production of these elements is dominated by Type II supernovae (SNe II). The alpha-abundance limits the number of SN II explosions that can have polluted the gas from which the star was made and, thus, contains estimates of the fraction of lost ejecta and/or IMF variations in the stellar populations of a galaxy through time. The iron peak elements (e.g. V, Cr, Mn, Co, Ni, Cu, Zn) are mostly believed to be the products of explosive nucleosynthesis. The level of the iron peak can (in principle) limit the most massive progenitor that can have exploded in the galaxy (e.g., Woosley & Weaver 1995). Heavy metals (Z > 30, e.g. Y, Ba, Ce, Sm, Eu) enable a distinction to be made between the fraction of s-process and r-process elements in a star, and this again puts detailed constraints on the number and type of past SN explosions. The [Ba/Eu] ratio can be considered an indicator of the contribution of AGB stars to the chemical evolution process. Since AGB stars have a several gigayear timescale for chemical contamination of the ISM they provide yet another type of clock.

With a 100m class E-ELT it will be possible to obtain Ca II triplet metallicites for old red giant branch stars (V=28) in the Virgo cluster, however high resolution spectroscopy and detailed abundance analysis of red giant branch stars is only possible out to M31 or CenA, even with a 100m telescope. Spectroscopic studies of old stars at the distance of Virgo will also require pre-imaging with photometric accuracy at the high spatial resolution and sensitivity of a 100m telescope to make detailed colour magnitude diagrams and select red giant branch star candidates for spectroscopy.

4.2.3 The resolved stellar population targets for the European Extremely Large Telescope

"Cosmic variance" requires that we study a statistically significant sample of each morphological type of galaxy in order to be able to confront theoretical predictions in a robust way. The distribution of galaxies in the nearby Universe is non-uniform. While the nearest dwarf galaxies are only tens of kpc removed, the nearest large spiral, M31, is ~750kpc distant. Farther away, at distances of ~2-3Mpc, many dwarfs and some large spirals are found in the nearby Sculptor and M81/M82 groups of galaxies. M82 is the nearest 'starburst' galaxy with a significant population of young massive star clusters. Centaurus A is a peculiar elliptical galaxy, providing one example at a specific place along the merger sequence. The well-known morphological-type vs density relation

Object	$(m-M)_0$	θ(1 pc)	RA	Dec
LMC	18.5	4"	05 23	–69 45
M31	24.3	0.3"	00 43	+41 16
Sculptor Group	26.5	0.11"	00 23	–38 00
M81/82	27.8	0.06"	09 55	+69 40
Cen A	28.5	0.04"	13 25	–43 00
NGC3115	30.2	0.02"	10 05	–07 42
Virgo Cluster	30.9	14 mas	12 26	+12 43
Antennae Galaxy	31.5	10 mas	12 00	–18 53
50Mpc	33.5	4 mas	...	...
Arp220	34.5	2 mas	15 34	+23 30
Perseus Cluster	34.5	2 mas	03 18	+41 31
Stephan's Quintet	35.0	2 mas	22 36	+33 57
Coma Cluster	35.0	2 mas	13 00	+28 00
Redshift z~0.1	38.5	0.5mas		...
Redshift z~0.3	41	0.2mas		...

Table 4.2 Potential targets for the European Extremely Large Telescope.

describes the fact that only in clusters of galaxies are there examples of elliptical galaxies of the whole range of luminosity; thus to gain an understanding of this morphological-type – density relation, and its importance in the physics of the Hubble Sequence, the Virgo or Fornax clusters, at a distance of ~15Mpc, must be within each. The Antennae galaxy system is the nearest example of an ongoing 'major merger'. NGC 3115 is an SO galaxy with a bimodal field stellar halo and globular cluster system, perhaps indicative of a merger event, and a well-established central supermassive black hole. Table 4.2 gives the distance moduli of these galaxies and clusters, and the angle subtended by 1pc at their distances.

For comparison, the diffraction limit of a 100m telescope is 0.8 milliarcsec at 300nm, 2.2mas at 800nm, and 6mas at K-band (2.2mm.) Note that these angular resolutions are comparable to those obtained by radio VLBI techniques, allowing very complementary observations on similar scales.

Determination of the age distributions of the stellar components of galaxies requires that the study include the oldest stars, those with a main sequence lifetime that is of order the age of the Universe. Stars like the sun, on the main sequence, with $M_V \sim +4.5$, $M_K \sim +3$, can, with a 100m-class telescope, be studied right out to, and including, the Virgo cluster. Evolved low-

mass stars, on the upper RGB (hence fainter than around M_V ~ –2.5, M_K ~ –6.5, TRGB/AGB (see fig.4.1)) can be studied all the way to redshifts of around z~0.1, while massive stars and star clusters will be accessible at cosmological distances, z above ~ 0.3.

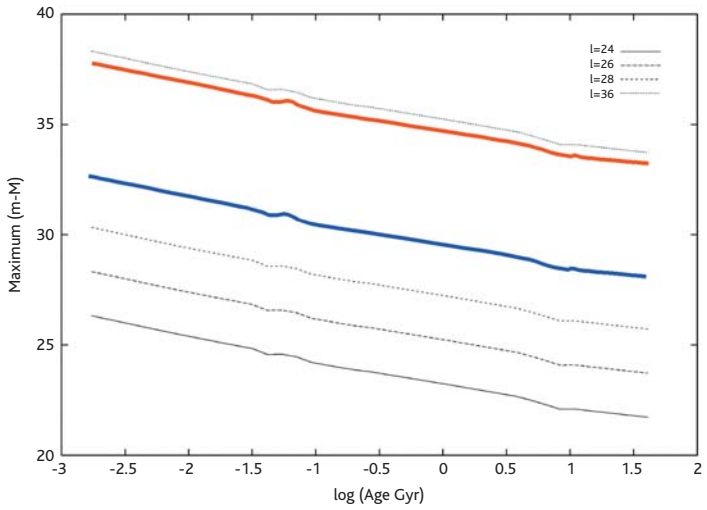

Fig.4.5

(From Frayn 2003) Results of simulations showing the maximum distance to which the main sequence turn-off can just be resolved as a function of population age and limiting magnitude. The thicker lines represent the limiting magnitude that can be reached with a 30m (lower, blue line) and 100m (upper, red line). Thus to detect the main sequence turn off for all stellar ages at the distance of Virgo (distance modulus of approximately m-M=+31.0) requires a 100m-class telescope.

4.2.4 Technical issues and design requirements

At the distance of the Virgo cluster, a solar metallicity, solar mass main sequence star has V ~ 35.5. Thus, provided one is not limited by crowding (see Table 4.4), a 100m class telescope will allow deep Colour-Magnitude Diagrams to below the oldest turn-off (see Figure 4.1), moderate resolution spectroscopy of the lower RGB (Figure 4.2), and high-resolution spectroscopy of the upper RGB/AGB (Figure 4.3), and of course of more massive stars.

Star type	M_V	M_K	10m	100m	10m	100m
			V		K	
Massive stars	**-2.5+**	**-1.5+**	35.1+	40.1+	28.2+	33.2+
TRGB/AGB	**-2.5**	**-6.5**	35.1	40.1	33.2	38.2
RGB stars	**-0.5**	**-2.5**	33.1	38.1	29.2	34.2
HB stars	**0.5**	**-2.0**	32.1	37.1	28.7	33.7
Old subgiants	**3.5**	**2.5**	29.1	34.1	24.2	29.2
Oldest turnoff	**4.5**	**3.0**	28.1	33.1	23.7	28.7
Oldest turnoff +1	**5.5**	**4.0**	27.1	32.1	22.7	27.7

Table 4.3

Photometric Limiting Distance Moduli for Imaging, Isolated Stars, Diffraction Limited (V=36.6, K=31.7). Assumed limiting magnitudes (S/N=10) are based on 10,000 sec integrations, $1e^-$ readnoise, sky background 21.5 (V), 12.5 (K) assuming a 100m aperture.

With a 100m telescope we would be able to obtain detailed images of galaxies out to the Virgo cluster and carry out photometry of main sequence stars (V=35, see below). We will also be able to carry out intermediate resolution (CaII triplet) spectroscopy of the red giant branch stars in Virgo (V=28). For high-resolution abundances we would be able to make observations of red giant stars at the distance of M31 and CenA (V=25 – see Table 4.4).

The science of stellar populations is a strong driver to deliver close to diffraction-limited performance in the optical. *Why the optical?* A significant factor is the higher diffraction-limited resolution in the optical (a factor of 3 to 4 higher than in the infrared, corresponding to magnitudes of depth in crowded fields) – most stellar population applications are confusion-limited rather than sky-background or photon-limited and typically attainable depths are 7 magnitudes fainter in V than in K (see Table 4.4). While OH line cancellation may be technically feasible in the H band, thermal emission at redward of 2 microns is an obstacle to deep imaging from the ground. Further, the derivation of stellar parameters such as age and metallicity is much more robust in the optical than in the near-IR – for spectroscopy, the resonance lines are in the optical/UV (electronic transitions are in the optical/UV, whereas it is molecules in the IR, and these are much more complicated). While the issue of ability to measure age and metallicity in the IR needs careful study, we can get a first idea from published isochrones. Figure 4.6 shows Bertelli et al. (1994) isochrones of J-K vs. M_K, V-I vs. M_V, and V-K vs. M_V, for metallicities of Z=0.0004 and Z=0.02 and ages of 8, 10, 11, and 12 Gyr (roughly spanning the evolution in stellar populations from redshift z=1 to z=3). Including an optical filter clearly gives better age discrimination near the turnoff and better metallicity discrimination from the RGB slope, by a factor of ~2.

	Massive stars	TRGB /AGB	RGB	HB	Old subgiant	Oldest TO	Oldest TO+1
Half-light of a Bulge	33.3 26.3	31.0 27.4	33.3 31.8	29.9 26.9	27.1 22.5	26.2 22.2	25.4 21.2
Spiral arms	34.3 27.3	34.3 32.8	32.0 28.4	30.9 27.9	28.1 23.5	27.2 23.2	26.4 22.2
Interarms	35.3 28.3	35.3 33.8	33.0 29.4	31.9 28.9	29.1 24.5	28.2 24.2	27.4 23.2
Disk edges	38.3 31.3	38.3 36.8	36.0 32.4	34.9 31.9	32.1 27.5	31.2 27.2	30.4 26.2
Center of E galaxy	27.3 20.2	27.3 25.7	25.0 21.3	23.9 20.8	21.1 16.4	20.2 16.1	19.4 15.1
Half-light of E galaxy	34.8 27.7	34.8 33.2	32.5 28.8	31.4 28.3	28.6 23.9	27.7 23.6	26.9 22.6
Edge of E galaxy	39.8 32.7	39.8 38.2	37.5 33.8	36.4 33.3	33.6 28.9	32.7 28.6	31.9 27.6
Center of GC	31.6 25.5	31.6 31.0	29.3 26.6	28.2 26.1	25.4 21.7	24.5 21.4	23.7 20.4
Edge of GC	37.3 31.2	37.3 36.7	35.0 32.3	33.9 31.8	31.1 27.4	30.2 27.1	29.4 26.1

Table 4.4

Limiting Distance Moduli, Diffraction Limited, 10% Photometric Accuracy, V/K bands. These limiting distances are set by the requirement that the rms background fluctuations per diffraction-limited resolution element ($1.22\lambda/D$, D=100m) not exceed 10% of the source brightness (fluctuations are calculated assuming the luminosity function of a 12Gyr-old solar metallicity population).

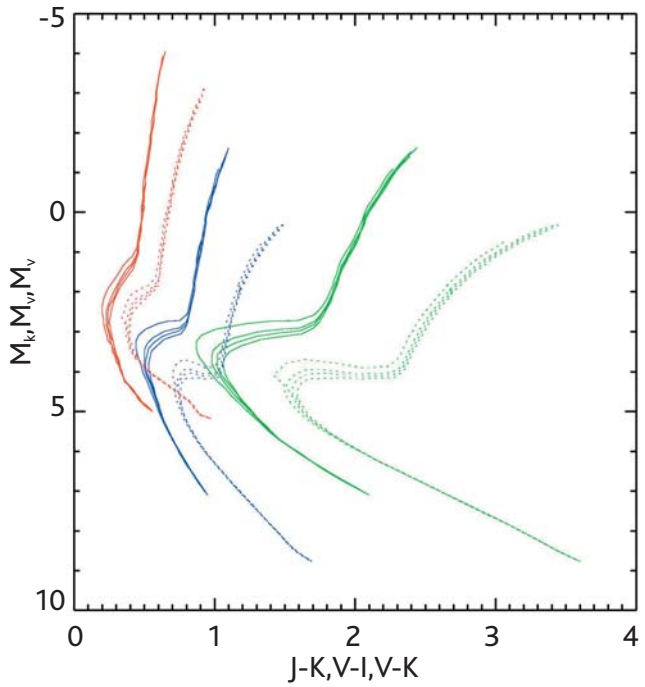

Fig.4.6 Bertelli et al. (1994) isochrones showing a comparison of optical with infrared colors. Red lines show J-K vs. M_K, blue lines V-I vs. M_V, and green lines V-K vs. M_V. The solid lines show low-metallicity (Z=0.0004) isochrones while the dotted lines represent Solar metallicity (Z=0.02). Each set of isochrones is plotted for ages of 8, 10, 11, and 12 Gyr. Note that the age and metallicity are much better discriminated if at least one optical band is utilised – such as V, I or if a V-magnitude is combined with an IR color. This is due to the higher sensitivity of the V band to metal-line blanketing.

Notes on Design Requirements

Imaging

Observation Type: Imaging

Field of View: 5 arcsec x 5arcsec or larger if possible

Spatial Resolution: Diffraction limited – the required Strehl will be determined from simulations of crowded fields. See also section 4.3 on stellar clusters. Much of this science case relies on the ability to perform high spatial resolution, crowded-field photometry at optical wavelengths. As much of this work is confusion, rather than photon, limited, it may be possible to work at quite low Strehl ratios, but detailed simulations are needed to test this. Also the limitations imposed by a PSF that is unstable in time, or rapidly varies across the field, need to be understood. Similarly, for spectroscopy of circumnuclear regions, simulations with real PSFs are required.

Spectral Resolution: R~5 (imaging)

Wavelength Range: optical and near-IR

Target Density: Crowded fields. Table 4.3 and Table 4.4 give the optical (V) and near-IR (K) magnitudes of important classes of stars, and the surface brightnesses at which confusion sets in (for 10% photometry) at the diffraction limit of a 100m telescope.

Dynamic Range constraint: to be determined from simulations

Telescope Size: 100m class telescope required to reach the MSTO for all ages at the distance of Virgo/Fornax.

Observing time: 10 hours to reach V=35, for a S/N~20

Notes on Design Requirements

Spectroscopy

Field of View: few arcmin or greater

Spatial Resolution: 2-20mas

Spectral Resolution: R=3000-8000 and R~20,000 – 40,000

Wavelength Range: V to K

Target Density: see imaging case above

Dynamic Range constraint:

Telescope Size: 100m class needed for faint targets and high spatial resolution.

Observing time: hours-days. For V=28 (e.g. Red giant branch stars in Virgo), intermediate spectroscopy with a FLAMES LR8 equivalent (i.e fibre spectroscopy), 17 hours will obtain a S/N~20; for a slit spectrograph like FORS this can be more like 5 hours. For high-resolution abundances of red giant stars at the distance of M31 and CenA (V=25), requires 16 hours to obtain S/N~40 using a FLAMES/HR fibre spectroscopy equivalent (R~20 000). Using a slit spectrograph like UVES at higher resolution (R~40 000) we could reach S/N~20 on a V=24 star in 15hours.

Other comments: wide field imaging and MOS would improve efficiency. M31 and Virgo are northern targets and Large Magellanic Cloud and Sculptor group are southern targets.

4.3 Resolved Stars in Stellar Clusters

Fig.4.7

HST images of extragalactic star clusters: M31-G1 (left) and NGC1705 (right). Credit: left – NASA and Michael Rich (UCLA), right – NASA, ESA and the Hubble Heritage team (STScI/AURA).

For studies of evolution, stellar clusters are fundamental. Normally, all stars in a cluster can be regarded as coeval and co-distant with common initial element abundance, later modified by evolution. With their similar age, initial abundance, distance and extinction, cluster stars are ideal for evolutionary studies. They are also, normally, easy to isolate from surrounding and super-posed populations. The cluster properties are normally little affected by the orientation of the parent galaxies. Calibrations of evolutionary parameters are regularly made with clusters as standards. An example is the initial mass function (IMF; Chabrier, 2003).

To date, the Milky Way and the Local Group galaxies have proved the best laboratory to study stellar and galaxy evolution since they host stellar populations spanning a wide range of ages, metallicities and environmental conditions. Their star cluster systems, in particular, have a double major impact in this respect. Being the best examples of Simple Stellar Populations of known single age and metallicity, they are unique laboratories to calibrate the evolutionary clock, the distance and metallicity scales, and the Initial Mass Function (IMF), which are all fundamental tools used to date distant galaxies. Moreover, being important channels of star formation, they are crucial tracers of galaxy assembly and galaxy chemical and dynamical evolution.

The detailed study of the star cluster systems in all the Local Group and beyond is a recent triumph of modern astrophysics (see e.g. Geisler et al. 2003; Brown et al. 2004), thanks to the improved imaging and spectroscopic capabilities of the current generation of ground-based and space instrumentation. The homogeneous and systematic investigation of their evolutionary, chemical and kinematical properties at the level of accuracy reached in Galactic star clusters represents a formidable opportunity to learn how galaxies formed, evolve and interact with neighbours in all possible environments, age and metallicity regimes, and a major step towards the comprehension of both the Local and distant Universe.

However, such a systematic study is well beyond the capabilities of the current generation of telescopes. Indeed, about two

order of magnitudes in sensitivity and spatial resolution need to be gained, in order to properly resolve and sample the cluster stellar populations up to a few Mpc distances, where faintness, crowding and confusion are major issues. This can be achieved only with a 50–100m class telescope with efficient adaptive optics systems.

Suitable Color-Magnitude Diagrams (CMDs) and Luminosity Functions (LFs) are fundamental spectro-photometric tools to characterise the evolutionary properties of the cluster stellar populations. In order to use them in the most efficient and fruitful way, the observed samples must be:

- complete, which means that virtually all the stars in a given area of the cluster are measured down to a given magnitude level, and that reliable corrections for incompleteness can be applied below that level;
- statistically significant, which means that observations should cover most of the cluster extension and total light, in order to properly sample also rapid evolutionary stages, intrinsically poorly populated;
- accurate and suitable for all sequences and environment, which requires UV-optical-IR multi-band observations (see e.g. Ferraro 2002; de Grijs et al. 2003a). A larger spectral baseline also allows a better definition of many stellar and population parameters. Moreover, it is of primary importance to be capable of modelling stellar populations over the full range of wavelengths, in order to correctly interpret the Spectral Energy Distribution of distant galaxies in terms of age, metallicity, and star formation history. In this respect, it is worth noticing that a multi-wavelength approach to the study of stellar and galaxy evolution has become a major issue in recent years, and many projects are now using ground-based and space facilities over the full spectral range in a co-ordinated way.

Among the several photometric features which play a major role in tracing the physical and chemical evolution of galaxies, here we mention two which have a major impact and for which a 50–100m telescope is needed.

- The Red Giant Branch (RGB) Tip: this is a bright, suitable standard candle for old stellar populations (Bellazzini et al. 2004, Valenti, Ferraro & Origlia et al. 2004). Bright RGB stars can be measured in star clusters up to the Virgo distance if the spatial resolution approaches 1 mas.
- The Main Sequence Turn Off (MSTO): this is the classical age indicator (Rosenberg et al. 1999). It can be measured in all the star clusters of the local group, if the point-source sensitivity can reach V=33 mag, the current limit.

A field of view of 10x10 arcsec and spatial sampling of the order of milli-arcsec are required to properly resolve cluster stars and sample a significant fraction of the cluster light at a few Mpc distance.

4.3.1 Modelling and Simulated observations of Stellar Clusters

With individual member stars down to and below the main-sequence turn-off point (MSTO) well observed, photometry is excellent for age determinations. When the MSTO is below the limit of reliable photometry, alternative age parameters can be used, such as the position of the horizontal branch (HB), the position and upper part of the asymptotic giant branch (AGB) and the position, inclination and upper part of the red giant branch (RGB).

With accurate photometry in intermediate band systems (such as the Strömgren *uvby* system), metallicity diagrams give excellent abundance estimates. Abundances can also be derived, with lower accuracy, from HB position and colour (Monaco et al., 2003). In the following discussion, MSTO and m_1 versus $(b\text{-}y)_0$ approaches are used as an illustration. Beyond distances adequate for direct MSTO, HB, AGB and RGB data, evolutionary data can be derived from the luminosity function. In addition, with

reduced information content, integral photometry for cluster evolution (Lata et al., 2002) can reach very large distances. This last method is useful as long as the spatial resolution permits safe identification of the cluster with respect to its surrounding field.

Detailed simulations of observations of stellar clusters with an ELT with a high performance adaptive optics system have been made for this case by Ardeberg and Linde and by Frayn and Gilmore. The method and results of the Ardeberg and Linde simulations are described below.

Observed data for an open cluster was used as the starting point of the simulations. In addition, a modelled and simulated young stellar cluster was used. The cluster was placed in a two-population star field at distances in the range 1–30 Mpc and sky background was added. Images and photometry of individual cluster stars was simulated. For this illustration, the Strömgren *uvby* photometric system was assumed. Cluster ages were derived from turn-off point photometry and [Me/H] from m_1 versus (*b-y*) using standard methods. For distances from 10 Mpc to 1 Gpc, integrated (*b-y*) data were measured for age determination. ELT MSTO age determination is of high quality out to the distances of the Virgo and Fornax clusters of galaxies.

An open cluster was modelled using the intermediate-age cluster NGC 6192 which has *uvby* data (Paunzen et al., 2003) as a template. [Me/H] = –0.1 was adopted and, from a large range of data, the age 700 Myr. To improve statistics, the number of stars observed was increased threefold, locating additional stars at random CMD positions, consistent with the distribution defined by observations (see Figure 4.8).

The cluster M15 (Yanny et al. 1994; van der Marel et al. 2002) was adopted as the template for globular cluster modelling and simulation. King (1962) density profiles were assumed. For younger metal-poor populations with an age of 100 Myr and [Me/H] = –1.8, a cluster with 50,000 stars was simulated using code by Meynet et al. (1994).

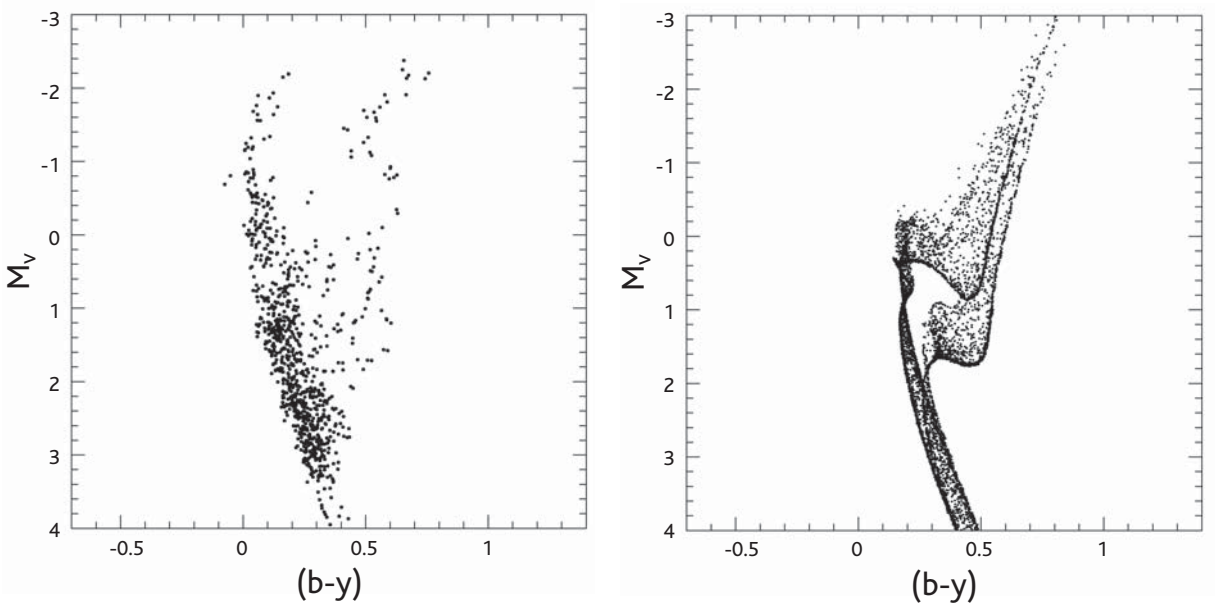

Fig.4.8

Colour-magnitude diagrams (CMDs) for the simulated cluster (left) and the cluster environment (right).

4.3.1.1 Cluster photometry with Adaptive Optics

From the assumptions listed in Table 4.5 a simplified PSF was derived (Ardeberg et al., 1999). The image profile was defined from a symmetric Airy function with a residual seeing-limited disc modelled with a Moffat function. Primary-mirror segmentation effects were neglected, as was the fact that the AO corrects the atmospheric PSF to a certain radius only, depending on actuator configuration.
For numerical reasons, the PSF was truncated. As far as can be verified, none of the simplifications should imply any significant influence on the results.

The quality of photometry delivered by an adaptive optics system depends on the on-line system corrections. In practice, the point-spread function (PSF) varies in time and with position in the field of view (Ardeberg, 2004). However, for this scientific application the fields observed would be small (of order 2arcsec by 2arcsec) and field-dependent variations should be tolerable. In contrast, time variations of the PSF require special consideration. Here it is assumed that the precision obtained is adequate for this purpose.

Image crowding dominates photometric errors significantly more than low photon flux, except for exposure times too short for this work (Ardeberg and Linde, 2004). The effects of the sky-background are insignificant compared to those of image crowding and limited photon flux. From a certain distance, the stars in a growing core region are excluded from meaningful photometry. Further out, the photometry and age and abundance analysis must increasingly rely on stars in the outer parts of the cluster. This decreases the contrast of cluster stars versus background stars, as described below. Given the strong contribution of image crowding to photometric imprecision, at larger distances an increased exposure time may well have only negligible effects on the resulting photometric quality.

Image size	2048 x 2048 pixels
Image scale	0.”001 / pixel
Field of view	2”x 2”
Pass bands	Strömgren *v, b & y*
Strehl factor in all pass bands	0.7
FWHM of seeing disc	0.”3
FWHM of PSF in all pass bands	0.”003
Maximum PSF definition size	512 x 512 pixels
Exposure time per pass band	36,000 seconds

Table 4.5

Simulation parameters.

4.3.1.2 Analysis and results

Colour-magnitude diagrams and metallicity distributions were constructed from the simulated images from 1–30Mpc (Figure 4.10). In all CMDs, zero-age main sequences were fitted and MSTO ages estimated to a nominal accuracy of 50 Myr. In the metallicity distributions, a global m_1 versus $(b\text{-}y)_0$ relation was fitted to the bright main-sequence data with a precision of 0.05 dex in [Me/H]. Beyond distances when it was possible to derive a CMD or a metallicity distribution, the cluster was measured with aperture photometry.

Figure 4.9 shows cluster images at four distances.

115 CMDs were derived, leading to the age versus distance relation in Figure 4.11. Figure 4.11 also shows integral (b-y) data and the results of the 115 metallicity distributions as a [Me/H] versus distance relation.

The visibility and ease of identification of the open and globular clusters is demonstrated in Figure 4.9 and 4.10, which shows the high quality of adaptive optics ELT CMD photometry. To 16 Mpc, the CMD retains all main features albeit with higher noise than at smaller distances. Measured data are lost due to core image crowding, increasing from 20 Mpc. Between 18 and 30 Mpc, the quality of age determinations decrease gradually. Further, there is a trend towards higher ages. This trend is a result of the relation between cluster and background stars. At modest distance, cluster stars are much more numerous in the field of

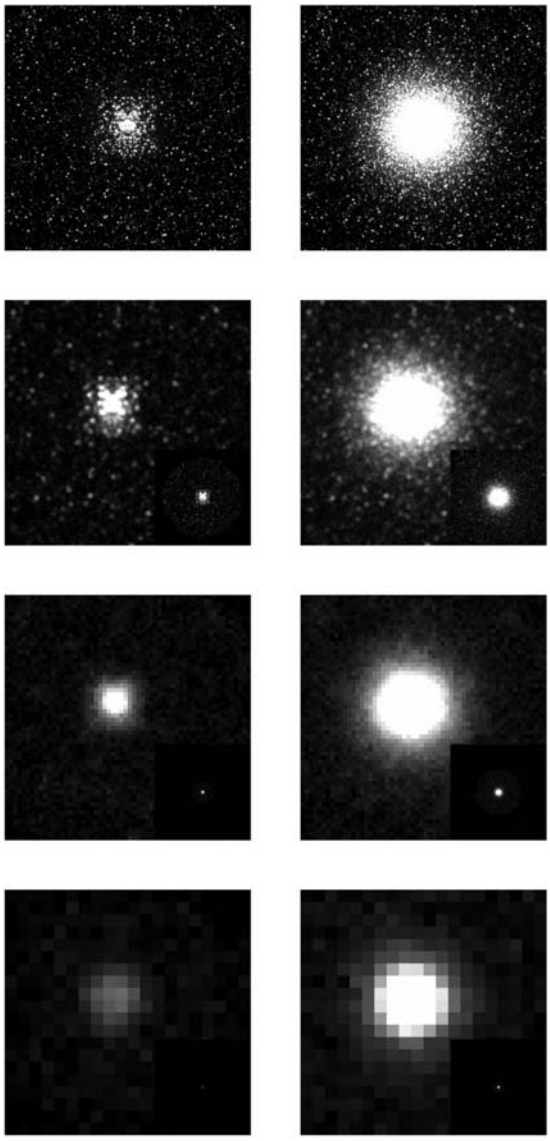

Fig.4.9

The simulated clusters as seen from distances corresponding to 10 (top), 40, 140 and 500 Mpc. To the left is the open cluster, to the right the globular. For each frame the linear size of the cluster has been kept, emphasising the decreasing image resolution. In the inset is shown the distance effect as related to 10 Mpc.

view than background stars and the CMD is virtually unaffected by field stars. With growing distance, image crowding increases from the core outwards. From 10 Mpc, the relative density of cluster and field stars changes steadily. The CMD density decreases due to loss of core stars. Field stars, of older populations, take over, and the estimated MSTO age increases. Still, to 30 Mpc, the age determinations, albeit influenced by field stars and with a large scatter, show a young cluster.

This result can be compared with that of Frayn (2003, and Figure 4.5), who considers field stellar populations. The results shown here are in good agreement with those of Frayn.

The morphology of the CMD reflects cluster evolution. Thus, the integrated colour of an open cluster is a measure of its evolution (Lata et al., 2002). Converting the Lata et al. B–V data to *b–y*, we can derive the cluster age and its apparent variation with distance (Figure 4.9 and Figure 4.10b). ELT resolution preserves the difference between a cluster and point sources to large distances, making cluster identification safe.

While high-quality MSTO data require a photometric accuracy of 0.04-0.05 mags, metallicity diagram abundances demand a colour-index precision around 0.02 mags. Hence, metallicity data are more vulnerable to photometric errors than CMD MSTO data. Figure 4.11 shows that the photometry supports a good over-all abundance accuracy out to 10 Mpc, while fair between 10 and 18 Mpc. The quality beyond 10 Mpc decreases gradually and is doubtful beyond 18 Mpc. As for the age data, in Figure 4.11, the number relation between cluster and field stars varies with distance. While the cluster stars dominate completely at smaller distances, cluster core star loss gradually modifies the relation between cluster and field stars, leading to gradually increased bias.

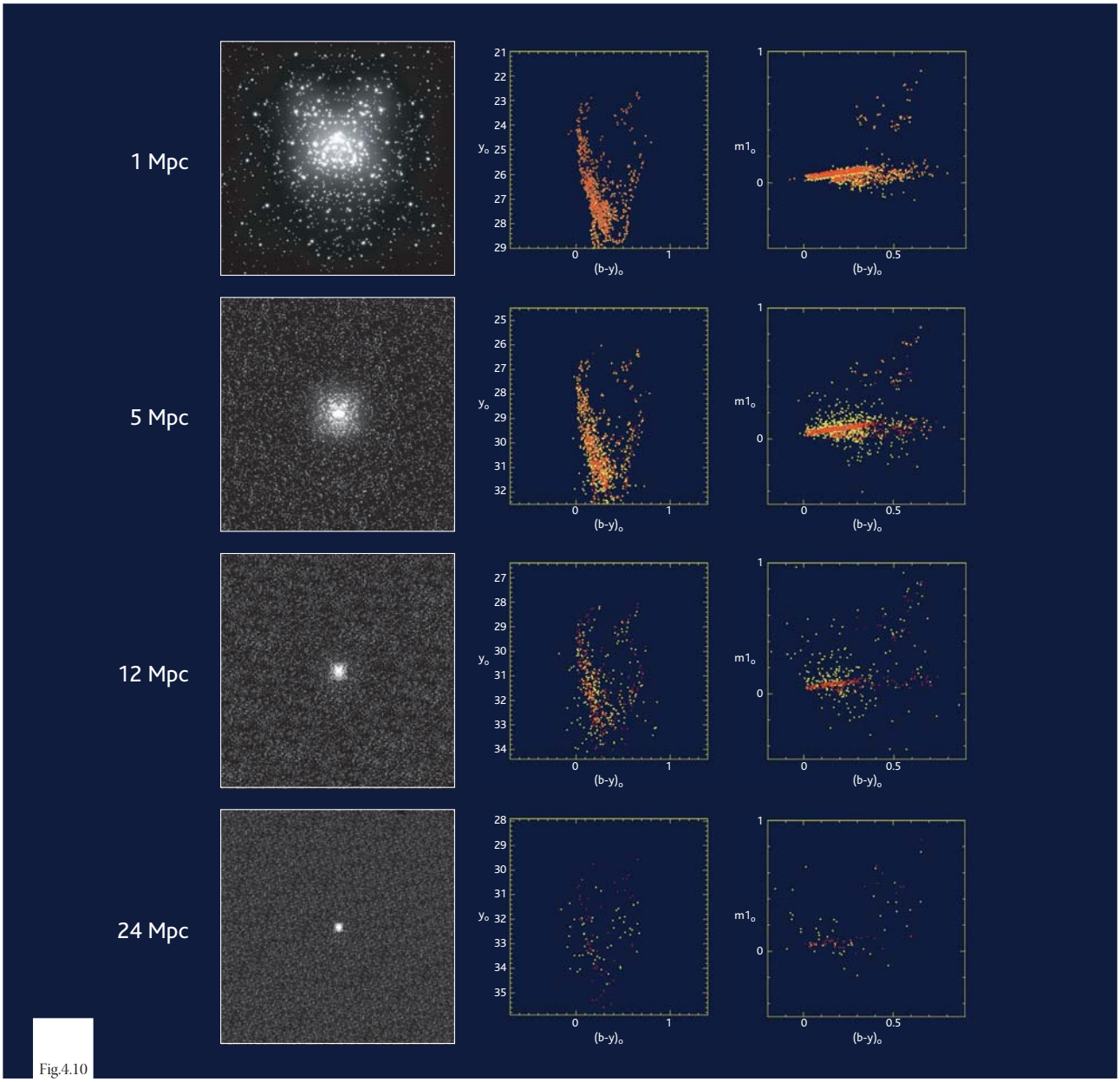

Fig.4.10

Resulting CMDs from simulated measurements of the cluster at selected distances from 1 to 24 Mpc. The yellow dots are observed values while the red dots correspond to input data.

4.3.1.3 Conclusions

For evolutionary studies of galaxies, the Virgo cluster is fundamental. The above simulations show that with E-ELT cluster photometry the evolutionary signatures of Virgo galaxies can be observed. MSTO age accuracy at 16 Mpc is good, that of abundances reasonable. Even beyond 20 Mpc, main sequence turn off ages are useful. Integrated colour data yield open cluster ages to 1 Gpc. Further work on these simulations and improvement of these methods are in progress.

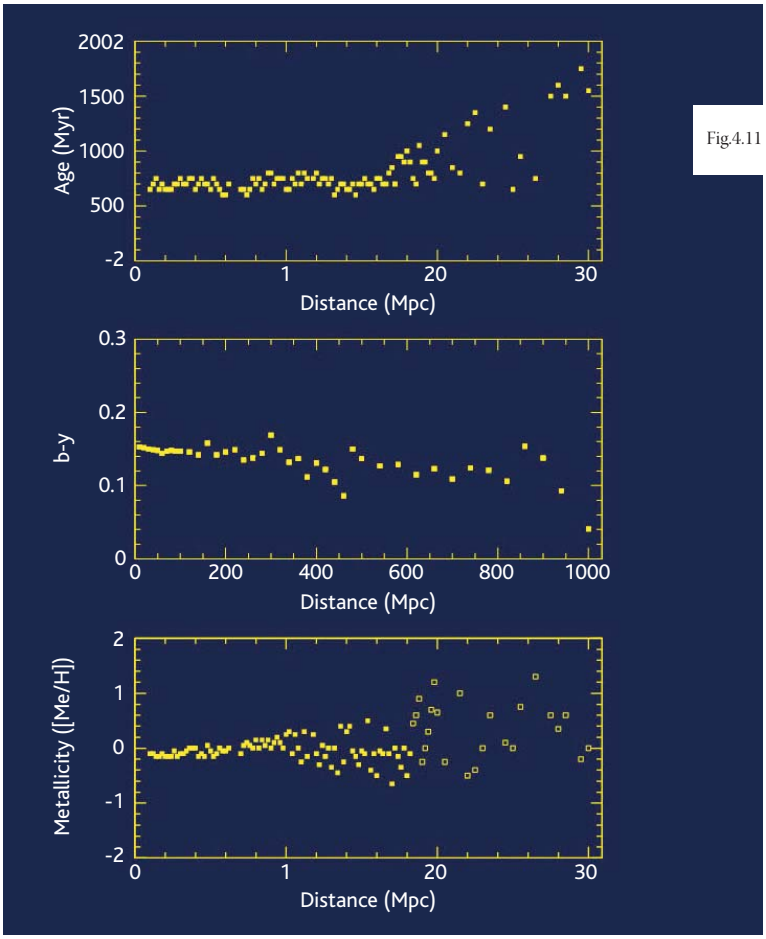

Fig.4.11

Top: Cluster ages, derived from MSTO estimation, as a function of distance. b) Middle: Cluster colour, derived from integral photometry, as a function of distance. c) Bottom: Cluster metallicity, derived from Strömgren m_1 photometry, as a function of distance.

Notes on Design Requirements

Observation Type: intermediate band (e.g. Stromgren) imaging

Field of View: 2arcsec x 2 arcsec assumed above

Spatial Resolution: 0".003

Adaptive Optics requirements for studies of Stellar Clusters

Although favourable in many respects, the small dimensions of clusters expose them to image crowding, especially at large distances. This has seriously limited the use of clusters as evolutionary probes of galaxies. With an image quality defined by the atmospheric turbulence, stellar clusters are difficult objects even in the Galaxy. However, ELTs with AO imply a new era of image quality. For example, a 50m AO ELT, such as the Euro50 (Andersen et al., 2003, 2004), will, at 1000 nm, give images close to diffraction limited, with a resolution around 0.005 arcsec. At 500 nm, it will give images with a resolution better than 0.003 arcsec.

The use of open clusters for evolutionary studies of distant galaxies has been studied preferentially here, although the use of globular clusters has also been studied. Open clusters have diameters typically around 5 pc. At 500 kpc, this matches the isoplanatic angle at good sites and single-conjugated AO would be adequate. In the wavelength interval assumed above, close to diffraction-limited image quality is assumed. With increasing cluster distance, the probability of finding member stars or surrounding stars adequate as AO reference objects decreases. Foreground stars suitable as reference objects will be available only exceptionally. With no bright object available, artificial reference objects is the solution. For cone-effect elimination, several artificial reference objects must be stacked.

Spectral Resolution: R~25 (intermediate band filters)

Wavelength Range: 0.4–0.6μm (Strömgren *b, v, y*)

Target Density: crowded fields

Dynamic Range constraint: to be determined from further simulation

Telescope Size: 50m assumed in the above simulations

4.3.2 Spectroscopic observations of star clusters

While photometric observations of star clusters provide fundamental information about their distance, age and overall metallicity, two other crucial issues must be investigated: kinematics and detailed chemical abundances. Accurate measurements of radial velocities, velocity dispersions and proper motions are indeed necessary to properly describe the dynamical status of star clusters and their host galaxy and to check for possible interactions (merging, streams, tidal stripping etc.) with neighbours.

Accurate abundance patterns of key metals like the *Fe-group, CNO*, *alpha* and neutron-capture (*s* and *r* processes) elements are crucial to disentangle primordial enrichment vs stellar nucleosynthesis (see e.g. McWilliam 1997).

Only when such a global set of fundamental information is available would it become possible to completely reconstruct the star formation history and the overall physical and dynamical evolution of the galaxies.

Medium-high resolution spectroscopy is required to obtain accurate spectral line measurements. A reasonable compromise between accuracy and depth can be found by setting as reference resolution R=30,000 with a few milli-arc seconds slits and S/N=30, which allows one to measure velocity fields down to a few *km/s* and relative abundances with about 0.1 *dex* accuracy.

Single bright giants in all the star clusters of the Local Group can be measured, while integrated spectroscopy can be performed up to the Virgo distance.

4.4 The Stellar Initial Mass Function

The distribution function of stellar masses, the *stellar initial mass function* (IMF), is one of the most fundamental astrophysical distribution functions. Only with a thorough knowledge of the IMF can the cosmological star formation history and the associated chemical enrichment of galaxies of various types, their mass-to-light ratios and photometric properties be calculated from a local evolution of baryon density, which in turn depends on the IMF through stellar feedback processes. It is thus of crucial importance to understand if and how the IMF varies with ambient physical conditions such as the temperature, pressure and chemical composition of the star forming gas. The IMF also dictates how rapidly a young star cluster evolves, first through the number of ionising photons and massive-stellar winds that expel its unused gas and later through mass-segregation, stellar-evolutionary mass loss from the cluster and relaxation.

The general form of the IMF is such that, above about 0.5$M_\odot$, the *standard stellar IMF* is a power-law with an exponent α_2=2.3 (approximately the "Salpeter" value), while at lower masses the IMF flattens (α_1 = 1.3) with a further flattening to α~0.3 below the hydrogen burning mass limit (Kroupa, Tout & Gilmore 1993; Kroupa 2002; Reid, Gizis & Hawley 2002). The mass distribution of objects that form from gravitational collapse of a molecular-cloud core thus extends from about 0.01 $M_\odot$ to about 150 $M_\odot$ where, as recent work shows, the occurrence of stars ends (Weidner & Kroupa 2004; Figer 2005; Oey & Clarke 2005). This fundamental maximum stellar mass limit appears to be rather insensitive to variations of the metallicity of the system. The average stellar mass is about 0.4 $M_\odot$.

To address the extremely important question as to whether the IMF does vary systematically with physical conditions, we need to have stellar samples for a variety of physical environments. Resolved star clusters, preferably of very young age, can provide such samples, because they constitute simple stellar populations of the same metallicity and age. Galactic-field populations, on the other hand, are complex populations with a mixture of ages and metallicities, and are composed of many dissolved star clusters. Galaxies are expected to have steeper integrated galaxial IMFs (IGIMFs) because the cluster mass function needs to be folded with the stellar IMF in each cluster. By the same argument, galaxies ought to have IGIMFs that vary in dependence on their star formation history and masses (Weidner & Kroupa 2005).

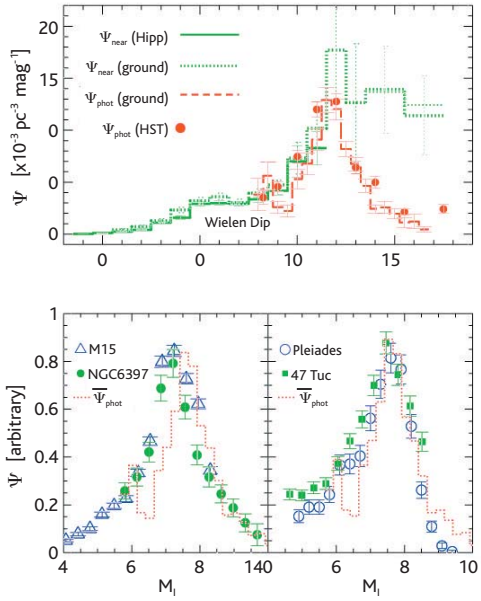

Fig.4.12

Upper panel: The V-band Solar-neighbourhood field-star luminosity function for nearby (green histogram, measured using trigonometric parallaxes) and distant (red histogram and filled dots, measured using photometric parallaxes) stars. The nearby Hipparcos sample extends to a distance limit of about 20pc, while the ground-based nearby (dotted) histogram extends only to about 5pc distance. The HST and ground-based distant LFs agree very well. The disagreement between the nearby and distant LFs is attributable to unresolved multiple systems in the latter. Lower panel: The I-band LFs of two globular clusters (left panel), and the globular cluster 47 Tuc and the young open cluster Pleiades (right panel). The red dotted histogram is the photometrical LF from the top panel, transformed to the I-band (from Kroupa 2002).

The standard stellar IMF has been measured for the typically 5Gyr old field stars in the Solar neighbourhood, and for a variety of young star clusters. It is beautifully consistent with the universal peak in the stellar luminosity function near M_V=12, M_I=9 (corresponding to a stellar mass of about 0.3 $M_\odot$) as seen in the Solar-neighbourhood luminosity function (LF) and in deep photometric surveys in the Galactic disk, as well as in metal-rich young and metal-poor old globular clusters (Figure 4.12). A systematic shift of the peak to brighter luminosities with decreasing metallicity is understood as a result of the brightening of metal-deficient stars (von Hippel et al. 1996; Kroupa & Tout 1997). Even exotic stellar systems, the dSph satellites which formed early in the cosmological time-frame and are believed to be the most dark-matter dominated objects known, appear to have had an indistinguishable IMF (Wyse et al. 2002). The chemical abundance patterns of different long-lived stellar populations also indicate an invariant IMF over large fractions of cosmological time despite very different physical conditions (Wyse 1998).

While today's mass-function measurements in virtually all clusters and OB associations, spanning a few orders of magnitude in stellar-number density, are consistent with the standard stellar IMF, one very different mass function has been measured for the young open cluster M35 below a few tenths of a Solar mass, where M35 shows a significant deficiency of stars. Global dynamical evolution cannot explain this difference because the Pleiades show a normal mass function while having a similar age (Figure 4.13). M35 has, however, a lower metallicity ([Fe/H]= –0.21) than the Pleiades ([Fe/H]=+0.01), and the M35 observations concentrate more on the central cluster region than the observations for the Pleiades. Different IMFs also seem to occur for massive stars (more massive than a few Solar masses), in that Scalo (1986) found $\alpha_{3\ field}$~2.8 for the Galactic field, while modern measurements of the massive-star IMF in very young clusters arrive at α_3=2.3 (Massey 1998). This may be a consequence of the expected difference between the IGIMF and the stellar IMF noted above.

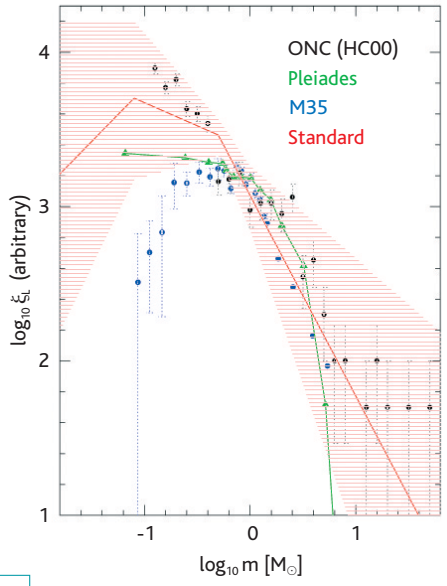

Fig.4.13

Three derived mass function for the Pleiades, the Orion Nebula Cluster (ONC) and M35, in comparison to the standard stellar IMF (from Kroupa 2002).

Thus, the only evidence for different IMFs in resolved stellar populations, in which the IMF can be deduced most straightforwardly, is M35 at low masses. While some massive, star-burst clusters appear to show a top-heavy IMF, most if not all of the reduction of α_3 in the inner cluster region can be attributed to mass segregation.

This general absence of variation, if verified, would exclude theories of star formation that sensitively depend on the cooling ability of the gas. Larson (1998) discusses the expected variation of the IMF with cosmological epoch showing that if the Jeans-mass argument holds then the average stellar mass ought to increase with redshift and decreasing metallicity. This is because the temperature of the background radiation field, below which a molecular cloud cannot cool, increases with redshift, and a lower metallicity inhibits cooling. This leads to higher temperatures during fragmentation and thus larger Jeans masses even under current conditions. Adams & Fatuzzo (1996) and Adams & Laughlin (1996) discuss a different model according to which stars control their own mass through feedback which limits the accretion, and also

find that the IMF depends on the physical conditions of the star forming gas, the characteristic mass increasing with decreasing metallicity and thus redshift. The apparent invariance of the IMF may be due to star formation being predominantly determined by the gaseous state rather than the collapse process during which the gas condenses to stars, as required by the above approaches. Compressible super-sonic turbulence in the interstellar medium may cascade down to small scales driven by shock-induced dissipation and form stars within a crossing time of the condensing molecular cloud. The spectrum of density fluctuations so produced leads to a mass distribution of gravitationally collapsing cores that resemble the observed power-law IMF form (Padoan & Nordlund 2002; Chabrier 2003).

Solutions to such fundamental questions would be advanced in a major way with improved constraints from more powerful telescopes. A 100m class telescope would allow direct imaging of individual stars down to the hydrogen burning mass limit in the local low-metallicity star-burst cluster R136 in the Large Magellanic Cloud, for example. While it has been established that R136 has a normal (Salpeter) power-law IMF above about 1 $M_{\odot}$ (Massey 1998), its form for low-mass stars is not known. To date we do not have a single star-bursting system in which the IMF is known for all stellar masses. There exists a dichotomy between the low-mass and massive parts of IMF determinations: In those very young clusters in which the massive end of the IMF has been well observed, there are no constraints for low-mass stars because such clusters are typically still hidden behind gas and dust in the Galactic disk and at large distance (more than a few kpc) or at very large distances (>50 kpc), owing to their rarity. Massive clusters that are accessible for observation are usually ancient globulars for which we do not have an observational handle on the massive-star IMF. Nearby clusters, on the other hand, are typically of low mass and do not sample the IMF for massive stars.

With a 100m class telescope many of the massive young clusters throughout the Local Group would become reachable for direct imaging of resolved stellar populations. Since a large variety of stellar systems with [Fe/H] differences over two dex would be studied, we would hopefully begin to see the systematic variations in the IMF expected from some elementary theoretical considerations. We would have a sizeable number of young massive clusters for which the IMF can be determined, for the first time, over the entire stellar mass range. By resolving individual stars in very young clusters throughout the Local Group we would also be able to significantly refine the fundamental maximum stellar mass limit, which current observations place near 150 $M_{\odot}$, and to verify that this limit does not depend on metallicity. Such data would lead to an increased effort in dynamical modelling of young and old clusters to address apparent IMF variations that will, undoubtedly, be discovered.

4.5 Extragalactic Massive Stars beyond the Local Group

The massive ($M > 8M_{\odot}$), young stellar populations of galaxies play a significant role in the chemical and dynamical evolution of their host systems – in particular via mass-loss from their stellar winds and ultimately as core-collapse supernovae. The current generation of 8-10m telescopes has enabled high-resolution spectroscopy of individual massive stars in Local Group galaxies, yielding their physical properties and chemical abundances. The main motivation of these studies has been to explore the dependence of stellar properties and stellar evolution on environment, particularly in the Magellanic Clouds which are metal-poor compared to the Milky Way (see e.g. Crowther et al. 2002; Evans et al. 2004). Key questions however remain unanswered; for instance, the behaviour of stellar winds at even lower metallicities, and the finding of nitrogen abundances for massive stars that are, in general, significantly larger than predicted by current evolutionary models (e.g. Trundle et al. 2004 cf. Maeder & Meynet 2001, 2004).

An ELT will open up a wide range of galaxies beyond the Local Group in which to expand such studies. Specifically, NGC 3109 at the edge of the Local Group is known to be metal-poor, with the main disk population thought to have a metallicity similar to that in the Small Magellanic Cloud (Minniti et al. 1999). Also nearby is the Sextans A dwarf, for which Kaufer et al. (2004) have found yet lower metallicities. Massive stars have been implicated in astrophysical phenomena such as gamma-ray bursts (e.g. Hjorth et al. 2003), and are candidates for the re-ionisation of the Universe at $z > 6$ (Haehnelt et al. 2001), so such studies would have far-reaching applications. With high-resolution (R~5,000–10,000) spectroscopy and a signal-to-noise ratio of ~100, detailed analyses of the most massive stars in NGC 3109 (with V~22–24) will be possible from integration times of a few hours; a multi-object capability would clearly increase the observational efficiency. High-quality spectra would permit accurate determination of light-element abundances and stellar parameters. These would serve as strong constraints on low-metallicity models of stellar evolution and, with successive generations of massive stars responsible for much of the chemical enrichment in their hosts, would impact on the chemical yields derived from population synthesis codes. The high spatial resolution of an ELT would also enable observations of the most massive stars in yet more distant galaxies; with a resolution of ~0.02 arcsec, stars in the Sculptor Group (at ~2Mpc) would be spatially resolved as those in the Magellanic Clouds are by current facilities. Although of lower signal-to-noise, basic physical parameters could still be derived from spectroscopy, giving us an insight into stellar physics in a very different region of the Universe from that of the Local Group.

Lower-resolution spectroscopy from an ELT would also be of considerable interest. Photometric colours of the most massive stars allow relatively little discrimination of their physical properties; only with spectroscopy can we study the upper mass-range of the IMF in clusters in systems such as M82. Furthermore, Kudritzki, Bresolin & Przybilla (2003) have advanced the so-called "Flux-weighted gravity-luminosity relationship" (FGLR) to employ the visually brightest stars in galaxies (late-B and early-A supergiants) as distance indicators. Their atmospheres are

Notes on Design Requirements

Observation Type: Intermediate to high-resolution spectroscopy

Field of View: ~1' (for e.g. NGC 3109/Sextans A)

Spatial Resolution: 0.1" to 0.02"

Spectral Resolution: R=1000 to 10,000

Wavelength Range: Primarily V and R; IJHK of some use

Target Density: A few tens per field

Telescope Size: 30–100m

Observing time: A few hours for each system

Date constraint: None

Other comments: MOS would improve efficiency

simpler to analyse than those of hotter stars and the observational requirements are less demanding. Indeed, small samples have already been observed with the VLT at low resolution (R~1000) in galaxies such as NGC 300 (at 2.0 Mpc, Bresolin et al. 2002) and NGC 3621 (at 6.7 Mpc, Bresolin et al. 2001). Kudritzki, Bresolin & Przybilla (2003) suggest that, with low-resolution spectroscopy and multi-colour photometry, the FGLR could be employed as a distance indicator almost out to the Virgo cluster using existing instrumentation. An ELT would extend the potential reach of such a technique, offering alternative distance estimates to those from other methods, e.g. from Cepheids.

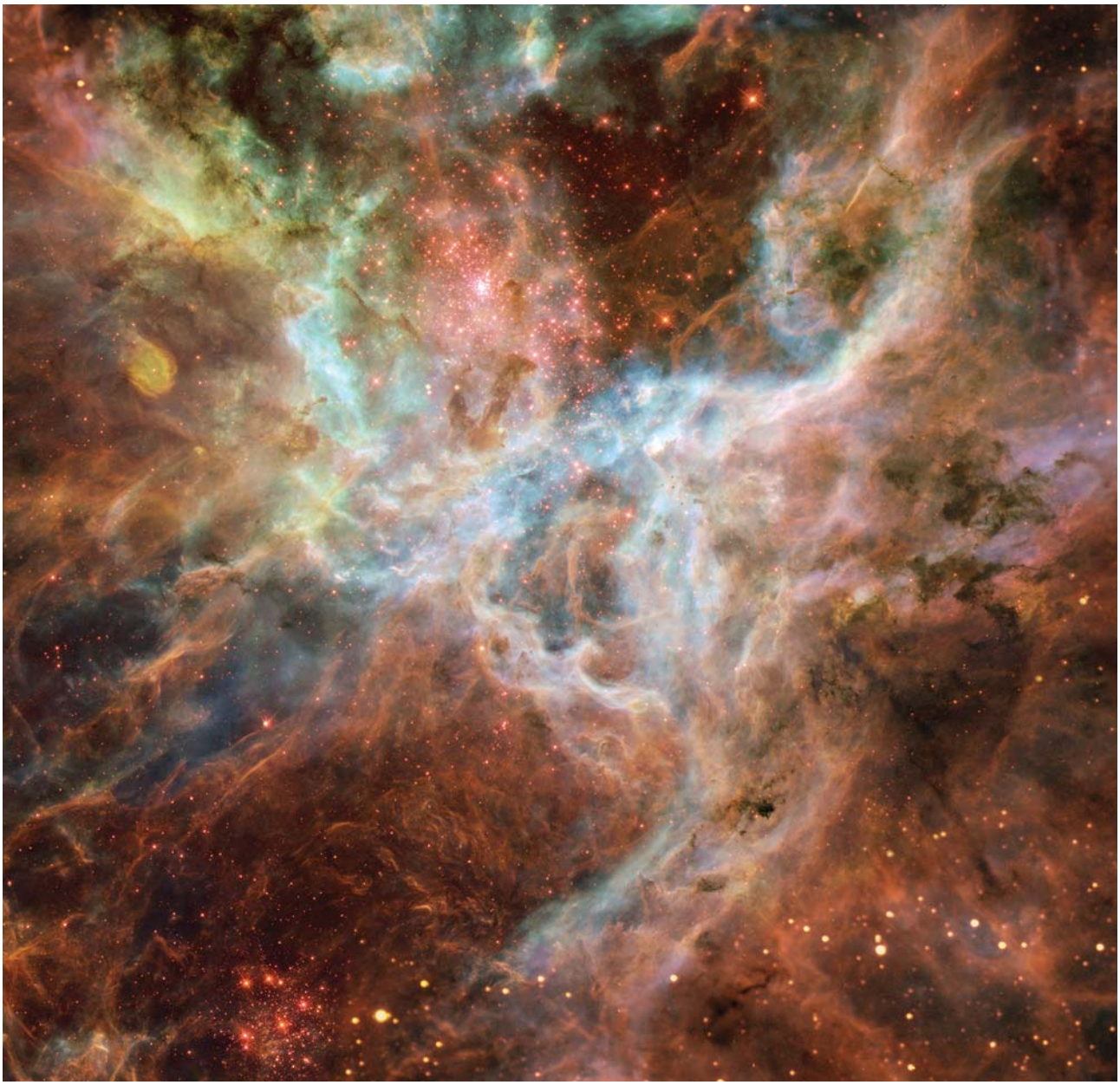

4.6 Stellar Kinematic Archaeology

Galaxies are fundamentally six dimensional objects, with as much information in the three components of velocity of their constituent stars as there is in their three spatial co-ordinates. Kinematic observations can provide unique information on two of the key properties of galaxies. First, the motions of the stars are dictated by their host galaxy's gravitational potential, so one can map out the mass distribution, and hence the arrangement of dark matter, from kinematic observations. Second, the orbits that the stars follow reflect the manner in which the galaxy was put together. Since the dynamical relaxation time of a galaxy, particularly in its outer parts, can be very long, the stellar orbits preserve an archaeological record of how the galaxy was put together.

There is, of course, nothing new in using the stellar kinematics of galaxies to try to understand their properties. However, to date most studies have had to make do with the integrated properties of the starlight to derive the stellar kinematics. At best, such studies can only extract basic measures of the dynamics of the constituent stars, such as the complete population's mean velocity, velocity dispersion, and some simple estimate of the degree to which the distribution of velocities differs from a Gaussian. These crude measures provide a horribly blurred view of the true distribution of stellar velocities; if there were some way to remove this blurring, then the gains would be at least as great as going from seeing-limited imaging to a diffraction-limited view of the spatial distribution of stars.

With an ELT, this will be possible for the first time. The spectra of individual stars that provide information on the chemical evolution of the population (see section 4.2.2) also provide the Doppler shifts of these stars. One then simply combines the inferred line-of-sight velocities for all the stars in each small region of a galaxy to obtain the complete line-of-sight velocity distribution.

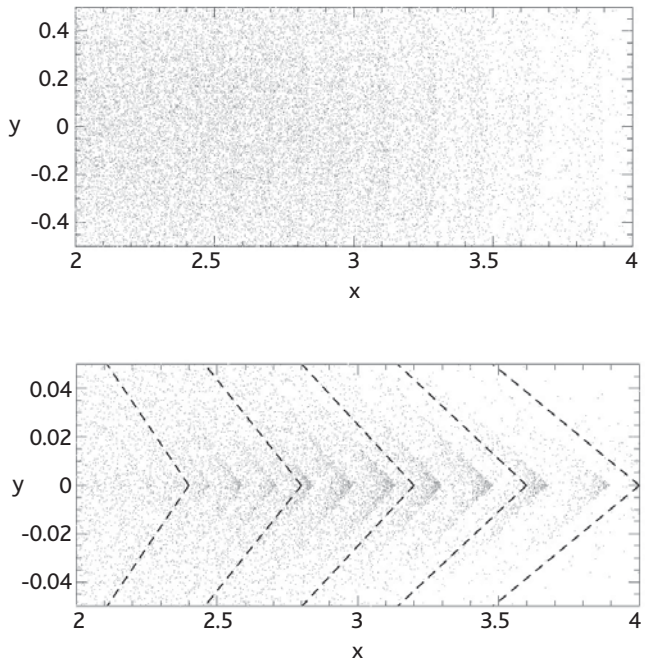

Fig.4.14

A simulation showing the stars from a minor merger that has formed a shell galaxy. The upper panel shows the observed spatial distribution of stars, in which the merger is almost undetectable, while the lower panel shows their line-of-sight velocities as a function of position, in which the signature of the successive shells of stars is readily apparent. The dashed lines show the pitch of the "arrow head" structures that one would expect on the basis of a simple dynamical model for a shell system orbiting in the adopted gravitational potential.

Some indication of the power of this technique can be inferred from the limited range of studies of individual stellar kinematics that has already been undertaken. In the Solar neighbourhood, Hipparcos demonstrated that there is a wealth of structure in the distribution of stellar velocities (Dehnen 1998). Some fraction of this structure can be attributed to the dispersing remains of the clusters in which the stars formed – the so-called "moving groups" – illustrating the long dynamical memories of galaxies as to the building blocks from which they were

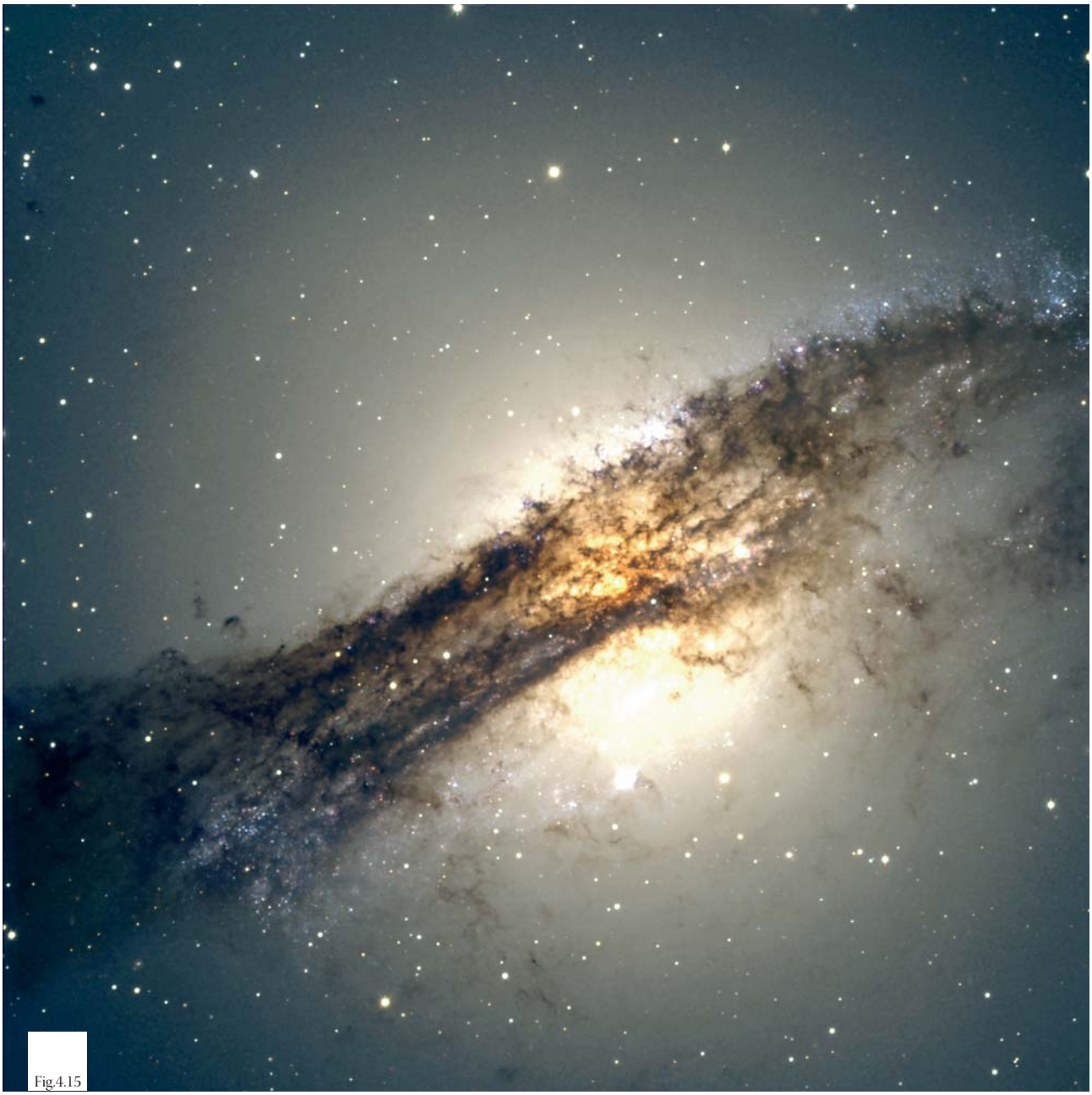

Fig.4.15

Centauris A, one of the nearest massive elliptical galaxies, still in formation as the dust lane indicates. A supermassive black hole lies at the centre of this galaxy, similar to those which power the quasars.

constructed. A little further afield, a study of the planetary nebulae in M31 has shown that a merging satellite galaxy can be traced all the way through the disk of the galaxy on the basis of its distinct stellar kinematics (Merrett et al. 2003). Even quite small samples of stars have been shown to produce intriguing results: Romanowsky et al. (2003) found that the line-of-sight velocities of stellar tracers (again in this case planetary nebulae) seem to drop in a Keplerian fashion at large radii in moderate-luminosity elliptical galaxies, perhaps indicative of a lack of a massive dark halo.

However, these results pale into insignificance when compared to what will be possible with an ELT. Extreme multi-object spectroscopy can obtain the requisite kinematic measurements for literally millions of giant stars in each galaxy. Further, target galaxies sampling the full Hubble sequence lie within reach of these measurements, allowing us to disentangle the formation histories of galaxies of all types in a range of environments. Such studies will be capable of picking out subtle elements of substructure that are currently well beyond what can be detected from integrated light studies. Indeed, minor mergers that are almost undetectable photometrically show up very clearly when the extra kinematic dimension is measured (see Figure 4.14). In fact it is thought that the entire halos of some disk galaxies could have been built from such mergers. The dynamical timescales in the outer parts of such halos are very long, so the signature of these mergers should be imprinted on the present-day phase-space distribution of halo stars (see Figure 4.15). Such observations will shed light not only on the merger history of the host galaxy, but, as Figure 4.14 shows, they determine the gravitational potential of the galaxy as well.

In fact, we can do even better. As we have seen in Section 4.2.2, each star is further identified by its metallicity. Thus, even subtler moving groups of stars can be pulled out from the kinematic data on the basis of their common metallicity, allowing the chemically-distinct building blocks of each galaxy to be disentangled. Similarly, parts of the galaxy of different ages can be isolated using their locations in the colour-magnitude diagram (Figure 4.1), providing a temporal view of the formation process.

The unprecedented size of the kinematic data sets accessible to an ELT also raises entirely new possibilities for the dynamical study of galaxies. For example, light escaping from stars near the centre of a galaxy will be redshifted by the energy it loses escaping the galaxy's gravitational potential. Typically, this signal will only be a few km/s (it scales as σ^2/c, where σ is the galaxy's velocity dispersion; Stiavelli & Seti 1993), which will be completely undetectable in each star when compared to the random velocity of hundreds of km/s in a typical elliptical galaxy. However, average together the velocities of a million stars, and the effect is detectable at the 10-sigma level for a galaxy in equilibrium. Such a measurement offers a completely novel way to determine the gravitational potential of elliptical galaxies.

Technically, the challenge is to obtain simultaneous spectra for as many stars as possible. In the outer parts of a galaxy, where crowding is not an issue, one possibility is to use slitless spectroscopy to disperse the light of all the stars. By limiting the spectral range to a small region around the calcium triplet (see Figure 4.2), the spectra can be kept to a limited size on the detector, preventing excessive blending. Even where crowding is an issue, it is worth noting that the individual stars can be "kinematically deblended": the lines in the calcium triplet have a natural width of only a few km/s, so even where the light from several stars is blended, their lines will still be distinct in any system with a velocity dispersion in excess of this low value. Not only can the velocities of the individual stars be reconstructed, but, by centroiding each individual absorption line from its contribution to the spectra in adjacent elements of an integral field unit, one can reconstruct the exact location of the star itself.

Notes on Design Requirements

Observation Type: Spectroscopy (slitless at large radii, IFU at small radii)

Field of View: a few arcseconds (with multiple observations across galaxy)

Spatial Resolution: Diffraction limited

Spectral Resolution: R ~ 10^4 to 10^5 to fully exploit "spectral deblending"

Wavelength Range: V to K

Target Density: plenty of nearby galaxies

Telescope Size: 100m

Observing Time: hours – days

Date Constraint:

Other Comments: chemical evolution data (see Section 4.2.2) are obtained from the same observations

4.7 The Intracluster Stellar Population

Cosmological simulations of structure formation predict that galaxies are dramatically modified by galaxy interactions during the assembly of galaxy clusters, losing a substantial fraction of their stellar mass which today must be in the form of intracluster stars (Murante et al. 2004). Observations now show that there is a substantial intracluster stellar population, which is observed as diffuse intracluster light (ICL; Bernstein et al. 1995; Feldmeier et al. 2002), or as individual stars, i.e. planetary nebulae (PNe; Arnaboldi et al. 2003; Feldmeier et al. 2004) and red giant stars (Durrell et al. 2002). The ICL represents up to 10% of the stellar mass in the Virgo cluster (Aguerri et al. 2005) and as much as 50% in rich Abell clusters (Feldmeier et al. 2002). The presence of a diffuse stellar component in clusters is relevant also for the discussion of the baryonic mass in clusters (Fukugita et al. 1998) and the efficiency of star formation (Balogh et al. 2001).

Within a distance of 100 Mpc, the clusters of Virgo, Fornax and Coma provide laboratories for studying the effects of different density environment on galaxy evolution and correlation of ICL properties with cluster dynamical status. Current studies of ICL in Virgo provide reliable estimates of the mean surface brightness in the Virgo core region of μ_b = 29.1 mag arcsec^{-2} (Aguerri et al, 2005); in the Coma cluster the ICL surface brightness is higher, i.e. μ_b = 25.7mag arcsec^{-2} (Bernstein et al. 1995). Assuming that the dominant population is older than a few Gyr, in the case of Virgo, we then expect of the order of a few tens of stars per square arcsec close to the turn-off, that is brighter than apparent magnitude 35. Using fields of a few tens of square arcsec with the E-ELT at a limiting magnitude of 35 in near-IR bands, it will become possible to study the HR diagrams of the ICL, and determine their age and formation history, setting important constraints on the time scales of the clusters' assembly and evolution.

The aim of the program is to obtain ages of the intra-cluster population in the Virgo Cluster measuring the magnitude of the turn-off point (TO). Given the low surface density, the intracluster population should appear as resolved using Adaptive Optics with a 100m class telescope even at the TO level. If the population is very old, with ages similar to those of galactic globular clusters (~13 Gyr), the turn-off is at M_J~2.5 and M_K~2. If the population is younger, then the TO should be brighter. It is however probable that the intracluster population shows a range of ages, with different TO's and jumps in the luminosity function corresponding to various episodes of stripping: a complete reconstruction of the history of formation of this population requires observation of the oldest TO's. Given the Virgo distance modulus (in the range $(m\text{-}M)_0$~31 to 32), the TO stars are expected to have J- and K-magnitudes of J~34 and K~33.5 respectively. Using the on-line Exposure Time Calculator of OWL, individual TO stars within the Virgo cluster should be observable in 3-4 hr exposure time at a S/N~10. A few nights of observations should be adequate for this program.

Notes on Design Requirements

Observation Type: imaging

Field of View: ~few tens of sq arcsec

Spatial Resolution: Diffraction limited – strehl required to be detemined

Spectral Resolution: 5 (imaging)

Wavelength Range: near IR (J and K)

Target Density: Few tens per sq arcsec

Telescope Size: 100m class telescope needed to reach the MS turnoff at Virgo

Observing time: Total of a few nights

4.8 The Cosmic Star Formation Rate from Supernovae

The detection and the study of high redshift supernovae (SNe) is important for at least two reasons. Firstly, their use as 'calibrated' standard candles in the local Universe (see Phillips 1993 and Hamuy 2003 for SNe-Ia and SNe-II respectively) provides a direct measurement of H_0 whereas their detection at z>0.3 allows measurements of the acceleration of the Universe and to probe the different cosmological models (Riess et al. 1998, Perlmutter et al. 1998, 1999). Secondly, the evolution of the cosmic SN rate provides a direct measurement of the cosmic star formation rate. In section 5.1 we discuss the former issue – here we illustrate the impact that the use of an ELT can have on the latter.

The rate of core-collapse SNe (II, Ib/c) is a direct measurement of the death of stars more massive than 8 $M_\odot$, although it is still a matter of debate whether stars with mass above 40 $M_\odot$ produce "normal" SNe-II and Ib/c, or rather collapse forming a black hole with no explosion, i.e. a collapsar (e.g. Heger and Woosley 2002). The rate of Type Ia SNe provides the history of star formation of moderate mass stars, 3–8 $M_\odot$, and helps to clarify the nature of their progenitors (single-degenerate or double degenerate scenarios e.g. Madau, Della Valle and Panagia 1998).

For a Salpeter IMF with an upper cut-off at 100 $M_\odot$, half of all SNII are produced by stars with masses between 8 and 13 $M_\odot$ and half of the mass in SN-producing stars is in the interval of mass 8–22 $M_\odot$.

A main sequence star with 13 $M_\odot$ has a luminosity of approximately 8000 $L_\odot$ and a temperature of 22000 K, and a star with 21.6 $M_\odot$ has L ~3.5×10^4 $L_\odot$ and T_{eff} ~27000 K. This means that more than half of the stars producing SNe are poor sources of ionising photons and of UV continuum photons, and that the bulk of the UV radiation, both in the Balmer and in the Lyman continuum is produced by much more massive stars. Actually, starburst models (e.g. Leitherer et al. 1999) suggest to us that stars above 40 $M_\odot$ produce 61% of the 912–2000A UV continuum and 87% of the Lyman continuum photons.

It follows that *both* the H-alpha flux *and* the UV flux are measurements of the very upper part of the IMF (about M>40 $M_\odot$) which is representative of only 8% of stars with masses larger than 8 $M_\odot$, and, therefore, are *not* good star formation rate indicators because (a) they require a huge extrapolation to lower masses, and (b) are very uncertain because their exact extrapolation depends crucially on the upper mass cutoff that is by no means a known quantity, nor a constant quantity in different environments (e.g. Bressan, Della Valle and Marziani 2002).

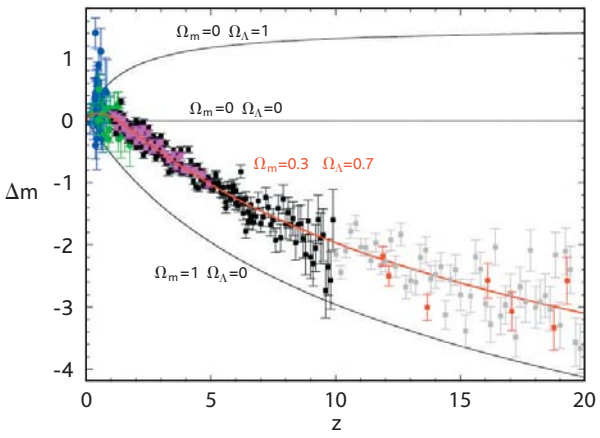

Fig.4.16

Simulated Hubble diagram, normalised to a cosmological model for an empty Universe, for supernovae out to redshift 20. Pink dots are simulated Type Ia SNe, black dots Type II (+Ib/c), blue and green dots are Ia SNe actually discovered by ground based telescopes (Perlmutter 1998, 1999; Riess 1998; Knop et al. 2003, Tonry et al. 2003) and from HST (Riess et al. 2004). The SNe have been distributed around the track Ω_M=0.3, Ω_Λ=0.7 after taking into account the intrinsic dispersion of the peak of the luminosity of type Ia and II SN populations, while the photometric errors have been derived from the S/N ratio that has been computed for each simulated observation. Red dots represent SNe from PopIII star population (see text for discussion of the rates of Pop III SNe).

If we are concerned that we may miss a SN because of extinction (e.g. Mannucci et al. 2003), we also note that a 'typical' SNII reaches typically a rest-frame B magnitude of –17.5 (Patat et al. 1994), whereas a starburst with a mass of 10^6 $M_\odot$, which produces as many Lyman continuum photons as our entire galaxy (10^{52} ionising photons per second) has an absolute B magnitude of only –15.2 and thus could be missed even more easily.

The expected number of SNe in a realistic ELT AO-corrected field of 2arcmin x 2arcmin has been computed by extrapolating the SN rates estimated by Madau, Della Valle and Panagia (1998) and Miralda-Escudé & Rees (1997). Mannuci, Della Valle and Panagia (2005) estimate ~ 4–7 SNe of Types Ia, Ib/c and II per field/yr up to z~5–8.

The explosion rate for PopIII SNe was taken from Mackey et al. (2003). However, recently Weinmann & Lilly (2005) found that this rate may be too high and it should be decreased by an order of magnitude. In this paper we assume as an estimate of the rate of PopIII SNe (up to z~15) in a 2 x 2 arcmin^2 ELT field:

$R_{SNe\text{-}III} \sim f \times d \times 5 \times 10^{-2}$/yr

where f is an efficiency factor ranging between 1 (Mackey et al. 2003) and 0.1 (Weinmann & Lilly 2005) and d the duration (in years) of the SN peak. According to Heger et al. (2001, their Fig. 3) *d* is about 1 (at 2-3μm, in the observer rest-frame), therefore, one should be able to observe, during a survey of 50 fields with an ELT, about

$f \times 5 \times 10^{-2} \times 50$ fields ~ f x 3 SNe.

Therefore, taking 4 exposures at time intervals of 3 months, one would expect to detect about 4–7 SNe/field/yr up to z ~ 5-8 (of Types Ia, Ib/c and II). Of these about 0.5 per field per year would be Type Ia. In the range z ~ 10-15 we would detect: $f \times d \times 5 \times 10^{-2}$/yr/field SNe from the Pop III stellar population.

In conclusion, E-ELT could generate a SN sample which provides a measurement of the star formation rate up to z~10 which is:

- *independent* from other possible determinations;
- *more direct,* because the IMF extrapolation is much smaller, and, possibly;
- *more reliable,* because it is based on counting SN explosions, i.e. explosion of STARS, rather than relying on identifying and correctly measuring the source of ionisation (if using the H-alpha flux) or the source of UV continuum.

Notes on Design Requirements

Observation Type: imaging (to find SNe) and spectroscopy (to obtain redshifts and types)

Field of View: 2 arcmin x 2 arcmin assumed above

Spatial Resolution: Calculation assumed a Strehl of 0.5 in K

Spectral Resolution: 5 (for imaging) and ~2000 for spectroscopy

Wavelength Range: near-IR : J,H and K bands

Target Density: About 4–8 SNe in a 2 x 2 arcmin field per year.

Telescope Size: D=100m has been assumed in these calculations (which also made use of the ESO ELT exposure calculator). A D=50m telescope is still acceptable.

Observing time: This project requires imaging 50 fields in the J(1h each), H(1h each) and K(1h each) bands at 4 different epochs for the 'Supernova search' complemented by 3 epochs in the K band for the photometric follow-up of about 350 SNe up to z ~ 10 and finally 4h to get the spectroscopic classification up to z~ 4.5/5. Thus the total time= 3 x 4h x 50(=600h) + 3h x 50(=150h) + 4h x 50(=200h)= 950h, equivalent to about 4 months, to study 400 SNe (200 of which also spectroscopically). This is not a huge number, indeed it is comparable to the size of current Treasury Programs (~ 450 orbits) or with the potential performances of the UWFC (on HST after WFC3) which is expected to discover about 500 SNe (at z <1.7) in about 6 months of time dedicated or with future performances of SNAP, about 2000 SNe at z <1.7 in 2 years.

4.9 Young, Massive Star Clusters

Stars, and in particular the most massive stars, rarely form in isolation. In fact, it is now well established that the vast majority of active star formation occurs in clusters of some sort. Star clusters are therefore both current and fossil records of episodes of higher-than-average star formation in their host galaxies.

In order to study the stellar content of clusters of various ages and at increasingly large distances, one would of course like to have access to diffraction-limited observations. While the theoretical diffraction limit of a 100m-class telescope is 1–2 orders of magnitude smaller than that of the current best instrument, the Hubble Space Telescope, ground-based observations are crucially dependent on the availability of adaptive optics. Assuming adaptive optics can be realised on an E-ELT, this is most likely the area where a 100m-class telescope has a real niche in the field of galaxy-scale starbursts and star formation processes: HST and its successors are less competitive due to their significantly smaller mirror diameters.

This is a fortunate situation, as it will allow us to probe right into the core of the most active, dust-enshrouded star forming regions. This will potentially help solve the key outstanding issue of how star formation actually occurs, proceeds and is triggered, as well as what the importance is of the interaction between the newly-born stars and their surrounding ISM. This is particularly important in view of our current knowledge of the process of star formation itself – these youngest dust-embedded clusters are full of very young, and therefore violently active, OB stars with strong winds and other forms of mass loss. We will be able to study their early evolution and the transformation from the youngest star forming cluster-like regions to more mature, partially virialised systems.

Thanks to the significantly larger collecting area of a 100m-class telescope compared to the current state of the art of 10m-class telescopes (a factor of 100), one will be able to extend studies of resolved stars in dense systems (star forming regions, young star clusters, etc.) to the Coma cluster, and study entire star cluster systems out to cosmological distances to similarly faint levels as currently possible for Virgo cluster member systems. This is an important advantage from a scientific point of view, as star cluster systems of various ages hold a key clue regarding the formation and evolution of galaxies themselves: it has recently been shown that the intermediate-age star cluster system in the very nearby starburst galaxy M82 has the potential of surviving until globular cluster-type ages (i.e., for a Hubble time). This provides an important benchmark for the evolution of star cluster systems, and supports the hierarchical galaxy formation models (de Grijs et al., 2003b, Goudfrooij et al. 2004). If these results could be confirmed in a wide variety of star cluster forming galaxies, this would have far-reaching implications for our understanding of not only star formation, but also of galaxy formation and assembly.

However, despite significant recent progress, the postulated evolutionary connection between the recently formed young massive clusters (YMCs) in starbursts and old globular clusters in the nearby Universe is still contentious. The evolution and survivability of young clusters depend crucially on their stellar IMF (cf. Smith & Gallagher 2001): if the IMF is too shallow, i.e. if the clusters are significantly depleted in low-mass stars compared to, for example, the Solar neighbourhood (where low-mass stars dominate the gravitational potential), they will likely disperse within about a Gyr of their formation (e.g. Gnedin & Ostriker 1997, Goodwin 1997, Smith & Gallagher 2001, Mengel et al. 2002).

As a simple first approach, one could construct diagnostic diagrams for individual YMCs, of mass-to-light (M/L) ratio (derived via dynamical mass estimates using high-resolution spectroscopy and the virial approximation) versus age (derived from the spectral features), and compare the YMC locations in this diagram with models of "simple stellar populations" (SSPs, i.e. single-age, single metallicity stellar populations) governed by a variety of IMF descriptions (cf. Smith & Gallagher 2001,

Mengel et al. 2002). However, such an approach, while instructive, has currently serious shortcomings and suffers from a number of fundamental problems as it stands at present:

(i) Firstly using a Salpeter-type IMF for YMC mass and M/L ratio determinations will lead to *overestimates* of the individual YMC masses and M/L ratios, by factors of a few (cf. de Grijs et al. 2003b) if the low-mass stellar IMF is significantly flatter than the Salpeter slope, as found observationally. Secondly, the observational data points can, in the case of this simple approach, be described by *both* variations in the IMF slope *and* variations in a possible low-mass cut-off; the models are fundamentally degenerate for these parameters.

(ii) While the assumption that these objects are approximately in virial equilibrium is probably justified at ages greater than about 10 Myr, the central velocity dispersion derived from high-resolution spectroscopy does not necessarily represent a YMC's total mass. It is now well-established that almost every YMC exhibits significant mass segregation from very early on (cf. de Grijs et al. 2002a,b,c, and references therein), so that the effects of mass segregation must be taken into account when converting central velocity dispersions into dynamical mass estimates.

(iii) With the exception of a few studies (e.g. M82-F, Smith & Gallagher 2001), the majority of nearby YMCs thus far analysed in this way have ages around 10 Myr. Around this age, however, red supergiants (RSGs) appear in realistic stellar populations. Unfortunately, the model descriptions of the RSG phase differ significantly among the various leading groups producing theoretical stellar population synthesis codes (Padova vs. Geneva vs. Yale), and therefore the uncertainties in the evolutionary tracks are substantial.

Thus, it follows that the essential conditions to make a major leap forward in this field are to obtain high-resolution spectroscopy and imaging of a significantly larger cluster sample than available at present (to distinguish between trends and coincidences), covering a much more extended age range. This is precisely what we propose here as a program for a 50–100m ELT. These observations will need to be backed up by detailed N-body simulations of clusters containing both a realistic number of test particles (upwards of several x 10^5) and all relevant physical processes occurring over the clusters' lifetimes.

Therefore, one needs to obtain (i) high-resolution spectroscopy of all clusters in a given cluster sample (requiring, therefore, a MOS approach) in order to obtain dynamical mass estimates, and (ii) high-resolution imaging (at close to diffraction-limited spatial resolution) to measure their sizes (and luminosities).

With a 50–100m-class ELT, we can now finally get close to resolving this potentially far-reaching issue conclusively. Using ELT-sized apertures will allow us to probe *both* the dynamics *and* the luminosity function of young and intermediate-age star clusters (and their host systems) out to cosmologically interesting distances, where we can obtain statistically significant samples of galaxy types spanning the entire Hubble sequence, and of their YMC systems.

Notes on Design Requirements

Observation type: Imaging and high-resolution spectroscopy

Field of View: ~2 x 2 arcmin

Spatial Resolution: 0.03-0.04 arcsec (or better) would allow clusters to be resolved to 30–50Mpc

Spectral Resolution: > 40,000

Wavelength Range: > 0.8μm

Target Density: numerous objects across the sky, particularly in the direction of Virgo and Fornax

Telescope Size: > 50m

Observing time: scaling from 8m-class telescopes, up to 1 night for spectroscopy per object

4.10 Black Holes – Studying the Monsters in Galactic Nuclei

4.10.1 Introduction

It is widely accepted that Active Galactic Nuclei (AGN) are powered by accretion of matter onto massive black holes. Under simple assumptions, accretion is limited by radiation pressure and the Eddington Luminosity represents the maximum luminosity that can be radiated for a given black hole mass. It is believed that most active galactic nuclei emit below or at their Eddington luminosity.

With the advent of the Hubble Space Telescope (HST) and ground based adaptive optics-assisted telescopes, important advances have been made in our understanding of the nuclear regions of galaxies. In recent years there has been a progression from massive black holes as a theoretical requirement for the energetic phenomena in active galactic nuclei (Lynden-Bell 1969) to direct estimates of massive black hole masses.

The observed evolution of the space density of AGNs implies that a significant fraction of luminous galaxies must host black holes in their nuclei with masses in the range 10^6–10^{10} $M_\odot$, which are relics of past activity (e.g. Soltan 1982, Marconi et al. 2004).

Indeed, a few low luminosity AGNs like M87 (Macchetto et al. 1997) and Centaurus A (Marconi et al. 2001) host supermassive (~10^8–10^9 $M_\odot$) BHs in their nuclei. They presumably sustained quasar activity in the past but are now emitting much below their Eddington limits. Supermassive BHs are also found in quiescent galaxies like our own galaxy (Genzel et al. 2000) and M32 (van der Marel et al.,1997). Already there are approximately ~40 galaxies where a super-massive black hole has been detected.

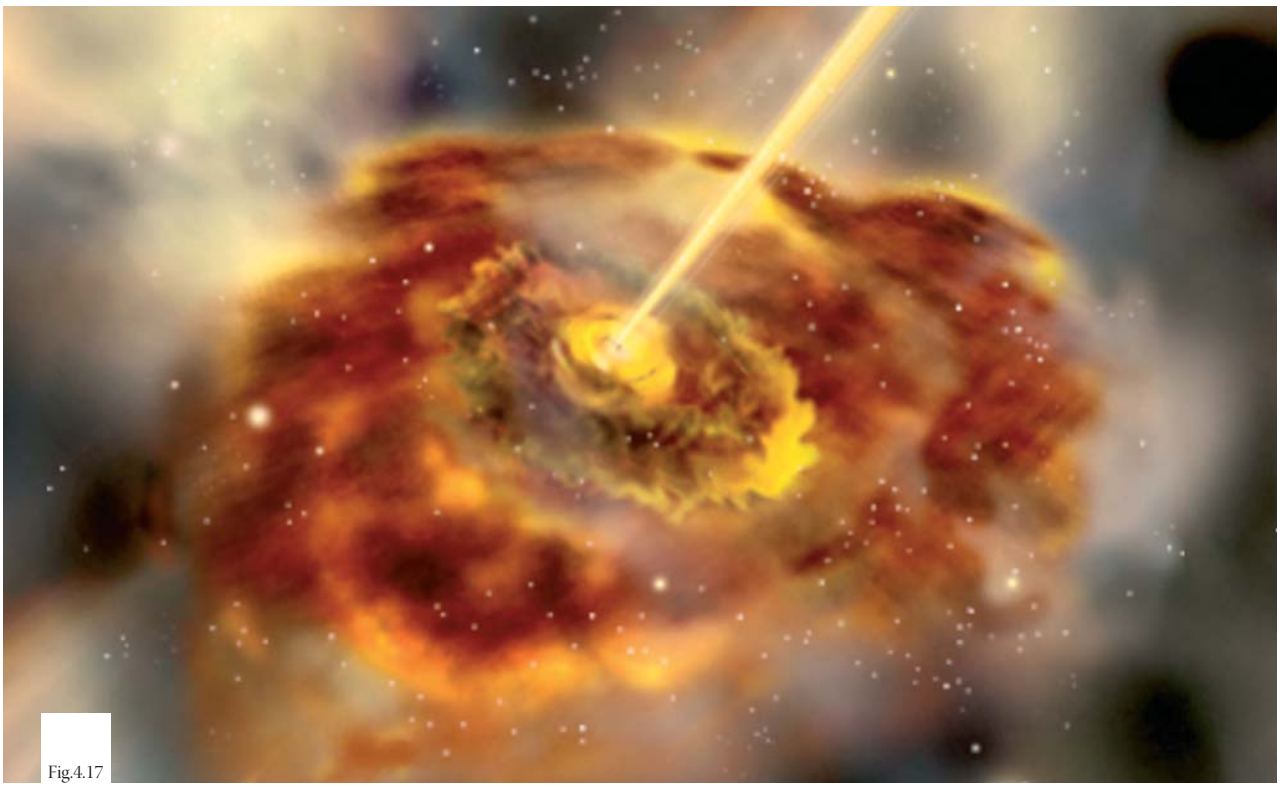

Fig.4.17

Artist's conception of an AGN with the BH surrounded by accreting material and ejecting a jet at relativistic velocities (credits: GLAST/NASA).

The goal of massive black hole research is to determine the demographics of massive black holes (over all redshifts) and to understand the relationship between massive black holes and their host galaxies. The ultimate aim is to establish both how massive black holes form and then grow, and to put this within the context of galactic evolution.

The reason massive black holes remained a theoretical requirement rather than an observational reality for so long was because of a lack of resolving power. We detect massive black holes by their gravitational effect on their environment. To confidently detect a massive black hole we need to probe the region over which the massive black hole dominates the galactic dynamics. This region is called the *sphere of influence* and its radius defined as:

$$r_i = GM_\bullet / \sigma^2$$
$$= 4.3\text{pc}\ (M_\bullet/10^7 M_\odot)(\sigma / 100\text{kms}^{-1})^{-2}$$

for a black hole mass of $M_\bullet$ and a stellar velocity dispersion of σ km/s. A typical scale for the sphere of influence is 7pc, and is almost independent of nuclear mass since larger bulges tend to have larger nuclei. Compared to the sizes of galaxies this region is small and we can only directly determine black hole masses by observations of the region of influence for galaxies at distances D < 100Mpc for the largest massive black hole masses and, more generally up to D ~ 20 Mpc. This severely hampers our ability to investigate the evolutionary history of massive black holes and their host galaxies in an unbiased manner.

Estimating massive black hole masses is best done through the direct dynamical analysis of the region of influence. Specifically, the principal methods for direct massive black hole mass estimates come from analysis of the kinematics of either gas (e.g. Marconi et al 2003, Barth et al 2001) or stars (e.g. Schödel et al 2002) in the region of influence. These direct massive black hole mass estimates have lead to the most important result to-date in massive black hole astrophysics; the discovery that the masses of massive black holes are correlated with other physical attributes of stellar bulges such as bulge mass and luminosity (e.g. Kormendy & Richstone 1995, Marconi & Hunt 2003), the stellar velocity dispersion in the bulge (Ferrarese & Merritt 2000, Gebhart et al 2000), the luminosity concentration in the central regions (Graham et al 2001) and the shape of the bulge surface brightness profiles (Graham et al 2002). These imply that the history of massive black holes is tied to the history of the formation of the galaxy. Indeed in recent models of galaxy formation it has been found that AGN feedback on the host galaxy (i.e. feedback from the BH during its accretion phase) can profoundly affect star formation (e.g. Granato et al. 2004, Menci et al. 2004). To get a complete view of galaxy evolution we need to understand the role played by the central massive black holes.

It is important to note that of the ~40 massive black hole mass measurements so far, for only 2 of these galaxies (our Galaxy and NGC4258) is a massive black hole *the only alternative*. For all the other cases it is still possible to construct a model where the central mass consists of other dark objects – e.g. stellar mass black holes, neutron stars etc. An important advantage of an ELT is that the spatial resolution will allow us to constrain the distribution of the dark mass to within volumes so small that a black hole is the only physical possibility.

4.10.2 The Future of massive black hole Astrophysics: New Opportunities with an E-ELT

What is required is direct kinematic measurements (gas or stars) of the nuclear regions of all types of galaxy at all redshifts. We can only get close to this goal with an ELT. The resolution obtained at 10mm will be 20mas, improving to a few mas at 1–2μm, where the adaptive optics system can deliver high Strehl imaging performance. This is more than an order of magnitude better than JWST at these wavelengths.

Figure 4.18 (top) shows that with a 100m ELT we can easily resolve the massive black hole sphere of influence (a mandatory requirement for a secure detection) for a massive black hole as small as $100M_{\odot}$ within 1Mpc. This means that a 100m telescope can easily detect intermediate mass black holes, if they exist, at the centres of globular clusters (see also section 3.4.4.3). Critically, an E-ELT will also allow us to determine if there are any small mass black holes in high mass bulges, something which would have important consequences for our current understanding of the MBH-host galaxy relationship.

A census of galactic nuclei in the local environment, to the distance of Virgo, would establish whether the relation between black hole mass and the host bulge holds also for dwarf galaxies. An E-ELT would probe the mass function 1–2 orders of magnitude further down than existing facilities can. Angular resolution is the key limitation here.

At the other end of the mass scale, Figure 4.18 (bottom) shows that a 100m telescope would allow us to measure the masses of all MBHs in the 10^6–10^9 range in the local Universe ($z < 0.1$), and we will for the first time be able to measure massive black holes with $M > 10^9 M_{\odot}$ at all redshifts (where they exist). This will mean that we can investigate massive black hole masses in Quasars at $z > 6$, an age when there would have been barely enough time to have formed massive black holes through accretion. An ELT will allow us to determine whether accretion or another channel (such as galaxy mergers) is the dominant mechanism for massive black hole growth.

The high resolution is ideal for studying the inner part of the accretion disks around MBHs in active galactic nuclei. For example, the famous Seyfert galaxy, NGC1068 lies at a distance of about 20Mpc and this resolution corresponds to a few pc, the expected size of structure. Even at cosmological distances at $1 < z < 6$ the physical resolution is of order 300 down to 30pc, clearly sufficient to resolve these objects spatially for the first time.

Production of Pa-α maps will resolve the Broad Line Region (BLR) in Active Galactic Nuclei (AGN). An ELT will allow us to (a) verify the reliability of estimates from reverberation mapping and, (b) to secure the relationship between the radius of the BLR and its luminosity. Such a relationship has been used (e.g Kaspi et al 2000, McLure & Jarvis 2002) to provide a quick method for estimating black hole masses in Seyfert I and Quasars.

If an Integral Field Unit is used in conjunction with a 100m telescope we will be able to use a powerful technique for detecting massive black holes. We will be able to separately resolve the absorption lines of individual stars in the galactic nuclei. This will allow us to reconstruct both the position of the stars (from the centroid of their absorption lines) and their line-of-sight velocity.

In summary, a 100m class ELT should allow:

- resolution of nuclear sub-structures of a few *pc* (or even down to ~0.1pc with a 100m ELT working close to the diffraction limit in the optical, i.e. ~1mas resolution) at distances of 20 *Mpc*, that is viewing through the accretion disk and measuring black hole masses with great accuracy, even in the low mass regime (see for instance the case of NGC 4258, Miyoshi et al. 1995);

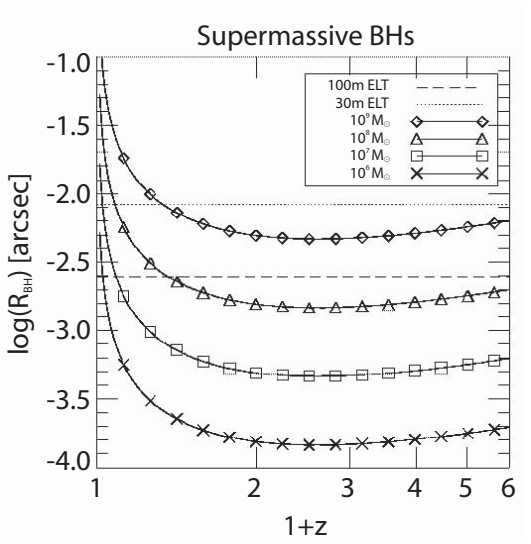

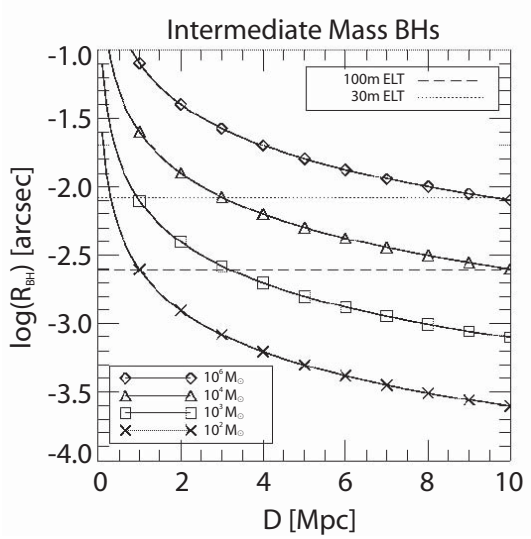

Fig.4.18

The impact of a 100m class telescope on studies of intermediate and massive black holes would be considerable. Shown here are the distances to which the sphere of influence can be resolved (for comparison, the resolution of a 30m telescope is also shown). With a 100m ELT we will be able to resolve the sphere of influence down to 100$M_\odot$ in the local Universe, allowing us to detect intermediate mass black holes at the centres of globular clusters. At the other end of the scale we will be able to detect 10^9 $M_\odot$ black holes at all redshifts. Here we assume a cosmology of H_0=70 km $s^{-1}Mpc^{-1}$, Ω_M=0.3 and Ω_Λ=0.7. The point spread function is given by 1.22λ/D, where D is 30m or 100m and λ=1μm.

- measurement of black hole masses greater than 10^9 $M_\odot$ at all redshifts (where they exist) with great accuracy
- resolution of bright stars in the circumnuclear region, and measurement of age, metallicity and velocity fields of the stellar populations of the host galaxy.

Combining the above points it will be possible to study the redshift evolution of the correlations between massive black hole-host galaxy properties thus shedding light on the galaxy formation process and its relation with BH growth. This information is fundamental to understand the formation and evolution of active nuclei and the connection with the evolution of their host galaxy, including the possible connection between AGN and starburst activity (see e.g. Oliva et al. 1999, Cid Fernandes et al. 2001, Kauffmann et al. 2003).

Notes on Design Requirements

Observation Type: High-res imaging and spectroscopy of gas and stars in galactic nuclei

Field of View: 5 arcsec

Spatial Resolution: A few mas – Diffraction limited at 1μm or optical if possible

Spectral Resolution: a few x 1000 for velocity measurements and OH avoidance in the near IR

Wavelength Range: optical and near IR (several nebular and stellar features)

Telescope Size: 100m or as large as possible for angular resolution

Other comments: Spectroscopic observations ideally suited to an IFU

5 Galaxies and Cosmology

Introduction

Progress in the field of galaxy formation and cosmology has accelerated in the past 10 years. We now have a general picture of how structure (galaxies, galaxy clusters and filaments) formed from the smooth very high redshift Universe. At the same time, the cosmological concordance model seems to indicate that we may have reached a consistent view of the evolution of the Universe as a whole.

Yet, there are still large gaps in our understanding of the "big picture", such as how star formation proceeded in galaxies, how galaxies assembled, the nature of the dark energy, what objects caused re-ionisation and what objects were the first to form in the Universe before re-ionisation.

New observational facilities in the coming decade will try to address these questions. Furthermore, new fundamental questions will arise: the evidence for dark energy was found only recently, and it added a new component to the Universe, the biggest component in terms of energy density at low redshift. We still have no idea of its nature and physical properties.

Below we present the science cases in the field of galaxy formation and cosmology. There are some special considerations for extremely large telescopes, which have to be taken into account when discussing their science cases. One is that galaxies are extended objects at all cosmological distances. The typical half-light radius of Ly-break galaxies at z~3 are about 0.2 to 0.3 arcseconds (Giavalisco et al. 1996). This means that for studies of their integrated light, it would be best to match the spatial resolution to this angular size. At higher redshifts the angular sizes are slightly lower (~0.1 arcsec at z=7), but this is still very much larger than the diffraction limit of ELT type telescopes.

On the other hand, point sources with angular size <1 mas will be studied: quasars, active galactic nuclei in general, Gamma Ray Bursts (GRBs) and supernovae (SNe). These benefit enormously from diffraction limited studies, as the sky background will be greatly suppressed. HII regions at larger redshifts are close to the diffraction limit. A regular HII region of about 50pc subtends about 0.005 arcseconds at z>1. The diffraction limit for a 30m in J is 0.01 arcseconds which probes to about 90pc at these redshifts. A 60m-telescope would be well matched to the size of such a HII region and a 100m telescope could just start to resolve such HII regions.

An ELT will have unique capabilities to detect the first objects emerging from the radiation epoch, peer with great detail into forming galaxies across the Universe and determine the parameters of the cosmological model with a much higher accuracy than currently possible.

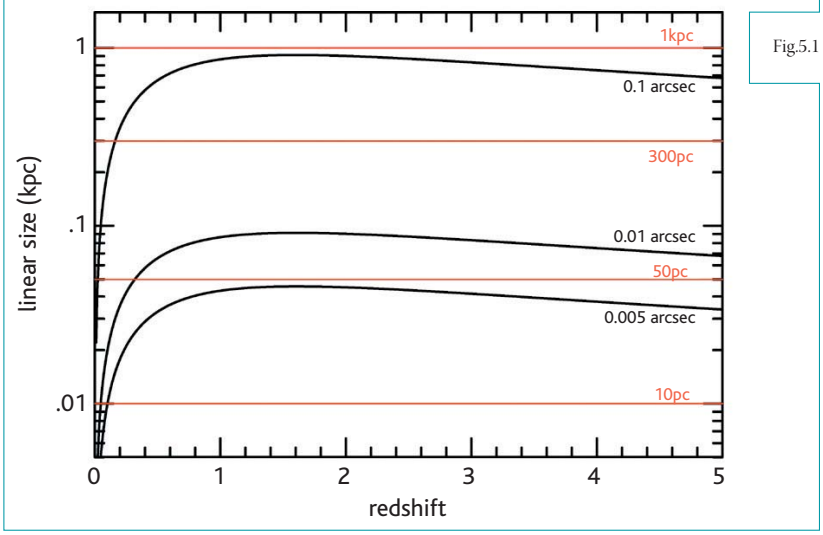

Fig.5.1 Linear size as a function of redshift. The underlying cosmology for this figure is H_0=65 km s^{-1} Mpc^{-1}, Ω_M=0.3, Ω_Λ=0.7. Typical linear sizes of a starburst region (1kpc), a giant HII region (300pc), a small HII region (50pc) and a globular cluster (10pc) are indicated.

5.1 Cosmological parameters

5.1.1 Dark energy

One of the most pressing problems in fundamental physics today is the nature of the force driving the acceleration of the Universe. Whether this is a signature of the cosmological constant as introduced by Einstein to balance his cosmological model or due to the release of energy from the potential of a fundamental particle field, like the inflaton responsible for the inflationary period following the Big Bang, remains to be determined. In either case, the dark energy appears to be the dominant constituent of the Universe. Whichever physical mechanism is at work, it decides the future of the Universe, which will remain undetermined until this cosmic riddle is solved.

Together with the flat geometry of space-time as determined by cosmic microwave experiments (e.g. WMAP results, Spergel et al. 2003) and the low matter density measured by large galaxy and galaxy cluster surveys (Hawkins et al. 2003, Allen et al. 2002), the expansion history forms a main pillar of the concordance cosmology.

There are currently several theoretical explanations entertained for the physics of the dark energy. These range from the classical cosmological constant (designated Λ), a decaying particle field (often referred to as quintessence), effects of higher dimension on gravity changing the effective Friedmann equation and entirely new cosmological models.

Several experiments are underway to determine the equation of state parameter of the dark energy. This parameter, ω, which relates the density ρ to the pressure p of the energy component via the equation

$$\omega = \frac{p}{\rho c^2}$$

also determines the expansion history through the energy conservation. The energy density scales with the co-moving volume (R is the scale factor) as

$$\rho \propto R^{-3(1+\omega)}$$

The classical cosmological constant has $\omega = -1$, while most particle fields likely have values different from this. The cosmological constant has no temporal evolution, while the decaying particle field will evolve with time. There are hence two ways to distinguish between the simplest theoretical proposals (Λ and quintessence). Current experiments such as the Supernova Legacy Survey (SNLS, Pritchet et al. 2004) and the ESSENCE project (Matheson et al. 2005 and references therein) will measure the integrated value of ω, and if it is found to be different from –1 will exclude Λ. The best redshift range for these experiments is $0.2<z<0.8$, where the transition from a decelerated Universe to the acceleration took place. First results are expected in a few years.

If Λ is ruled out by the current experiments, we have to contend with at least two physical fields, which have changed the expansion history of the Universe in dramatic fashions. Given such a situation, it is quite likely that there are more such 'quintessence' fields, which have influenced the cosmic evolution.

The second method, to look for a time variation of ω, will also be attempted in the coming decades. Observations of distances across a large redshift range ($0<z<2$) are required for such an experiment. Below we discuss two possible distance indicators that could be observed to such redshifts with an ELT.

5.1.1.1 Type Ia Supernovae as distance indicators

Type Ia supernovae have provided convincing evidence for the existence of dark energy and the expansion of the Universe (Perlmutter et al 1999, Riess et al 1998, Leibundgut 2001, Riess et al 2004, Tonry et al. 2003, Knop et al 2003).

Measuring the time variation of ω out to redshift z~1.7 is best achieved with a dedicated satellite such as the proposed SNAP/JDEM mission (through luminosity distances to SNe Ia and weak lensing). Although JWST is also planning to observe SNe Ia, it is unlikely to achieve the required statistical sample for an accurate measurement of the time derivative of ω. A large ground-based telescope will be required to provide a reliable classification of the supernovae with z>2 and accurate redshifts for them. The weak lensing experiment will rely on statistical redshifts and will not depend on spectroscopy. It would, however, be prudent to have a spectroscopic programme on an ELT to check on the photometric redshifts.

As shown in Section 4.7, an ELT would be capable of finding and following supernovae of all types to much higher redshifts than currently possible. Specifically, an ELT can provide spectroscopic redshifts for SNe Ia to z=4, if of 100m diameter. The redshift range decreases to z~1.7 for a 30m telescope. The important issue here is that with a 100m telescope the first half of the universal expansion history can be mapped. Any additional 'quintessence' field active during this period would be detectable, if a coordinated programme between JWST and an ELT could be run.

An additional benefit would be the systematic characterisation of distant supernovae with high S/N spectroscopy. The underlying assumption,

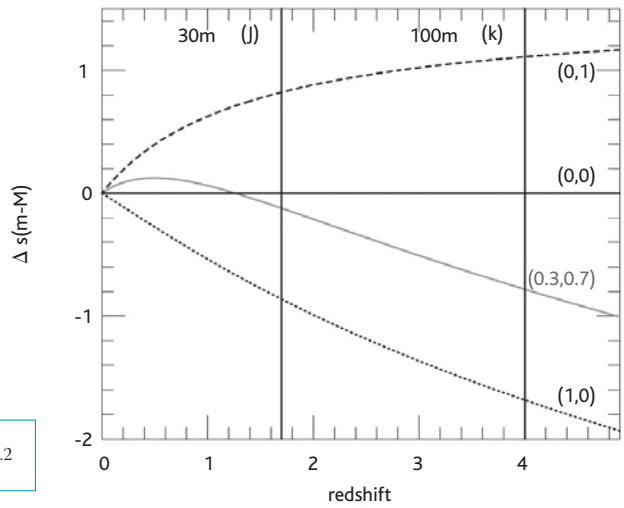

Fig.5.2 Hubble diagram for various cosmological models, normalised to the model for an Empty Universe. Spectroscopic limits of a 30m and a 100m telescopes for the classification of SNe Ia are indicated. The cosmological models are described by the parameter pairs (Ω_M, Ω_Λ).

tested with many photometric methods like colours, light curve shapes, and luminosity scatter, that SNe Ia do not considerably change their luminosity as a function of universal age and other parameters (most prominently metallicity) is best checked through detailed spectroscopy. Qualitative comparisons of spectra at low and high-z have been performed using 8–10m class telescopes on supernovae up to z~1 (Figure 5.3; Lidman et al 2005, Matheson et al 2005) and the first quantitative comparisons have recently been attempted (Hook et al 2005, Garavini et al in prep) but the low signal-to-noise obtainable allows only first-order comparisons to be made. Detailed high signal-to-noise spectroscopy will only be possible with the next generation of ELTs.

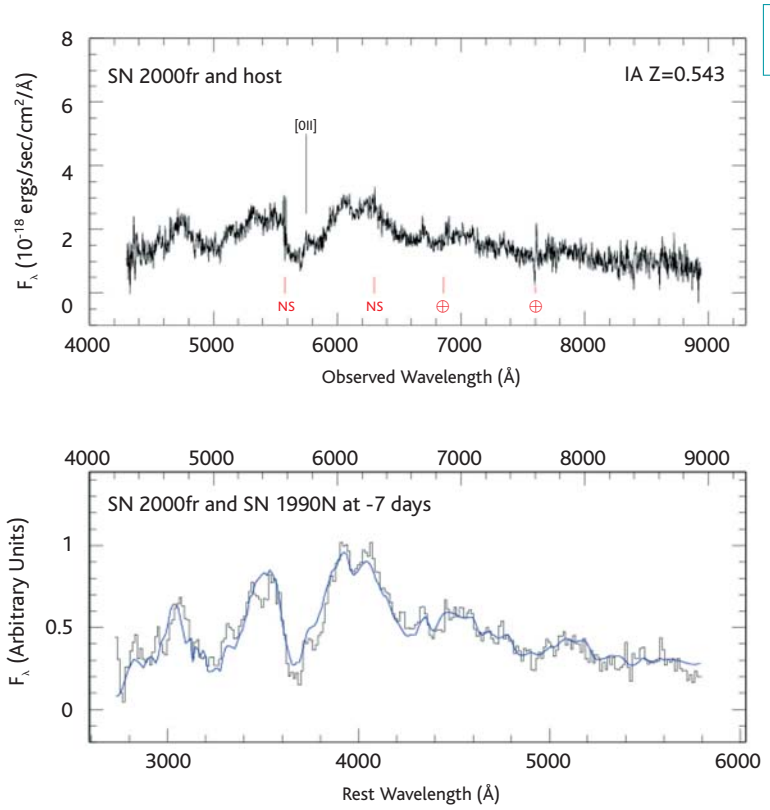

Fig.5.3

(From Lidman et al 2005) A VLT spectrum of SN 2000fr, a SN Ia at z=0.543, showing unambiguous detection of Si II at 4000 Å, confirming that this is a Type Ia SN. In the upper spectrum, the unbinned spectrum is plotted in the observer's frame and is uncorrected for host galaxy light. Night sky subtraction residuals are marked with the letters "NS" and telluric absorption features are marked with the "earth" symbol. In the lower spectrum, contamination from the host is removed and the spectrum is rescaled and rebinned by 20 Å. For comparison, the best fitting nearby supernova is overplotted in blue. A spectrum of the host galaxy (not shown here) shows emission in [OII] and [OIII] as well as Balmer absorption lines, from which the redshift was measured.

Notes on Design Requirements

(see also section 4.7)

Observation Type: imaging (to find SNe) and spectroscopy (to obtain redshifts and types, and detailed comparisons of spectral features at all redshifts)

Field of View: 2 arcmin x 2 arcmin (imaging)

Spatial Resolution: diffraction limited (Strehl =0.5 in K) assumed above

Spectral Resolution: *R*~5 (for imaging) and R~2000 for spectroscopy. Note that although only low resolution is needed (since SN features are broad), higher spectral resolution may be needed to reduce the effects of night sky lines in the IR.

Wavelength Range: near-IR : J,H and K bands

Target Density: Approx 0.5 SNela will be found in a 2 arcmin x 2arcmin field per year (see section 4.7). Follow-up spectroscopy could be done one object at a time or simultaneously with SNe of other types in the field. Approx 4-7 SNe in total are expected in a 2 arcmin x2 arcmin field. Thus MOS would be feasible if an AO-corrected spectrograph with a patrol field of 5 arcmin on a side could be built.

Observing time: The Type Ia SNe would be found as part of a survey for supernovae of all types (see section 4.7). This requires imaging 50 fields in the J(1h each), H(1h each) and K(1h each) bands at 4 different epochs for the supernova search complemented by 3 epochs in the K band for the photometric follow-up of about 350 SNe (of all Types) up to z ~ 10 and finally 4h to get the spectroscopic classification up to z~ 4 to 5 (depending on type). Thus the total time= 3 x 4h x 50(=600h) + 3hx50(=150h) + 4hx50(=200h)= 950h to study 350 SNe (220 of which also spectroscopically). The result would be a sample of approximately 25 spectroscopically confirmed SNe Ia per year up to z~4.

Date constraint: Repeated observations

5.1.1.2 Gamma-Ray Bursts as distance indicators

In addition to extending far beyond z=2 in order to overcome the problem of parameter degeneracy of the cosmological models, it is desirable to use distance indicators which are free of extinction as an alternative to SNe Ia. Gamma Ray Bursts (GRBs) potentially fulfil these requirements.

GRBs are extreme extragalactic sources. Their isotropic emitted energy, in the γ-ray band (i.e. above few keV) is $E_{iso}=10^{51-55}$ erg and they have already been detected up to redshifts of z=4.5. Since they are discovered in the γ-ray band, GRB detections are not affected by dust absorption and optical extinction by Ly-α clouds. Therefore, they should be discoverable out to extremely high redshifts, i.e. z~15–20 (Lamb & Reichart 2000).

The properties described above suggest GRBs could be a good candidate class of sources to probe the cosmological models of the Universe. However, the huge dispersion (four orders of magnitude) of the isotropic GRB energy E_{iso} makes them everything but standard candles. This problem is only partially solved if the GRB energetics are corrected for their jet opening angle θ_{jet} (Frail et al. 2001): the collimation corrected energy $E_\gamma=(1-\cos\theta_{jet})E_{iso}$ clusters around 10^{51} erg with still a considerable scatter (~two orders of magnitude) which prevents GRBs from being used as standard candles.

The recent discovery of a very tight correlation between the collimation corrected energy E_γ and the GRB spectral peak energy E_{peak} (Ghirlanda et al. 2004a) with a scatter of only 0.1 dex allowed, for the first time, use of GRBs as standard candles to constrain the cosmological parameters (Ghirlanda et al. 2004b). This correlation, similar to the 'stretch-luminosity' correlation of SNIa, already gives encouraging results, even with a still limited number of 15 GRBs, for the density of dark energy and dark matter and for the investigation of the recent acceleration era (Firmani et al. 2005). GRBs, observable at intermediate redshift between SNIa and the last scattering surface of the CMB, are a valuable complement to SNeIa and CMB for constraining the present cosmological parameters and studying the dynamics of the Universe.

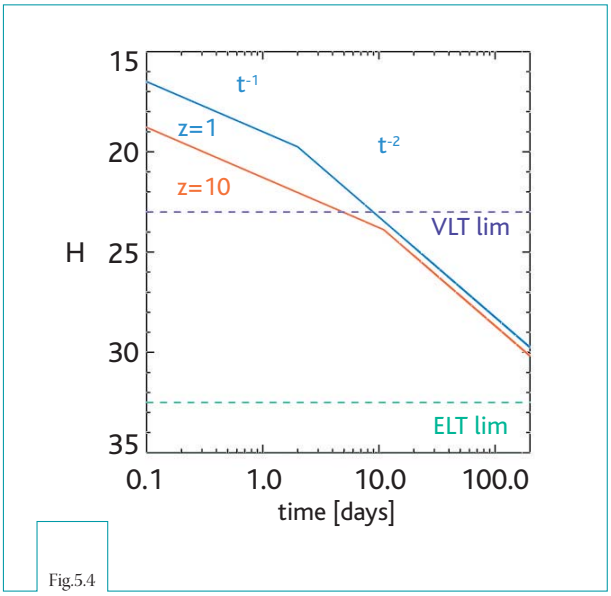

Fig.5.4

GRB H-band afterglow light curve. The blue curve is the template afterglow light curve of a z=1 GRB (e.g. GRB990510, Israel et al. 1999) with a jet break time of 2 days. The same GRB light curve at redshift z=10 (red solid line) would show a jet break at 11 days. The dotted line represents the limiting magnitudes for a 1 h exposure with average sky conditions at VLT (blue) and 100m ELT (green). To measure the jet break time, a crucial parameter for the use of GRBs in cosmology, for a high redshift GRB a 100m-class telescope is required.

The prospects for the use of GRBs as standard candles clearly depend on the increase of the number of detected GRBs which satisfy the E_{peak}–E_γ correlation. Many events are required to test and fully calibrate this correlation. Clearly the extension of the sample in coming years will also extend the present GRB redshift limit to higher values. This will offer the unprecedented opportunity to investigate the nature of dark energy beyond what can be reached by SNe Ia.

Cosmology with GRBs through the E_{peak}–E_γ correlation requires a set of observables, which are derived both from the GRB high energy emission (i.e. the γ–ray prompt phase) and from the afterglow observations in the optical and IR band. In particular, the afterglow spectroscopic observation should provide the GRB redshift, while the long term (days to weeks) photometric monitoring of the afterglow emission allows measurement of the break

time. The latter allows us to estimate the GRB opening angle θ_{jet} and, therefore, to derive the collimation corrected energy E_γ.

Typically, the GRB Optical-IR afterglow flux decays in time as F(t) proportional to t^{δ} with $\delta \sim -1$ before the jet break time t_{break}, while it steepens (i.e. $\delta \sim -2$) after t_{break}. In most cases GRB afterglows are so faint (V ~ 23 at 1 day after the burst occurrence) that large telescopes are required to monitor their emission up to the late phase in order to observe the characteristic jet break time. At present, the most successful monitoring campaigns rely on the use of 10m-class telescopes. However, in order to measure the GRB jet break time, monitoring timescales of order weeks are required, especially for very high redshift (z>10) events. This will only be possible with >50m telescopes.

As a case study we consider a high redshift z=10 GRB. Due to Ly-α absorption this burst is best monitored in the H-band. The typical magnitude of a "local" z=1 GRB is H~19 at ~1 day after the burst. We assume that its light curve decays in time as described above and also assume the average jet break time, as measured with the present GRB sample, i.e. t_{break} ~2 days. Note that these are only fiducial values as GRBs display a large variety of observed magnitudes and different scaling laws. Scaling the z=1 GRB observed light curve to redshift z=10 we find that the jet break time should be observed at ~11 days with an expected afterglow magnitude of H~24. Figure 5.4 shows the light curve of the z=1 burst (solid blue line): its t_{break} magnitude is well in reach of the VLT (for a 1h exposure in normal sky conditions and S/N=5). The same light curve scaled at z=10 instead shows that it cannot be sufficiently monitored by a 10m telescope. In this case with the 100m ELT exposure calculator, we find that a 1h exposure, in normal observational conditions, allows sufficient signal-to-noise (S/N=5) up to ~200 days, and therefore, precise measurement of the jet break time of this high redshift burst.

One of the greatest advantages of the use of GRBs for observational cosmology through the E_{peak}-E_γ correlation is the possibility of detecting them out to very high redshifts. In principle also a limited number of GRBs between redshift 5 and 15 would strongly contribute to pin-pointing, for example, the two cosmological parameters Ω_M and Ω_Λ. As an example we simulated a sample of 50 high redshift GRBs as they would be detected by Swift (Lazzati et al., in preparation). If the jet break time of these events can be measured, the constraints on the cosmological parameters would be determined with a high accuracy with GRBs alone and even better when GRBs

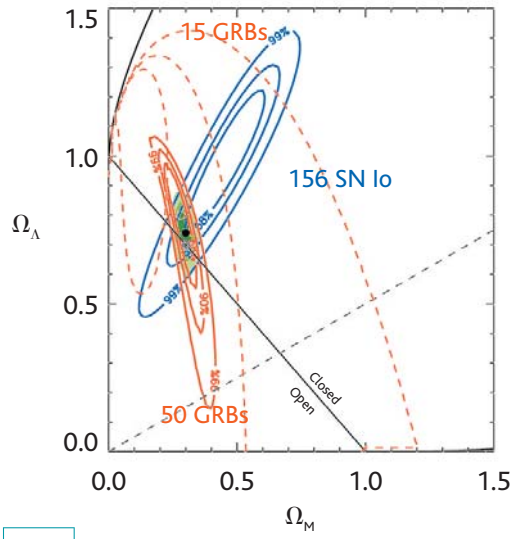

Fig.5.5

Constraints on the cosmological parameters Ω_M and Ω_Λ (from Ghirlanda et al. 2004b) obtained with 15 GRBs through the E_{peak}-E_γ correlation (dashed red contours) and from the gold sample of 156 SNIa from Riess et al. 2004 (blue solid contours). The solid red contours represent the result of a simulation of 50 high redshift GRBs (with 5<z<15), which obey the E_{peak}-E_γ correlation. The simulation assumes that GRBs follow the SFR2 of Prociani & Madau (2001) and that their luminosity function is only slightly evolving with time as found in Firmani et al. (2004). Jet break times following the log-normal distribution found by Ghirlanda et al. (2005) were assumed. The green shaded region represents the joint fit of the cosmological parameters obtained with the 50 simulated GRBs and the 156 observed SNIa.

are combined with SNIa. Figure 5.5 shows the results (dashed red contours) obtained with the limited sample of 15 GRBs used to constrain the cosmological parameters Ω_M and Ω_Λ (Ghirlanda et al. 2004b) and the sample of 156 "gold" SNIa (Riess et al. 2004 – blue contours). Clearly a few GRBs are not competitive at this stage with SNIa, although the higher redshift distribution of GRBs makes their contours orthogonal to those determined with SNIa. With a larger sample of high redshift GRBs it will be possible to accurately constrain with GRBs alone (solid red contours) or together with SNIa (green filled contours) the cosmological models.

Notes on Design Requirements

Observation type: Photometry and spectroscopy

Field of view: <5x5 arcmin (but might depend on the X-ray facilities positional accuracy)

Spatial resolution:

Spectral resolution: R=8000 to 10000

Wavelength range: 0.8 to 2.4μm

Target density: single target monitoring

Telescope size: 100m or as large as possible for sensitivity to point sources. A 50m or 30m could also make an important contribution.

Observing time: nightly observations per GRB for a typical total of 1 month monitoring (depending on object visibility and magnitude) Comments: the observation should be performed in ToO, depending on the GRB discovery by high energy satellites.

5.1.2 Expansion history

5.1.2.1 Cosmic Expansion history from primary distance indictors

During the last few years distances based on primary distance indicators have been investigated in many theoretical and empirical studies. HST has provided sizable samples of classical Cepheids in stellar systems located well beyond the Local Group (Freedman et al. 2001; Saha et al. 2001). At the same time, microlensing experiments (EROS, OGLE, MACHO), collected a huge amount of photometric data of variable stars in the Magellanic Clouds and in the Galactic bulge. Detailed evolutionary and pulsation models provided new and homogeneous predictions concerning the dependence of mean brightness and colours on chemical composition (especially iron and helium). A comparison between distance determinations based on predicted and empirical relations indicates that they are in plausible agreement. However, the wealth of new results has also revealed new inconsistencies. Recent findings suggest that the Cepheid Period-Luminosity (PL) relation might depend on the metal abundance and also be nonlinear over the entire period range (Sandage et al. 2004; Romaniello et al. 2004). As far as RR Lyrae are concerned, a nonlinear dependence has also been suggested for the correlation between visual magnitude and metalicity (Caputo et al. 2000). Current uncertainties on the input physics adopted to construct Horizontal Branch models hamper the use of evolutionary predictions to supply very accurate distance estimates (Cassisi et al. 1998).

New instruments such as the VLTI available at ESO are providing very accurate "geometric" distance determinations for a few Galactic Cepheids (Kervella et al. 2004). In the near future, the use of VLTI auxiliary telescopes and J-band observations will provide the opportunity to estimate the distance for approximately three dozens of nearby Cepheids. For a substantial improvement in the global accuracy of distance measurements, we need to wait for *Gaia*. The impact of *Gaia* on this topic is twofold: (a) according to current plans *Gaia* will supply the trigonometric parallax for a substantial fraction of Galactic Cepheids with an accuracy of better than 2%. The same applies to field and cluster RR Lyrae and HB stars; (b) *Gaia* will also supply accurate homogeneous, multi-band photometry down to limiting magnitudes of V≈20-21, and medium resolution spectroscopy down to limiting magnitude of V≈15 mag. This will allow us, for the first time, to supply a robust estimate of the systematic errors affecting different distance indicators, and in turn, to properly calibrate current methods.

With such a solid calibration, the next step can only be provided by a diffraction-limited Extremely Large Telescope. The absolute optical magnitude of classical Cepheids ranges from –2.5 to approximately –7.5. This means that these objects can be observed both in optical (V,I) and in near-infrared bands not only in the spiral arms of early type galaxies in the Coma cluster (m-M≈35), but also in the disk edges of spiral galaxies at redshifts roughly equal to 0.1 (m–M≈39). This unprecedented opportunity will allow us to measure, for the first time, the local expansion field and the Hubble constant (H_0) using primary distance indicators alone. With the mean optical magnitude of RR Lyrae stars equal to 0.5, a 100m ELT will detect and measure in the optical bands RR Lyrae stars not only in the external regions of globular clusters in the Virgo cluster (m-M≈31) but also in the external regions of elliptical galaxies in the Coma cluster. This means that these low-mass stars can be adopted to supply an independent estimate of the Hubble expansion and constant.

The brightness of the tip of the Red Giant Branch (RGB), whose magnitudes are: M_V~ –2, M_I~ –4 and M_K~ –6, is one of the most powerful standard candles for old stellar populations. In particular, it is well suited to the low surface brightness, external regions of galaxies, which are not affected by significant crowding. Even if one accounts for the need of measuring the luminosity function down to 2-3 magnitudes below the tip of the RGB in order to obtain a safe estimate of its brightness, the Coma cluster appears well within the reach of a 100m-class telescope. Note that quoted estimates account for both the limiting magnitude and for the confusion limiting magnitude of individual targets (Arnold 2001).

The quoted distance indicators supply a robust calibration with a large sample overlap of secondary distance indicators such as Type Ia supernovae and the Tully-Fisher relation. Note that current calibration of the absolute luminosity of SNe Ia is based on a dozen spiral galaxies in which classical Cepheids have been identified. The use of both RR Lyrae stars and tip of RGB will provide the opportunity to use the same primary distance indicators to calibrate SNe Ia in early and in late type galaxies, and in turn to constrain any systematic effect when moving from metal-poor and metal-intermediate (globular clusters, halo of spiral galaxies) to metal-rich stellar systems (halo of elliptical galaxies).

Finally, it is worth mentioning both RR Lyrae stars and classical Cepheids are excellent stellar tracers of low- and intermediate-mass stars. Therefore, the radial distribution of these objects can be safely adopted to trace the different stellar populations across the entire Hubble sequence, in different environments (field and cluster galaxies) and at different epochs.

Notes on Design Requirements

These are similar to those for "resolved stellar populations" – see Section 4.2 and 4.3.

5.1.2.2 CODEX: the COsmic Differential EXpansion experiment

In an expanding Universe the redshift is inversely proportional to the scale parameter of the Universe. So for any galaxy, its redshift must vary with time under the braking and accelerating actions of the energy components. The expansion is driven by the dominating energy components, such as radiation, ordinary matter, dark matter and dark energy. As a consequence, the cosmic redshift drift is a cosmic reflex motion which is expected to be isotropic across the sky and dominant with respect to peculiar accelerations of individual galaxies. The point was first made by Sandage (1962), who also realised how discouragingly small this redshift drift is compared to the length of a human life. In fact, the expected velocity shifts of extragalactic objects are of the order of only a few metres per second, or a $\delta z \sim 10^{-8}$ over a century. It increases with redshift, but not substantially over the range of redshifts spanned by known sources.

The predictions of models with different cosmological parameters are shown in Figure 5.6 taken from Grazian et al (2005). The figure

illustrates how the measurement of this cosmic drift can be used to derive the fundamental parameters that define the cosmological model. Redshifts are free from evolutionary properties of the sources and the detection of their variations would represent a new and direct approach in observational cosmology, alternative to that based on luminosity and apparent-size distances, including Type Ia SNe, or microwave background anisotropies.

In recent years the drive to discover planets orbiting around nearby stars by means of the small periodic radial velocity variations they induce on the stellar motion has led to the development of special calibration techniques and to the construction of dedicated spectrographs. The accuracy of radial velocity measurements has been pushed down to the 1 m s^{-1} range over a period of years and of $\delta v \sim 10$ cm s^{-1} scale over a few hours. This is not yet sufficient to detect the cosmic signal of the redshift drift, but comes very close.

The cosmological structure of neutral hydrogen producing the Lyman-α forest in quasar spectra may supply the necessary probes to reveal the universal drift, in a similar way to the use of stellar atmospheric lines to reveal exoplanets. The basic concept calls for measuring the radial velocities of Lyman-α clouds in the spectra of ~100 distant QSOs. The radial velocities of these clouds, with redshifts between 2.5 and 5, need to be monitored over at least a decade. Only ELTs with a diameter larger than 50m can provide sufficient photons needed to make the measurements at both the resolution and the pixel sampling required to control the systematics which become significant at this level of precision.

These expectations led ESO, the Observatory of Genève, the Institute of Astronomy in Cambridge and the Observatory of Trieste-INAF to join forces in CODEX, the COsmic Differential Expansion collaboration. The aim of the study phase is the identification of the optimal strategy for the measurements and the development of an instrument concept for a 100m ELT. This work is on-going and results are expected in approximately one year.

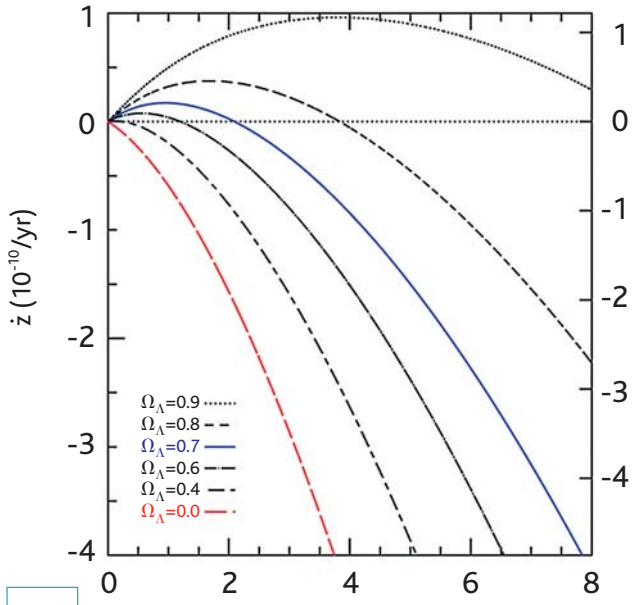

Fig.5.6

(From Grazian et al 2005) Expected change in the cosmic expansion rate as a function of redshift.

Notes on Design Requirements

Observation Type: High-resolution absorption-line spectroscopy

Spatial Resolution: 0.2"

Spectral Resolution: >100000; ideally 400000

Wavelength Range: 0.4–0.7μm

Target Density: single objects

Telescope Size: > 50m for sufficient S/N and control of systematics

Observing time: Assuming a 100m telescope, 50 nights per epoch (~100 targets – possibly once a year)

Date constraint: Repeated observations required over a period of ~ 10 yrs

Other comments: Very high stability required (a few cms^{-1} per year over a period of 10 yrs). E.g. vacuum spectrograph (HARPS-like), IFU. Require extremely high S/N (>1000 per resolution element) with multiple short exposure times. Global S/N >10000 combining all objects.

5.2 Highlight Science Case: First light - The First Galaxies and the Ionisation State of the Early Universe

Fundamental to our understanding of how the Universe evolved is how its properties changed during the first billion years after the Big Bang. Central to this issue is that of "first light": when and how the first galaxies formed. Understanding the key parameters of the earliest galaxies (masses, star formation histories, metallicities and their effect on the gas that fills the Universe around them) will give us crucial insight into the precise details of how the Universe evolved during its youth.

5.2.1 Introduction

A central issue in astrophysics is how and when the first stars and galaxies formed and what impact they had on the intergalactic medium (IGM) that surrounds them. Recent progress in observational cosmology coupled with detailed theoretical and computational predictions of how structure should develop in the Universe has pushed the issue of "first light" to the forefront of astrophysics.

After the Big Bang, the Universe cooled. 380,000 years after the Big Bang its temperature was low enough for the hydrogen-dominated IGM that pervades the Universe (the repository for all Baryons at that time) to became neutral. Today, that same IGM is fully ionised, heated by the integrated ultraviolet emission from galaxies and AGN. Exactly how and when the IGM turned from neutral to fully ionised is a matter of great debate. Observations of the highest redshift quasars indicate the transition to a fully ionised IGM had occurred no later than about 1Gyr after the Big Bang, by a redshift of $z\sim6$ (e.g. Becker et al 2001), whereas observations of the Cosmic Microwave Background with the WMAP satellite (e.g. Kogut et al 2003) imply that the IGM may have been half-ionised by $z\sim11$, some 500 Myr earlier. Together, these two results imply that the IGM had an extended and potentially complex re-ionisation history. Whether the re-ionisation occurred slowly over this period, or there were several sporadic periods of ionisation due to more than one distinct generation of ionising sources is completely unknown.

The fundamental questions of how and when the IGM was re-ionised are directly related to those of how and when the first stars and galaxies formed: presumably it is these first objects that produce the UV radiation field that re-ionises the IGM. In our current picture of the process, these galaxies started to form from over-densities in the inhomegeneous matter field at high redshift which over time collapsed and grew dense enough that star formation was able to occur within them. The UV photons output by the hot young stars or mini AGN in each protogalaxy ionised a small region, a bubble, in the surrounding IGM. Over time, the UV output of each galaxy and the number of such galaxies grew sufficiently that the individual bubbles around every source overlapped and eventually merged so that the entire IGM was ionised. So the formation of the first substantial population of galaxies was accompanied by the evolution of the IGM from completely neutral, through a "Swiss cheese" phase where ionised bubbles were surrounded by neutral gas through to a completely (or essentially completely) ionised phase. Figure 5.7 shows a visualisation of a simulation of this process.

As the first galaxies trace the evolution of the most over-dense structures in the early Universe, they are also key (and potentially simple) probes of how early structures evolved. At later epochs, interpreting how galaxies relate to the underlying distribution of matter in the Universe is more complicated as there has been more time for multiple complicating physical processes to take place.

In just the past few years, 8m telescopes have allowed progress in understanding the nature of star forming galaxies at $z\sim5$–6, galaxies

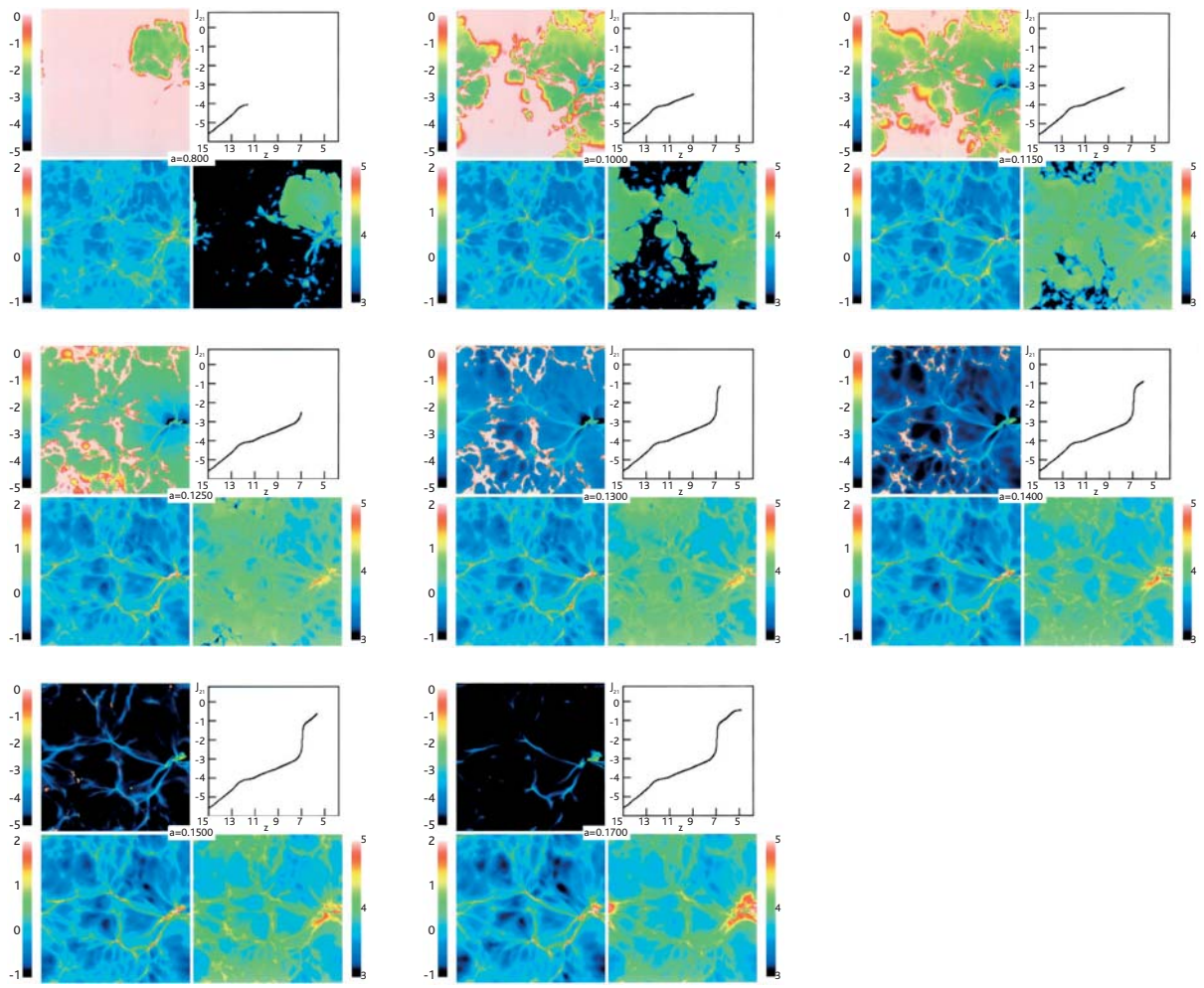

Fig.5.7

Slices of a simulation of the early Universe at eight different epochs: (a) z = 11.5, (b) z = 9, (c) z = 7.7, (d) z = 7, (e) z = 6.7, (f) z = 6.1, (g) z = 5.7, (h) z = 4.9. Shown are logarithm of neutral hydrogen (upper left), logarithm of gas density (lower left), logarithm of gas temperature (lower right), and logarithm of ionising intensity as a function of redshift (upper right). Ionisation fronts propagate from high-density regions where stars and proto-galaxies form. HII regions slowly extend from high-density regions and progressively overlap. As time goes more and more ionising photons are emitted and eventually ionise the entire space (source: Gnedin 2000).

seen after re-ionisation of the IGM was completed. Limited work has been possible on sources at 6<z<6.5, with the highest redshift sources discovered to date at redshifts no higher than z=7. Some of these sources show evidence for stellar populations that formed at higher redshifts (e.g. Egami et al 2005, Eyles et al 2005, Verma et al, 2005 in prep), but no galaxies at z>7 have yet been discovered (see Bremer et al 2004a). To make real progress on sources during the epoch of re-ionisation will require far more sensitive optical and near-IR observations with an ELT. Such observations will allow detailed study of the key properties of galaxies out to z~10. Additionally, an ELT is necessary to survey and spectroscopically identify the most distant high redshift galaxies. These are crucial steps in our understanding of how the first galaxies formed and evolved and how they affected the surrounding IGM. Thus, we are currently only able to investigate the end of re-ionisation with the current generation of telescopes. Where 8m telescopes have allowed us to efficiently survey for galaxies at z~5–6, 100m-class telescopes will allow similar surveys for the faintest sources at z>10 as the increased distance modulus to these sources and the increased sky brightness at

>1μm is directly compensated for by the increase in collecting area.

ELT observations will elucidate the key properties of the first galaxies: their luminosity and mass functions, star formation histories, metallicities, sizes and morphologies, their effect on the surrounding IGM (both through ionisation and chemical enrichment), and crucially for the understanding of the growth of structure, their clustering and dynamics. In addition to direct observations of the first galaxies, we can use bright AGN, supernovae and Gamma-Ray Bursts (GRBs) to probe the properties of the intervening IGM between them and us, sampling multiple typical sightlines through the gas at an epoch when it is undergoing strong evolution (both in ionisation state and also possibly chemical enrichment). This dual track approach should give us a detailed picture of the evolution of both the earliest galaxies and the early IGM and how they influence each other. This detailed and broad picture can only be obtained using an ELT; no existing ground-based or planned space mission can give as complete a picture of the Universe at the time of re-ionisation as an ELT.

5.2.2 The Highest Redshift Galaxies (z>10)

The highest spectroscopic redshift measurements to date lie at z~6–7, corresponding to the approximate end of re-ionisation. The existence of bright quasars at the same redshifts indicates that rather massive galaxies existed at this very young epoch, and it is likely that these started to form at much higher redshifts. SPITZER observations of high redshift galaxies imply that at least some started significant star formation at z>7. One of the important challenges in current day astronomy is to find these very early galaxies, which may have already been a significant population by z>10, if the epoch of re-ionisation started at that time, as indicated by early WMAP results.

Obviously, we currently know very little about z>10 galaxies. At the time of writing, the galaxy with the highest spectroscopically-confirmed redshift is at z=6.6. We can estimate the possible source density of more distant galaxies using reasonable extrapolations from that of z=5–6 sources and from counts of z=7–8 candidates in the albeit small-volume fields of ultra-deep HST observations. Extrapolating from the number counts in Lehnert & Bremer (2003, 2004) and Bremer et al (2004b), Bremer & Lehnert (2005a) estimated the surface density of UV bright galaxies at z=9–10 at AB=27 to be as high as 0.2 per square arcminute. Using broad-band imaging with HST-NICMOS, Bouwens et al (2005) found spectroscopically-unconfirmed candidates at z=7–8 with a surface density of 1 per sq. arcmin, at a typical magnitude of 27 (AB). Given that multiple studies (e.g. Lehnert & Bremer 2003, Bunker et al 2004, Bouwens et al 2005) indicate that the space density of these galaxies is likely to be significantly lower than that of similar star forming galaxies at z=3–4, the very high redshift population is both faint and rare.

If we assume no evolution in the luminosity function between z=7 and z > 10 population, we expect to find galaxies with typical brightness of AB=27.5 and fainter at the highest redshifts. These magnitudes are expected to be beyond the capabilities of continuum spectroscopy with JWST, which should reach magnitudes of 27 in extremely long exposures. Hence, this epoch may be studied using a combination of JWST and ELT observations. Ultra deep imaging by JWST should identify z>10 candidates over large areas and to very faint magnitudes (to AB ~ 31.4 in 10 hours). However, JWST itself would not be able to carry out continuum spectroscopy to these levels. In order to carry out spectroscopy to these depths, and hence, unambiguously determine redshifts for a large number of sources requires an ELT. In typical integration times of 100 hours one can expect to achieve a depth of about 28.5–29 depending on the source sizes with a 60m telescope (S/N of 10 in H-band at a resolution of R=100). Given these long integration times and the rather low surface density, it is clear

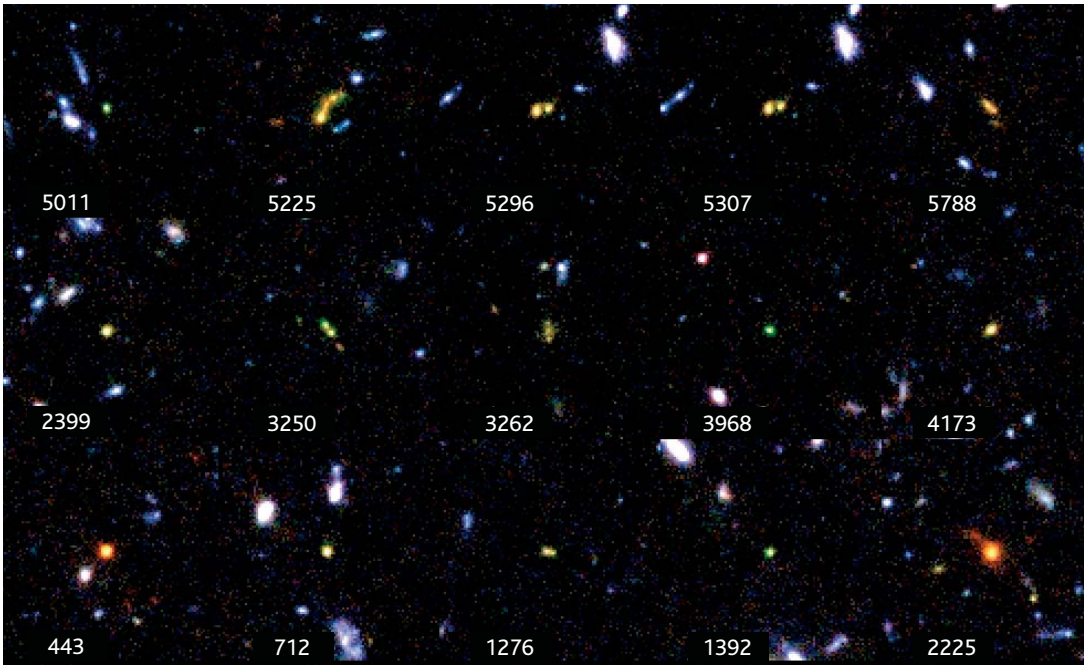

Fig.5.8

HST/ACS images of high redshift (z~5-6) galaxies from Bremer & Lehnert (2005b) showing the small but resolved nature of the galaxies, with typical half light radii of 0.1-0.2 arcsec (1-2 kpc).

that the ELT must have a relatively wide-area spectroscopic capability (though not necessarily a filled focal plane for the spectroscopy – see notes on requirements). Given the expected source densities, a 5x5 arcmin is the minimum requirement, being matched to the field size of NIRCAM on JWST. The desired area is 10x10 arcmin, which is of sufficient area and volume-grasp to allow studies of large scale structure at these redshifts, providing 10 or more such fields are studied to overcome cosmic variance.

Although various studies have shown that galaxies become smaller with increasing redshift (e.g. Roche et al 1998, Bremer et al 2004b, Bouwens et al 2004a), the high redshift galaxies observed to date are resolved with typical half-light radii of 0.1–0.2 arcsec (Figure 5.8 and Figure 5.9). Consequently, diffraction-limited performance is not necessary, it is more important to have sufficient image quality to concentrate the light from galaxies on the 0.1–0.2 arcsec scale.

We note that this work can extend to z=13.8, where the Ly alpha emission line disappears in the atmospheric extinction feature at wavelengths of 1.8–2μm. Longward of 2μm, the emission from the telescope and the atmosphere significantly affects the ability to reach the depths indicated above. In the following three paragraphs we detail key observational diagnostics of the highest redshift galaxies that can be studied uniquely with an ELT.

The highest redshift galaxies exist in a Universe with a density more than 1000 times higher than that in the current Universe. Hence the processes occurring in these galaxies may be qualitatively different from those occurring in nearby galaxies. Below we discuss some basic parameters that an ELT can measure even for these very first galaxies.

Clustering

Galaxies are expected to condense and form within dark matter haloes, consequently a key diagnostic of the properties of these haloes is the clustering of the galaxies. Indeed large-scale structure has been found in the highest redshift galaxy samples to date at z~5.7 (Ouichi et al 2005). Quantifying this in a statistically useful manner at the highest redshifts requires large samples with

spectroscopic redshifts. Models for the growth of galaxies can be directly probed using statistical tools such as the galaxy-galaxy correlation and the halo masses can be probed through other measurements, such as the local density of galaxies. The combination of these measurements will be particularly strong tests of the models for the early growth of structure, for example the correlation between local density and galaxy properties is an invaluable tool to determine the relationship between halo mass and galaxy properties.

Ionisation state and population III

It might be expected that the earliest galaxies have dramatically different spectral properties from z=3–5 galaxies. At extremely low metallicities, the emission lines of NIV, CIV, HeII, etc. are expected to become very strong (as the mean temperature of the ISM is thought to be higher than at low redshift due to the lack of coolants, hence the lines from highly ionised species). These unique diagnostic lines can be used to determine the ionisation state of the gas and thereby constrain its metallicity.
The same spectral information will allow determination of the spectral properties of the earliest stars, possibly allowing identification of galaxies with a substantial population III component (e.g. Schaerer 2003). At high redshift, many of these lines shift into the thermal infrared, but at least CIV is accessible out to z=10.5 from the ground.

In general, dedicated searches behind galaxy clusters may significantly ease the detection and characterisation of the most distant objects (see e.g. Hu et al. 2002 and Kneib et al., 2004 for successful detections using this technique at z~6.5). Cluster lenses typically provide magnifications higher than 10 over typical sizes of ~10 x 10arcsec^2 in the source plane. Dedicated searches behind a large number of clusters could yield tens of gravitationally amplified high-z objects.

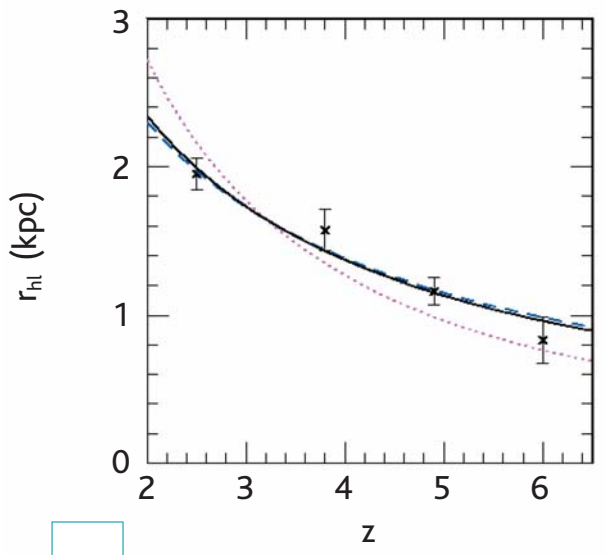

Fig.5.9

Mean half-light radius vs. redshift for objects of fixed luminosity (0.3-1.0 L*, z=3). Shown are data (crosses with 1σ errors on the mean) from a z=2.5 HDF-N + HDF-S U-dropout sample and UDF B-, V-, and i-dropout samples plotted at their mean redshifts of z=3.8, z=4.9 and z=6.0, respectively. The dotted magenta line shows the $(1+z)^{-1.5}$ scaling expected assuming a fixed circular velocity, and the dashed blue line shows the $(1+z)^{-1}$ scaling expected when assuming a fixed mass (Mo et al. 1998). A least-squares fit favours a $(1+z)^{-1.05\pm0.21}$ scaling (solid black line). Source: Bouwens et al. (2004a).

5.2.3 Galaxies and AGN at the End of Re-ionisation (5<z<10)

One of the most astrophysically important questions is: what are the sources responsible for the re-ionisation: star forming galaxies or AGN? The end of the re-ionisation epoch is where the influence of galaxies and AGN emitted sufficient ionisation radiation to begin to completely ionise the IGM. Given the rates necessary, it is also the epoch when galaxies likely started to take on the characteristics that we associate with galaxies in the local Universe. Their metallicities were likely to be similar to the most metal poor objects observed locally; since the metal enrichment of the IGM and proto-cluster environments had been enriched by early generations of stars, characteristics of their stellar populations were probably similar to that we observe at lower redshifts.
In addition, we can investigate the nature of

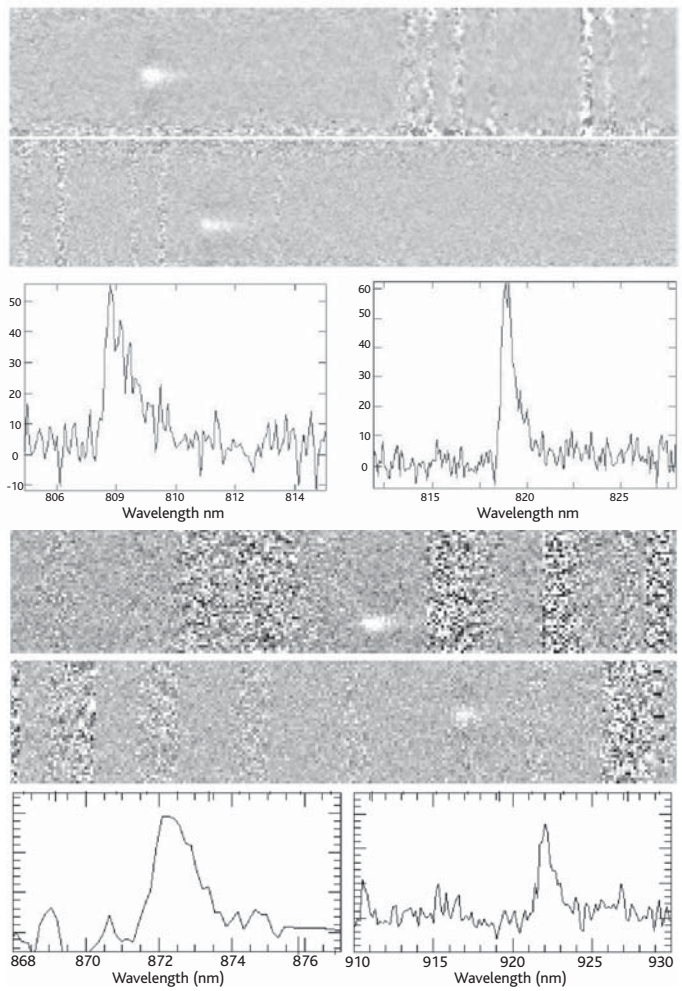

Fig.5.10

(Top) 2D spectra and (below) 1D extracted spectra showing the Ly-α line in high redshift galaxies at z=5.65 and 5.74. The lower panels show similar 2D and extracted spectra for galaxies at 6.17 and z=6.58. The characteristic shape of the line and the drop in the continuum from red to blue across the line (both caused by absorption by intervening Ly-α) identifies the line unambiguously as Ly-α. Source: Bremer & Lehnert (2005b), Cuby et al (2003) and Cuby (private communication).

the neutral IGM and the influence of galaxies on the IGM in detail. In this redshift regime, we should see signs of the recombination haloes around galaxies that are in the process of ionising the surround IGM, as well as observing significant metal enrichment as the most active star forming galaxies and powerful AGN eject metals, energy and momentum into the IGM. Most importantly, perhaps unlike the first objects, many of these galaxies will be bright enough to probe directly and in detail with an ELT. Thus, it is in this redshift regime that we can gain a detailed understanding of important physical processes and influences that shape the nature of galaxies in the early Universe.

Galaxies at redshifts of z=5–6 are the most distant systems that have been studied in any depth. These have been discovered in two ways, either from their strong Ly–α line emission (Figure 5.10) or from their strong rest-frame UV emission. Both of these are clear signatures of recent and ongoing star formation.

The strong UV emitters have recently had many of their broad properties determined. They are young galaxies: for most of these, the star formation we are seeing is the first large-scale event in the system, having lasted no more than a few tens of millions of years. A minority are older, having initiated significant star formation at z~8 or earlier. The size of the star forming region is typically 1–2 kpc across (Figure 5.9) and the dynamical time of the region is comparable to the age of the starburst. Spectroscopy of a typical Ly–α line (Figure 5.10) shows it to have the characteristic shape of a strong out-flowing wind, consistent with the star formation density indicated from the UV-luminosity, up to a few tens of Solar masses per year in a region with a surface area of about 1 kpc^2. The wind is out-flowing into the surrounding medium at speeds of up to several thousand km s^{-1}. It is likely that the stellar population has sub-solar metallicity, given that little star formation seems to have occurred previously.

The above represents the limit of what can be achieved with a modern 8m telescope. ELTs have a key role to play in the deeper understanding of these objects and in studying even more distant galaxies. The deepest spectroscopy of z~5 galaxies carried out to date (~100 hour exposures) can at best identify several absorption lines in the spectrum of the most UV luminous objects. As UV luminosity increases with the stellar mass and age of a starburst region, the limited ability of 8m telescopes to carry out this work means that

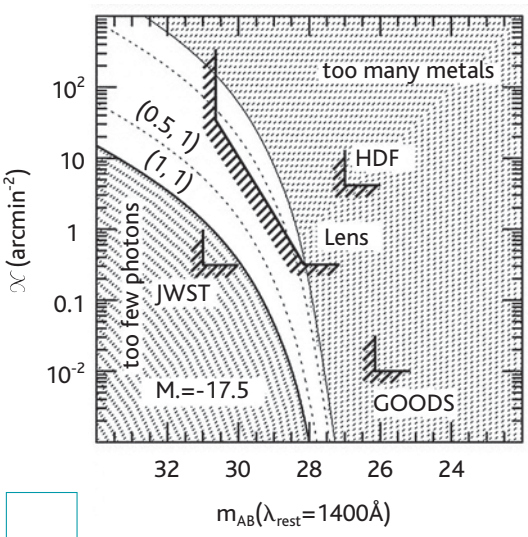

Fig.5.11

Surface density vs. apparent AB magnitude of reionisation sources per unit redshift with a broad luminosity function. The lower solid line represents the minimum surface brightness model. The upper thin solid line represents the global metallicity constraint. The thin dotted lines give predictions for different models. The adopted luminosity function has faint-end slope $\alpha=-1.6$ and knee $M^*_{1400}=-17.5$. The non-shaded area is the only one available to reionisation sources with this luminosity function. (Source: Stiavelli et al. 2004).

the results are unlikely to be typical of the majority of the galaxies at these redshifts.

With a suitable moderate-order adaptive correction, a 30–100m could obtain a spatially-resolved spectrum of the same objects on the same (100hr) timescale. This would directly determine the dynamics and total mass of the stellar population in these galaxies. Assuming optical correction is possible, z=5–6 galaxies can be studied spectroscopically in a 3x3 or 10x10 pixel data cube, depending on telescope size. Given that the half-light radius of these sources is typically 0.2 arcsec, a spatial resolution substantially better than this (of order 0.02") is required for a full 100m study.

Higher redshift sources would also be observable in a similar manner, though at z>9 the study would be carried out in the J-band and would be limited to those spectral features falling in favourably dark regions of the sky spectrum. Assuming that during the era of ELTs, the JWST will be operating, use of an ELT to follow up JWST-discovered z>9 galaxies will be the crucial method to understand how these earliest galaxies formed and evolved.

As well as studying the stellar continuum of these sources, the ELT will be able to carry out exquisite spatially-reduced studies of the emission lines for these sources. The lines have a far higher surface brightness than the continuum, allowing for very high spatial and spectral resolution structure. At the diffraction limit of a 100m ELT, individual HII regions could be identified and the kinematics and spatial structure of the emission lines can be elucidated in a level of detail comparable to current studies of low redshift star forming galaxies. This will allow direct comparison of the evolution and properties of low and high redshift starbursts.

Similar studies can be carried out on Ly–α–detected high redshift galaxies. These are related to the UV-luminous objects: they are a subset of the lower UV luminosity counterparts with large Ly–α equivalent width, indicating that these are extremely young starbursts, even younger than the UV-luminous objects. This star formation has lasted for a few million years at most and the UV emission has had little time to build up. Detection of their comparatively weak continuum is equally-well carried out using a 100-m ELT or the JWST, with the ELT having the advantage at lower redshifts because of the decreased terrestrial sky brightness in the optical. However, the detailed high-resolution study of the properties of the Ly–α emission described earlier can also be carried out by an ELT on these objects (they have Ly–α luminosities comparable to the UV-bright sources). Such studies cannot be carried out by the JWST.

What kind of source densities can we expect for both these populations?

UV-bright (Lyman break) galaxies.

At z=5-6 the surface density is ~1/3 arcmin^{-2} to AB=26 per unit redshift, about 1/40 arcmin^{-2} with $f_\lambda>10^{-17}$ erg s^{-1}cm^{-2} for Ly–α and ~1/10 arcmin^{-2} for $f_\lambda>2\times10^{-18}$ erg s^{-1}cm^{-2}. The sources have flat continuum spectrum (zero colour in AB).

Assuming no change in luminosity function, at z=7–9 there is the same volume/ arcmin^{-2} as at 5<z<6. There is about a factor 2 decrease in flux for the same luminosity so the above numbers apply to AB=27 and f_λ>5x10^{-18} erg s^{-1}cm^{-2} and 1x10^{-18} erg s^{-1}cm^{-2}, respectively. Evolution is likely to affect the luminosity function towards lower object densities and luminosities, and reaching AB=28 is required (see Figure 5.11).

A 100m telescope can achieve S/N of ~ 10 in 100 ksec in spectroscopy at a resolution of 5000 (for OH suppression and dynamical studies) on objects with AB=27.5-28 depending on source size. Obviously, higher S/N can be obtained when emission lines such as Ly–α or HeII are present, allowing in turn more detailed dynamical analyses.

Therefore, multi-object spectroscopy will allow simultaneous observations of a few tens of objects at once provided that the field of view of the telescope is large enough (a few arcmin in diameter) and that AO image enhancement can be performed over the full field or in parts of it.

Lyα sources.

To f_λ~10^{-17} erg s^{-1}cm^{-2} with a 1.5% filter there are 1/45 arcmin^{-2} at z=5.8. Therefore, over Δ z=1 (a ~15% filter) there is 1/4.5 arcmin^{-2}. For a reasonable luminosity function, we can expect about 1/arcmin^2 at f_λ~10^{-18} erg s^{-1}cm^{-2}. These can be found using large-area IFUs, slitless spectroscopy or narrow-band imaging. Assuming no evolution, we get comparable numbers for z=7-9. Of course, increasing (and wavelength dependent) sky brightness in the red limits the actual volume that can be probed. So, the surface density is relatively high, but they are harder to identify than UV-bright sources.

A problem in studying these is the number of line-only sources that are at lower redshift, which have surface densities at least an order of magnitude higher than the z>5 Ly–α emitters. These interlopers can be identified by deep multi-band and multi-wavelength observations.

Considerations about the size of the targets

1 kpc corresponds to 170 mas at z=6 and 0.5 kpc corresponds to 100 mas at z = 8. Typical half-light diameters are therefore of the order of 200-300 mas. Therefore, a spatial resolution of the order of 20 mas is required to optimise the signal to noise ratio and to allow spectroscopic and dynamical studies of these objects in cubes of the order of 10x10 spatial elements.

Notes on Design Requirements

Observation Type: Imaging and spectroscopy (for continuum and emission lines)

Field of View: 5 arcmin or more – a goal of 10x10 arcmin is desirable. Note that an ELT is likely to be faster than JWST for individual sources, but without a large FOV this gain would be lost (see Annex B for discussion). The FOV would not need to have contiguous instrumentation. Deployable IFUs would be suitable (see below).

Spatial Resolution: Local (along line of sight to targets) AO correction with a goal of at least 50% encircled energy within 0.01 to 0.02 arcsec for a 100m telescope. More relaxed AO constraints are appropriate for spatially-unresolved spectroscopy of the most distant sources – in this case the light should be concentrated in apertures matching the source size (around 0.1–0.2 arcsec).

Spectral Resolution: 5000–10000. Lower resolution (R~ a few hundred) is sufficient for simple redshift determinations of very high redshift sources (although higher resolution may still be needed for sky background suppression).

Wavelength Range: 1.0–2.4μm. Continuum spectroscopy of the faintest sources may be best done at λ<1.8μm where the sky background is lower.

Target Density: 0.2–5 per arcmin^2

Telescope Size: 100m or as large as possible for collecting area. 50m could make an important contribution and a 30m could also make some contribution.

Observing time: Several tens to hundreds of hours per field

Other comments: multiple IFU required. 10 to 50 IFUs with about 1" individual FOV and about 20 mas spatial sampling. Note that at this spatial resolution and for spectral resolutions up to R~10,000, observations are background limited between the OH lines after a few minutes.

5.2.4 Probing the Re-ionisation History

The first "fairly bright" objects are not only markers of the beginning of the re-ionisation epoch, but are also crucial for probing the inhomogeneous structure and metal enrichment of the IGM from metal absorption lines in their spectra due to intervening ionised structures. The short-lived gamma-ray bursts (GRBs) are an obvious bright population and can be detected up to z~15–20 (depending on telescope size, see Table 5.1). Explosions of population III stars (events fainter than GRBs) can be used to probe the IGM at z~<12, although this population rapidly disappears with time for regions with metal enrichment higher than 1/10000 of the Solar value. Although the epoch of quasar formation is a fully open question, the SDSS quasars at redshifts around 6 are powered by supermassive black holes, thus intermediate mass black holes (corresponding to quasars of intermediate luminosity) must exist at earlier epochs (up to at least redshifts of about 10).

These rare objects will be detected by dedicated missions/telescopes in the case of GRBs and the supernovae resulting from the explosions of population III stars. The highest redshift quasars are likely to be discovered during the next decade by the JWST space mission.

Probing the physics of the IGM at redshifts from 10 to 20 requires intermediate/high resolution spectroscopy in the near IR, which can only be carried out with telescopes of the 60–100m class due to the predicted low fluxes of these first "background" objects. The extremely fine diffraction limit of large apertures concentrates the light from unresolved objects such that there is little or no effective background contamination from sky emission. Shortward of 3μm, an ELT will be far superior to any planned orbiting observatory at studying these objects, being able to do so in a more flexible way given the instrumentation possibilities of a ground-based ELT.

Object	$f_\nu$obs (μJy)	λobs (μm)	m_{AB}	S/N	Δt (hr)	S/N	Δt (hr)
				100m		30m	
Gamma Ray Burst (GRB) at z=10, observed with R=10⁴							
Very bright GRB 10 days after burst (similar to bulk of GRB population at 1 day after burst)	1.5	2	K=23.6	40	1.8	15	15
Bulk of GRB population at +10 days	0.04	2	K=27.4	15	90	X	X
Very bright GRB 1 day after burst	30	2	K=20.3			40	2.7
Population III Supernova							
at z~9	0.65	1.24	J=24.4	40	1.7	40	75
observed with R=10⁴							
observed with R=2x10³						40	8
at z~12	0.44	1.60	H=24.8	40	4	X	X
observed with R=10⁴							
observed with R=2x10³						40	50
at z~16	0.30	2.1	K=25.2	40	14	X	X
observed with R=10⁴							
observed with R=2x10³						20	70
High redshift Quasar							
at z~9 observed with R=2x10³	0.008	1.24	J=29.1	20	50	X	X
at z~12 observed with R=2x10³	0.019	1.60	H=28.2	20	50	X	X
at z~16 observed with R=2x10³	0.033	2.1	K=27.6	20	50	X	X

Table 5.1

Estimated signal-to-noise ratios and exposure times needed to observe various types of unresolved, very high redshift object (GRBs, population III supernovae and quasars) with a 100m and a 30m ground-based telescope. Entries marked by "X" are infeasible observations with a 30m telescope.

The strong HI absorption by the IGM implies observations in the near IR: J to K bands for z~9, H and K bands for z~12 and K band for z~16. Spectroscopic observations in the near IR of the first objects can be performed with ELTs at different resolution and signal to noise for the 3 populations of object. In Table 5.1 we compare theoretical signal-to-noise estimates for various types of object observed with a 100m and 30m ground-based telescope, derived using the ESO on-line ELT exposure time calculator. Cosmological parameters of Ω_M=0.3, Ω_Λ=0.7 and H_0=70 kms^{-1} Mpc^{-1} have been assumed.

The more luminous GRB afterglows at z=10 should have fluxes at λ~2μm of 30μJy and 1.5 μJy at 1 and 10 days after the burst respectively, while mean expected fluxes are 1.5 and 0.04 μJy at 1 and 10 days after the burst (Lamb & Reichart 2000). For GRBs at z=10, spectroscopic observations of similar quality can be obtained with 30 and 100m telescopes although at different times after the burst. As shown in Table 5.1, for a spectral resolution R=10^4 a 30m telescope could not observe the bulk of the GRB population at 10 days after the burst (but could observe very bright GRBs and/or GRBs within ~1 day of the burst).

Population III SNe

Massive stars (140-260 $M_\odot$) should explode as very bright supernovae and could then be detectable from the ground out to z~16 for about one month after the explosion, and at even higher redshift, thus longer observed duration, from space. For a broad range of rest-frame UV frequencies, the monochromatic luminosities of population III SNe remain about constant for a substantial fraction of the time. Theoretical models (Heger et al 2001) give peak AB magnitudes of 25.5 at z=20 for λ_{obs} in the range 1.5–5μm. From this we derive fluxes of 650, 440 and 300 nJy at λ_{obs} =1.2μm (z~9), 1.6μm (z~12) and 2.1μm (z~16), respectively. Because high spectral resolution data (R~10^4) are needed to derive the physical properties of the ISM and IGM at z>10, such studies can only be conducted with ELTs of very large size (70–100m).

QSOs

The bright 6.0<z<6.5 QSOs discovered in the Sloan Digital Sky Survey (SDSS, Fan et al 2003) have magnitudes z'_{AB}~20. Assuming that they radiate at the Eddington limit, their black-hole mass is equal to ~ 4x10^8$M_\odot$. There are very few such objects: currently 6 in 2870 deg^2. Fainter QSOs, up to z~5, have been searched for in the COMBO-17 survey (Wolf et al 2003) and the luminosity function of z~5 QSOs has roughly the same luminosity dependence ($L^{-1.5}$) as that found at z~3. For a population one hundred times fainter than the z~6 SDSS QSOs, the expected fluxes are 200, 140 and 95 nJy at z~9 (1.2μm), z~12 (1.6μm) and z~16 (2.1μm) respectively. It should noted that QSOs with rest-frame monochromatic luminosities equal to those of z'_{AB}~24 QSOs at z~6 would have apparent fluxes similar to those of population III SNe at the same redshift.

Black hole masses, thus luminosities, of high redshift QSOs are limited by the time available for mass accretion onto black-hole seeds. Even if the latter are massive (~10^3$M_\odot$) population III stars, black-hole masses at z~10–15 may not exceed 10^5–10^6 $M_\odot$ (Ricotti & Ostriker 2004). Consequently, the UV luminosities of high redshift QSOs may be at most ~1x10^{44}erg s^{-1} which gives expected fluxes of 42 and 29 nJy at z~9 (1.2μm), and z~12 (1.6μm) respectively.

QSOs at high redshift may be ten times less luminous than population III SNe. If so, they would be too faint to be observed with 30m telescopes at a spectral resolution of R=2x10^3. A spectral resolution of R=2x10^3 remains of interest to explore e.g. the metal-enrichment of the IGM at early times from the study of the CIV forest. This could be done with 100m class telescopes. The minimum flux limits for S/N=20 in 50 hr for spectroscopy at R=2x10^3 with 100m telescopes are shown in the lower three rows of Table 5.1. For Eddington rest-frame luminosities, these correspond to black-hole masses of (1.5, 5 and 13) x10^5$M_\odot$ at z~9, 12 and 16, respectively. To get such high masses at z~16 would imply either seed black holes at z~25–30 with masses larger than 10^3$M_\odot$ or efficient merging of black holes in dense stellar clusters at early times.

Notes on Design Requirements

Observation Type: High-resolution absorption-line spectroscopy

Field of View: Single point sources

Spatial Resolution: Diffraction-limited for best point-source sensitivity

Spectral Resolution: R=10^3 to 10^4

Wavelength Range: Near-IR (JHK)

Target Density: single objects

Telescope Size: As large as possible for better point source sensitivity. See Table 5.1.

5.2.5 Early Chemical Evolution of the IGM

Understanding the heavy element enrichment of the Universe, and the effect of galaxies on the environment in which they form is one of the most outstanding problems in astrophysics. It is not only important for understanding the star formation history of the Universe, but also may influence the characteristics of the star formation itself by changing the modes by which gas cools and forms stars. Thus, without a thorough understanding of how and when the metals in the Universe were created and dispersed, we have no hope of understanding the evolution of galaxies and the growth of structure.

Recent studies (e.g. Adelberger et al 2003) have shown that galactic winds from starburst galaxies are likely to play an important role in enriching the intergalactic medium. What is less clear is the mechanism, the degree of enrichment, and its range. We do not even know whether galaxies formed early enough to enrich the whole of the intergalactic medium which we see at redshifts z≈2–5. Some attempts have been made to investigate the metallicities of regions of the intergalactic medium (Schaye et al. 2003; Simcoe et al. 2003). Generally these apply mostly to overdense regions which are predominantly near galaxies, with extrapolated or averaged suggestions that metallicity upper limits for [C/H] (or [O/H]) are of order –3.5 for the lower density gas. However, limits of below 10^{-4} of Solar are the important ones, since it is at that level that the presence of heavy elements is not expected to significantly change the way the regions evolve, and in particular the stellar mass function when they form stars (e.g. Bromm & Larson 2004).

Probing gas densities close to the Universe mean density is difficult with presently available instruments. If we choose the mean density at redshifts 3.0 and 4.5 as points at which we might wish to measure metallicities then we can, using the Schaye (2001) HI column density versus hydrogen number density estimates, the Haardt-Madau (2001) ionising flux estimates and the CLOUDY (Ferland 2004) photoionisation code, arrive at estimates for the CIV and OVI column densities in these regions. The results, giving the expected column densities (given as log*N*) for heavy element abundances at uniformly 10^{-4} Solar, are shown in the following table:

Redshift z=	3.0	4.5
Density n_H (cm^{-3})	10^{-5}	3 x 10^{-5}
log*N*(HI) (cm^{-2})	13.5	14.4
log CIV/C	–2.8	–1.6
log*N*(CIV)	8.4	9.6
log OVI/O	–1.5	–1.0
logN(OVI)	10.0	10.5

Note that OVI is in any case hopeless because of blending with the Ly–α forest lines, but was included since it is likely to have the strongest lines in the available wavelength range. CIV is often in a clear region of the spectrum since its rest wavelength is above that of Ly–α, and at redshifts z≈3 and 4.5 is clear of significant

absorption in the Earth's atmosphere. However, its detection at this level is challenging, since current detection limits from high S/N high resolution spectra are about log*N*(CIV)≈11.5. Even with a 100m telescope the achievement of a S/N 5000-10000 spectrum for a 17.5mag object is hardly a realistic prospect, though with 10% efficiency a S/N of about 2000 should be achievable in about 60 hours exposure time, giving a metallicity limit for a single system in the high redshift case of [C/H]≈–3.5. A S/N level of order 10000 would then be achieved by averaging the signal from 25 or so such systems. At this level the redshifted CIVλλ1548, 1550 lines for such systems at redshift z≈4.5 would be detected.

The figure of 25 such systems per object is a realistic one. It is based on counting those with log HI column densities in the range 14.3< log(*N*(HI))<14.5 with accurate redshifts 4.0<z<4.5 in the Keck spectrum of the high redshift QSO BR2237-0608. There will be some velocity smearing of the average from uncertainties in the Lyman line redshifts, but the trade-off between S/N and velocity uncertainty can be assessed from the data.

At a S/N of 10000 there is the possibility that weak absorption in the Earth's atmosphere will be significant. There are two ways of removing this problem – the extensive HITRAN line database covers a wide range of atmospheric transitions, and should be useful at this level. Also, any signal seen could easily be checked by re-observing at some time later, when the Earth's velocity projected along the line of sight has changed by a few km s^{-1}. The atmospheric lines will not move, and the object ones will be displaced by a known amount. Small variations in the detector response can be removed in a similar way – either with the atmospheric lines or by shifting the wavelengths on the detector by a small amount.

Notes on Design Requirements

FOV: Small (<10 arcsec plus guide star)

Spatial resolution: Not important (if image sliced to get spectral resolution)

Spectral resolution: R~10000

Wavelength range: 0.4–0.9μm

Observation type: Absorption line spectroscopy

Target density: Single targets

Special requirements: None

Telescope size: As large as possible. 100m is most sensitive to point sources. 50m would also make a very significant contribution.

Observing time: 100m ~60 hours/object

Date constraints: None

Comments: JWST would not be able to carry out this science

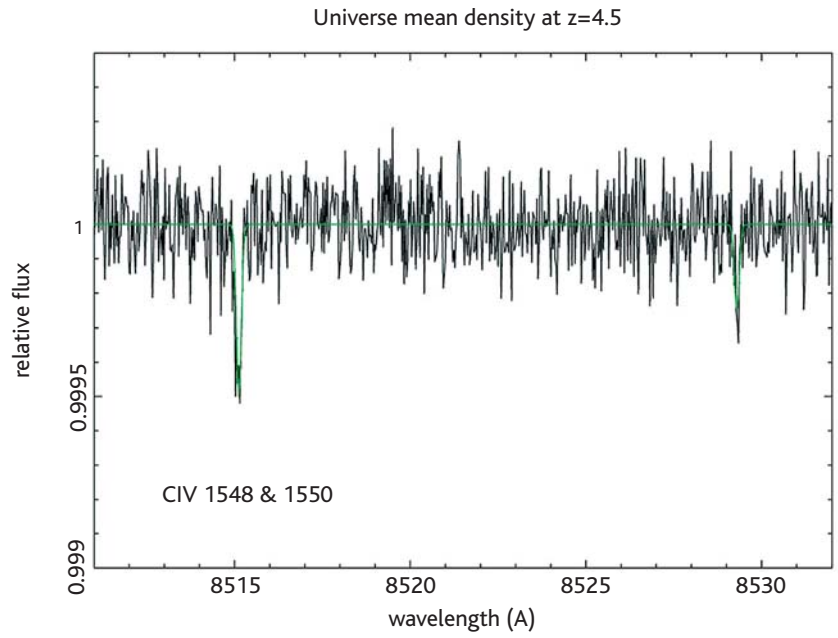

Fig.5.12 The expected strengths of the CIV doublet lines for 10^{-4} Solar abundances in a system with the mean Universe density at redshift z=4.5. The data at S/N=10000 are shown in black, and the noise-free signal in green. The assumed spectrograph resolution is 3 km/s, which is the same as the assumed line width; note the vertical scale.

5.3 Evolution of galaxies

The current generation of largest space- and ground-based telescopes have made rapid progress and allowed us to place preliminary constraints on the global cosmic evolution of star formation and mass assembly. However, this is not sufficient to understand the interplay between the baryonic and dark matter, to study the complex physics of baryon evolution (merging, star formation, feedback, AGN, ...), and to trace the formation and evolution of galaxies in detail. Questions we would like to address are: how has the dark and baryonic matter in galaxies grown from the first cosmological seeds? What physical mechanism is responsible for metallicity gradients in galaxies and the mass-metallicity relationship observed in the local Universe? What were the characteristics of the galaxies that merged in the early Universe to form the galaxies we see today? What is the role of feedback from intense star formation and super-massive black holes on the ensemble characteristics of galaxies? What is the relative fraction of dark and baryonic mass as a function of redshift, total mass, and radius from the centre of mass of the galactic system?

Over the next 20 years, one of the major goals of astrophysics will be to map spatially resolved parameters of individual galaxies and the matter distribution at moderate to high redshift (z=1–5). These goals can be accomplished with an ELT by mapping the spatially resolved kinematics, star formation, and chemical abundances of individual massive galaxies, as well as measuring the kinematics of their satellite objects. We can then investigate the past history as well as constrain the future evolution of a statistically significant number of galaxies. This is a unique avenue to understand the growth and evolution of both the baryonic and dark matter components of high redshift galaxies that has not been possible to date.

5.3.1 Introduction

Over the last decade, observational cosmology has made rapid and substantial progress (Table 5.2). The results of WMAP have been a significant step toward the adoption of a concordance cosmology with accurate determinations of many of the cosmological parameters. This (now) standard model includes a fairly mature view of the hierarchical structure formation, under the sole influence of gravity. The basic premise of all models of large scale structure is that fluctuations in the mass density of the early Universe grow through simple gravitational aggregation/collapse. The collapse depends purely on the initial conditions, now thought to be well constrained by observations.

The same is not true for our understanding of the evolution of galaxies – the evolution of the baryonic component does not simply follow the hierarchical merging of dark matter structures. The opposing forces of cooling, angular momentum exchange and loss, and feedback due to star formation and active galactic nuclei largely drive it. Phenomenological ("semi-empirical" or "semi-analytical") models have been developed to describe the formation and evolution of galaxies. These models rely heavily on simple parameterisations of the physical mechanisms that are likely to drive galaxy evolution. Thus, this type of modelling relies heavily on specific observations to determine the correct parameterisations and relationships between complex and perhaps interacting/opposing physical processes. The most important ingredients are metallicity, angular momentum, stellar initial mass function, and spatial distribution of the gas, the frequency of mergers, as well as the star formation and feedback processes such as radiation pressure and mechanical energy injection from both stars and super-massive black holes. Models differ in prescriptions for this physics (Figure 5.13).

The most direct way to verify these prescriptions is to observe both the earliest and most rapidly growing galaxies, and

measure their physical properties. Through detailed observations of high redshift galaxies, we ultimately would like to know their spatially-resolved star formation histories, extinction, and metallicities, and most importantly for the growth of structure, their clustering and the dynamics of individual sources and satellite/companion galaxies. These last two are especially crucial as they determine the mass scales of the galaxies and their dark matter haloes, and allow insight into the role of feedback in shaping the properties of the ensemble of galaxies. These detailed studies must be done using sufficiently large parent population samples (numbering thousands) and over large enough volumes in order to rule out field-to-field variations ("cosmic variance") and temporal variations biasing the results.

The ability to conduct studies of these types is one of the main drivers of the capabilities of any ELT. To understand the evolution of galaxies across a wide range of redshifts will require (i) a telescope of large aperture to study the low surface brightness emission to obtain spatially resolved properties, (ii) an instrument with high spatial and spectral resolution in order to investigate galaxies on physical sizes of HII regions/complexes and velocities of the lowest mass galaxies or smallest velocity gradients, (iii) an instrument with a high multiplexing advantage and efficiency to obtain the necessary signal-to-noise on large numbers of objects simultaneously, and (iv) instruments covering a wide range of wavelengths in order to use the important diagnostic lines in the rest-frame UV and optical to constrain the physical properties of galaxies across the redshifts where most of the mass in galaxies was put into place.

Redshift range	$0.5 < z < 1.3$	$1.3 < z < 2.6$	$2.6 < z < 6$	$z > 6$
Number of objects with spectroscopic redshifts	several 10000	~2000	~1000	~10
Relative mass range probed	Dwarf galaxies	M*	>M*	Unknown
Epoch of	Disk formation?	Disk/elliptical formation?	Massive Elliptical formation?	First Objects/ young galaxies
Star Formation Rate – Extinction	LIRG dominated	LIRG/ULIRG Dominated	Unknown	Unknown
Integral of Stellar mass – photometry	~50% of the mass formed	~25% of mass formed	<10–20% of mass formed	Unknown
Metallicities	~100 galaxies with R_{23}, evidence for some evolution	A handful of galaxies with R_{23}	A handful of galaxies with reliable R_{23}	Unknown
Dynamical Mass Estimates	50 objects (3D) Rotation/dispersion dominated?	10s of galaxies Rotation/dispersion dominated?	10–20 objects Rotation/dispersion dominated?	1 QSO Unknown
Stellar populations Metallicity/dynamics	Rough mass metallicity relations	Unknown	Unknown	Unknown
UV escape fraction	~10% z=0	Challenging to measure directly	~10–50%	Unknown
IGM metal abundance	Good estimates	Good estimates	Puzzling results in the evolution of metallicity density	Pre-enrichment?
Clumping factor of neutral IGM	~0	~0	~0 to unknown	Unknown

Table 5.2

Summary of our current understanding of the properties of galaxies in various redshift ranges.

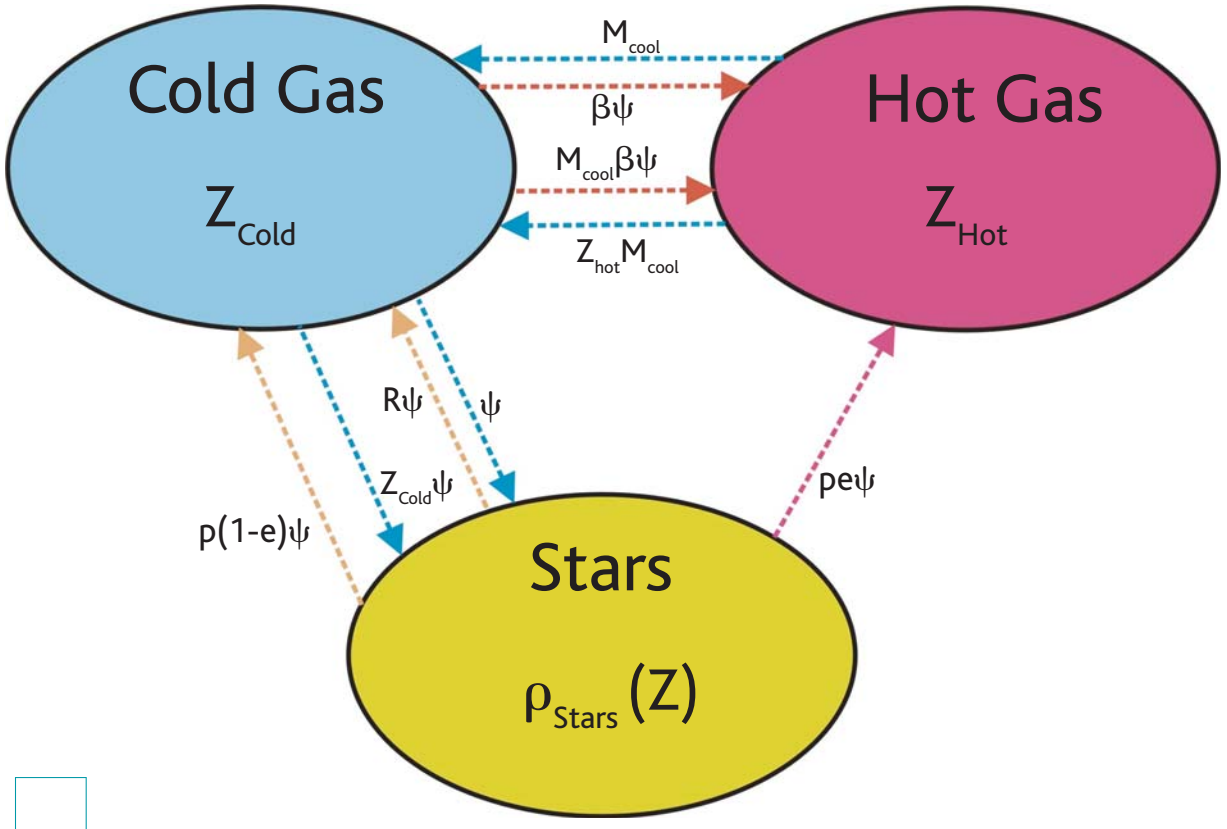

Fig.5.13

Schematic representation of the physical processes likely to be involved in the formation of stars and the relative balance of phases in the interstellar medium (based on a similar diagram presented by Carlos Frenk). This balance is largely controlled by the processes of stellar and AGN feedback, the energy released through gravitational collapse, and dissipation. In this balance, the rate and quality of star formation play key roles and thus an important constraint in modeling galaxy evolution is the initial mass function and feedback as a function of environment and metallicity. The symbols represent: M_{cool}=mass cooling rate of hot gas, ψ=star formation rate, β=shock heating rate, Z_{cold}=metallicity of cold gas, Z_{hot}=metallicity of hot gas, R=star formation efficiency, p=yield, and e=fraction of gas converted to hot phase by supernovae and stellar winds.

5.3.2 Physics of High Redshift Galaxies

What are the physical processes that were responsible for shaping the properties of the ensemble of local galaxies? We are beginning to understand the co-moving mass density and star formation rate as a function of redshift. While this achievement is providing powerful insight into how the whole population of high redshift galaxies grew, we still do not understand why high redshift galaxies are very different from nearby galaxies. As such, the determination of average mass density and star formation rate has only broad implications for the physical processes that drive the evolution of galaxies. The important physical processes within galaxies at high redshift are not understood. For a good understanding of the galaxies, we must consider: the non-linear collapse of gas on scales spanning from the formation of individual stars and HII regions to the global rate of star formation in a galaxy halo (i.e. less than a parsec to many 10s of kpc); the initial mass function and how its shape changes with environment (e.g. metallicity, gas pressure, temperature, ambient radiation field, etc); feedback from stellar winds/supernova and active galactic nuclei; the cooling and heating of the interstellar medium down to scales of individual star forming regions and stars; various gas and stellar dynamical processes

that lead to redistribution of gas and stars allowing for processes that may change the star formation rate and the growth of super-massive black holes, and many other processes (see Figure 5.13).

How will we probe such physics in the high redshift Universe? Telescopes with significantly larger apertures and instruments with deployable integral field units are clearly required to provide dramatically enhanced spatial resolution and sensitivity. This will allow us to detect emission and absorption lines at very high resolution out to the low surface brightness outer regions of high redshift galaxies. Instruments capable of obtaining high spectral resolution (R~5000–10000) in both the optical and infrared are required in order to use the rest-frame UV and optical emission and absorption lines to investigate the various physical processes shaping galaxies at high redshift. The availability of an AO system will also allow detailed studies of the stellar distribution, gas distribution and kinematics, winds, etc.

With such a combination of high spectral and spatial resolution and massive light gathering capability, an ELT will be capable of measuring the following.

1. Column densities of the many species in the rest-frame UV relative to the column density of Hydrogen (either obtained from the Lya absorption or from HI studies with future generations of radio telescopes) which will allow us to estimate the ionization state and metallicity of the interstellar medium of high redshift galaxies.

2. Spatially resolved optical emission line ratios such as R_{23}=[OII]λλ3726, 3729 + [OIII]λλ4959, 5007/Hβ, Hα/Hβ, [NII]λ6583/Hα, [SII]λλ6716, 6731/Hα, etc. to constrain the metallicity, the ionisation state of the emission line gas, coupled with line width, velocity, and emission line morphology, to determine whether or not the galaxies are driving large scale outflows – "superwinds" (e.g. Lehnert & Heckman 1996) or are hosting active galactic nuclei.

3. The strength of the rest-frame UV and optical interstellar and stellar absorption lines such as Mgb, Balmer series, and various metal lines (such as CIV and FeII) to estimate the age and metallicity of the stellar population.

4. The relative velocities of the rest-frame UV and optical interstellar and stellar absorption lines to investigate the dynamical state of the interstellar medium – are these galaxies driving superwinds and what are the energy, momentum, metallicity, and dust content of these outflows (e.g. Heckman et al. 2000)?

5. Dynamical masses compared to the characteristics of the stellar population estimated from their absorption lines and spectral energy distributions, which will allow us to constrain the stellar initial mass function over a wide range of redshifts.

6. General properties of galaxies hosting active AGN and those which are not. From such a comparison we can elucidate the processes responsible for the growth of super-massive black holes and its relationship to star formation within the galaxy.

Obviously, this is just a sampling of what a combination of an ELT and a set of very efficient, highly-multiplexing optical and near-infrared spectrographs could accomplish in understanding the properties of high redshift galaxies.

Notes on Design Requirements

Determining the relative velocities and spatially resolved characteristics of galaxies with a wide range of magnitudes and surface brightness distributions requires an instrument with a high multiplex and deployable integral field units. To obtain the necessary sensitivity and physical scales necessary to probe the individual star forming regions and complexes requires a robust adaptive optics system. In order to probe individual regions of galaxies, which have the physical size of a hundred pc or less, will require resolution near that obtainable with a 30 to 100 m telescope. Fields of view of about tens of arcmin^2 will be necessary to study 10s of galaxies simultaneously. This multiplexing advantage is absolutely crucial since to reach the surface brightnesses necessary in the extended galaxy continuum will require exposure times of perhaps several nights, even with the largest aperture telescopes. Obviously, the observable number of individual galaxies is proportional to the field size which would also then drive the number of deployable IFUs. To construct the table below of required instrumental parameters, we have assumed that we are observing galaxies in the redshift range $1.7<z<3.5$, where all of the important rest-frame UV and optical emission and absorption lines from rest-frame Ly–α to [OIII]λ5007 or Hα are available in the atmospheric windows from 0.3 to 2.5 microns, and the number of suitable targets is roughly ≥ten≥arcmin^{-2} (down to m_{AB}=26 in the near-infrared).

Specs	minimum	goal	Note
Observation type			Multi-object integral-field spectroscopy
FOV (diameter)	2 arcmin	10 arcmin	if small FOV, the program requires duplicate observations to cover > 10 arcmin scales
Spatial resolution	50 mas	10-20 mas	Size of HII complexes ~0.1–0.2 kpc
Spectral resolution	5000	10000	OH sky requires > 3000 Resolving ISM lines ~10–20 km/s
Wavelength range	0.5–2.5μm	0.3–2.5μm	
IFU type Number and Size	20 with 2x2 arcsec FOV		To map abs. and emission line velocities, metallicities, extinction, and ionisation
Pixel size Number/IFU	50 mas 40x40	20 mas100x100	
Minimum space between IFUs	Few arcsec	Few arcsec	To investigate mergers and massive companions
Target density	~0.1 to ~10 arcmin^{-2}		
Special Requirement			IFU
Telescope size	30m	100m	
Observing time			Of order ~1 night per field. Depends on multiplex and required statistics
Comments			JWST does not have multiple IFUs and will likely not observe down to 0.3μm

5.3.3 The Assembly of Galaxy Haloes

How have galaxies grown from the first cosmological seeds? Despite the general concordance on the ΛCDM cosmological model, the question of how and when the present-day galaxies formed and assembled still remains open. In the generally accepted framework, galaxies assemble and increase their mass gradually through the merging of dark matter haloes (Figure 5.14 and Figure 5.15). In this scenario, the young Universe is expected to be populated by small mass objects which are the first to form, whereas the most massive galaxies are the last products of this "merging tree" evolution.

Unlike the complexity and the large number of (non-linear) physical processes that are relevant in the growth of the baryonic component of galaxies, the growth of the dark matter component should be through simple gravitational, non-dissipative accretion and merging of individual "clumps" of dark matter, which is driven by dynamical friction and angular momentum exchange. These are driven by the large-scale distribution of dark matter that is not uniform, but is simply set by the initial conditions of the early Universe. All these effects are calculable with the only limitation that there is a size and mass scale below which the current

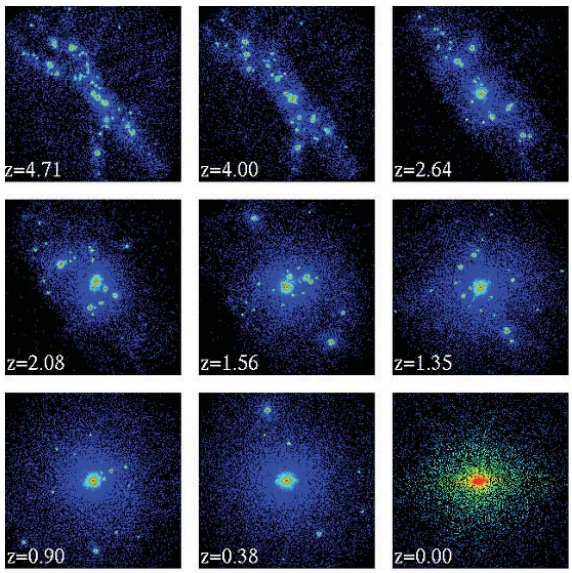

Fig.5.14 A realisation of the evolution of a dark matter halo from Abadi et al. (2003). Each panel shows the distribution of dark matter particles in a cube of 320 physical kpc on a side. The bottom panel shows the inner most 40 kpc and each particle is coloured according to its dark matter density. The redshift is indicated in the lower left corner of each panel.

generation of computers cannot yet model. Unfortunately, this size is currently too large to resolve many important aspects of galaxy formation and evolution.

As described in the previous section, while we think we have a reasonable understanding of the boundary conditions of galaxy evolution, we do not have even a basic understanding of the detailed baryonic physical processes or their relative efficiencies. More fundamentally, studying the baryonic component of galaxies alone is equally inadequate, since the mass of any structure in the Universe is dominated by dark matter and because of the complexity of the physical processes that control the growth of the baryonic components of galaxies (shocks, feedback from massive stars and AGN, merging, interplay between dark and baryonic matter, etc).

Thus, it is clear that over the next 20 years, one of the major goals of astrophysics will be to map the distribution and to understand the physical processes responsible for the growth of both the baryonic and dark matter components of galaxies at moderate to high redshift (z=1–5). This can be accomplished with an ELT by mapping the spatially resolved kinematics, star formation, and chemical abundances of individual massive galaxies as well as measuring the kinematics of their satellite objects (both their internal kinematics and their velocity relative to the most massive galaxy dominating the dark matter halo). By mapping these properties, we can estimate the past history as well as constrain the future evolution of a statistically significant number of galaxies. This is a unique avenue to understand the growth and evolution of both the baryonic and dark matter components of high redshift galaxies that has not been possible so far.

A local census of the distribution of the baryonic mass reveals – albeit with large uncertainties – that of the baryons presently locked in stars and stellar remnants, a majority reside in spheroids (as opposed to disks; Fukugita, Hogan, & Peebles 1998). When and how did all these baryons come to reside in spheroids and disks? There are two competing explanations. The classical pictures are the “monolithic collapse” of Eggen, Lynden-Bell, & Sandage (1962) versus the (hierarchical) merging model of Searle & Zinn (1978). As mentioned above, the hierarchical picture of galaxy formation and evolution is, for many reasons, widely favoured (e.g. Ellis 1998). It predicts that small galaxies formed first and that massive galaxies grew at

later times by the accretion and merging with smaller (proto-) galaxies. Monolithic collapse, as the name suggests, is a simple process in that the gas collapses over a few crossing times and the star formation proceeds rapidly. When including realistic feedback mechanisms from the intense star formation, such collapse is stretched out to about 1 Gyr. The debate is not between which model is correct, as merging obviously plays an important role in galaxy evolution, the real question is how did star formation proceed in galaxies, are processes like merging a function of epoch, are there galaxies that formed "anti-hierarchically", and is our understanding of the hierarchical frame-work complete. Recent observations have shown the existence of high redshift, old (a few Gyr), early-type/spheroidal galaxies (up to z~2) with stellar masses similar to those of the most massive galaxies in the local Universe, thus indicating that the formation of massive galaxies started much earlier and occurred much faster than expected from the classical hierarchical merging models (Figure 5.16 and Figure 5.16; e.g. Cimatti et al. 2004; Glazebrook et al. 2004; Fontana et al. 2004; McCarthy et al. 2004).

One of the main observational goals remains to derive the masses of galaxies over a wide range of redshifts and cosmic time. However, estimating dynamical masses for high redshift galaxies is extremely difficult – very often impossible – with the current generation of 8-10m-class telescopes, due to their faintness and small angular sizes. Rotation curves or velocity gradients have been measured for samples of disk galaxies up to z≈1 (e.g. Vogt et al. 1996; Ziegler et al. 2002; Boehm et al. 2004), a few virial mass estimates have been made for Lyman-Break Galaxies (LBGs) using the velocity dispersion of emission lines (e.g. Pettini et al. 2001; Erb et al. 2003; van Dokkum et al. 2004), and millimetre interferometry has been used to estimate the dynamical mass of a submm-selected galaxy at z~2.8 (Genzel et al. 2003). More recently, a few velocity fields have been established for galaxies from z=0.5 to z=2.5 using integral field units (Flores et al, 2004; Förster Schrieber et al. 2005 in preparation, see Figure 5.17). For early-type galaxies, most observations have been performed for cluster and field ellipticals at z<1 in order to derive the velocity dispersion of absorption lines (e.g. Treu et al. 2005).

A "cheap" alternative method to overcome the current limitations is to estimate the stellar masses based on fitting the galaxy multi-band spectral energy distributions (SEDs) with spectral synthesis stellar models and to derive the mass-to-light ratio and the stellar mass as free parameters ("photometric stellar masses"; e.g. Brinchmann & Ellis 2000; Dickinson et al. 2003; Fontana et al. 2003; 2004). However, the reliability of these estimates (especially for high-z galaxies) is still an open question.

To map the dark matter haloes of galaxies from redshifts from when the Universe was half to only 5% of its current age (z≈1–5) will require us to obtain spectra of very faint and physically small galaxies. This is necessary because we wish to probe the dynamics of galaxies in the haloes and also obtain redshifts of possible background sources that have been lensed by the gravitational potential of individual galaxies.

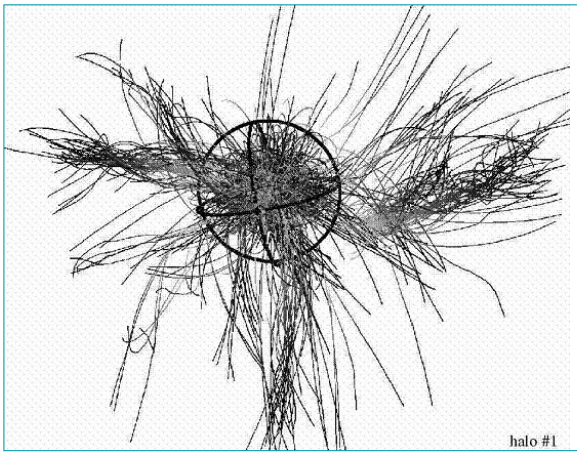

Fig.5.15 A realisation of a merger history of a dark matter halo from Gill et al. (2004). The time covered by this history is approximate 8 Gyr and shows the richness and frequency of the merger history of a relatively massive halo. It is the dynamics of these merging halos that we wish to trace with an ELT.

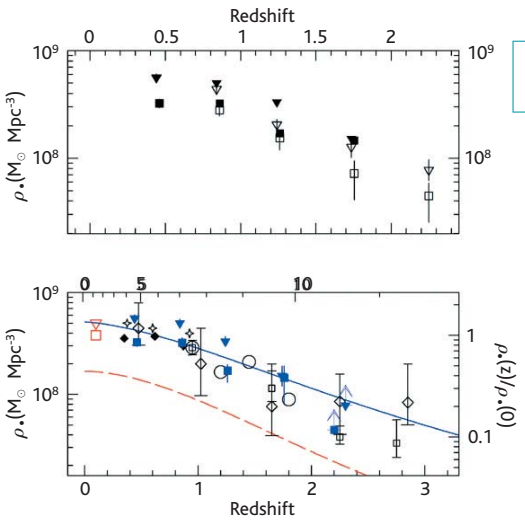

Fig.5.16

The evolution of the cosmological mass density as a function of redshift (Fontana et al. 2004). Upper panel: observed cosmological mass density as observed in the K20 data. Squares correspond to best fit estimates, triangles to "maximal mass" estimates. Empty points represent the observed values, with the corresponding Poisson noise. Filled points represent the values corrected for incompleteness. Lower panel: The global evolution of the cosmological mass density from z=0 to z=3 as observed from the K20 and other surveys.

Through such statistical measurements it is possible to estimate the halo masses of the galaxies. Coupled with spatially resolved measurements of the dynamics of the parent (most massive) galaxy in the dark matter halo, it is possible to construct a mass versus radius relation as a function of their estimated baryonic mass and angular momentum. Since any one halo is likely to be populated by several tens of galaxies, many of which may be too faint to obtain the required measurements, one has to observe many galaxies with similar total baryonic mass content. Making such measurements yields the total dark matter mass and the fraction contributed by the baryons ("the bias factor"). In addition, the measurement of the dynamics of the objects in the halo allows us to estimate the likely merging time scale, the rate of growth of mass and angular momentum, and to investigate whether or not interacting with the parent galaxy and its halo retards the development of the nearby companions and satellite galaxies. Since the mergers are driven by dynamical friction, tidal shear, stripping, and

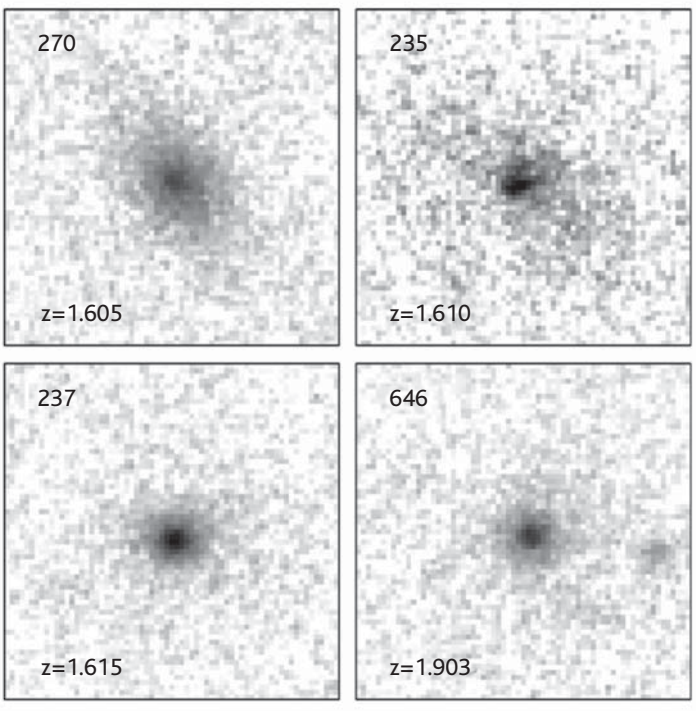

Fig.5.17

HST images (ACS+F850LP) of four old and massive galaxies at 1.6<z<2.0 (Cimatti et al. 2004). Their stellar masses are estimated to be $>10^{11}\ M_\odot$ according to the fitting of their multi-band spectral energy distributions. Their spectra being typical of elliptical galaxies (i.e. absorption-line spectra), a direct estimate of their dynamical masses through a measurement of the velocity dispersion σ is currently beyond the capabilities of optical and near-IR spectroscopy with 8-10m-class telescopes due to the faintness of these objects.

stirring, we would expect to see signs of these interactions influencing the growth and evolution of the companion/satellite systems.

Larger telescopes than those presently available are clearly required to allow the estimate of high-z galaxy dynamical masses through moderate- to high-resolution integral-field unit (IFU) spectroscopy (rotation curves for disk-like systems with emission line and velocity dispersion for absorption-line galaxies, especially early-type galaxies). The main aims of such observations will be measuring the cosmic evolution of the Tully-Fisher, Fundamental Plane and other scaling relations, the evolution of the galaxy mass assembly rate as a function of redshift and mass, comparison with the photometric stellar masses, comparison with the predictions of galaxy formation/evolution in order to provide stringent constraints for the models. High spatial resolution will also allow deriving structural parameters such as the effective radius (Re) and surface brightness (μ_e) that are needed to place the target galaxies in the scaling relations.

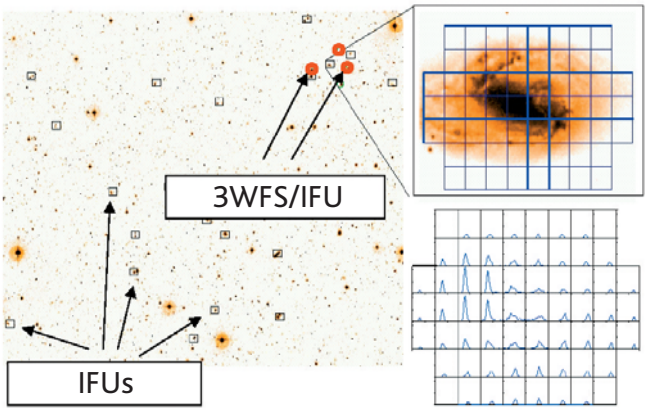

Fig.5.18 Concept for a multi-IFU observation of multiple galaxy haloes. Left: example placement of IFUs on the sky. Right top: detail showing arrangement of IFU pixels on a target galaxy, Right lower: typical resulting map showing emission line strength and velocity field as a function of projected position on the galaxy. The Wavefront sensors (WFS) provide AO correction close to the target location (similar to the concept of the FALCON instrument, Hammer et al 2003).

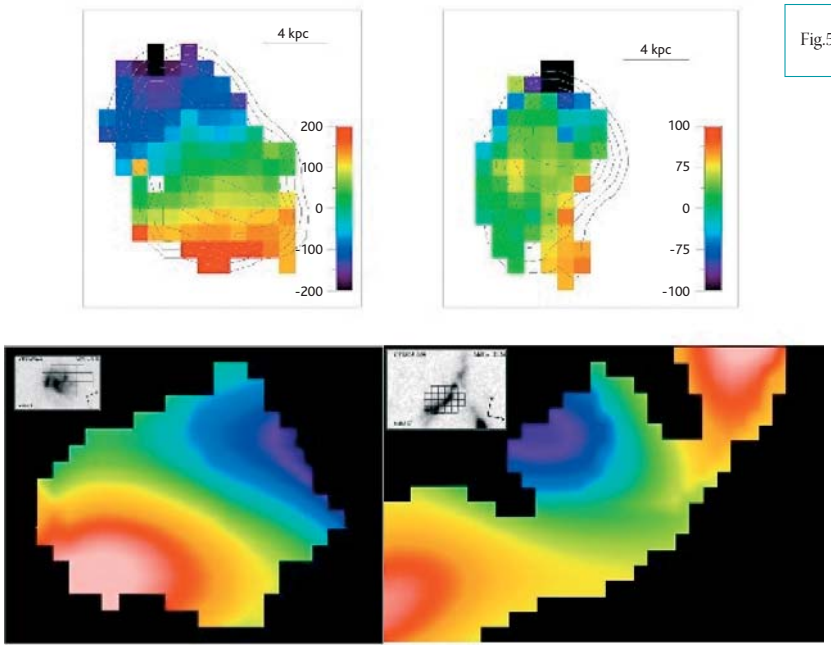

Fig.5.19 Examples of 3D velocity fields of distant galaxies observed with the integral field units SINFONI (top, Förster Schreiber et al. 2005, in prep) and GIRAFFE (bottom, Flores et al. 2004) both on the ESO-VLT. In the top two panels, the contours represent the distribution of the Hα emission, while in the lower two panels, the insets show HST/WFPC2 images of the galaxies with the GIRAFFE field of view super-imposed. To obtain detailed velocity fields, metallicities, star formation intensities or extinction maps on sub-kpc scales will require a substantial improvement in the coupling of the resolution within apertures <0.1 arcsec. Only adaptive optics correction on the target can provide the necessary resolution and only an ELT has the light gathering power to obtain sufficient signal-to-noise to sample faint galaxies at such fine physical scales.

Notes on Design Requirements

The galaxies in individual dark matter haloes will be moving relative to the parent galaxy at velocities of several tens of km s^{-1}. Low mass star forming local galaxies that populate the haloes at low redshift typically have emission line luminosities of $10^{39–40}$ ergs s^{-1} cm^{-2}. Hα, [OIII]λ5007, [OII]λ3727 are the strongest optical emission lines in low-mass, low-metallicity galaxies, which are likely to be the most appropriate targets in the haloes. At z=3, the luminosity distance in the currently favoured cosmology (H_0= 70 Mpc km s^{-1}, Ω_M=0.3, and Ω_Λ=0.7) is 7.85 x 10^{28} cm. The typical flux of the halo galaxies is then about 10^{-19} to 10^{-20} ergs s^{-1} cm^{-2}. Thus, even on a 100m telescope, the integration time is nights for each field.

Determining the relative velocities and spatially resolved kinematics and metallicities of sources in a common halo requires an instrument with a high multiplex with integral field units (deployable IFUs, see e.g. Figure 5.18). To obtain the necessary sensitivity and physical scale of star forming regions in individual galaxies requires a sophisticated adaptive optics system. In order to probe individual dark matter haloes, which have the physical size of several hundred kpc will require fields of view of about 1 $arcmin^2$ with the desire to cover several haloes in the same field simultaneously. The observable number of individual haloes is proportional to the field size which would also then drive the number of deployable IFUs. To construct the table below of required instrumental parameters, we have assumed that we are observing galaxies in the redshift range 1<z<5 [emission and absorption lines from rest-frame 3727Å (OII up to z~5.6) to 5200Å (MgI, OIII, up to z=1– 4) and to 6563Å (Hα, up to z=2.6)], and the number of targets per halo is roughly several tens $arcmin^{-2}$ (down to m_{AB}=28 at 4000Å, rest-frame with about 10 massive haloes $arcmin^{-2}$).

Specs	minimum	goal	Note
Observation type			Multi-object integral-field spectroscopy
FOV (diameter)	2 arcmin	10 arcmin	if small FOV, the program duplicates observations to cover > 10 arcmin scales
Spatial resolution	100 mas	50 mas	Size of satellites (Magellanic clouds) < 1 kpc
Spectral resolution	5000	10000	OH sky requires > 3000; « Size » of satellites < 10 km/s
Wavelength range	1–2.5µm	0.7–2.5µm	
IFU type 1 Number and Size	10 with 2x2 arcsec FOV		To map velocity/metallicity/dust of the major galaxies
IFU type 2 Number and Size	100 with 0.5x0.5 arcsec FOV	400	400 Idem, for satellites/ From 10 to 40 satellites per galaxies
Pixel size **Number/IFU1** **Number/IFU2**	50 mas 40x40 10x10	25 mas 80x80 20x20	
Minimum space between IFUs	Few arcsec	1 arcsec	To catch all satellites in haloes (halo mass)
Target density	~0.1 to ~10 $arcmin^{-2}$		
Special Requirement			IFU
Telescope size	30m	100m	
Observing time			Of order ~1 night per field. Depends on multiplex and required statistics
Comments			JWST will also have a significant impact with complementary observations at λ>2.5µm

5.3.4 The star formation rate over the history of the Universe

Thanks to the Hubble Space Telescope (HST), ground-based 10-m class telescopes and sub-mm facilities, the universal star formation density has been explored to within the first Gyr after the Big Bang. However, the invested amount of exposure time is very large and we are reaching the limit with current telescopes. Firstly because of sensitivity, but secondly because star formation is not confined to one wavelength range: a multi-wavelength analysis is needed to gather photons carrying information on star formation. Depending on the rest-frame wavelength (ultraviolet, visible, far-infrared), different physical characteristics (mass, dust attenuation, star formation histories, etc.) are observed. In order to interpret the data correctly, selection biases must be understood by observing several samples of galaxies at several redshifts.

One of the biggest questions is the role of the dust attenuation and how observational selection affects the shape of the diagram. Indeed, sub-millimetre surveys suggested that optical surveys may have substantially underestimated the star formation density in the distant Universe, which would reach a plateau at z>1.5 and would not decrease as in e.g. Smail, Ivison & Blain (1997) but more likely at a much higher redshift. Several caveats remain however: firstly the correction for the dust attenuation is difficult to estimate. This makes the UV-only plot not representative of the global star formation history. Secondly, the equivalent limiting UV luminosity is about 0.3 L* at z=3: only the most massive galaxies are observed. Thirdly, the highest redshift point is based on only four objects.

To fully estimate the star formation rate history, we need to account for all photons produced by stars, detected either directly in the rest-frame UV or in the rest-frame far infrared through the re-processing of UV photons by dust (although note that an alternative method for measuring the cosmic star formation rate, based on detecting individual supernova explosions out to very high redshift, would be possible with an ELT, as described in sections 4.7 and 5.1.1, although the dust problem remains).

To fully account for all photons produced by stars requires more than rest-frame UV imaging (e.g. from JWST) as shown in Figure 5.21. To carry out this kind of observation on a large sample of galaxies we need rest-frame FIR observations with an instrument similar to SCOWL (see Annex B).

It seems that more massive (or more luminous) galaxies are generally dustier than lighter ones. Even though the latter galaxies are intrinsically faint, we are still able to observe them in the local Universe because of their small distance. However, in the more remote Universe (and the high redshift one), we do not know whether galaxies like these even exist.

A hierarchical scenario is very likely to explain at least a part of the galaxy formation process. Following this idea, the size/mass of galaxies should decrease with the redshift as is observed. Small galaxies (10^9–10^{10} $M_\odot$ or about L<0.1 L*) should therefore be more numerous in the early history of the Universe. Containing a small amount of dust, they undergo a low

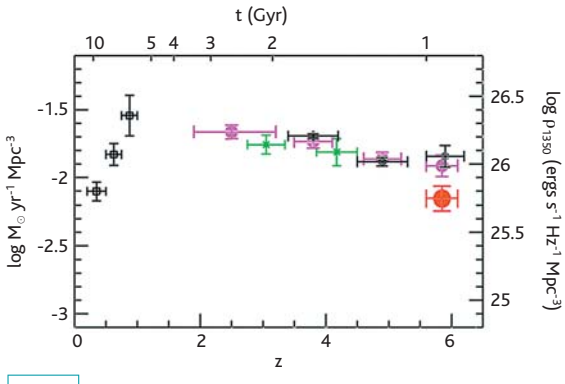

Fig.5.20

An updated version of the Madau plot (Bouwens et al. 2004) containing data points up to about z≈6. This diagram, not corrected for dust attenuation, is based on objects with a UV luminosity equivalent to 0.3 L* at z=3. Note that the highest redshift point is based on only four objects.

attenuation and are very faint in the rest-frame FIR. If we cannot see them in UV, where they can most easily be detected, we will underestimate the cosmic star formation rate.

The core program should observe a sample of fields separated by more than about 150 comoving Mpc to avoid problems with the cosmic variance but also a large number of galaxies to sample several important parameters (mass, dust attenuation, etc.). One can build several selected samples that would be representative of characteristic observational programmes:

- A UV-selected sample similar to HST-observed Lyman Break Galaxies (LBGs).
- A visible-selected sample similar to ground-based observations.
- A FIR-selected sample.

The size of an individual observed field needs to be above 10–20 Mpc on a side i.e. 3 arcmin on a side. Such a field should contain about 1 L* galaxy at z=1 and the total number of L* galaxies (and/or the sub-L* progenitors) would be a few tens/hundreds over the observed redshift range. The expected limiting magnitude (in imaging mode) for galaxies in the range $0.01<L/L^*<0.1$ at z=7 would be $31.2<m_{AB}<33.7$, respectively. The individual exposure time to reach m_{AB} = 32.0–33.7 (i.e. 0.05 L* / 0.01 L* at z=7) for 5 filters

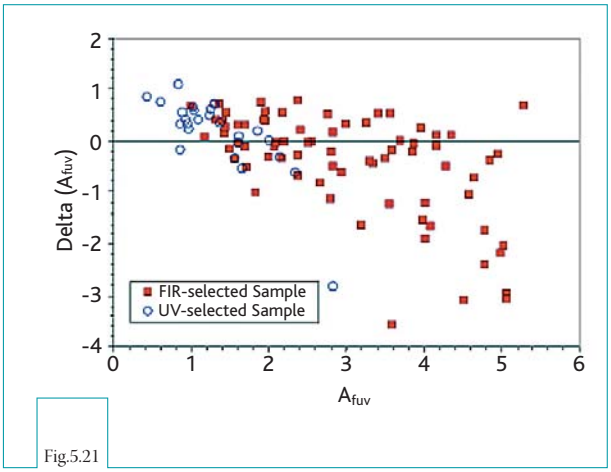

Fig.5.21

The estimation of the dust attenuation A_{FUV} is biased and introduces large errors Delta(A_{FUV}) when the dust attenuation is evaluated without the far-infrared flux i.e. UV reprocessed photons (Burgarella et al. 2005). Not accounting for both UV and FIR fluxes implies a poor estimate of the complete star formation rate of galaxies (A zero value of Delta A_{FUV} implies a good estimate).

(depending on the redshift) is estimated to be at least 15 nights per observed field. It remains to be determined whether the fainter galaxies in this range could be observed. About 5 fields would need to be observed in order to reach about 1000 galaxies and work with large enough numbers in each bin (assuming 10 bins per parameter). The total amount of time would therefore be about 75 nights for a 100m telescope.

Notes on Design Requirements

FOV	3x3 arcmin^2	10x10 arcmin^2	Observe representative piece of the Universe and statistical samples
Spatial resolution	0.1 arcseconds	0.05 arcseconds	Size of large HII regions
Spectral resolution	Imaging	Imaging	
Wavelength range	0.5–2.2μm +FIR	0.3–2.2μm +FIR	SCOWL(?)/ALMA
Observation type	Imaging	Imaging	
Target density	A few tens per arcmin^2	Few per unit z and per arcmin^2	Tentative
Special requirements	Rest-frame UV & FIR mandatory		
Telescope size	100m would have the largest impact. 50m and 30m could also make a significant contribution		

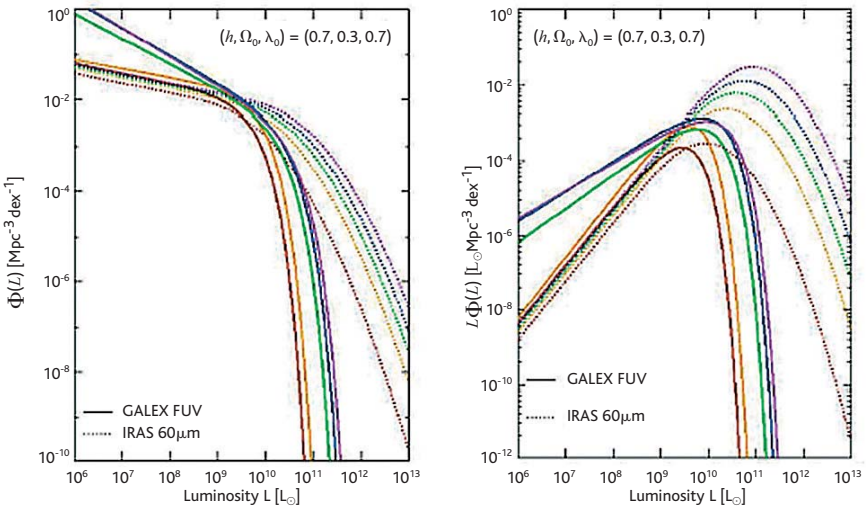

Fig.5.22

The FUV and FIR luminosity functions (Takeuchi & Buat 2005) in the left panel show that low-mass galaxies should be observed in the rest-frame UV (low dust attenuations) and massive galaxies in the rest-frame FIR (large dust attenuations). In terms of energy (right panel), the FUV cannot be neglected if we want to estimate the total star formation rate of galaxies and the inferred star formation density. Redshift increases from red to blue (i.e. from bottom to top) from z=0 to z=1.

5.4 Fundamental constants

Fundamental constants play a central role in our understanding of nature. They are fundamental because their numerical value can not be deduced from first principles and are supposedly universal and invariable quantities. Thus, the fundamental constants *capture at once our greatest knowledge and our greatest ignorance about the Universe (Barrow 2002).*

Testing the variability of the constants is a test of fundamental physics. Measured variations in space and time would have far reaching consequences: they would point the way to a unified theory of fundamental interactions, shedding some light on a possible scalar field acting in the late Universe or on the existence of extra spatial dimensions. In higher dimensional theories, such as string or M-theory, the constants are defined in the full higher-dimensional space and our more familiar four-dimensional constants become only effective and dynamical quantities. The values of the constants in our space-time depend on the value of several scalar fields and on the structure and sizes of the extra dimensions. Any evolution of the extra dimensions would lead to *varying constants* in our four dimensional space.

Testing for variations in the constants is an active area of precision laboratory physics. Experiments using atomic clocks restrict the variation of the fine structure constant, α, to the level of 10^{-15}yr^{-1} and the ACES space mission foreseen to fly on the International Space Station in 2006 is expected to improve this sensitivity by about *two orders of magnitude*. However, astrophysics provides unique information about the values of the fine-structure constant, α, in the distant past and about remote regions of the Universe. In 1999 observations of spectral lines of distant astronomical objects brought first hints that α might change its value over time and/or space. The Many-Multiplet method, applied to Keck/HIRES QSO absorption spectra, has yielded the first tentative evidence for a varying α by Webb et al. (1999) and this evidence has only become stronger with successively larger HIRES samples (Murphy et al. 2001; Webb et al. 2001; Murphy et al. 2003). The most recent and robust HIRES constraint comes from 143 absorption systems over the range $0.2 < z_{abs} < 4.2$ (Murphy et al. 2004) – see Figure 5.23 (left panel):

$$\Delta\alpha/\alpha = (-0.57 \pm 0.11) \times 10^{-5}$$

However, more recent observations of quasars are consistent with a null result. Chand et al. (2004) have analysed 23 absorption systems in somewhat higher signal-to-noise ratio spectra from a different telescope and spectrograph, the VLT/UVES, over the range $0.4 < z_{abs} < 2.3$ – see Figure 5.23 (right panel):

$$\Delta\alpha/\alpha = (-0.06 \pm 0.06) \times 10^{-5}$$

No variability has been found in individual absorption systems by Levshakov et al. (2004) and Quast, Reimers & Levshakov (2004).

At present, the debate over the possible variability of α is very open and a significant improvement demands an ELT with a high resolution spectrograph. The primary objective would be to resolve even the sharpest of metal absorption lines in the quasar spectrum, which are of order ≈1 km s^{-1} wide. Thus, with a 60-100-m ELT and a spectrograph with R≈300,000 covering most of the optical range, an effective precision gain of *two orders of magnitude* can be achieved. This will only be possible if a high precision wavelength calibration is in place at the ELT. Murphy (in prep.) and ESO are currently pursuing the design of a laser 'frequency comb' system which will achieve 1 cm s^{-1} precision (per observation). The spectrograph will also need to be fibre-fed so as to scramble guiding and atmospheric effects at the entrance slit. Additionally, as shown by the ESO/HARPS experience, the stability gained by placing the spectrograph in a temperature-controlled, vibration-isolated vacuum chamber is crucial to providing reliable wavelength calibration.

A two order-of-magnitude gain in precision will keep the astronomical observations competitive with the laboratory tests of variations in α and would constitute the most precise test of fundamental physics outside our Solar System. If a variation is detected (or

current hints at a variation are confirmed at high confidence), these measurements would be our first window into the extra dimensions of space-time postulated by modern unified theories. Even if no variation is detected, the limits obtained will be one of the most potent constraints on future theories.

Notes on Design Requirements

Observation Type: High-resolution absorption-line spectroscopy

Field of View: Single point sources

Spatial resolution: 0.01" or better for maximum sensitivity to point sources

Spectral Resolution: 300,000

Wavelength Range: Optical

Target Density: single objects

Telescope Size: 60–100m

Other comments: High precision spectrograph needed, similar to that for CODEX

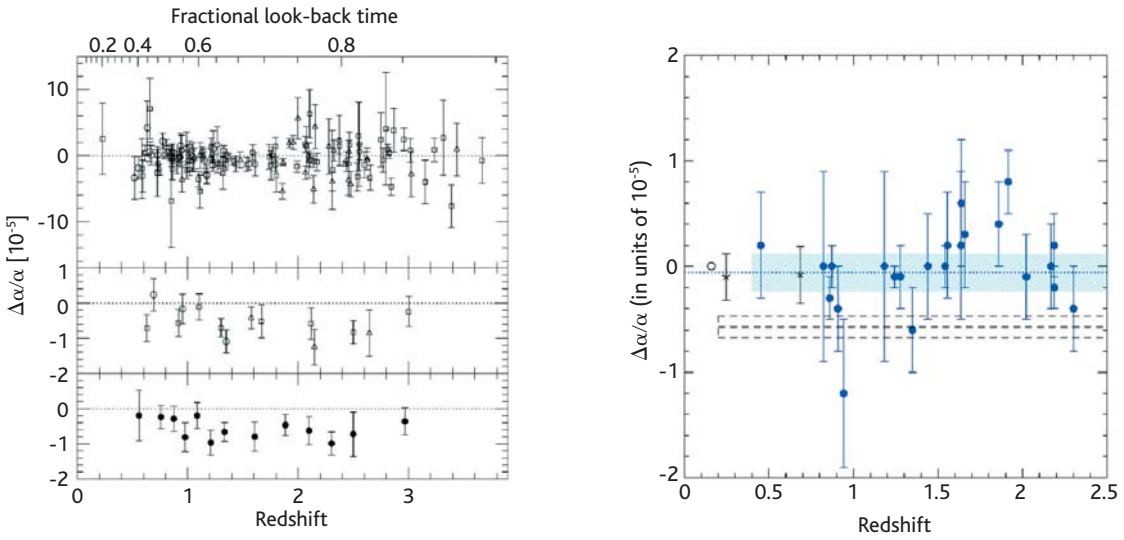

Fig.5.23

$\Delta\alpha/\alpha$ and 1-σ errors for the three Keck/HIRES samples of Murphy et al. (2004). Upper panel: unbinned individual values. Middle panel: binned results for each sample. Lower panel: binned over the whole sample. Right: VLT/UVES results from Chand et al. (2004). The shaded region is the 3-σ error in the weighted mean and the dashed region represents the 1-σ error from Murphy et al. (2003).

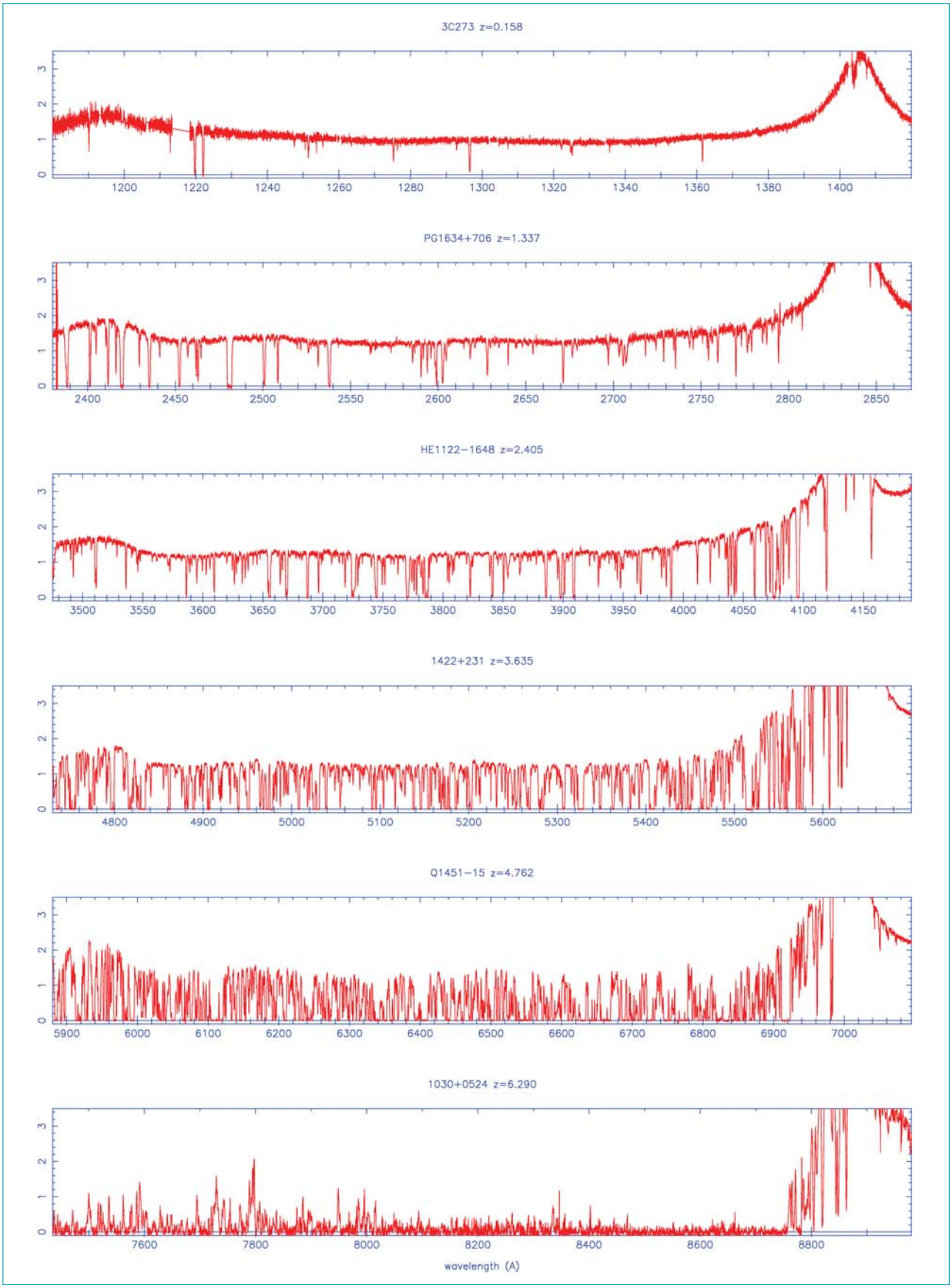

Spectra of quasars of increasing redshift illustrating the increase in absorption due to intervening neutral gas with increasing redshift. At the highest redshifts these show a 'Gunn-Peterson' absorption trough – the complete absorption of light at wavelengths shortward of the Lyman – α line of atomic hydrogen – implying that the re-ionisation epoch which began at redshift ~20 must have continued until redshift ~6.

Annex A: Summary of the dependence of the science cases on telescope aperture

Several teams worldwide have begun development of the next generation of Extremely Large ground-based Telescopes (ELTs). A range of designs and telescope apertures from 20m–100m is being considered.

In the following sections some highlights from the ELT science case are presented, showing what can be achieved with ELTs of various sizes from 20m to 100m. In some cases there is a continuum of improvement as telescope diameter increases, but there are also a few important "threshold points" where a telescope above a certain size enables a whole new branch of study. Rather than discussing all the topics covered in the science case, three key areas are considered, all of which have been identified by various ELT science groups as key scientific drivers. These are, (1) detection and study of extrasolar planets, (2) study of galaxy formation via observations of resolved stellar populations, and (3) exploring the very high redshift Universe.

A1.1 Exoplanet detection from ground-based ELTs

As described in the "Planets and Stars" section of this science case, direct detection of extrasolar planets is a major technical challenge. This is because planets are many orders of magnitude fainter than their parent star, while those of exceptional scientific interest, occupying the 'habitable zone', where water-based life may be found, lie very close to their parent star, with both considerations ensuring that reflected light and intrinsic emission from the planet is swamped by the glare from the star. In the next ten years, astronomers using current 8–10m class telescopes expect to perform the first direct detections of gaseous giant planets, using advanced adaptive optics and coronographic techniques to suppress the glare from the planets' parent stars by factors of up to 10^7.

Extremely Large Telescopes, however, offer spectacular potential advances even beyond this expected progress. Apart from their sheer collecting area, which is essential for studying such faint objects as Earth-like extrasolar planets, a large telescope's small diffraction limit allows cleaner separation of a planet from the image of the star. As a result, one of the most exciting prospects for future ELTs is the ability directly to detect *and study* large samples of planets in other Solar Systems, including terrestrial planets.

Several simulations have modelled such observations, showing that a 30m telescope at a "standard" site with appropriate performance from its adaptive optics system should be capable of studying massive gas-giant planets out to several tens of light years. As shown in Annex B, and in the "Planets and Stars" section of the main case, study of Jupiter-like planets is within reach of ELTs over 30m diameter.

In principle it would be possible for a 30m-class telescope to detect Earth-like planets in their parent star's habitable zone to distances of several pc (requiring star rejections of order 10^9). However, the number of suitable stars within the few-pc range of a 30m telescope is low (a few tens) and current (albeit conservative) estimates are that only ~1% of Solar-like stars may host an Earth in a stable orbit within their habitable zones. Thus, optimistically there is perhaps a 50:50 chance of finding a single earth-like planet with a 30m telescope. Although such a discovery would have a profound impact, we would still be unsure as to whether this prototype object was an unusual case, even if it were to be discovered.

By contrast, a 100m ELT will be able to survey for such planets around the ~1000 Solar-like stars which exist within 30pc of the Sun,

providing a statistically meaningful sample of such planets. The key here is the combination of collecting area, to detect the faint light reflected by a planet from its parent sun, and the extremely high spatial resolution needed to reach and resolve distant exoplanetary systems. Earth, for example, would appear only 0.1arcsec from the Sun if the Solar System were observed from a distance of 10 parsecs or ~30 light years. A characteristic size of the habitable zone around a Sun-like parent star is the Earth-Sun distance, 1AU, which is equivalent to 33milliarcsec at an observing distance of 30pc. The volume of space, and consequently the number of stars, accessible to a telescope of diameter D scales as D^3, while the time to reach a given signal-to-noise for planet observations (background-limited observations of point sources) is proportional to D^4, thus the gain in performance for a 100m telescope compared to a 30m is huge.

Only a 50m–100m class telescope would be capable of studying a significant sample of Earth-like planets. Indeed, such telescopes would allow a crucial determination of the fraction of extra-solar Systems that host earth-like planets even if that fraction is lower than the current (gu)estimates, something which a 30m could not do with a non-detection or even a single detection – see also Annex B for a comparison with space-based planet-finding missions, and other telescope apertures and locations.

By repeated imaging, planets will be followed around their orbits. Variations in their apparent brightness during this process can then be used to determine many properties. For example, their albedos (reflectivities) determine their surface temperatures and for larger planets the photometric signature of rings like those around Saturn would be detectable. On a range of timescales, brightness changes because of diurnal rotation, weather and even seasons offer a powerful technique for investigating surface and atmospheric conditions. Because of weather, seas, forests, deserts and ice-caps, Earth's brightness changes much more on all time-scales than that of Mars or of Venus.

Ultimately, a 100m telescope will be capable of obtaining *spectra* of Earth-like exoplanets out to distances of several tens of light years, with the possibility of detecting "Biomarkers" such as water and oxygen (ozone). By doing this we can determine directly whether our own Solar System is unique and, if not, establish whether other planetary systems could, or in fact do, support life.

Table A.1 – Summary: Exoplanet study capability as a function of ELT size

20m
– Direct detection of Jovian-mass planets in wide orbits around nearby Solar-like stars
– Radial velocity search on fainter stars (increasing available volume by a factor of 200)

30m
– Imaging of young (<10Myr) Jovian planets around stars in star-forming regions up to 75pc away
– Detection and classification of mature Jovian planets around stars within 10–20pc
– Possible detection of one Earth-like planet within ~5pc

100m
– Survey of 1000 Solar-like stars and direct detection of Earths within 30pc
– Time-resolved photometry of Earth-like planets (albedo & weather)
– Spectroscopy of earth-like planets and search for "Biomarkers"
– Study of entire exoplanetary systems

A1.2 Resolved stellar populations

It is now believed inevitable that mergers between galaxies play an important part in the build-up of the galaxies we see today (see the "Stars and Galaxies" section), in which case we would expect to see evidence of these past mergers. Indeed, recent studies of individual stars in our own Milky Way galaxy have revealed sub-populations of stars with distributions of ages and chemical composition which seem to be a discrete perturbation on the main distribution function, providing clues as to the timing of the main mergers in the Milky Way's history. However, up until now these studies have been limited to our own Galaxy and its satellites.

Future wide-field (with field of view of over a degree in diameter) multi-object spectrographs on 4m–8m telescopes will allow the structure of the Milky Way halo to be mapped in unprecedented detail, by measuring radial velocities and chemical abundances for several 100,000 stars out to the limits of the stellar halo. Such instruments will also be used to study evolved Red Giant Branch stars in the M31 "Andromeda" galaxy in our Local Group, but can not observe apparently fainter stars.

A 20–30m telescope would allow studies of resolved stellar populations to be extended to galaxies beyond our own Milky Way and its satellites, and into the Local Group. Figure A-1 shows a simulated colour-magnitude diagram for M32 (a dwarf galaxy within our Local Group) as observed with a 30m telescope. Simulations (e.g. Olsen et al) have shown that distinct stellar populations can be recovered from such observations, allowing analysis of that galaxy's star formation and assembly history. Indeed, a 30m telescope could study the star formation and chemical enrichment histories of galaxies out to the 5Megaparsec distance of NGC5128 (Centaurus A), the nearest galaxy with an active super-massive black hole in its nucleus, and also an evident product of a recent major merger event.

However, as described in the "Stars and Galaxies" section of the main science case, a real understanding of galaxy evolution requires us to know the range of possible merger histories which can lead to superficially similar galaxies today. To study a representative section of the Universe requires reaching at least the nearest large galaxy clusters, which are the closest places where large elliptical galaxies are found. This requires observing galaxies in the Virgo or Fornax clusters at distances of 16 or 20 Megaparsecs respectively. To achieve this outstanding science requires an ELT larger than about 50m. Initial feasibility studies look promising – simulations show that a 100m class telescope could observe individual stars within galaxies in the Virgo cluster, and determine their ages (even for the oldest, hence faintest stars) and composition with sufficient accuracy that a direct map of the galaxy's history could be derived (see Fig A.1).

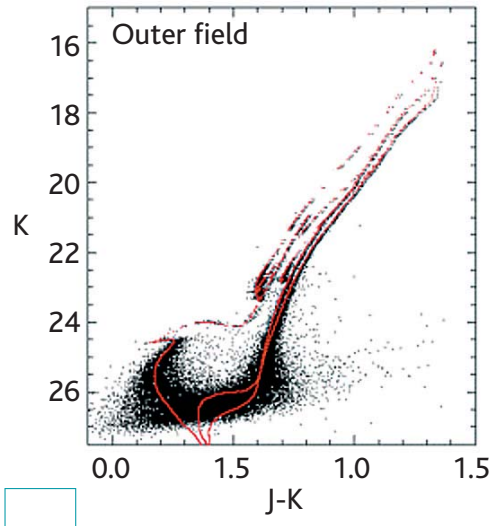

Fig.A.1

(From the GSMT science case) A simulated colour-magnitude diagram for M32 as observed with a 30m telescope. Several distinct stellar populations are visible, allowing analysis of the star formation and assembly history of this galaxy.

Table A.2 – Summary: Resolved Stellar Populations capability as a function of ELT size

20m
- Resolve oldest stellar populations in Magellanic Clouds and Local Group dwarf spheroidals (Sculptor, Fornax, Carina) and the Sagittarius dwarf
- Resolution of the brightest giant stars in galaxies in the Virgo cluster
- Observations of halo giants in Local Group galaxies (high-resolution spectroscopy)

30m
- Age/metallicity measurements of resolved populations in M31/M32 at ~750kpc (imaging)
- Determination of star formation and chemical enrichment histories of galaxies out to Cen A (nearest active galaxy)

100m
- Age/metallicity measurements of resolved populations in M87 (in Virgo cluster at 16Mpc)
- Detailed study of galaxy formation in a representative sample of the Universe

A1.3 The very high redshift universe

The aftermath of the Big Bang and the era of recombination left the early Universe filled with cool neutral gas (mostly H and He). Yet today, and indeed for most of the history of the Universe, almost all the gas has been warmed sufficiently to become ionised, and transparent. A key goal of astrophysics is to understand how and when the first luminous objects in the Universe formed from that gas, what they were, and how they contributed to heating, ionising, and enriching the gas with heavy elements.

Many tantalising questions about the re-ionisation history of the Universe are raised by recent results, with hints but few answers. Current results from the Wilkinson-MAP Cosmic Microwave Background probe suggest that the gas in the Universe was re-ionised by about 200 million years after the Big Bang (that is, by a redshift z ~ 17), while observations of the highest redshift quasars, seen at a time of about 900 million years after the Big Bang (that is, at redshift z ~ 6), demonstrate that enough of the intergalactic (IGM) medium remained *un*-ionised at that time to absorb almost completely all radiation shortwards of the Lyman-α recombination line of HI. It may be that there were two re-ionisation epochs, the earlier caused by a first generation of massive stars, followed by considerable gas cooling, and a later caused by the first quasars and galaxies. Alternatively, a slower, highly inhomogeneous re-ionisation process may have occurred over the whole extended period between the two epochs at which we currently have information.

These possibilities can be tested if we can observe the ionisation state of the IGM by the absorption features it produces in the spectra of very distant "background" objects. There are a few populations of sources that could be observed at such very high redshift with Extremely Large Telescopes. Gamma-ray bursts (GRBs), probably extreme supernova events from massive stars, are intrinsically extremely bright optical transients for a short time, and should be detected up to redshifts of 15–20 if they exist at these early times. "Normal" supernova explosions of population III stars would be intrinsically and apparently fainter than GRBs, but could be used to probe the Inter-Galactic Medium at redshifts up to about 12. An interesting expectation for population III supernovae is that the population disappears in regions with metal enrichment higher than 1/10000 of the Solar value, a result itself of considerable interest if proven. Although the epoch of quasar formation is an open question (see the "Galaxies and Cosmology" section), quasars being found today by the SDSS survey at redshifts around 6 are apparently powered by super-massive black holes, so we infer that intermediate mass black holes, corresponding to quasars of intermediate luminosities, must exist at earlier epochs, up to at least redshifts of about 10. Probing the physics of the IGM at redshifts from 10 to 20 requires

intermediate/high resolution spectroscopy of these "background" sources in the near infrared. Apart from the brightest GRBs (and/or GRBs caught very early) which could be observed with a 30m class telescope, spectroscopic observations of these faint background objects can only be carried out with telescopes of the 50–100m class.

The first galaxies probably compete with the first quasars for the reionisation of the IGM. Although less luminous than quasars, proto-galaxies are far more numerous: their number and nature can be directly investigated with Extremely Large Telescopes. Candidate star forming galaxies out to redshift about 6 have already been discovered, and a few have even been confirmed spectroscopically. These known galaxies, which are high redshift analogues of the well-known Lyman Break Galaxies, currently studied at redshifts of 3, are spatially resolved on 0.1–0.2 arcsec scales. The objects detected thus far typically have AB magnitudes of i=25.5 and z=25.5, with a surface density of 500 and 160 per square degree, per unit redshift at redshift 5.5 and redshift 6.0 respectively.

Given these observational properties, an Extremely Large Telescope will allow detailed study of the astrophysics of these objects. For example, a 30m telescope would be able to produce spectra of the same quality as are provided by current 8–10m telescopes, but could do this at each point on a 3x3 grid over the surface of the galaxy, rather than, as today, integrated over the entire source. Thus, the objects could be resolved into their main components (disks/bulges?). A 100m telescope could provide proportionately higher resolution – and in imaging mode could resolve individual HII regions out to a redshift of 5, quantifying local star formation and chemical enrichment rates.

If there are galaxies at much higher redshifts which are similar to those galaxies currently known at redshift 6, they would have magnitudes of J_{AB}=27 and K_{AB}=28 at redshift 9 and redshift 16 respectively. Such objects are expected to exist for two main reasons. Firstly, the results from WMAP indicate the presence of ionising sources in place at redshifts greater than 10, presumably ultra-violet emission from the first objects. Secondly, the amount of time between redshift 10 and redshift 6.5 is so short in cosmological terms (about 300million years), there is simply too little time to go from a Universe containing no galaxies at redshift ten to the Universe we see at redshift 6.5.

Such very high redshift objects will be discoverable with the James Webb Space Telescope with broad-band photometric Lyman-Break imaging techniques. How will we study them? In spectroscopic mode, a 20m ELT would be more sensitive than JWST for detecting star formation from Lyman-alpha emission-line spectroscopy. However, only a 100m-class ELT can provide key diagnostics of both the inter-stellar medium and stellar populations in these galaxies, by intermediate resolution spectroscopy in the near IR at redshifts up to 15–17.

Table A.3 – Summary: Studies of the high redshift Universe as a function of ELT size

20m
- Ly-alpha emission-line spectroscopy from 6<z<10
- Possible detection of z~10 objects (depending on their nature)

30m
- Possible detection of z~10 objects (depending on their nature)
- Spectroscopy of "earliest galaxies" found by JWST
- IGM studies to z~10 using brightest GRBs as background sources

100m
- Detection of z>10 objects
- Spectroscopy of "galaxies" to z~20 (depending on their nature). Such objects may even be resolved with a 100m
- IGM studies at z>10 (GRBs, QSOs, PopIII SNe as background)

A1.4 Summary

Science Case		20m	30m	60m	100m
Solar System		Y	Y	Y	Y
ExoPlanets (direct detection):	Gas Giants	Y	Y	Y	Y
	Exo-Earths	N	N	Y?	Y
Proto-Planetary disks		Y	Y	Y	Y
Resolved Stellar Population:	Local Group	N?	Y	Y	Y
	Virgo	N	N	N	Y
Massive Black Holes		Y	Y	Y	Y
Star formation History of the Universe		Y	Y	Y	Y
Physics of Galaxies and Dark Matter, z=1–5		Y	Y	Y	Y
Dark Energy		Y	Y	Y	Y
High-z Universe :	Sources of re-ionisation	?	?	Y	Y
	$R=10^4$ on GRB at z>10	N	N	Y	Y
The Unexpected		Y	Y	Y	Y

Table A.4

A comparison of the scientific capabilities of ground-based Extremely Large Telescopes as a function of aperture size. The symbol "Y" indicates that there is a significant advantage for an Extremely Large Telescope of a particular size compared to the next smaller size. The symbol "N" indicates that an Extremely Large Telescope of that size cannot make a significant contribution in that scientific area. This summary should be treated as indicative rather than quantitative, since the assessment depends on the level of astrophysical detail required in each scientific area. In each case, the assessment assumes an excellent typical high mountain site (e.g. Mauna Kea), rather than Antarctica "Dome C".

In Table A.4, we attempt to summarise some of the science achievable with Extremely Large Telescopes of various sizes, and show some of the potential "critical-points", where new areas of study become possible. Each increase in telescope size improves the science achievable in many areas, and also enables new fields of research. The ultimate "killer applications" discussed in this document, including spectroscopy of Earth-like planets and resolving old stellar populations at Virgo distances, are only achievable with a 100m-class telescope.

Annex B: New scientific opportunities in the Extremely Large Telescope era

Extremely Large Telescopes represent the next major technological and scientific advance for Optical-InfraRed astronomy. As shown in the previous chapters, the science case for these facilities is spectacular in its own right: yet these facilities are not being developed in isolation. Major advances are being made towards the next generation of other facilities on the ground and in space, to operate at other wavelengths from radio to gamma-rays, and beyond the electro-magnetic spectrum. Major efforts are being made to co-ordinate approaches on an international scale between particle physics, fundamental physics and astrophysics. It is becoming increasingly understood that astronomical discoveries – dark energy, dark matter, neutrino mixing – are driving the frontiers of particle physics, and more than ever that developing understanding of elementary particle physics, quantum gravity, and possibly quantum optics is essential to allow progress in understanding the Universe and its contents.

At an implementation level, developments in computing power, data storage and fast communications are already revolutionising the way astronomers collect and use data, demonstrated by the growth of data archives and Virtual Observatories. These advances and facilities, in combination with advances in technology for adaptive optics, astronomical instrumentation and detectors, mean that Extremely Large Telescopes will be far more powerful facilities than even their sheer collecting area alone would suggest.

In the following sections we place the Extremely Large Telescope in the context of forthcoming complementary facilities, and highlight a few areas where future technical and intellectual developments, as yet developed only to a very preliminary extent, show considerable promise to extend the scientific bounty and the discovery potential of Extremely Large Telescopes beyond even that which is described in earlier chapters.

B1.1 The physics – astrophysics connection

An influential recent US National Research Council policy review is entitled 'Connecting Quarks with the Cosmos'. Both the existence of this report and its title illustrate the increasing overlap between forefront research in particle physics, fundamental physics and astrophysics. The Universe is recognised as the largest high-energy laboratory available for scientific study. Astrophysics is understood to provide natural sources of extremely energetic, highly relativistic, events, and extreme gravitational fields, as well as being the only place where major discoveries of the nature of reality – dark energy, dark matter, inflationary expansions, extremely energetic particles – are currently happening. While no-one yet knows how physics will develop over the next decades, it is already clear that the Universe is the physics laboratory *par excellence*. The increased precision of measurement, and the inevitable continuing discoveries, which will follow the next generation Extremely Large Telescopes, are just as certain to redefine progress in physics as in astrophysics.

B1.2 The next generation of ground-based astronomical and related facilities

Dramatic progress in astronomical technology is being made across and beyond the electromagnetic spectrum.

In Cosmic Ray physics, the study of high-energy particles reaching the Earth's upper atmosphere from large distances, there are extremely exciting new challenges. Among the most dramatic is the ability to study directly individual sources of ultra-high energy particles, and so to begin to understand the acceleration mechanisms which can generate particles with highly relativistic energies. These sources are most likely gravitationally collapsed sources – neutron stars and black holes formed in supernovae, super-massive black holes, explosive transients – and such studies will allow a new and complementary approach to their study and identification. The most ambitious facilities becoming available are the Pierre Auger cosmic ray facility, an international facility located in Argentina (www.auger.org), and the HESS cosmic ray facility located in Namibia (www.mpi-hd.mpg.de/hfm/HESS/HESS.html), together with many other facilities worldwide (MAGIC, Whipple, VERITAS, CANGAROO, CAT, with INTEGRAL and GLAST in space). One of the greatest challenges for these facilities is verification and study of the most extreme energy cosmic rays. These particles have such high energies they should self-immolate by scattering against photons from the cosmic microwave background radiation. Thus, if real, they are (on a cosmological scale) local, and indicate new extreme particle acceleration locations. These particles are rare – the detection rate is one particle per 5 sq km per century – but they may indicate new physics of considerable importance. Detailed analysis of their sources, when identified, will become a major astrophysical challenge for all available facilities.

Astrophysical Neutrino detection requires huge masses. In addition to experiments at essentially every high-energy physics laboratory, major facilities are under development under water (ANTARES, Baikal, DUMAND, NEMO) and under ice (AMANDA, ICE-CUBE, RAND, RICE, km^3...). Neutrino oscillation studies using the Sun as a source have already detected an unexpected non-zero neutrino mass. SN1987A has been detected as the first extra-Galactic neutrino source. While large-scale structure analyses from cosmology show that neutrinos cannot contribute much more to the Universe mass-energy budget than do stars, the existence proof of neutrino mass from current data illustrates the power of astrophysical analyses, in combination with particle physics experiments, to probe the nature of matter. Future detections of astrophysical transient neutrinos by the new facilities will, as in the case of SN1987A, provide early warning of an impending extreme event available for astrophysical study with an ELT.

Direct detection experiments to identify dark matter particles of course are derived directly from local astronomical analyses. These experiments, of which very many are in operation and under development, have defined a whole new subject, astro-particle physics. The local mass density of dark matter at the earth, 0.3GeV/cc, which defines all direct detection experiments, is deduced directly from analyses of Solar neighbourhood stellar kinematics and distances (Kuijken & Gilmore 1991). Our knowledge of the existence of dark matter and dark energy is entirely based on astrophysical observations. The extreme dominance of dark energy in the current universal energy budget is of course derived entirely from astronomy. It is difficult to imagine that substantial progress in attempts to generalise the standard model of particle physics will succeed until they can include what astronomers have shown are the dominant forms of matter and energy in existence.

The other major new window on the Universe which is soon to open is gravitational wave astronomy. LIGO, GEO600, VIRGO, and TAMA are currently establishing the subject, with the spacecraft array LISA to follow in the next

decade. Gravitational wave astrophysical sources will be dominated by compact objects in strong gravitational fields, allowing a next generation of tests of gravity theory, but also identifying sources which will merit, and probably require, detailed astrophysical analysis using all available approaches to allow an understanding.

An active collaboration between these facilities across all approaches to knowledge will be required, and will be mutually beneficial for astrophysics and physics.

There are also other major new ground-based facilities, which, like the Extremely Large Telescope, probe the electromagnetic spectrum. Both optical/near infrared and radio wavelengths require physically large observatories, and can operate from the ground from appropriate sites through a relatively transparent atmosphere.

On the ground, radio interferometry provides the only facilities which can equal the spatial and spectral resolution and sensitivity of diffraction-limited optical telescopes. The major radio observatories of the future (ALMA under construction, LOFAR, MWA, Allan Array,..., in the medium term, SKA later, at sub-millimetre and low frequencies respectively) will complement the ELT by probing non-thermal phenomena, the molecular Universe and highly obscured regions.

Facility	Wavelength range, type	Estimated operation	Greatest complementarity with ELT
ALMA	0.3 to 10 mm milli-arcsec imaging R up to 10^7 spectral resolution	2011	Resolving protoplanetary discs. Star formation and dust at all z. Imaging close to black holes and jet collimation regions. High–z CO.
LOFAR, Allen Array, PaST, MWA	SKA prototypes	2010?	Early SKA science
SKA	> 1cm milli-arcsec to arcsec imaging R up to 10^7 spectral resolution	2015+	Early Universe in HI and CO. Black holes and high energy astrophysics. Star formation history. Supernovae. Gravitational lensing. Astrometry (with VLBI)
Pierre Auger Array, HESS, etc	Cosmic rays	2006+	Discover extreme acceleration sources, possible new physics
LIGO, VIRGO, GEO600,etc	Gravitational Wave observatories	2008+	Discover extreme gravity events before optical events – require redshifts, location, context
ICE-CUBE, AMANDA, etc	Neutrino physics observatories	2005+	Probe neutrino mass, identify first component of dark matter

Table B.1

Some forthcoming ground-based astrophysical facilities.

B1.3 Future astronomical space missions

The next generations of space observatories, operating at wavelengths from the far infrared to X-rays, and extending beyond the electromagnetic spectrum, will need the complementary spectroscopy that only an extremely large optical telescope can provide. The table below list some planned future space missions and their likely requirements for ground-based observations.

Mission	Wavelength range, type	Launch Date	ELT follow-up and support required
GAIA	1.7m optical tel. for stellar kinematics: ESA	2011	ELT exploits catalogue of Solar Systems for exo-earth search; catalogue available ~2017
SPICA	3.5m 5K MIR/FIR telescope; imaging and spectra: Japanese-led	2010+	High-resolution MIR imaging and spectroscopy of newly-found sources
JWST	6.5m 30K NIR/MIR telescope; imaging & multi-object spectra: NASA/ESA/CSA	2012	Spectroscopy and high-resolution imaging of extremely faint sources
LISA	Gravity-wave detection ESA/NASA	2012+	Detection of extreme gravity events across the Universe: ELT essential for identification and detailed analysis
TPF & DARWIN	Coronograph and interferometer; exo-Earth imaging and spectra: NASA & ESA	2014–2020	50-100m ELT: complementary approach to terrestrial planet finding and spectroscopy
XEUS/ ConstellationX	Future X-ray astronomy NASA and ESA	2015+	Discovery of the first massive clusters and the first black holes

Table B.2

Some Future Space Missions and their ground-based complementarity.

B1.3.1 Comparison with JWST imaging sensitivity

The synergy between ground- and space-based observations in the optical and near-IR has been clearly demonstrated by the vast number of discoveries which required *both* HST and 8–10m ground-based telescopes in order to produce the result (usually using HST for imaging, and large ground-based telescope for spectroscopy). Although this will continue to apply for the next generation of observatories, their great aperture means that ELTs can in fact out-perform space-based telescopes in many regimes despite the reduced background in space. Thus, ELTs will be complementary to, but not reliant on, JWST.

Below we briefly consider two regimes: observations of (a) point sources and, (b) extended sources (in particular distant galaxies).

a) Point sources

The table below gives a comparison of point-source sensitivity for ELTs of various sizes compared to JWST. The calculations are based on initial calculations by Gillett & Mountain (1998), and details are given in Hawarden (2000). Since no high-resolution spectroscopic capability is proposed for any space IR telescope, an ELT is essential to deliver the spectroscopic science implied by table B.3.

b) Extended sources

For extended sources the gain of an ELT compared to JWST is not so great because the smaller diffraction limit does not help reduce the background "under" the object. However, again their sheer aperture allows ELTs to complement or out-perform JWST depending on the application.

M. Franx has considered the specific case of low spectral resolution (R=100) near-IR (H-band) observations of very high redshift (z>7) galaxies. An initial comparison of a 60m ELT with NIRSPEC on JWST produced the following conclusions, assuming that the ELT can work between the sky lines in the near-IR.

- ELT is faster by factor of ~16 on individual objects, but the large field of view of JWST-nirspec (10 sq arcmin) would have it lose that, unless ELT has at least the same field size. A field size of 10x10 arcmin is needed to make a really big step forward for this application.
- It is unlikely that ELT will go beyond an AB magnitude of 30 for extended objects. AB=28.5 is a more realistic estimate (R=100, S/N=10, exposure time =100 hours). These long integration times strengthen the case for a large multiplex.

λ (μm)	Imaging (R=5)				Spectroscopy (R=10,000)			
	20m	30m	50m	100m	20m	30m	50m	100m
1.25	2.1	3.6	10.2	34.8	5.8	9.1	15.8	30.6
1.6	1.2	2.3	6.2	22.7	5.8	9.1	15.8	30.4
2.2	0.92	2.1	4.0	6.1	4.5	7.4	13.2	25.8
3.5	0.036	0.080	0.221	0.86	0.50	1.1	2.9	10.9
4.9	0.005	0.020	0.054	0.20	0.042	0.095	0.27	1.00
12	0.012	0.030	0.079	0.30	0.088	0.200	0.54	2.15
20	0.004	0.031	0.088	0.33	0.045	0.107	0.30	1.15
25	0.004	0.031	0.088	0.33	0.039	0.088	0.24	0.92

The red boxed area defines where JWST outperforms an ELT

Table B.3

(From Hawarden 2000) IR performance of several ELTs is compared to that of the JWST space telescope. In the near-infrared an ELT outperforms a 6.5m cold (~30K) space telescope such as JWST (i.e. the point source sensitivity ratio ELT/JWST is >0.5 – see the unshaded regions above).

B1.4 EXOPLANET DETECTION FROM SPACE

Angel (2003) provides a detailed comparison of various space- and ground-based telescopes for detecting extrasolar Earth-like planets. As can be seen from Table B.4 (based on the summary in that paper), a ground-based 100m telescope at a regular site could out-perform planned space-based facilities in terms of signal-to-noise, particularly at shorter wavelengths.

Apart from improved signal-to-noise, one of the main advantages of a 100m-class ground-based telescope is its sensitivity – the distance at which exo-planets could be observed – and consequently the number of stars that can be surveyed (which is roughly proportional to the cube of this distance). Whereas the Darwin and the Terrestrial Planet Finder (TPF) space missions are expected to reach systems at distances of ~50 light years from us, a 100m ELT could reach to ~100 light years away. This greatly increases the number of suitable stars that can be surveyed from of order 100 to of order 1000. Thus, if ~1% of Solar-like stars host Earth's in stable orbits within their habitable zones, the chance of finding earth-like planets is increased such that a discovery becomes probable, and such that statistical studies of their frequency of occurrence and properties become possible.

Other differences between the ground and space-based approaches are:

- Difference in wavelength
  - study of different parameters or same parameters in different conditions
  - (In)sensitivity to exo-zodiacal emission. E-ELT may complete the survey for the *still unknown* percentage of stars for which Darwin will be blinded by exo-zodiacal light
- Length of "mission": an ELT is likely to be available for a longer lifetime and is more easily fitted with new instrumentation to adapt to scientific results.

Telescope	Size	λ (μm)	mode	S/N (earth at 10pc, t=24h)	
Space interferometer	4x2m	11	Nulling	8.4	Darwin, TPF-I
Space filled	7m	0.8	Coronograph	5.5-34	
Antarctic	21m	11	Nulling	0.52	GMT
		0.8	Coronograph	5.9	
Ground	30m	11	Nulling	0.34	TMT
		0.8	Coronograph	4.1	
Ground	100m	11	Coronograph	4.0	OWL
		0.8	Coronograph	46	
Antarctic	100m	11	Coronograph	17	BOWL=better OWL
		0.8	Coronograph	90	

Table B.4

(Adapted from Angel 2003). Comparison of the performance of various space and ground-based telescopes for detecting extra-solar Earth-like planets. The signal-to-noise obtainable for a 24hr observation of an Earth-like planet at 10pc is given for various telescope types and sizes.

B1.5 Supporting multi-wavelength science via the Virtual Observatory

In future astronomical research, much science will be enhanced or enabled by the analysis of data from other astronomical facilities together with that from the ELT. For instance, in the study of the earliest galaxies (see section 5.2.1), comparison of mid-IR data from the JWST and the near-IR data from the ELT will be naturally complementary in furthering our understanding of the physical processes at work in the epoch of re-ionisation. Many science problems will only be addressable with the incorporation of data from supporting high quality facilities, largely because of the need for full wavelength coverage or temporal data.

A challenge is to provide an astronomer with the tools and system to facilitate these comparisons of multi-sourced data, and to provide appropriate science focused tools to enable the manipulation and interpretation of the federated data sets.

To meet these challenges, Europe is now developing Virtual Observatories, both through national programmes such as AstroGrid (www.astrogrid.org) in the UK, and wider preliminary design studies through the Euro-VO (www.euro-vo.org) and through the precursor Astrophysical Virtual Observatory (AVO) projects. Similar projects are underway in North America (NVO) and other countries, co-ordinated through the International Virtual Observatory Alliance (IVOA).

Vital interoperability standards, addressing issues such as common astronomical ontologies, registries for resource discovery, data models, and access protocols, are currently being developed through the International Virtual Observatory Alliance (www.ivoa.net). This standards body involves the participation of all global VO projects, and thus representatives of the entire global astronomical community. Thus, in addition to partners from Europe, the IVOA includes the USA National Virtual Observatory (NVO), Japanese, Chinese, and many other VO projects.

Scientific results based on the usage of VO systems are already appearing, these made possible through the ability to seamlessly access and mine multi-wavelength data (e.g. Padovani et al 2004).

In the timeframe of the E-ELT, it is anticipated that mature VO infrastructures will be in place throughout Europe. This VO will integrate the major compute and data services available to the European astronomical community, bringing access to ELT and all other data and information resources required by the community.

In summary, the Euro-VO will be the vital framework through which ELT data products will be made accessible to the end-user community, for inter-comparison with complementary data from other contemporaneous missions and archival datasets.

B1.6 Developments in instrumentation

B1.6.1 Adaptive optics modes for ELTs

As is emphasised in the science cases and comparison table above, near diffraction-limited imaging, provided by Adaptive Optics (AO), is recognised to be essential to deliver their full scientific potential by all ELT projects, even though natural-seeing or "improved-seeing" operational modes are also envisioned. Recent developments in facility AO systems on current 8-10m class telescopes, including the first use of laser guide stars, demonstrate the clear potential for AO on future large telescopes. More complex systems such as Multi-Conjugate Adaptive Optics (expected to provide AO-corrected images with uniform image quality across a field of view of a few arcminutes) are now being developed and are expected to be in operation on current 8m facilities within the next few years. Most ELT designs have AO designed into them as an integral part of the telescope, using large deformable mirrors. This allows higher performance than does the retro-fitting of a facility AO capability, as was required for the current generation of telescopes. Thus, high-performance AO is a critical-path requirement and, as with all other critical-path items, will have to pass suitable reviews before the project proceeds.

B1.6.2 The use of ELTs at mid-infrared wavelengths

The mid-IR can contribute to a large number of topics in the ELT science case, and indeed some applications are dominated or enabled by mid-IR imaging and spectroscopy. The highlight cases for the mid-IR can be summarised as follows:

A. The formation of stars and the evolution of circumstellar disks: (dynamics of interstellar and circumstellar media, organic molecules in planet forming zones, H_2 pure rotational lines in proto-planetary disks, dust processing in disks.

B. The structure and conditions in nearby Starbursts, ULIRGs and AGN: unit scales of massive star formation, trigger mechanisms of starbursts, probing the inner parts of AGN with silicates, circum-nuclear starbursts, (sub)structures in the densest star forming environments – ULIRGs and UCHIIRs.

C. QSOs, AGN, and GRBs at high redshift.

The potential benefits of mid-IR observations on an ELT are manifold:

- The high point-source sensitivity makes it possible – in many cases for the first time – to do first class mid-IR science from the ground, i.e. comparable, or in some cases, even better than from space.
- The spatial resolution of 0.025 arcsec at 10μm will provide images comparable with what we know from HST, enabling high resolution studies over a large waveband. This opens up a significant discovery space.
- Many interesting objects will be too dust enshrouded to be studied at shorter wavelengths in a meaningful way. In addition, the mid-IR provides access to important diagnostic features (e.g. silicates, molecules, low-excitation H_2 and fine structure lines) which are not accessible at shorter wavelengths and cannot be detected by ALMA.
- A lot of the Galactic science depends on molecular tracers that require very high spectral resolution, not offered by any space based mid-IR observatory now or in the foreseeable future.
- Observations with ISO-SWS/LWS and Spitzer-IRS have shown the importance of spectroscopy at high angular resolution – different regions have different properties and spatially averaging spectra often hides the underlying physics.

B1.6.2.1 Design considerations for an ELT operating in the mid-IR

There are a number of implications on telescope design for optimal mid-IR observing. As with the sub-mm case below, these will be balanced against many other factors when considering telescope design parameters and choice of site:

(i) "the higher the site the better" in terms of precipitable water vapour. On a site like the South Pole or the peaks above the ALMA plateau the transmission at Q-band (about 18–24μm) would be greatly improved and new atmospheric windows longward of 24μm would open up. Some of these contain very important diagnostic spectral features for Galactic astronomy, some of these windows may be of interest for objects at higher redshift. In short, the precipitable water vapor content (and hence the altitude) will essentially define whether science longward of 13 microns can be done;

(ii) "the simpler the telescope the better" in terms of the number of warm mirrors and pupil shape definition. Obviously, a design with multiple warm optical correction elements is not the first choice for the thermal infrared. However, AO at thermal wavelengths would benefit from the presence of at least one adaptive correction element (with several thousands degrees of freedom) as part of the telescope itself. A possibility for chopping at the pupil would be desirable.

B1.6.3 The use of ELTs at sub-mm wavelengths

Astrophysics at submillimetre wavelengths (300μm to 2mm) is essentially the study of cool gas and dust, with for example the blackbody emission of a 10K source (or a 40K source at z=3) peaking at around 300μm. Such very cold material is associated with objects in formation, that is, the mysterious earliest evolutionary stages of galaxies, stars and planets. Furthermore most formation processes are deeply hidden within dust clouds, where the optical extinction can be many tens of magnitudes; but the extinction at submillimetre wavelengths is negligible. So understanding the *origins* of these objects requires observations to be conducted at submillimetre wavelengths.

The premier facility for *high-resolution* millimetre astronomy in the next decade will clearly be ALMA. Yet a 100m ELT offers the opportunity to observe with a similar geometric collecting area to ALMA, but with a near perfect dish surface accuracy and a single aperture. Thus, the *effective* collecting area of a 100m-class ELT (such as the proposed OWL telescope), if it could observe at short submillimetre wavelengths, will be approximately twice that of ALMA. A wideband bolometer array (dubbed SCOWL, Sub-mm Camera for OWL: Holland et al., 2003, SPIE, 4840, 340) would provide a facility which would surpass ALMA in several respects. The larger effective collecting area and the wider bandwidth of SCOWL will mean a factor of up to 20 improvement in point-source sensitivity to a given mass of dust (see table below). But with the proposed large-format focal plane array in SCOWL, the most significant gain will be in large-scale mapping speed. The table shows that projects to map square degrees at high sensitivity become feasible with SCOWL.

	SCOWL (100m)		ALMA	
	850μm	450μm	850μm	450μm
Flux sensitivity (mJy/√sec)	0.3	0.6	1.9	11
Dust mass sensitivity (cf SCUBA-2)	70	170	11	9
Resolution (arcsec)	2.1	1.1	0.02	0.01
Confusion limit (mJy)	0.01	0.005	4×10^{-4}	2×10^{-4}
Mapping speed (time per square degree to 0.01mJy)	2 days	10 days	7yr	900yr

B1.6.3.1 Design considerations for an ELT operating in the submillimetre

1. Telescope site. This is critical, as the true submillimetre windows only open up when the precipitable water vapour content is <1mm, and preferably <0.5mm. Figure B.1 shows the transmission in the main submillimetre windows at 350, 650 and 850GHz for three levels of precipitable water vapour. Sub-mm observations require an excellent, and generally high, site and this should be considered as one of the many factors when choosing the ELT site.

2. Operational aspects. Several options may be available for a sub-mm camera on an ELT: either it could be used when the optical conditions are non-optimum (e.g. poor seeing, cirrus), it could operate in the daytime (likely between dawn and midday, when the sky is still stable), it could compete directly with optical/IR projects, or it could operate in a hitchhiker mode (simultaneously with optical/IR). In any mode, sub-millimetre operation will allow more science to come from the ELT, with more potential observing time available. However, the hitchhiker mode is particularly appealing, as an astronomer could be doing a comprehensive project such as searching for faint planets around a star, whilst simultaneously looking for zodiacal or Kuiper Belt dust.

3. Optics design. To maximise the sensitivity, the optics should be designed to avoid a significant fractional blockage from warm sub-mm absorbers.

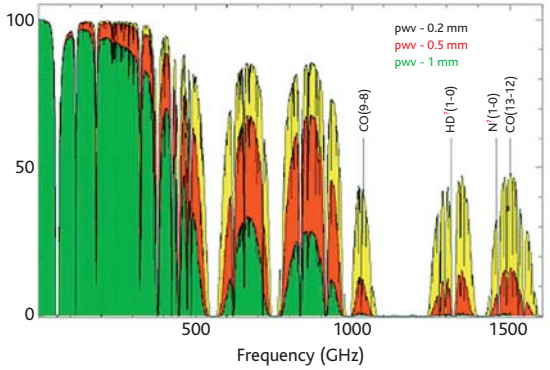

Fig.B.1

Transmission in the main submillimetre windows at 350, 650 and 850GHz for three levels of precipitable water vapour.

B1.6.4 The potential of astronomical quantum optics

Almost all of astronomy involves interpretation of the information content of electromagnetic radiation from celestial sources. The only exceptions are neutrino detections; gravitational-wave searches; direct detection of particle cosmic rays; and physical studies of planetary-system bodies. This electromagnetic radiation is collected by a telescope, and recorded by an appropriate instrument and detector.

Astronomical telescopes are equipped with auxiliary instruments which may give an impression of being inherently different from one another. However, a closer examination of the physical principles involved reveals that they all are measuring either the spatial or temporal coherence of light, or some combination of these. All imaging devices (cameras, interferometers) are studying aspects of the spatial coherence, albeit in various directions, and for different angular extents on the sky. All spectral analysis devices measure aspects of the temporal coherence, with different temporal/spectral resolution, and in the different polarisations. Although a gamma-ray satellite may superficially look different from a long-baseline radio interferometer, the basic physical property they are measuring is the same.

These spatial and temporal coherences can be traced back to be properties of the electromagnetic field amplitude and can be ascribed to individual photons, or to groups of individual photons. Thus, all existing astronomical instruments are limited to studies of such one-photon properties. However, light can carry information also

beyond this [first-order] coherence, e.g. encoded in the temporal distribution of photon arrival times. Photons that arrive from the given directions with the same energy (wavelength) will generate the same astronomical images and spectra, although the light might differ in its statistics of photon arrival times. These statistical distribution functions can be well-understood, as is observed in chaotic, maximum-entropy black-body radiation, which follows Bose-Einstein statistics, corresponding to the specific pattern of *bunching* in arrival times appropriate for any group of bosons with integer quantum spin. However, the statistics might also be quite different if the radiation is not in a maximum-entropy state, which would be the case if it originated in stimulated laser-type emission or had undergone scattering on the way to the observer.

Different physical processes in the generation of light may thus cause quantum-statistical differences, apparent as a different distribution of photon arrival times, between light with otherwise identical spectrum, polarisation, intensity, etc. Studies of such non-classical properties of light are actively pursued in laboratory optics.

Classical physics integrates all the quantum-statistical information in radiation of a certain wavelength into the quantity "intensity". When treating radiation as a three-dimensional photon gas, other parameters become significant, including higher-order coherence and the temporal correlation between photons. The best-known non-classical property of light is the bunching of photons, first measured by Hanbury Brown and Twiss in the experiments that led to the astronomical intensity interferometer.

Such properties may be revealed by studying second- and higher-order degrees of coherence, which reflect correlated properties of two or more photons in the light from the source. For example, in stimulated emission there is a causal coupling between a first photon, that is stimulating the emission, and the stimulated photon: stimulated emission thus is a property that can not be ascribed to a single photon; there must always be at least two. An idealised laser emits light whose photons are evenly distributed in time: in contrast to thermal emission there is no 'bunching'. The observation of such coherent effects exemplifies non-linear optical instrumentation: measuring the second- (or higher-) order coherence involves finding the probability that two (or more) photons arrive within the same time interval.

The second-order signal is proportional to the conditional probability that a second photon is detected immediately after the first. Since the signal is thus proportional to the intensity of the first photon multiplied by the intensity of the second one, it therefore increases as the square of the observed light intensity or the fourth power of telescope diameter. Higher-order coherences increase even more rapidly with telescope size. While such effects of non-linear optics are familiar in the laboratory, they are not [yet] familiar to astronomers. Thus far, the only astronomical instrument to exploit the second-order coherence of light was the stellar intensity interferometer, developed long ago by Hanbury Brown & Twiss; today that would be seen as a quantum-optical instrument (albeit usable for maximum-entropy, chaotic light only), and its legacy actually is quite valuable when discussing future astronomical observations.

In the laboratory, many effects of non-linear optics became accessible thanks to the intense light from lasers. In astronomy, the observability of non-linear effects in the photon stream from astronomical sources may become accessible thanks to the intense light collectable by Extremely Large Telescopes. Although the observability of more complex photon statistics in astronomical sources is not yet established, quantum optics could ultimately offer a fundamentally novel information channel also for astronomy.

For more detailed discussion of such issues see Dravins (1994, 2000, 2001). For an example of how higher-order studies of light may reveal radiation processes in specific objects, see Johansson & Letokhov (2005).

There exist other effects of quantum optics which are as yet less well-understood, but

which have the potential to be exploited in astronomy in the age of Extremely Large Telescopes. One important example follows from the recent realisation that individual photons may carry orbital angular momentum, in addition to the classically known angular momentum associated with photon spin and polarisation. Photon orbital angular momentum can already be measured for individual photons. This orbital angular momentum, which is in the direction of propagation, is characterised by an integer L in units of ħ, so that an absorber placed in the path of such a beam will, for each photon absorbed, acquire an angular momentum L. The integer L counts the orbital angular momentum state of the photon, and determines in a quantum information sense how many bits of information can be encoded in a single photon. Photons have now been prepared with L up to the order of 300, which implies that single photons may carry [at least] 8 bits of information, of considerable interest for quantum computing, and a main reason for the current interest in these phenomena.

Of course, in an astronomical context, the question arises whether, and in which astronomical sources, photons with such properties might be produced?

Light from astronomical sources can in principle be manipulated at the telescope using this same methodology, which might become a basis for a future instrument. For example, interference of light with orbital angular momentum produces a dark spot on the optical axis (irrespective of how tightly it is focused), but normal intensities outside. By suitable manipulation of starlight from a parent star with a planetary system, one might induce different amounts of angular momentum to the light from the central star, relative to its nearby exoplanet, thus enhancing the observable contrast by several orders of magnitude. In a sense, such light may thus act as its own coronagraph.

For an introduction to the orbital angular momentum of light, see Padgett, Courtial & Allen (2004). For a general discussion of the astronomical potential of light with orbital angular momentum, see Harwit (2003). For a discussion of high-contrast imaging using such light see Swartzlander (2001), and for a discussion of means for detecting photons with different orbital angular momentum see Leach et al (2002).

That a single photon, of any given wavelength and polarisation, and coming from any given direction, still can have hundreds of different states regarding its orbital angular momentum has come as a surprise to many, who naively believed that photon properties were already well understood. Perhaps the main conclusion to be drawn from these quantum studies is that light, and its photons can be much more complex, and carry much more information than was commonly believed in the past.

For astronomy, this poses an opportunity and a challenge: since our understanding of the Universe is based upon a delicate decoding of the information content of light from celestial sources, we need to exploit every opportunity to extract additional information, especially when moving into uncharted and unknown territory, where we cannot know beforehand what type of information will be conveyed. Quantum optics offers such an opportunity, while the forthcoming Extremely Large Telescopes promise the first opportunity to detect quantum-optical effects in the distribution of photons arriving from astronomical sources.

Credits

Contributors

This science case has been developed at a series of meetings within Europe over the last four years, sponsored by the EC network OPTICON. The OPTICON ELT Science Program and this document are co-ordinated by Isobel Hook and Gerry Gilmore. For more information on the OPTICON ELT Science Program and its participants, see www-astro-opticon.org/networking/elt.html

Document editor

Isobel Hook, University of Oxford, U.K.

Science working group co-chairs

Scientific contributions were co-ordinated by the co-Chairs of the Science Working Group, listed below.

Planets and Stars	Rafael Rebolo	IAC, Tenerife, Spain
	Hans Zinnecker	AIP Potsdam, Germany
Stars and Galaxies	Mike Merrifield	University of Nottingham, U.K.
	Sergio Ortolani	Padua University, Italy
Galaxies and Cosmology	Jacqueline Bergeron	IAP Paris, France
	Bruno Leibundgut	ESO

The EC FP6 Infrastructure Co-ordination Network, OPTICON, is co-ordinated by Gerry Gilmore, University of Cambridge, U.K.

This science case supports the EC FP6 ELT Design Study, Project Co-ordinator: Roberto Gilmozzi (ESO), Project Manager: Philippe Dierickx (ESO), Project Scientist: Piero Salinari (INAF-Arcetri, Italy).

References

Section 1

Andersen, T., Ardeberg, A., Owner-Petersen, M., 2003, Euro50, A 50 m Adaptive Optics Telescope, Lund Observatory

Andersen, T., Ardeberg, A., Riewaldt, H., Quinlan, N., Lastiwka, M., McNamara, K., Wang, X., Enmark, A., Owner-Petersen, M., Shearer, A., Fan, C., Moraru, D., 2004, SPIE 5489, 407

Dierickx P., Brunetto E., Comeron F., Gilmozzi R., Gonte F., Koch F., le Louarn M., Monnet, G., Spyromilio J., Surdej I., Verinaud C., Yaitskova N., 2004, Proc. SPIE 5489, in press

Gilmozzi R., 2004, Proc. SPIE, 5489, in press

Section 3

Alcock C. et al. 1997, ApJ, 486, 697

Arnold L., Schneider J., 2004, A&A, 420, 1153

Arnold L., Gillet S., Lardiere O., Riaud P., Schneider J., A&A, 2002, 392, 231

Babel J., Montmerle T., 1997, ApJ, 485, L29

Bally J., Zinnecker H., 2005, AJ, 129, 2281

Baumgardt H., Hut P., Makino J., McMillan S., Portegies Zwart S., 2003a, ApJ, 582, L21

Baumgardt H., Makino J., Hut P., McMillan S., Portegies Zwart S., 2003b, ApJ, 589, L25

Baumgardt H., Makino J., Hut P., 2005, ApJ, 620, 238

Bedin L., Anderson J., King I., & Piotto G., 2001, ApJ, 560, L75

Beers T. C., Suzuki T. K., Yoshii Y., 2000, in The Light Elements and Their Evolution, IAU Symp., Vol. 198, eds. L. da Silva, M. Spite, J. R. de Medeiros, PASP, p. 425

Bonnell I. A., Bate M. R., Zinnecker H., 1998, MNRAS, 298, 93

Burrows A., Marley M., Hubbard W. B., Lunine J. I., Guillot T., Saumon D., Freedman R., Sudarsky D., Sharp C., 1997, ApJ, 491, 856

Butler R. P., Marcy G. W., Fischer D. A., Brown T. M., Contos A. R., Korzennik S. G., Nisenson P. & Noyes R. W., 1999, ApJ, 526, 916

Cayrel R. et al., 2001, Nature, 409, 691

Chauvin G., Lagrange A.-M., Dumas C., Zuckerman B., Mouillet D., Song I., Beuzit J.-L., Lowrance P., 2004, A&A, 2004, 425, L29

Christlieb N., et al., 2004, A&A, 428, 1027

Clark R. N., 1999, Manual of Remote Sensing, ed. A. Rencz (J. Wiley and Sons, New-York)

Davis C. J., Whelan E., Ray T. P., Chrysostomou A., 2003, A&A, 397, 693

Dyudina U. A., Sackett P. D., Bayliss D. D. R., Seager S., Porco C. C., Throop H. B., Dones L., 2005, ApJ, 618, 973

Gebhardt K., Rich R. M., Ho L. C., 2002, ApJ, 578, L41

Gerssen J., van der Marel R. P., Gebhardt K., Guhathakurta P., Peterson R. C., Pryor C., 2002, AJ, 124, 3270

Goriely S., Arnould M., 2001, A&A, 379, 1113

Goriely S., Clerbaux B., 1999, A&A, 346, 798

Hainaut O., Rahoui F., Gilmozzi R., 2004, in proceedings of the Berlin-4 meeting "Exploring the Cosmic Frontier", Springer-Verlag series "ESO Astrophysics Symposia", ed. A. Lobanov

Henning Th., Feldt M., Stecklum B., Klein R., 2001, A&A, 370, 100

Hill V. et al. 2002, A&A 387, 560

Fracassini M., Pasinetti L.E., Manzolini F., 1981, A&AS, 45, 145

Kulkarni S. R., Hut P., McMillan S., 1993, Nature, 364, 421

Lardiere O., Salinari P., Jolissaint L., Carbillet M., Riccardi A., Esposito S., 2003, in: Proceedings of the Second Backaskog workshop on ELTs, 9-11 September 2003, Backaskog, Sweden, eds A. Ardeberg and T. Anderson. SPIE, 5382, 550

Le Louarn M., Verinaud C., Yaitskova N., Fedrigo E., Korkiakoski V., Hubin N., 2004, Proc. SPIE 5490, in press

Lucas P.W., Roche P. F., 2000, MNRAS, 314, 858

Lucas P. W., Roche P. F., Riddick, F., 2003, in E. Martin, ed., Proc. IAU Symp 211, (ASP: San Francisco), p63

Mackey A. D., Gilmore G. F. 2003a, MNRAS, 338, 85

Mackey A. D., Gilmore G. F. 2003b, MNRAS, 338, 120

Marley M. S., Gelino C., Stephens D., Lunine J. I., Freedman R., 1999 ApJ, 513, 879

Marcy G. W., Butler R. P., Fischer D. A., Laughlin G., Vogt S. S., Henry G. W., Pourbaix D., 2002, ApJ 581, 1375

Mayer L., Quinn T., Wadsley J., Stadel J., 2004, ApJ, 609, 1045

MacLow M.-M., Klessen R. S., 2004, Rev. Mod. Phys., 76, 125

McCaughrean M. J., Zinnecker H., Andersen M., Meeus G., Lodieu N., 2002, ESO Messenger, 109, 28

Naef D., Mayor M., Korzennik S. G., Queloz D., Udry S., Nisenson P., Noyes R. W., Brown T. M., Beuzit J.-L., Perrier C., Sivan J.-P., 2003, A&A, 410, 1051

Pasquini L., Bonifacio P., Randich S., Galli D., Gratton R. G., 2004, A&A, 426, 651

Portegies Zwart S. F., McMillan S. L. W., 2002, ApJ, 576, 899

Reeves, H., Fowler, W.,A., Hoyle, F. 1970, Nature, 226, 727

Schneider J., Aronold L. & Borkowski V., 2003. New approaches for the search for binary planets and moons of extrasolar planets. In SF2A-2003: Semaine de l'Astrophysique Française, eds. F. Combes, D. Barret, T. Contini, and L. Pagani. EdP-Sciences, Conference Series, p. 151.

Shu F. H., Adams F. C., & Lizano S, 1987, ARA&A, 25, 23

Stern A., Spencer J. 2003, New Horizons: the First Reconnaissance Mission to Bodies in the Kuiper Belt. In 'The First Decadal Review of the Kuiper Belt', editors J.K Davies and L. H Barrera, Kluwer Academic Publishers, Netherlands p 477

Sigurdsson S., Hernquist L., 1993, Nature, 364, 423

Sudarsky D., Burrows A., Hubeny I., 2003, ApJ, 588, 1121

Suzuki T. K., Yoshii Y., Kajino T. 2001, ApJ 522, L125

Thi W.-F., van Dishoeck E. F., Blake G. A., van Zadelhoff G.-J., Hogerheijde M. R., 1999, ApJ, 521, L63

Valle G., Ferrini F., Galli D., Shore S. N., 2002, ApJ 566, 252

Wanajo S., Itoh N., Ishimaru Y., Nozawa S., Beers T. C., 2002, ApJ, 577, 853

Williams D. M., Knacke R. F., 2004, Astrobiology, 4, 400

Zapatero-Osorio M. R., Béjar V. J. S., Martín E. L., Rebolo R., Barrado y Navascués D., Bailer-Jones C. A. L., Mundt R., 2000, Science, 290, 103

Zuckerman B., Song I.. 2004, ARA&A, 42, 685

Section 4

Adams F.C., Fatuzzo M., 1996, ApJ, 464, 256

Adams F.C., Laughlin G., 1996, ApJ, 468, 586

Aguerri J.A.L. et al. 2005, AJ, in press (astro-ph/0502420)

Andersen T., Ardeberg A., Owner-Petersen M., 2003, "Euro50, a 50m Adaptive Optics Telescope", Lund Observatory

Andersen T., Ardeberg A., Riewaldt H., Quinlan N., Lastiwka M., McNamara K., Wang X., Enmark A., Owner-Petersen M., Shearer A., Fan C., Moraru D., 2004, SPIE 5489, 407

Aparicio A. & Gallart C., 2004, AJ 128 1465

Ardeberg A., 2004, SPIE 5489, 23

Ardeberg A., Linde P., 2004, SPIE 5382, 47

Ardeberg A., Linde P., Owner-Petersen M., 1999, ESO Conf. and Workshop Proc. No. 57, 20

Arnaboldi M. et al. 2003, AJ, 125, 514

Balogh M. et al. 2001, MNRAS, 326, 1228

Barth A.J., Sarzi M., Rix H., Ho L.C., Filippenko A.V., Sargent W.L.W. 2001, ApJ, 555, 685

Bastian N., Taylor V.A., Windhorst R.A., 2003d, MNRAS, 342, 259

Beckers J. M., Owner-Petersen M., Andersen T., 2004, SPIE 5382, 510

Bellazzini M., Ferraro F.R., Sollima A.,

Pancino E., Origlia L. 2004, A&A, 424, 199

van den Bergh S., 2000, "The galaxies of the Local Group", Cambridge Univ. Press, Cambridge, New York

Bernstein G. M., Nichol R. C., Tyson J. A., Ulmer M. P., Wittman D., 1995, AJ, 110, 1507

Bresolin F., Kudritzki R.-P., Mendez R. H., Przybilla, N., 2001, ApJ, 548, 159L

Bresolin F., Gieren, W., Kudritzki, R.-P., Pietrzynski, G., Przybilla, N., 2002, ApJ, 567, 277

Bressan A., Della Valle M. and Marziani P., 2002, MNRAS, 331, L25

Brown T. M., Fergusson H. C., Smith E., Kimble R. A., Sweigart A. V., Renzini A., Rich R. M., VandenBerg D. A., 2003, ApJ, 592, L17

Brown T. M., Ferguson H. C., Smith E., Randy A., Swigart A. V., Renzini A., Rich R. M., Vandenberg, D. A., 2004, ApJ, 613, L125

Burstein D., Li Y., Freeman K. C., Norris J. E., Bessell M. S., Bland-Hawthorn J., Gibson, B. K., Beasley M. A., Lee H.-c., Barbuy B., Huchra J. P., Brodie J. P., Forbes D. A., 2004, ApJ, 614, 158.

Chabrier G., 2003, PASP, 115, 763

Ciardullo, R., Durrell, P. R., Laychak, M. B., Herrmann, K. A., Moody, K., Jacoby, G. H., Feldmeier, J. J., 2004, ApJ, 614, 167

Cid Fernades, R., Heckman, T. Schmitt, H., Gonzalez Delgado, R., Storchi-Bergmann T. 2001, ApJ, 558, 81

Combes F., Debbasch F., Friedli D., Pfenniger D., 1990 A&A, 233, 82

Crowther P., Hillier D.J., Evans C.J., Fullerton A.W., De Marco O., Willis A.J., 2002, ApJ, 579, 774

Dall'Ora, M., Storm, J., Bono, G., Ripepi, V., Monelli, M., Testa, V., Andreuzzi, G., Buonanno, R., Caputo F., Castellani V., Corsi C. E., Marconi G., Marconi M., Pulone L, Stetson, P. B., 2004, ApJ, 610, 269

Dehnen W., 1998, AJ, 115, 2384

Durrell P. R., Harris W. E., Pritchet C. J., 2001, AJ. 121, 2557

Durrell P.R., Ciardullo R., Feldmeier J. J., Jacoby, G. H.; Sigurdsson, Stein, 2002, ApJ, 570, 119

Edvardsson B., Andersen J., Gustafsson B., Lambert D. L., Nissen P. E., Tomkin, J., 1993 A&A, 275, 101

Evans C. J., Lennon D. J., Trundle C., Heap S. R., Lindler D. J., 2004, ApJ, 607, 451

Feldmeier J. J., Mihos, J. C., Morrison H. L., Rodney, S. A., Harding, P., 2002, ApJ, 575, 779

Feldmeier J J., Ciardullo, R., Jacoby G. H., Durrell, P. R., 2004, ApJ 615, 196

Ferguson A. M. N., Irwin M. J., Ibata R. A., Lewis G. F., Tanvir N. R., 2002, AJ. 124, 1452

Ferraro F. R., 2002, in Observed HR Diagrams and Stellar Evolution, edited by T. Lejeune & J. Fernandes, ASP Conf. Proc., 274, 268

Ferraro F. R., Origlia L., Testa V., Maraston C., 2004, ApJ, 608, 772.

Ferrarese L. & Merritt D. 2000, ApJL, 539, L9

Figer D.F., 2005, Nature 434, 192

Frayn C., 2003, PhD Thesis, University of Cambridge

Fukugita M., Hogan C. J., Peebles P. J. E., 1998, ApJ, 503, 518

Gebhardt K.et al. 2000, ApJL, 539, L13

Geisler D., Grebel E. K., Minniti D., de Grijs R. 2003, Book Review: "Extragalactic star clusters", The Observatory, 123, 1174, 165

Genzel R., Pichon C., Eckart A., Gerhard O.E., Ott T., 2000, MNRAS, 317, 348

González R. A., Liu M. C., Bruzual A., G., 2004, ApJ, 611, 270

Goudfrooij P., Gilmore D., Whitmore B.C., Schweizer, F., 2004, ApJ, 613, 121

Graham A.W., Erwin, P., Caon, N., & Trujillo, I. 2001, ApJL, 563, L11

Graham A.W., Erwin, P., Caon, N., & Trujillo, I. 2002, astro-ph/0206248

Granato G.L., et al., 2004, ApJ, 600, 580

de Grijs R., Johnson R.A., Gilmore G.F., Frayn C.M., 2002a, MNRAS, 331, 228

de Grijs R., Gilmore G.F., Johnson R.A., Mackey A.D., 2002b, MNRAS, 331, 245

de Grijs R., Gilmore G.F., Mackey A.D., Wilkinson M.I., Beaulieu S.F., Johnson R.A., Santiago B.X., 2002c, MNRAS, 337, 597

de Grijs R. Bastian N., Lamers H. J. G. L. M., 2003a, ApJ, 583, L17

de Grijs R., Fritze-v. Alvensleben U., Anders P., Gallagher J.S., Bastian N., Taylor V.A., Windhorst R.A., 2003b, MNRAS, 342, 259

Gnedin O.Y. & Ostriker J.P, 1997, ApJ, 474, 223

Goodwin S.P., 1997, MNRAS, 286, 669

Haehnelt M., Madau P., Kudritzki R., Haardt, F., 2001, ApJ, 549, 151L

Hamuy M., 2003, ApJ, 582, 905

Heger A., Woosley S. E., 2002, ApJ, 567, 532

Heger A., Woosley S.E., Baraffe I., Abel T., 2001, in proc. MPA/ESO/MPE/USM Joint Astronomy Conference "Lighthouses of the Universe: The most Luminous Celestial Objects and their use for Cosmology" (astro-ph/0112059)

Hill V., Francois P., Spite M., Primas F., Spite F., 2000, A&A, 364, L19

von Hippel T., Gilmore G., Tanvir N., Robinson D., Jones D.H.P., 1996, AJ 112, 192

Hjorth J. et al., 2003, Nature, 423, 847

Kaspi S., Smith P.S., Netzer H., Maoz D., Jannuzi B.T., Giveon U. 2000, ApJ, 533, 631

Kaufer A., Venn K., Tolstoy E., Pinte C., Kudritzski R.-P., 2004, AJ, 127, 2723

Kauffmann G., 1996, MNRAS, 281, 487

Kauffmann G. et al. 2003, MNRAS, 346, 1055

King I. R, 1962, AJ. 67, 471

Kormendy J., 1977, ApJ, 218, 333

Kormendy J. & Richstone D. 1995, ARA&A, 33, 581

Knop R. et al., 2003, ApJ, 598, 102

Kroupa P., 2002, Science 295, 82

Kroupa P., Tout C.A., 1997, MNRAS 287, 402

Kroupa P., Tout C.A., Gilmore G., 1993, MNRAS 262, 545

Kudritzki R.-P., Bresolin F., Przybilla N., 2003, ApJL, 582, 83

Lacy J. H., Evans N. J., II, Achtermann J. M., Bruce D. E., Arens J. F., Carr J. S., 1989, ApJ 342, L43

Larson R.B., 1998, MNRAS 301, 569

Lata S., Pandey A. K., Sagar R., Mohan V., 2002, A&A, 388, 158

Leitherer C., Schaerer, D., Goldader J. D., Delgado R. M. G., Robert C., Kune D. F., de Mello D. F., Devost, D., Heckman, T. M., 1999, ApJS, 123, 3

Lejeune Th., Cuisinier F., Buser R., 1997, A&AS 125, 229

Lynden-Bell, D.,1969, Nature, 223,690

Macchetto F., Marconi A., Axon D. J., Capetti A., Sparks W., Crane P. 1997, ApJ, 489, 579

Mackey J., Bromm V., Hernquist L., 2003, ApJ, 586, 1

McLure R.J. & Jarvis M.J. 2002, MNRAS, 337, 109

McWilliam A. 1997, ARA&A, 35, 503

Madau, P. Della Valle, M. and Panagia, N. 1998, MNRAS, 297, 17L

Maeder A. & Meynet G., 2001, A&A, 373, 555

Maeder A. & Meynet G., 2004, A&A, 422, 225

Massey P., 1998, ASP Conf. Ser. 142: The Stellar Initial Mass Function (38th Herstmonceux Conference), eds. Gilmore G., Howell D., 142, 17

Merrett H. et al, 2003, MNRAS, 346, L62

Mannucci F., Maiolino R., Cresci G., Della Valle M., Vanzi L., Ghinassi F., Ivanov V. D., Nagar N. M., Alonso-Herrero A., 2003, A&A 401, 519

Mannucci F., Della Valle M. and Panagia N., 2005, in prep.

Marconi A. et al. 2003, ApJ, 586, 868

Marconi A., Capetti A., Axon D.J., Koekemoer A., Macchetto D., Schreier E.J., 2001, ApJ, 549, 915

Marconi A., Hunt L. K., 2003, ApJ, 589, L21

Marconi A., Risaliti G., Gilli R., Hunt L.K., Maiolino R., Salvati M., 2004, MNRAS, 351, 169

Melendez J., Barbuy B., Bica E., Zoccali M., Ortolani S., Renzini A.; Hill V., 2003, A&A, 411, 417

de Mello D. F, Daddi E., Renzini A., Cimatti A., di Serego Alighieri S., Pozzetti, L., Zamorani G., 2004 ApJ, 608, L29

Menci N., Cavaliere A., Fontana A.,

Giallongo E., Poli F., Vittorini V., 2003, ApJ, 587, L63

Mengel S., Lehnert M. D., Thatte N., Tacconi-Garman L.E., Genzeil R., 2001, ApJ, 550, 280

Meynet G., Maeder A., Schaller G., Schaerer D., Charbonnel C., 1994, A&AS 103, 97

Minniti D., Zijlstra A. A., Alonso M. V., 1999, AJ, 117, 881

Miralda-Escude J., Rees M., 1997, ApJ, 478, 57L

Miyoshi M., Moran J., Herrnstein J., Greenhill L., Nakai N., Diamond P., Inoue M., 1995, Nature, 373, 127

Monaco L., Bellazzini M., Ferraro F. R., Pancino E., 2003, ApJ, 597, L 25.

Murante G., Arnaboldi M., Gerhard O., Borgani S., Cheng L. M., Diaferio A., Dolag K., Moscardini L., Tormen G., Tornatore L., Tozzi P., 2004, ApJ, 607, L83

Oey M.S., Clarke C.J., 2005, ApJL, 620, L43

Oliva E., Origlia L., Maiolino R., Morrwood A. F. M. 1999, A&A, 350, 9

Owner-Petersen M., Gontcharov A., 2004, SPIE 5382, 544

Pagel B. E. J.,Tautvaisene G., 1998, MNRAS, 299, 535

Padoan P., Nordlund Å., 2002, ApJ 576, 870

Patat F., Barbon R. Cappellaro E., Turatto M., 1994, A&A, 282, 731

Paunzen E., Maitzen H. M., Rakos K. D., Schombert J., 2003, A&A, 403, 937

Perlmutter S. et al., 1998, Nature, 391, 51

Perlmutter S. et al., 1999, ApJ, 517, 565

Phillips M. M., 1993, ApJL, 413, 105

Reid I.N., Gizis J.E., Hawley S.L., 2002, AJ 124, 2721

Riess A. et al.,1998, 116, 1009

Riess A. et al, 2004, ApJ, 607, 665

Romaniello M., Robberto M., Panagia N, 2004, ApJ, 608, 220

Romanowsky A.J., Douglas N. G., Arnaboldi M., Kuijken, K. Merrifield M. R., Napolitano N. R., Capaccioli M., Freeman K. C., 2003, Science, 301, 1696

Rosenberg A., Saviane I., Piotto G., Aparicio A., 1999, AJ, 118, 230

Salow R. M., Statler T. S., 2004, ApJ, 611, 245

Scalo J.M., 1986, Fundamentals of Cosmic Physics 11, 1

Schödel R. et al. 2002, Nature, 419, 694

Smith L. J., Gallagher J.S., 2001, MNRAS, 326, 1027

Soltan A., 1982, MNRAS, 200, 115

Spännare S., 2003, private communication

Stephens A. W., Frogel J. A., DePoy D. L., Freedman W., Gallart C., Jablonka P., Renzini A., Rich R. M., Davies R., 2003, AJ, 125, 2473

Stetson P., 1987, PASP, 99, 191.

Stiavelli M. & Setti G., 1993, MNRAS, 262, L51

Thacker R.J. & Couchman H.M.P., 2001, ApJ, 555, 17L

Tolstoy E., Irwin M. J.; Cole A. A., Pasquini L., Gilmozzi R., Gallagher J. S., 2001 MNRAS, 327, 918

Tolstoy E., Venn K. A., Shetrone M., Primas F., Hill V., Kaufer A., Szeifert, T., 2003 AJ, 125, 707

Trundle C., Lennon D. J., Puls J., Dufton P. L., 2004, A&A, 417, 217

Valenti E., Ferraro F.R., Origlia L. 2004, MNRAS, 354, 815

van der Marel R. P., Gerssen J., Guhathakurta P., Peterson R. C., Gebhardt K., 2002, AJ. 124, 3255

van der Marel R. P., de Zeeeuw P., Rix H.-W., Quinlan G. D. 1997, Nature, 385, 610

Villar-Martin et al. 2004, MNRAS, 355,1132

Weidner C., Kroupa P., 2004, MNRAS 348, 187

Weidner C., Kroupa P., 2005, ApJ, in press

Weil M. L., Eke V. R. & Efstathiou G., 1998, MNRAS, 300, 773

Weinmann S. M. & Lilly S. J., 2005, ApJ, in press (astro-ph/0412248)

Williams S. J., Shafter A. W., 2004, ApJ. 612, 867

Woosley S. E. & Weaver T. A., 1995 ApJS, 101, 181

Wyse R.F.C. & Silk J., 1989, ApJ, 339, 700

Wyse R.F.C., 1998, ASP Conf. Ser.142: The Stellar Initial Mass Function (38th Herstmonceux Conference), ed: Gilmore G., Howell D., 142, 89

Wyse R.F.G., Gilmore G., Houdashelt M.L., Feltzing S., Hebb L., Gallagher J.S., Smecker-Hane T.A., 2002, New Astronomy 7, 395

Yanny B., Guhathakurta P., Bahcall J. N., Schneider, D. P., 1994, AJ, 107, 1745

Section 5

Albadi M. G., Navarro, J. F., Steinmetz, M., & Eke, V. R. 2003, ApJ, 597, 21

Adelberger K. L., Steidel C. C., Shapley A.E. & Pettini M., 2003, ApJ, 584, 45

Allen A. W., Schmidt R. W., & Fabian A. C. 2002, MNRAS, 334, L11

Arnold L. 2001, Semaine de l'Astrophysique Francaise, Eds. F. Combes, D. Barret, F. Thevenin, to be published by EdP-Sciences, Conference Series, p. 597

Barrow J. D. 2002, From Alpha to Omega: The constants of Nature, London: Jonathan Cape

Becker R. et al 2001, AJ, 122, 2850

Bennett C. L., et al. 2003, ApJS, 148, 1

Boehm A. et al. 2004, A&A, 420, 97

Bouwens R. et al., 2004a, ApJ, 611, L1

Bouwens R. et al., 2004b, ApJ, 616, 79

Bouwens R. et al., 2005, ApJ, 624, 5

Bremer M. et al 2004a, ApJ, 615, 1

Bremer M. et al 2004b, MNRAS, 347, 7

Bremer M. & Lehnert M., 2005a, in proc "Exploring the Cosmic Frontier", Berlin 2004, Springer-Verlag series "ESO Astrophysics Symposia", Ed. A. Lobanov.

Bremer M. & Lehnert M., 2005b, in proc "The Evolution of Starbursts" AIP Proc 331. Heraeus Seminar: The Evolution of Starbursts Eds. Huettemeister, Manthey, Aalto, Bomans

Brinchmann J. & Ellis R. 2000, ApJ, 536, L77

Bromm V. & Larson R. B., 2004 ARA&A, 42, 79

Buat et al 2005, ApJ, 619, 51L

Bunker A., et al., 2004, MNRAS, 355, 347

Burgarella et al, 2005, MNRAS, in press

Caputo F., Castellani V., Marconi M. & Ripepi V. 2000, MNRAS, 316, 819

Cassisi S., Castellani V., degl'Innocenti S. & Weiss A. 1998, A&ASS, 129, 267

Chand H., Srianand R., Petitjean P., Aracil B. 2004, A&A, 417, 853

Cimatti A. et al. 2004, Nature, 430, 184

Cole S. et al. 2001, MNRAS, 326, 255

Cuby J.-G., Le Fèvre O., McCracken, H., Cuillandre, J.-C., Magnier, E., Meneux, B., 2003, A&A, 405, 19L

Dickinson M. et al. 2003, ApJ, 587, 25

van Dokkum P. et al. 2001, ApJ, 553, L39

Egami E., et al. 2005, ApJ, 618, L5

Eggen O. J., Lynden-Bell, D., Sandage, A. R. 1962, ApJ, 136, 748

Ellis R. 1998, Nature, 395, 3

Erb D. et al. 2003, ApJ, 591, 101

Eyles L., et al. 2005, MNRAS, submitted (astro-ph/0502385)

Fan X. et al. 2003, AJ, 125, 1649

Ferland G. J., 2004, at website: http://www.nublado.org/

Firmani et al. 2005, astro-ph/0501395

Firmani et al. 2004, ApJ, 616, 1033

Fontana A. et al. 2003, ApJ, 594, L9

Fontana A. et al. 2004, A&A, 424, 23

Frail D. A. et al. 2001, ApJ, 562, L55

Freedman W.L., Madore B.F., Gibson B.K., Ferrarese L., et al. 2001, ApJ, 553, 47

Fukugita M., Hogan C. J., Peebles P. J. E. 1998, ApJ, 503, 518

Genzel R. et al. 2003, ApJ, 584, 633

Ghirlanda G. et al. 2004a, ApJ, 616, 331

Ghirlanda G. et al. 2004b, ApJ, 613, L13

Ghirlanda G. et al. 2005, astro-ph/0502186

Giavalisco M., Steidel C. C., Macchetto F. D. 1996, ApJ, 470, 189

Gill S. P. D., Knebe A., Gibson B. K., & Dopita M. A. 2004, MNRAS, 351, 410

Glazebrook K. et al., Nature, 430, 181

Gnedin N. Y. 2000, ApJ, 535, 530

Grazian et al., 2005, in preparation

Haardt F. & Madau P., 2001, in XXXVI Rencontres de Morions on: Galaxy Clusters and the High Redshift Universe Observed in X-Rays. Website: http://pitto.mib.infn.it/~haardt/cubaintr.html

Hammer F. et al, 2003, SPIE, 5382, 727

Hawkins E., Maddox S., Cole, S., et al. 2003, MNRAS, 346, 78

Heckman T. M., Lehnert M. D., Strickland D. K, & Armus L. 2000, ApJS, 129, 493

Heger A., Woosley S.E., Baraffe I., Abel T., 2001 (astroph/0112059)

Hook I. et al 2005, AJ, submitted

Hu E., Cowie L., McMahon R., Capak P.; Iwamuro F.; Kneib J.-P., Maihara T.; Motohara K., 2002, ApJ, 568(2), L75

Israel et al. 1999, A&A, 384, L5

Kervlla P., Bersier D., Mourard D., Nardetto N., Fouqué P. & Coudé du Foresto V. 2004, A&A, 428, 587

Kneib J.P., Ellis R., Santos M., Richard, J., 2004, ApJ, 607, 697-703

Knop R. et al., 2003, ApJ, 598, 102

Kogut A. et al., 2003, ApJS, 148, 161

Lamb D. Q., Reichart D. E., 2000, ApJ, 536, 1

Lehnert M. D. Bremer M., 2003, ApJ, 593, 630

Lehnert M. D., Bremer M., 2004, ESO Messenger, 115, 27

Lehnert M. D., & Heckman, T. M. 1996, ApJ, 462, 651

Leibundgut B. 2001, ARA&A, 39, 67

Levshakov S. A., Centurión M., Molaro P., D'Odorico S. 2004, A&A, in press (astro-ph/0408188)

Lidman C. et al 2005, A&A, 430, 843

McCarthy P. J. et al. 2004, ApJ, 614, L9

Matheson et al. 2005, AJ, in press (astro-ph/0411357)

Mo H. J., Mao, S., White, S. D. M. 1998, MNRAS, 295, 319

Murphy M. T., et al. 2001, MNRAS, 327, 1208

Murphy M., T., Webb, J. K., Flambaum V. V. 2003, 2003, MNRAS, 345, 609

Murphy M. T. et al. 2004, in "Astrophysics, Clocks and Fundamental Constants," eds. S. G. Karshenboim and E. Peik, Lecture Notes in Physics, 648,.131

Ouichi M. et al, 2005, ApJ, 620, 1, L1

Pentericci L. et al. 2002, AJ, 2158

Perlmutter S. et al., 1999, ApJ, 517, 565

Pettini M. et al. 2001, ApJ, 554, 981

Pritchet C. et al 2004, proceedings of "Observing Dark Energy" (NOAO/Tucson proceedings), astro-ph/0406242

Prociani & Madau 2001 ApJ, 584, 522

Quast R., Reimers, D., Levshakov, S. A. 2004, A&A, 415, L7

Ricotti M. Ostriker J., 2004, MNRAS, 352, 547

Rigopoulou D. et al. 2002, ApJ, 580, 789

Riess A. et al.,1998, 116, 1009

Riess A. et al, 2004, ApJ, 607, 665

Roche N., Ratnatunga K., Griffiths R.E., Im M., Naim A., 1998, MNRAS, 293,157

Romaniello M., Primas F., Mottini M. & Groenewegen M. 2004, IAU Colloquium 193, eds D.W. Kurtz and K.R. Pollard, p. 426

Saha A., Sandage A., Thim F., Labhardt L., et al. 2001, ApJ, 551, 973

Sandage A. 1962, ApJ, 136, 319

Sandage A., Tammann G.A. & Reindl B. 2004, A&A, 424, 43

Schaerer D., 2003, A&A, 397, 527

Schaye J., 2001, ApJ, 559, 507

Schaye J., Aguirre A., Kim T.-S., Theuns T., Rauch M. & Sargent W. L. W. 2003, ApJ, 596, 768

Searle L., Zinn R. 1978, ApJ, 225, 357

di Serego Alighieri S. et al. 2005, A&A, submitted

Simcoe R. A., Sargent W. L. W. & Rauch M. 2003, in Carnegie Observatories Astrophysics Series, Vol. 4: Origin and Evolution of the Elements ed. A. McWilliam & M. Rauch (Pasadena: Carnegie Observatories).

Smail I., Ivison R.J. & Blain A.W., 1997, ApJ, 490, 5

Spergel D.N., et al., 2003, ApJS, 148, 175

Stiavelli M. et al, 2004, ApJ, 600, 508

Tonry J. L, et al., 2003, ApJ, 594, 1

Treu T. et al. 2001, MNRAS, 326, 221

Treu T. et al. 2002, ApJ, 564, L13

Treu T. et al. 2005, ApJ, in press (astro-ph/0503164)

Van Dokkum P. et al. 2004, ApJ, 611, 703

Vernet J. et al. 2005, A&A, submitted

Vogt S. et al. 1996, ApJ, 465, L15

Webb J. K., Flambaum V., Churchill C. W., Drinkwater, M. J., Barrow J. D., 1999. PhRvL, 82, 884

Webb J. K., et al. 2001, PhRvL, 87, 091301

Wolf C. Wisotski L., Borch A., Dye S., Kleinheinrich M., Meisenheimer K., 2003, A&A, 499, 514

Ziegler B. et al. 2002, ApJ, 564, L69

Annex A

"Giant Magellan Telecscope – Science Goals" Draft November 2003, available from the GMT web pages http://helios.astro.lsa.umich.edu/magellan/

"Frontier Science enabled by a Giant Segmented Mirror Telescope" by the GSMT science working group, available at http://www.aura-nio.noao.edu/gsmt_swg/SWG_Report/SWG_Report_7.2.03.pdf

The Euro-50 web pages http://www.astro.lu.se/~torben/euro50/

Annex B

Angel R., 2003 in: Proceedings of the Conference on Towards Other Earths: DARWIN/TPF and the Search for Extrasolar Terrestrial Planets, 22-25 April 2003, Heidelberg, Germany. Edited by M. Fridlund, T. Henning, compiled by H. Lacoste. ESA SP-539, Noordwijk, Netherlands: ESA Publications Division, ISBN 92-9092-849-2, 2003, p. 221-230

Dravins D.: Astrophysics on Its Shortest Timescales,ESO Messenger No.78, 9-19 (1994)

Dravins D., 2000, "Beyond Imaging, Spectroscopy and Interferometry:Quantum Optics at the Largest Telescopes", in T.Andersen, A.Ardeberg, R.Gilmozzi, eds. Proc. Backaskog Workshop on Extremely Large Telescopes, ESO Conf. Workshop proc. No.57, 36-42

Dravins D., 2001, Quantum-Optical Signatures of Stimulated Emission, in T.Gull, S.Johansson, K.Davidson, eds.Eta Carinae and Other Mysterious Stars: The Hidden Opportunities of Emission Line Spectroscopy, ASP Conf. ser. No.242, 339-345

Gillett F. & Mountain M., 1998, Science With The NGST, edited by Eric P. Smith and Anuradha Koratkar, ASP Conference Series vol. 133, p. 42

Hanbury Brown R., Twiss R. Q., 1956, Nature, 178, 1046

Harwit M., 2003, ApJ 597, 1266

Hawarden T., 2000, ISAS Report SP No.14, 249 (Dec 2000), Proceedings of a workshop on large space M/FIR telescopes focussing on SPICA

Holland W. et al., 2003, SPIE, 4840, 340

Johansson S. & Letokhov V.S., 2005, "Possibility of Measuring the Width of Narrow Fe II Astrophysical Laser Lines in the Vicinity of Eta Carinae by means of Brown-Twiss-Townes Heterodyne Correlation Interferometry", astro-ph/0501246, New Astron., in press

Kuijken, K; Gilmore, G., 1991, ApJL, 367, L9

Leach J., Padgett M.J., Barnett S.M., Franke-Arnold S., CourtialV., 2002, Phys.Rev.Lett. 88, 257901-1

Padgett M., Courtial J., & Allen L., 2004, Phys.Today, 57, 35

Padovani P., Allen M. G., Rosati P., Walton N. A., 2004, A&A, 424, 545.

Swartzlander G.A., 2001, Opt.Lett., 26, 497

SKA documentation is available at http://www.skatelescope.org/

The ALMA Science Case is available in ASP Conference Series Vol. 235 "Science with ALMA" and at http://www.eso.org/projects/alma/science/alma-science.pdf

Section authors

The following contributed significant text to this document:

Section 3

A. Baglin
P. Bonifacio
C. Catala
Gerry Gilmore
Dougal Mackey
E. Michel
J. Schneider
B. Sicardy

Section 4

Andy Adamson
Arne Ardeberg
Magda Arnaboldi
D. Axon
R. Davies et al.,
Massimo Della Valle
Chris Evans
Colin Frayn
Gary Fuller
Raffaele Gratton
Roberto Gilmozzi
Richard de Grijs
M.A. Hughes
P. Kroupa
Peter Linde
A. Marconi
Mike Merrifield
Livia Origlia
Eline Tolstoy
Doug Whittet

Section 5

J. Bergeron
G. Bono
M. Bremer
D. Burgarella et al.
R. Carswell
S. Cassisi
J.-G. Cuby
M. Della Valle
M. Franx
G. Ghirlanda on behalf of the DEEP Group
F. Hammer
I. Hook
M. Lehnert
B. Leibundgut
P. Molaro and the CODEX team

Annex A

Malcolm Bremer
Matt Burleigh
Roger Davies
Gerry Gilmore
Tim Hawarden
Mike Merrifield
Simon Morris
Tim Naylor

Annex B

Bill Dent
Dainis Dravins

General contributors

In addition, many people contributed ideas and text during the various science case meetings. These include:

Andy Adamson
João Alves
Arne Ardeberg
Luc Arnold
David Axon
Roland Bacon
Eric J. Bakker
Stefano Basso
Slimane Bensammar
Jacqueline Bergeron
Antonio Bianchini
Peter Bizenberger
Michel Blanc
Lorenzo Brandi
Malcolm Bremer
Jane Buckle
Denis Burgarella
Matt Burleigh
Marcella Carollo
Matthew Cassie
Fabienne Casoli
Alain Chelli
Andrea Cimatti
Dave Clements
Françoise Combes
Garret Cotter
Pierre Cox
Jean-Gabriel Cuby
Colin Cunningham
John Davies
Jon Davies
Roger Davies
Chris Davis
Massimo Della Valle
Michel Dennefeld
Vik Dhillon
Philippe Dierickx
Ewine van Dishoeck
Kjetil Dohlen
Janet Drew
Jim Dunlop
Mike Edmunds
Nicolas Epchtein
Jose E. Espinosa
Chris Evans
L Falomo
Marc Ferrari
Marijn Franx
Colin Frayn
Malcolm Fridlund
Flavio Fusipecci
Carme Gallert
Ramón García López
W Gassler
Mauro Ghigo
Giancarlo Ghirlanda
Gerry Gilmore
Roberto Gilmozzi
Raffaele Gratton
Richard de Grijs
Oliver Hainaut
Francois Hammer
Tim Hawarden
Tom Herbst
Isobel Hook
Mark Hughes
Masanori Iye
Pascal Jagourel
Laurent Jorda
Andres Jordan
Eric Josselin
Sarah Kendrew
Johan Knapen
Konrad Kuijken
Robert Laing
Agnes Lebre
Matt Lehnert
Bruno Leibundgut
Peter Linde
Roger Malina
Laura Maraschi
Alessandro Marconi
Eduardo Martín Guerrero
Eric Maurice
Alain Mazure
Mark McCaughrean
Richard McMahon
Mike Merrifield
George Miley
Lance Miller
Paolo Molaro
Guy Monnet
Anna Moore
Alan Moorwood
Simon Morris
Mohamed Mouhcine
Matt Mountain
Denis Mourard
Ulisse Munari
Tim Naylor
Paul O'Brien
Knut Olsen
Livia Origlia
Sergio Ortolani
Steve Phillipps
Didier Queloz
Andreas Quirrenbach
Suzie Ramsay-Howat
Sofia Randich
Rafael Rebolo
Mike Redfern
Anita Richards
Francois Rigaut
Adrian Russell
Penny Sackett
Piero Salinari
Agustin Sanchez-Lavega
Renzo Sancisi
Jean Schneider
Marc Seigar
Steve Serjeant
Ray Sharples
Ian Smail
Stephen Smartt
John Spencer
William Sutherland
Chris Tinney
Eline Tolstoy
Yvonne Unruh
Paul van der Werf
Christophe Verinaud
Paolo Vettolani
Rosie Wyse
Natalia Yaitskova
Frédéric Zamkotsian
Tim de Zeeuw
Hans Zinnecker

the EC FP6 Infrastructure Co-ordination Network
OPTICON is co-ordinated by
Gerry Gilmore, Institute of Astronomy,
Cambridge University, UK

Email: gil@ast.cam.ac.uk

the EC FP6 ELT Design Study is co-ordinated by
Roberto Gilmozzi, European Southern Observatory,
Garching bei Munchen, Germany

Email: rgilmozz@eso.org

WWW sites for further information:

http://www.astro-opticon.org/networking/elt.html

http://www.eso.org/projects/owl/

Designed and produced by Holly Benson Communications